UQAC
Université du Québec
à Chicoutimi

Using analytical and numerical methods to assess the influence of the structural parameters of fractured-rock on controlling water flow in underground excavations

By

Alireza Shahbazi

Under supervision of Prof. Ali Saeidi and co-supervision of Prof. Romain Chesnaux

Thesis presented to the University of Quebec at Chicoutimi with a view to obtaining the degree of doctor of philosophy (PhD) in engineering (Civil)

Defended on February 18, 2022

Board of examiners:

Prof. Duygu Kocaefe, department of Applied Sciences at UQAC, President of the board of examiners

Prof. Mohamed El Tani, Lebanese association for underground space, External Member of examiners

Prof. Silvain Rafini, department of Applied Sciences at UQAC, Internal Member of examiners

Prof. Ali Saeidi, department of Applied Sciences at UQAC, Supervisor, Internal Member of examiners

Prof. Romain Chesnaux, department of Applied Sciences at UQAC, Co-Supervisor, Internal Member of examiners

Québec, Canada

ABSTRACT

Water seepage into underground excavations is one of the most important challenges in aboveground and underground civil works. This phenomenon may hinder the excavation rate, and increase the risk of rockfall from wall of the tunnel and subsidence of aboveground buildings. Since most of the underground and aboveground structures are built in rocky formations, the permeability of the fractured rock mass is the main parameter that determines the amount of discharge that occurs through the rock mass. In this regard, the hydraulic conductivity of rock mass has been focused by many researches to evaluate the fluid flow, and has been studied by empirical, analytical and numerical methods. In the present thesis, the amount of flow through the rock mass has been investigated by using analytical and numerical methods (3DEC software), and due to the practicality of the topic, the amount of inflow rate to the tunnel in the present study is more focused. For this purpose, the tunnel inflow rate and its dependence on the geometrical characteristics of the discontinuities have been formulated using analytical and numerical modelling methods. In addition, the effect of the geometry of joint sets and tunnels as well as the groundwater regime on the amount of inflow rate to the tunnel has been investigated using the response surface methodology and numerical simulation method. In order to ensure the representativeness of numerical models for calculation of the inflow rate to the tunnel, same as what is referred in the literature as REV, a new concept, called STL, has been introduced to determine the representative length of the tunnel in terms of geometric characteristics of discontinuities. Apart from the effect of joint set characteristics on the inflow rate to the tunnel, the effect of rock block geometries such as block volume, block surface and volumetric fracture intensity (P_{32}) on the inflow rate to the tunnel has been investigated by numerical and analytical methods. In this regard, new analytical methods have been developed to calculate block surface area, block volume and volumetric fracture intensity. The analytical method for calculating block volume has been developed to modify previously developed analytical models.

Keywords: rock mass, hydraulic conductivity, inflow rate, circular tunnel, 3DEC, analytical modelling, block volume

RÉSUMÉ

L'écoulement de l'eau dans les ouvrages souterrains est un défi important des travaux de surface et de sous surface effectués dans le domaine du génie civil. En effet, ces ouvrages peuvent retarder les travaux d'excavations, ainsi qu'augmenter le risque de rupture des parois rocheuses de la structure et créer un affaissement des bâtiments. Étant donné que de nombreuses structures (i.e. souterraines et en surface) sont construites en contact avec les formations rocheuses, la transmissivité du massif rocheux est un paramètre clé pour spécifier le débit généré dans les fractures. Afin d'évaluer correctement la transmissivité, de nombreuses investigations considèrent la conductivité hydraulique du massif rocheux à l'aide de méthodes empiriques, analytiques et numériques. Cette thèse de doctorat propose une étude sur le débit d'un fluide à travers un massif rocheux et est essentiellement basée sur des méthodes analytiques et numériques (i.e. logiciel 3DEC) en fonction de l'applicabilité du sujet. Ici, le débit d'entrée à l'intérieur du tunnel est le paramètre principalement ciblé. Le débit entrant dans le tunnel, ainsi que sa dépendance aux caractéristiques géométriques des discontinuités du massif rocheux ont été formulés en utilisant des méthodes de modélisation analytique et numérique. De plus, l'effet des géométries des ensembles de joints du tunnel et le régime des eaux souterraines du débit entrant dans celui-ci ont été étudiés en utilisant la méthodologie de surface de réponse (RSM) et la méthode de simulation numérique. Afin d'assurer la représentativité des modèles numériques appliqués pour le calcul du débit entrant dans un tunnel et demeurer fidèle à la littérature existante sur le REV, un nouveau concept est proposé afin d'identifier la longueur représentative du tunnel en lien avec les caractéristiques géométriques des discontinuités du massif rocheux: le STL. Outre l'effet des caractéristiques des ensembles de joints sur le débit entrant dans le tunnel, l'impact des géométries des blocs rocheux telles que le volume des blocs, la surface des blocs et l'intensité de la fracture volumétrique (P_{32}) sur le débit entrant ont été étudiés à l'aide de ces méthodes numérique et analytique. Dans le but d'améliorer les modèles analytiques antérieurs, de nouvelles méthodes ont été développées afin de calculer la surface d'un bloc, le volume d'un bloc et l'intensité volumétrique de la fracture.

TABLE OF CONTENTS

LIST OF TABLES

LIST OF FIGURES

LIST OF SYMBOLS

(.): Inner product of a pair of vectors (a number)

(×): Cross product of a pair of vectors (a vector)

a_1: longest dimension of a block (m)

a_3: Shortest dimension of a block (m)

a: Ratios of hydraulic conductivities

A: The area of the observation zone (m²)

A_i: Surface area perpendicular to the direction of the fluid flow (m²)

$\vec{A}, \vec{B}, and\ \vec{C}$: Edge vectors of the intact block

b: aperture of the fracture (m)

C_f: Fracture compressibility (kPa^{-1})

$D_1, D_2,\ and\ D_3$: Dip of the joint set 1, 2 and 3 (º)

$DD_1, DD_2,\ and\ DD_3$: Dip direction of the joint set 1, 2 and 3 (º)

DIP: Dip angle of the joint set (º)

DD: Dip direction of the joint set (º)

D_T: Diameter of the tunnel (m)

e_i: Average hydraulic aperture of ith set (m)

E_{doa}: Erosion, discontinuity orientation adjustment

E_{ij}: Hydraulic aperture of the jth fracture of the ith set at ground surface (m)

f'_i: Apparent frequency of the ith set at the wall of the tunnel (m^{-1})

f_i: Real frequency of the ith set (m^{-1})

g: Gravitational acceleration (m.s^{-2})

Δh_x, Δh_y and ∂h_z: Variations of the hydraulic head isolines in the x, y and z directions (m)

h: Hydraulic head (m)

HC: Hydraulic conductivity index

i_{ij}: Hydraulic gradient in the plane of ith set

i_r: Radial component of the hydraulic gradient

i_x, i_y, i_z: Hydraulic gradient in x, y and z direction, respectively

J_a: Joint alteration number

J_{Cond}: Joint condition

J_n: Number of joint sets

J_o: Joint aperture (m)

J_r: Joint roughness number

J_s: Relative block structure

J_v: Number of joints intersecting a volume of 1m^3 of rock (m^{-3})

K: Hydraulic conductivity tensor of the fractured rock

K_1, K_2 and K_3: Principal hydraulic conductivities (m.s^{-1})

K_{2y}, K_{1x}: Principal sub-vertical and sub-horizontal hydraulic conductivities (m.s^{-1})

K_{eq}: Equivalent hydraulic conductivity (m.s^{-1})

K_f: Hydraulic conductivity of the fracture (m.s^{-1})

K_{ij}: Hydraulic conductivity matrix

k_{ij}: Permeability matrix

K_{ni}: Initial joint stiffness of ith set (N.m^{-1})

l_i: The joint length of set i (m)

L: The characteristic length of the rock mass (m)

N: Total number of sets of discontinuities

n_i: Normal to joint set i vector

N_{J1}, N_{J2}, and N_{J3}: Normal vectors to joint set J$_1$, J$_2$, and J$_3$ plane

N_r: Number of random joints in the real location

P: Plunge of the tunnel direction (^{o})

P_{32}: 3D volumetric fracture intensity (m^{-1})

P_i: Joint persistent of set i

P_{iT}: Perimeter of the trace of ith set plane on the wall of the tunnel (m)

q: Discharge rate (m^3/s)

r: Distance from the centre of the tunnel (m)

R: Tunnel radius (m)

R^2: Coefficient of determination

RBL: Representative block of a fractured rock mass

RBLS: Surface area of the representative block (m^2)

RBLV: Volume of the representative block (m^3)

S: The average joint spacing measured along the drill core (m)

S_a: Average joint spacing of all sets (m)

S_b: Block surface area (m^2)

S_i: Average spacing of joint set i (m)

S_{pi}: Apparent spacing of the joint set i at the wall of the tunnel (m)

T_T: Trend of the direction of the tunnel (º)

T: Transmissivity (m^2/s)

uL: Lugeon

$\overrightarrow{u_A}, \overrightarrow{u_B},$ and $\overrightarrow{u_C}$: unit vectors of $\vec{A}, \vec{B},$ and $\vec{C}$

V_b: Volume of blocks (m^3)

$V_b{}^A$: The analytically calculated block volume (m^3)

ΔV_{ij}: Aperture closure of ith set as a result of the overburden load (m)

V_{mij}: Average maximum closure of of ith set's aperture (m)

Z: Depth of the tunnel centre below the groundwater table (m)

β: Form factor of the blocks

γ_1, γ_2, and γ_3: Angle between each pair of joint sets (°)

γ_{AB}: Angle between edge vector A and B (°)

γ_i: Angle between joint sets (°)

θ_{iT}: Angle between tunnel direction and normal to i^{th} set plane (n_i) (°)

θ_i: Angle between edge vector and S_i (°)

μ: Dynamic viscosity of water (Pa.s)

ρ: Fluid density (kg.m^{-3})

σ_n: Normal stress (N.m^{-2})

LIST OF ABBREVIATIONS

3DEC: Three-dimensional distinct element code

ANOVA: Analysis of Variances

BHTV: Borehole televiewer

CCD: Central Composite Design

CGD: Gouge Content Designation

CV: Coefficient of Variation

DFN: Discrete fracture network

D_I: Depth index

Equivalent Permeability: A constant tensor in Darcy's law representing flow in a heterogeneous medium

FLAC: Fast Lagrangian Analysis of Continua, numerical modelling software for advanced geotechnical analyses

FISH: FLAC-ISH or the language of FLAC software

GSI: Geological strength index

JCS: Joint wall compressive strength

JRC: Joint roughness coefficient

LCM: Least Common Multiple

LPI: Lithology Permeability Index

REV: Representative Elementary Volume (m^3)

RMR: Rock mass rating

RMSE: Root Mean Square Error

RQD: Rock quality designation

RSM: Response Surface Methodology

SGR: Site Groundwater Rating

STL: Specific Tunnel Length (m)

TIC: Tunnel Inflow Classification

wJd: weighted joint density (m^{-1})

DEDICATION

To my loved ones, Maryam and Ayhan

"A mes proches, Maryam et Ayhan"

ACKNOWLEDGMENTS

I would like to express my sincere appreciation to my research supervisor, *Prof. Ali Saeidi*, for his trust, continuous support, kindness and care during my PhD. I enjoyed every minute of work under his supervision.

I would like to warmly thank my co-supervisor, *Prof. Romain Chesnaux*, for his support and kindness. I learned many things from *Romain*, either scientific or ethical.

I would like to express my gratitude to *Prof. Alain Rouleau*, for his valuable feedbacks and technical support during my research. Collaborating with him is a valuable asset that I have gained.

I am deeply grateful to the members of my committee, *Prof. Duygu Kocaefe, Prof. Mohamed El Tani* and *Prof. Silvain Rafini*, for their worthwhile guidance and support.

I would like to thank the Itasca Consulting Group in Minneapolis for the IEP Research Program, especially Jim Hazzard, for his valuable technical help and advice.

Last but not least, I would like to sincerely thank my family and friends for all the love and support they provided me throughout my studies.

CONTRIBUTION OF THE AUTHORS

JOURNAL ARTICLES

A review of existing methods used to evaluate the hydraulic conductivity of a fractured rock mass, Engineering geology, Volume 265, February 2020, 105438, *https://doi.org/10.1016/j.enggeo.2019.105438*

A new combined analytical-numerical method for evaluating the inflow rate into a tunnel excavated in a fractured rock mass, Engineering geology, Volume 283, 20 March 2021, 106003, *https://doi.org/10.1016/j.enggeo.2021.106003*

The specific length of an underground tunnel and the effects of rock block characteristics on the inflow rate, Geosciences 2021, 11(12), 517; *https://doi.org/10.3390/geosciences11120517*

Rock block volume calculation by analytical method for geological engineering applications*,* Submitted to "Journal of Rock Mechanics and Geotechnical Engineering" journal

Effects of fracture system geometrical parameters on the inflow rate into a tunnel in rock: a numerical modelling experiment, Submitted to "Quarterly Journal of Engineering Geology and Hydrogeology" journal

Development a practical method for calculation of the block volume and block surface in a fractured rock mass, will be submitted soon

CONFERENCE PAPERS

Numerical modelling for determining the local vertical hydraulic gradient at the wall of a tunnel*,* GeoCalgary Conference, September 2020, Calgary, Canada

Numerical investigation of the relationship between the inflow rate to the tunnel, block volume and block surface area, The Evolution of Geotech- 25 Years of Innovation, 141, *https://doi.org/10.1201/9781003188339-19*

Dependency of the average inflow rate to the tunnel that is excavated in a fractured rock mass

to its Length and direction, GeoNiagara Conference, September 2021, Niagara Falls, Canada

CHAPTER 1

INTRODUCTION

1.1 STATEMENT OF THE PROBLEM

The fluid flow through a fractured rock mass may cause various problems for structures that are supposed to be constructed (excavated) in rocky formations. Seepage to the underground tunnel may increase the risk of rockfall from the tunnel wall and reduce the excavation rate. Waste of the water that has seeped from the rims of dams diminishes the available water for agriculture and drinking purposes. These problems pose difficulties, and given that most underground and aboveground structures are constructed in a rock mass, the water transferability of rock mass is a parameter that governs the flow of the fluid in rocky formations. Compared with the rock matrix (intact rock), discontinuities are the main route for transferring the water through a fractured rock because the permeability of the intact rock is low enough for the rock to be considered an impermeable body. As a result, the fluid flow rate through the fractured rock mass is largely dependent on the hydraulic conductivity of its fractured network.

Calculation of the fluid flow rate through a rock mass and its hydraulic conductivity has been the subject of various investigations and studied using empirical, analytical, and numerical methods. Since the late 18th century, the empirical method based on field data has been used to formulate the permeability of a rock mass and the inflow rate to the tunnel. Such empirical investigations mostly focused on the effect of depth on the inflow rate. Moreover, the hydraulic conductivity of rock mass has been formulated through regression analysis of permeability data on one hand and by using effective parameters on the other hand. The main weakness of empirical methods is that they ignore the geometrical characteristics of discontinuities and regard the rock mass as a homogeneous and isotropic formation. Given that empirical methods are basically founded on the existence of large series of field data, analytical and numerical methods were developed in parallel as alternatives to empirical methods; they can estimate the hydraulic characteristics of rock mass within a shorter time and at a lower cost. Regarding rock mass as a homogeneous formation is a basic assumption in the

development of existing analytical methods for the calculation of the inflow rate to the tunnel and the hydraulic conductivity of a rock mass.

Numerical simulations are also used to model the fluid flow through fractured networks. Generally, 2D numerical simulations are utilized to study the inflow rate to the tunnel. 3D models are often adopted for a simulation of the inflow rate to the tunnel in specific cases of fractured rock mass, but they have not been used to study the impact of geometrical characteristics of the joint sets on the inflow rate to the tunnel. On the basis of this information, the drawbacks encountered in determining the inflow rate to a tunnel that is excavated in a fractured rock mass are listed below.

- Existing analytical methods for the calculation of the inflow rate to a tunnel excavated in a fractured rock mass mainly assume that the rock mass is a homogeneous and isotropic formation. As a result, the effect of fracture network geometry on the inflow rate is not properly included in analytical methods. Existing analytical methods are suitable for 2D analysis only.

- Numerical methods for the calculation of the inflow rate to a tunnel that were developed using 2D simulation demonstrate a specific condition of the joint sets and tunnel direction. In this case, the tunnel is always perpendicular to the normal of the joint sets, implying that the traces of the joint sets at the tunnel wall are always in the direction of the tunnel. However, the angle between the tunnel and joint sets may deviate from what is applied in 2D numerical modeling.

- The first step in implementing a 3D numerical simulation for the calculation of the inflow rate to a tunnel is to ensure that the size of the model is representative of the unlimited size of the formation. In hydrogeological investigations, this concept is introduced as representative elementary volume (REV). However, for the case of a tunnel excavated in a fractured rock mass, the representative size of the numerical model is not properly focused on by previous studies, and the predefined REV of the formation is not applicable to the case of a tunnel because the fluid flows toward the center of the tunnel.

☐ Given that joint sets are the main routes of the fluid flow into the tunnel and that the permeability of the intact rock is often assumed to be negligible in numerical modeling, the inflow rate to the tunnel can be formulated in accordance with the geometrical characteristics of the joint sets, tunnel geometry, and level of the water table. The development of such an equation can help in the estimation of the inflow rate to the tunnel.

☐ The geometry of the rock block is one of the most applicable parameters of a rock mass in geomechanics, but it has rarely been considered in hydrogeological studies. The relationship between rock block characteristics, such as block surface or block volume, and the inflow rate to the tunnel has not been investigated by previous researchers.

☐ No analytical method exists for the calculation of the surface area of the rock block. In addition, the results of existing analytical methods for the calculation of block volume show a noticeable difference with real values. Performing a reasonable estimation of the two parameters is necessary for determining a reliable relation between block geometry and inflow rate to the tunnel.

1.2 RESEARCH OBJECTIVES

The main objective of this thesis is to establish a relationship between the fluid flow through the rock mass, especially the inflow rate to a tunnel that is excavated in a fractured rock mass, and the geometrical characteristics of the discontinuities by using 3D numerical simulation. To achieve the main objective, the following sub-objectives are defined.

☐ Development of an analytical model for predicting the inflow rate to a tunnel that is excavated in a fractured rock mass in consideration of the geometrical characteristics of the fractured network, level of the water table, tunnel depth, and tunnel radius.

☐ Introduction of the REV of the numerical model (or representative elementary length of the tunnel) to the numerical simulation of the inflow rate to the tunnel. The concept of REV when used for geological or hydrological characteristics of a rock mass has

already been introduced; however, this concept should be modified when referring to the hydrological characteristics of the tunnel.

☐ Determination of the impact of the geometrical characteristics of the joint sets on the inflow rate to the tunnel by using 3D numerical simulation and evaluation of the effect of the interaction between parameters on the inflow rate to the tunnel by using the response surface methodology.

☐ Development and validation (via the 3D numerical simulation method) of analytical methods for the calculation of the area and volume of rock blocks and the volumetric fracture intensity of a rock mass that includes three persistent joint sets. Notably, the analytical method for block volume calculation is supposed to yield more accurate results than previously developed models.

☐ Definition of the relationship between block geometries, including block surface area, block volume, and volumetric fracture intensity (P_{32}), and inflow rate to the tunnel by using the 3D numerical simulation method.

1.3 RESEARCH METHODOLOGY

The specific methodology used to achieve the principal and sub-objectives of this study is briefly illustrated in Fig 1-1.
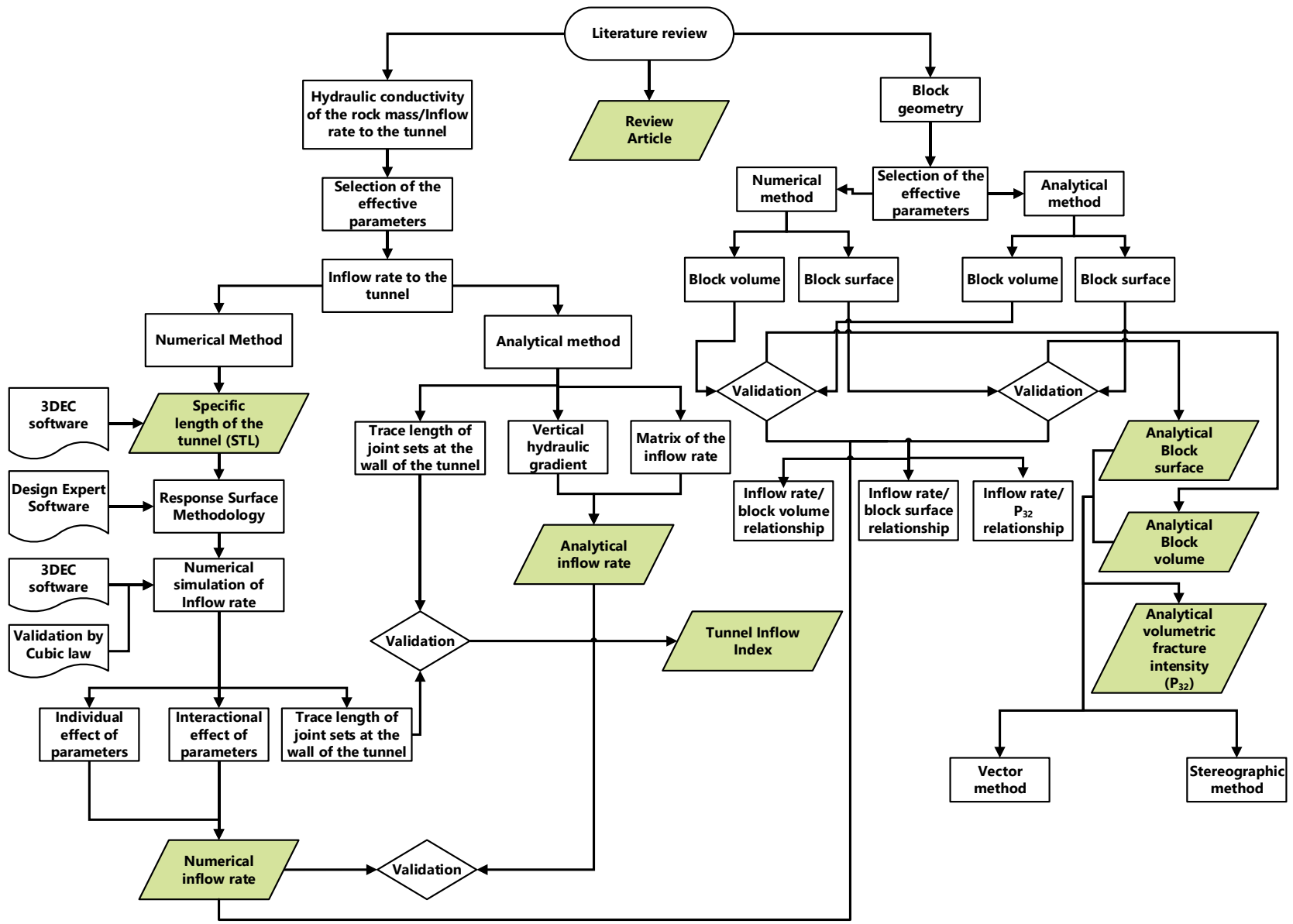
Fig 1-1. The methodology for reaching to the main and sub-objectives of this thesis. The green boxes are the objectives of the thesis.

The first and most important step of the methodology is to review literature and existing publications related to the hydraulic conductivity of rock mass, especially the inflow rate to the tunnel. By conducting this review, various existing methods for achieving the objectives of the study are identified. In addition, the parameters that affect the amount of flow entering the tunnel are determined. After determining the effective parameters, as the second step of the research, an analytical method is developed for the calculation of the inflow rate to a tunnel that is excavated in a fractured rock mass in the steady state condition and laminar flow mode. When calculating the inflow rate to the tunnel, this method considers the geometrical characteristics of the discontinuities. The development of the analytical model consists of two steps. The first is to determine the matrix of the hydraulic conductivity of the rock mass, and the second step is to define the existing hydraulic gradient at the wall of the tunnel. Rocscience RS2 software is used to develop an empirical–numerical equation for the vertical hydraulic gradient at the wall of the tunnel. After obtaining the matrix of hydraulic conductivity and the equation of the hydraulic gradient, the inflow rate can be calculated analytically.

The third step of the research is to calculate numerically the inflow rate to the tunnel. For this purpose, Itasca 3DEC software version 7 is adopted to perform numerical simulations. 3DEC is one of the best software for the simulation of the geomechanical and hydrogeological responses of rock mass, and it is designed to evaluate fractured networks. Meanwhile, the response surface methodology is used to achieve the principal objective of the study, which is to define numerically the relationship between the inflow rate to the tunnel and the effective parameters. For this purpose, 88 numerical simulations are defined using Design Expert software to determine the individual and interaction effects of each parameter on the inflow rate to the tunnel and to derive the relationship between inflow rate and effective parameters. To ensure the accuracy of the numerical model results, the calculated numerical flow through a fracture is compared and validated using the cubic law; then, the inflow rate determined by the numerical method is validated using the previously developed analytical model.

Aside from the geometrical characteristics of the discontinuities, block geometry is considered in this research to determine the relationship between inflow rate to the tunnel and block size. Block volume, block surface, and volumetric fracture intensity (P_{32}) are the geometrical characteristics of the block that are discussed in this work, and for this purpose, block geometries are calculated using analytical and numerical (3DEC) methods. Given that no analytical method is available to calculate the block surface, a method is developed in this work for the case of three persistent joint sets. In addition, a new analytical method is established for the calculation of block volume; this method is more accurate than previously developed models, and as a result, the volumetric fracture intensity can be analytically determined by dividing the block surface by block volume. All of the developed analytical models for the calculation of block geometries are validated through the numerical simulation method by using 3DEC software. Then, after obtaining the inflow rate to the tunnel and the block geometries, the relationship between them is investigated.

1.4 ORIGINALITY AND CONTRIBUTION

The main objective of this study is to evaluate the fluid flow through a fractured rock mass, with focus on the inflow rate to the tunnel. In this regard, new concepts are introduced in this dissertation and discussed in this section.

As the first step of this research, existing literature is reviewed, and contemporary methods for the evaluation of the hydraulic conductivity of rock mass and inflow rate to the tunnel are studied. On this basis, a literature review article has been published as the first innovation of this thesis.

An analytical method is developed for the calculation of the inflow rate to the tunnel. This method has a significant difference from other methods because it is developed based on the fluid flow in the fracture network. By contrast, existing methods are developed by considering an equivalent medium instead of fractured rock mass and hence require predefining the hydraulic conductivity of the rock mass prior to using analytical equations.

The specific length of the tunnel is introduced in this work as the representative length of the tunnel for numerical simulations. Notably, thus far, no criteria that should be considered in numerical simulations have been defined for tunnel length. Tunnel length has an important effect on the average inflow rate to the tunnel, and as the length changes, the inflow rate changes accordingly.

The hydraulic gradient on the wall of the tunnel plays an important role in the value of flow velocity into the tunnel because when it increases, the amount of inflow increases in the same proportion. Investigation of the hydraulic gradient on tunnel walls has rarely been performed in previous studies, although a few studies have mentioned tunnel depth as the only parameter affecting the hydraulic gradient. However, this work confirms that in addition to tunnel depth (water head above the tunnel), the values of principal hydraulic conductivity and their directions are other parameters that affect the hydraulic gradient on the tunnel wall.

Although several studies have focused on the effect of discontinuity geometries, tunnel geometry, and groundwater levels on tunnel inflow rate in 2D simulation, 3D sensitivity analysis has not been sufficiently performed. 2D numerical simulation of the amount of inflow rate to the tunnel cannot approximate the real situation compared with 3D modeling because only a special case of the orientation of the joint sets in relation to the direction of the tunnel is considered, i.e., the case where the tunnel is always perpendicular to the normal of the joint sets. In this study, a sensitivity analysis is performed on the aperture, spacing, and orientation of the joint sets; tunnel radius; and water head above the tunnel by using 3D numerical models. Apart from the individual effect of the parameters, the effect of their interaction on the inflow rate is also studied in this research.

Usually, the dip and dip direction of the joint sets and the orientation of the tunnel are regarded as effective parameters when studying the effect of joint set orientation on the inflow rate to the tunnel. However, instead of these parameters, the angle between the normal to the joint sets and the direction of the tunnel is considered in this work. This substitution is reasonable because the traces of the joint sets on the wall of the tunnel are the sole pathway for transferring the fluid to the tunnel and depend merely on the angle between the joint set and the direction of the tunnel.

Block geometry is often used to develop geomechanical indices of rock mass, such as GSI and RMR, but not to evaluate its hydrogeological properties. In this study, the correlation between fluid flow through rock mass and block geometry is investigated through 3D numerical simulation. The volume and surface of the block and the volumetric fracture intensity (P_{32}) are the geometric characteristics of the blocks that are considered in this work.

Thus far, no analytical method is available for calculating the surface area of blocks created by the intersection of three persistent joint sets. In addition, existing methods for calculating block volume show discrepancies with actual values. In this study, an analytical method is developed for the calculation of the surface of blocks created by the intersection of three persistent joint sets, and it is validated through numerical methods. In addition, a new analytical equation is established to calculate the block volume. Through a comparison of the results of the developed and existing methods with the results of numerical simulations, the accuracy of the developed models is confirmed. Then, the incompatibility and application area of previous models are investigated. The volumetric fracture intensity is also determined analytically by using the developed method to calculate the block surface and block volume. This study provides an important innovation in the calculation of block geometry and can affect a wide range of geomechanical indices of rock mass that are based on previously developed methods for calculating block volume.

1.5 THESIS OUTLINE

A review article and five journal papers are the outcome of this thesis, and they are presented separately in Chapters 2 to 7. The general structure of the articles comprises the Abstract, Introduction, Methodology, Discussion, and Conclusion.

CHAPTER 1 describes the overall structure of the thesis by explaining the statement of the problems first. On this basis, the objectives of the research are presented. Then, the methodology used to achieve the principal and sub-objectives of the study are described, and the originality and novelty of the thesis are explained.

CHAPTER 2 presents existing literature regarding the evaluation of the hydraulic conductivity of fractured rock mass and the inflow rate to the tunnel. The pros and cons of the methods and the limitations in the application of each model are also discussed.

CHAPTER 3 introduces the newly developed analytical method for the calculation of the inflow rate to the tunnel excavated in a fractured rock mass. This chapter consists of two parts. In the first one, an analytical model is developed based on Darcy's law and cubic law. In the second part, the hydraulic gradient on the wall of the tunnel is formulated using an empirical–numerical equation obtained with Rocscience RS2 software.

In CHAPTER 4, the correlation between the inflow rate to the tunnel and block volume, block surface, and volumetric fracture intensity (P_{32}) is investigated. For this purpose, the representative length of the tunnel for hydrogeological purposes (STL) is determined first for numerical simulation. Then, a new analytical method is developed based on vectoral multiplication for the determination of the surface area of the blocks that are created by the intersection of three persistent joint sets. The correlation between inflow rate to the tunnel and block geometries is investigated by performing numerical simulations and regression.

In CHAPTER 5, the relationship between the inflow rate to the tunnel and the geometrical characteristics of the discontinuities, tunnel radius, and groundwater level is formulated by implementing a numerical simulation with 3DEC and designing numerical experiments with the response surface methodology (RSM).

As mentioned, the relationship between block geometries and inflow rate to the tunnel is investigated in CHAPTER 4. However, the discrepancy between the analytically calculated block volume and the block volume from 3DEC software requires the development of another analytical method for the calculation of block volume. Thus, in CHAPTER 6, an analytical model based on vectoral multiplication is developed to calculate the volume of the blocks that are formed by the intersection of three persistent joint sets. The model is validated using 3DEC software.

The vectoral methods for the calculation of block volume and block surface (also volumetric fracture intensity) in CHAPTER 4 and CHAPTER 5 may be not simple enough to be used by practitioners or geologists. In this regard, in CHAPTER 7, the stereographic projection method is adopted to develop analytical equations for the calculation of the volume, surface area, and volumetric fracture intensity of rock mass that includes three persistent joint sets. The inconsistency of each method is examined using RSM and Design-Expert software.

CHAPTER 8 presents the most important outcomes of the present work and the directions for future research. Supplementary data related to CHAPTER 5 are presented in CHAPTER 9.

CHAPTER 2

Article 1: A review of existing methods used to evaluate the hydraulic conductivity of a fractured rock mass

Alireza Shahbazi, Ali Saeidi, Romain Chesnaux

Université du Québec à Chicoutimi, 555 boulevard de l'Université, Chicoutimi, Québec G7H 2B1, Canada

Email: alireza.shahbazi1@uqac.ca

2.1 HIGHLIGHTS

- Existing methodologies for investigating the hydraulic conductivity of a rock mass are reviewed comprehensively

- Hydraulic conductivity of a rock mass can be assessed by empirical, analytical, and numerical methods

- The advantages and disadvantages of existing methods for rock mass permeability are summarized

- Future direction for assessing the hydraulic conductivity of a rock mass are discussed

2.2 ABSTRACT

We review the existing methods for evaluating the hydraulic conductivity of a rock mass. Rock mass permeability may be assessed using empirical, analytical and numerical approaches. Empirical methods use data from in situ field tests to derive the relationship between depth and permeability by applying a curve-fitting method and establishing the relationship between hydraulic conductivity and a geological index. Analytical methods rely on Darcy and cubic laws to estimate the permeability of a rock mass by taking into account the geometrical characteristics of the joint sets. Analytical equations of the flow rate into underground excavations are also developed by solving the Laplace equation for homogeneous and isotropic aquifers under various boundary conditions. Numerical modelling can evaluate the outcomes of both empirical and analytical approaches (and vice versa) and can provide a sensitivity analysis of the parameters that affect rock mass permeability. The importance of stress

and joint set characteristics is often investigated via numerical modelling, as are the scale effect and directional permeability. In this review paper, we provide a comprehensive review of these approaches for studying rock mass permeability. We summarize the advantages and disadvantages of existing methods and highlight potential future research directions.

Keywords: Hydraulic conductivity, Permeability, Rock mass, Empirical method, Analytical model, Numerical model

2.3 INTRODUCTION

The seepage of water into underground excavations from groundwater or aboveground reservoirs is an important aspect of water resource management. Quality information related to seepage is essential for a wide range of scenarios. Knowledge of the seepage rate from the rock foundation of a dam can help assess the feasibility of dam construction. This information can also help adequately modify the base and reservoir rims [1-3]. In underground water reservoirs, the hydraulic properties of the rock formation govern the discharge rate of water wells; it is thus essential to obtain a reliable evaluation of these properties. Before construction of an underground excavation, a comprehensive understanding of the hydraulic properties of a rock formation is necessary to properly evaluate the stability of the cavity walls and possible means of evacuating seeped water from the excavation area [4-6]. Finally, the leakage of radioactive waste or petroleum reservoirs [7, 8] poses another risk potential that can only be accurately assessed through knowledge of the hydraulic characteristics of the surrounding rock mass.

Studies assessing water inflow into underground excavations were some of the first to begin looking at the in-depth permeability of rock masses. The works of Snow [9], Carlsson and Olsson [10], and many others, through to Chen et al. [2] published numerous equations to address the problem of evaluating rock mass properties. Given that the rock type (sedimentary, metamorphic, and igneous) and class (*GSI*, *RMR*, etc.) vary between most studies sites, each developed equation is, however, valid only for a specific setting.

In general, permeability decreases with depth; the rate of change is highest at subsurface depths and the rate of change decreases with depth. An existing set of equations link the empirical equations of

permeability and rock mass indices derived from core log data [11-13]. Of these various rock mass indices (i.e., *RMR*, *RQD*, and *GSI*), *RQD* is the most readily available data obtained from boreholes, and therefore the RQD-permeability relationship is the one most frequently determined [11-15].

In parallel with these empirical investigations, researchers developed analytical formulations of permeability by considering effective parameters and applying Darcy and cubic laws as well as the Laplace equation. The Laplace equation and the assumption of a homogeneous and isotropic medium are fundamental aspects of all permeability models that are developed to measure water inflow rates into underground tunnels. Differences between models stem from variable initial boundary conditions and the specific approaches that are used. Muskat and Meres [16] and Goodman et al. [17] published the initial elementary models that were further developed by Park et al. [18].

One of the earliest classic models of the permeability tensor of a rock mass was developed by Snow [19]. He introduced a model that considered the geometrical characteristics of the joint sets. Oda [20] developed a rock mass permeability tensor by defining the crack tensor and using the probability of the presence of cracks. More recently, in addition to the parameters considered previously when evaluating the permeability tensor of the rock mass, Zhou et al. [21] added the effect of stress and joint interconnections and developed a set of analytical equations to predict water flow into tunnels.

Numerical modelling can be applied to the sensitivity analysis of joint geometry [22, 23], as well as to the assessment of how the mechanical properties of fractures [23, 24], stress [25-27], and scale effects [28, 29] affect rock mass permeability. Modelling can also evaluate tunnel inflow rates [22, 23, 30]. Because numerical models of rock mass permeability are applied most often to evaluate in-depth permeability, and because stress increases with depth, the developed models have focused mainly on the effect of stress on permeability. Normal stress decreases permeability [25, 31, 32], whereas shear stress increases permeability [25, 33, 34]. Furthermore, sensitivity analysis demonstrates that increased joint frequency (which is the opposite of spacing) [22, 23] and interconnection [22, 30, 31] promote permeability. The effect of mechanical and physical properties of fractures on rock mass permeability have also been modelled numerically [23, 25, 33]. The relevance of the representative elementary volume (REV) in evaluating the

hydrological properties of a rock mass has been investigated [25, 28, 29]. Based on directional hydraulic conductivity, the scale of the discrete fracture network has been shown to mainly affect hydraulic conductivity values.

The accuracy of a numerical model is governed mostly by the degree to which the fracture network generated for use in the modelling effort is representative of reality. To generate the discrete fracture network (DFN), it is possible to collect in situ data [35] or to generate the DFN either stochastically [36] or mechanically [36]. In this regard, considering the correlation between the geometrical parameters of the rock mass in the DFN results produces a more realistic fracture network.

This review paper presents a comprehensive state of the art of methods used to assess hydraulic conductivity in fractured rock environments. It aims to serve as a reference document and guide for characterizing the hydraulic properties in fractured rock; such a guide may be useful for both practitioners and consultants. We present the empirical, analytical and numerical methods, respectively. For each approach, we detail its development, evolution as well as advantages and drawbacks.

Empirical equations are useful for the formations for which they have been developed; in consequence, utilization of rock mass indices (RMR, RQD, etc.,) developed specifically to determine geomechanical characteristics may be less appropriate for assessment of hydraulic behaviour. Analytical equations are economical and rapidly accessible tools that may yield a rough estimation of the permeability of the rock mass; future research on analytical equations aim to increase the effectiveness of parameters as well as consideration of uncertainties in these parameters. The assumption of rock mass as a homogeneous and isotropic media for predicting inflow rate to underground tunnels is limited by the fact that hydraulic conductivity of fractured media is highly dependent on the direction of the measurement. Numerical models require greater time (and cost) expenditures than other methods, but they accommodate a higher number of influential parameters and they offer the possibility of conducting sensitivity analyses.

2.4 EMPIRICAL METHODS

Evaluating the hydraulic conductivity of a rock mass using an empirical approach relies on in situ permeability data and establishing correlations between permeability, depth [37-39], and the geological characteristics of the rock mass. In this section, we present the most important empirical investigations of permeability and fluid flow through a rock mass. In the first part, we survey developed permeability-depth equations. We then discuss efforts to relate permeability with existing geological indices.

2.4.1 Depth-permeability relationship

Empirical studies of permeability as a function of depth represent some of the earliest and most common investigations of permeability [37, 39, 40]. The experimental routine for measuring in-depth permeability consists of applying the double-packer test [2, 41, 42] and/or Lugeon test [2, 43] at various depths. Regression analysis of this data produces a depth-hydraulic conductivity curve; however, permeability values obtained via this method are not very representative of the actual permeability in fractured rock. The permeability values obtained by such tests depend on the test location and are applicable only to the rock formation in the immediate vicinity of the tests. Results cannot be applied to the overall rock mass, as geological characteristics are not homogeneous throughout the entire rock mass [44].

In empirical investigations, in situ stress is the most important parameter affecting the in-depth permeability of a rock mass; gravity stress is the most common source of this stress. In situ stress directly affects the fracture aperture, i.e., the main route of fluid flow in the rock mass, and consequently modifies the permeability of the rock formation [45-47]. Unlike aperture, which decreases with depth due to gravity stress, discontinuous spacing usually increases with depth [48] and has less of an effect than aperture on the in-depth variations of permeability [42]. Snow [49] originally argued in favour of the existence of a relationship between depth and joint spacing, although there is now general agreement that a change of aperture and spacing with depth does not occur [45].

Generally, there is also agreement that the depth-related variation in hydraulic conductivity of a rock mass is a decreasing trend; however, there are different formulations of the hydraulic conductivity–depth

relationship. Piscopo et al. [45], propose a relationship between rock mass depth, spacing, and hydraulic conductivity by arguing that the decrease of K with depth is related to a decreased hydraulic aperture. They define K as:

$$K = K_0 \exp(-\beta d) \qquad\qquad (2\text{-}1)$$

where K is the hydraulic conductivity (m s^{-1}), K_0 is ground surface hydraulic conductivity (between 0.84×10^{-7} and 3.64×10^{-7}, where its arithmetic mean is 2.75×10^{-7}), β is a constant of approximately 9.3×10^{-3} (m^{-1}), and d is depth (m).

In the manner of Piscopo et al. [45], various forms of the hydraulic conductivity–depth relationship have been published (these are listed in chronological order in Table 2-1. Given that the experimental approach of all the equations is generally the same, differences between the equations are due to their application to differing rock formations.

Table 2-1. Recommended empirical formulations for assessing the hydraulic conductivity of a rock mass with depth

Equation	Reference	Parameters	Rock type
$Log\ k = -8.9 - 1.671\ Log\ z$	Snow [9]	k, permeability (ft^2); z, depth (ft).	Sandstone and limestone
$K = K_0\ \exp(-ad)$	Louis [50]	K, hydraulic conductivity (m/s); K_0, hydraulic conductivity at ground (m/s); varies between 0.84×10^{-7} and 3.64×10^{-7}; d, depth (m); a, empirical coefficient between 3.4×10^{-3} and 7.8×10^{-3}.	Igneous and metamorphic rocks
$K = 10^{-(1.6Logz+4)}$	Carlsson and Olsson [10]	K, hydraulic conductivity (m/s); z, depth (m).	Gneiss granite (crystalline)
$Log\ K = -5.57 + 0.352\ Log\ z - 0.978\ (Log\ z)^2 + 0.167\ (Log\ z)^3$	Burgess [38]	K, hydraulic conductivity (m/s); z, depth (m).	Metamorphic rock
$K = K_i \left[1 - \dfrac{z}{58 + 1.02z}\right]^3$	Wei et al [40]	z, depth (m); K, hydraulic conductivity (m/s); K_i, hydraulic conductivity near ground surface (m/s); varies between 0.84×10^{-7} and 3.64×10^{-7}.	Igneous and metamorphic (crystalline) rocks
$K = K_0\ \exp(-\beta d)$	Piscopo et al. [45]	K, hydraulic conductivity (m/s); K_0, hydraulic conductivity near ground surface (m/s); varies between 0.84×10^{-7} and 3.64×10^{-7}; d, depth (m) (85–140 m); β, empirical coefficient at 9.3×10^{-3} (l/m).	Mainly andesite and secondary metamorphic (igneous and metamorphic) rocks
$K = 2 \times 10^{-6}\ d^{-0.48}$	Chen et al. [2]	K, hydraulic conductivity (m/s); d, depth (m).	Igneous and metamorphic rocks

To better visualize the equations presented in Table 2-1, a selection of these equations is illustrated in Fig 2-1. Average ground surface hydraulic conductivity (K_0) is equal to 2.75×10^{-7} and the arithmetic mean of "β" is used for equation (2-1). Trends for equations are very similar; differences are attributed to rock type and discontinuities. The Louis [50] and Piscopo et al. [45] equations describe a linear relationship for log K-depth, whereas the other equations are curvilinear in form. The Snow [9] and Carlsson and Olsson

[10] curves are almost identical, although the rate of the change of *K* with depth is predicted almost identically by Burgess [38] and to a slightly greater difference by Wei et al. [40].
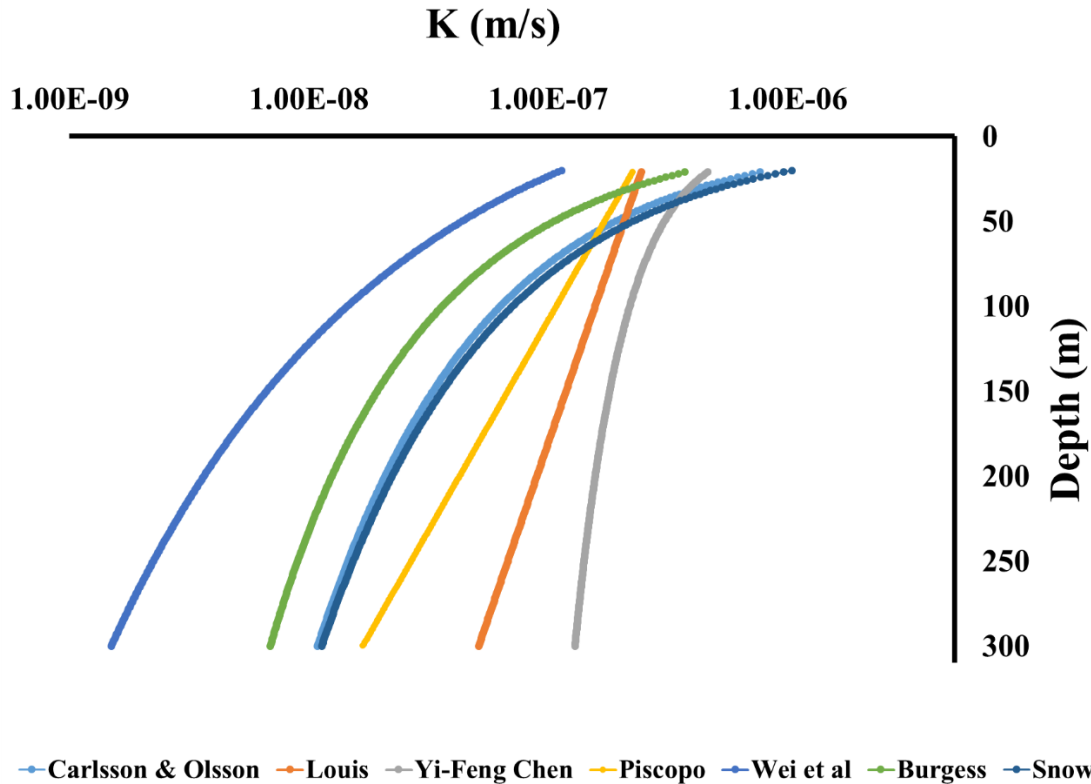
Fig 2-1. Variation in the hydraulic conductivity of a rock mass with depth using a harmonized K_0 and based on $K = K_0 \, exp \, (ad)$-type equations

2.4.2 Formulation using rock mass indices

In rock mass geomechanical studies, indices used for assessing stability include the rock mass rating (*RMR*), geological strength index (*GSI*), and rock quality designation (*RQD*). Some researchers have tried to establish an empirical relationship between these indices and hydraulic conductivity [12, 14, 15]. Jiang et al. [15], defining the *RQD* from borehole data at a depth of 11 to 88 m, posited a relationship between rock mass transmissivity and the *RQD*. From the core log of the borehole, they first defined the joint spacing. Using the Priest and Hudson [51] equation for relating *RQD* and joint spacing, Jiang et al. (2009) then defined the *RQD* for each borehole. From linear regression, the change of *RQD* with depth can be expressed by Eq.(2-2). Note, however, that any formulation for relating *RQD* to depth was rejected by Piscopo et al. [45].

19

$$RQD = 0.2875h + 65.751 \qquad (2\text{-}2)$$

where h is depth. Then, based on the packer test data, the relationship between transmissivity and depth is also fitted using regression analysis based on the Swan model [52] ($\sqrt[3]{T} = -A_1 h + A_2$), and demonstrated by Eq.(2-3):

$$\sqrt[3]{T} = 0.116 \log h + 0.3695 \qquad (2\text{-}3)$$

Finally, by comparing equations (2-2) and (2-3), Jiang et al. published Eq.(2-4) to correlate K and RQD (Fig 2-2):

$$K = 0.4892 \exp(-0.0543 \times RQD) \ (R^2 = 0.7809) \qquad (2\text{-}4)$$
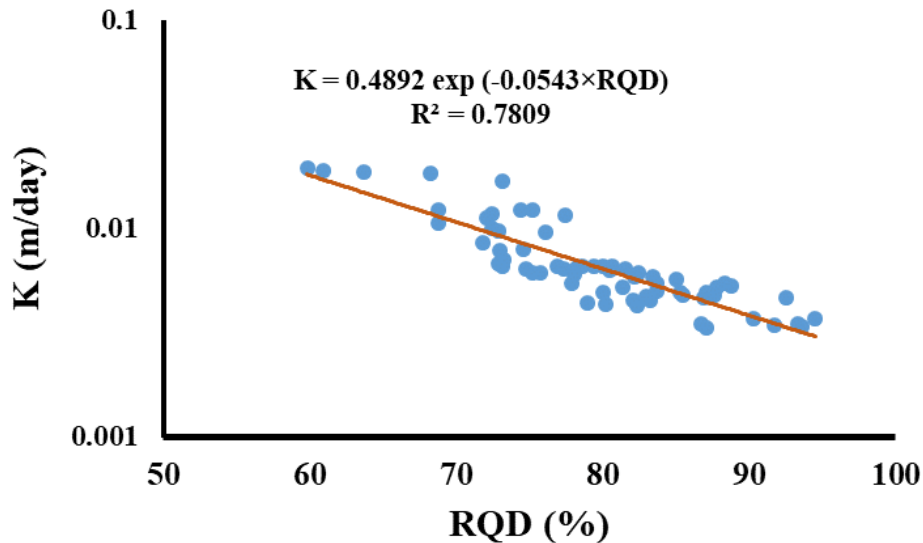
Fig 2-2. Scatterplot of mean hydraulic conductivity versus mean RQD [15]

By the same method, other relationships between hydraulic conductivity and *RQD* [11, 12], *GSI-RQD* [11], and *RMR-RQD* [13] have been developed (Table 2-4). Fig 2-3 summarizes the existing relationships between hydraulic conductivity and RQD, as listed in Table 2-4.
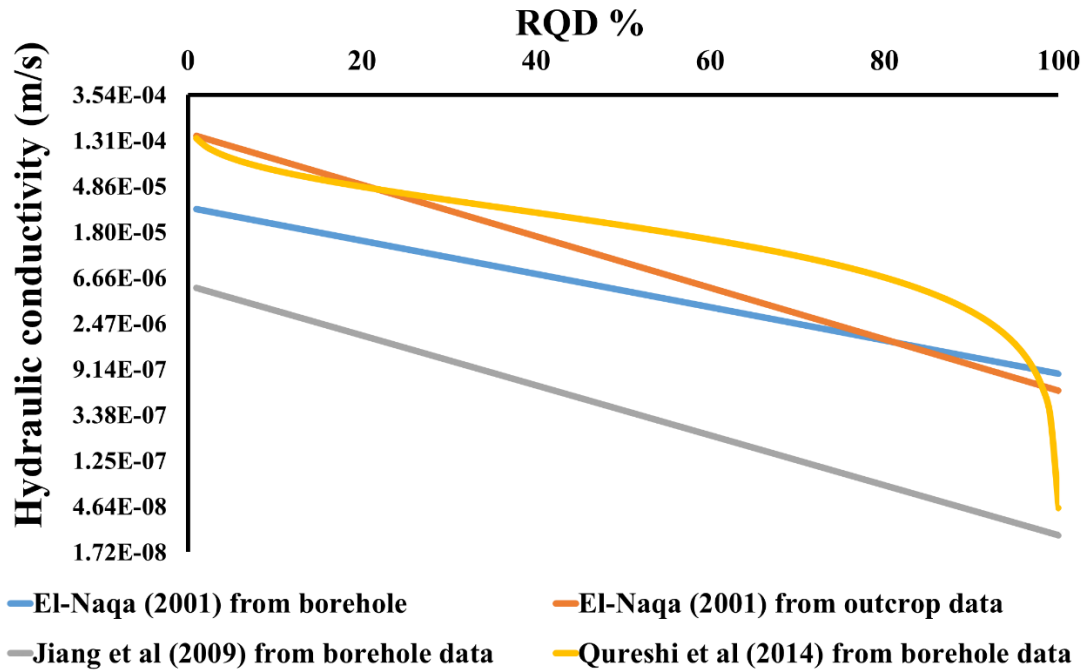
Fig 2-3. Existing relationships between hydraulic conductivity and RQD based on the published equations of Table 2-4

Ku et al. [53] defined another index of rock mass permeability. They relied on the geological parameters of *RQD*, depth index (*DI*, influence of the depth on permeability), gouge content designation (*GCD*), and the lithology permeability index (*LPI*, influence of mineral composition, grain size, texture, colour, and so forth on permeability). This new index, *HC*, evaluates the hydraulic conductivity of a rock mass and is defined according to equation (2-5):

$$HC = (1 - RQD)(DI)(1 - GCD)(LPI) \qquad (2\text{-}5)$$

The definitions and formulas of each parameter of equation (2-5) are presented in Table 2-2.

Table 2-2. Description of the parameters of rock mass permeability indices as published by Ku et al. [53]

Parameter	Formula	Remarks
Depth index (DI)	$DI = 1 - \dfrac{L_c}{L_T}$	L_T, total length of the borehole (m); L_c, depth in the middle of a double-packer test interval in the borehole (m).
Gouge content designation (GCD) index	$GCD = \dfrac{R_G}{R_T - R_S}$	R_S, cumulative length of core pieces longer than 100 mm in a run (m); R_T, total length of the core run (m); R_G, total length of gouge content (m).

Lithology permeability index (LPI)	According to Table 2-3	
Rock quality designation (RQD)	$RQD = 100\left(1 + \dfrac{1}{10s}\right)\exp\left(-\dfrac{1}{10s}\right)$	s, joint spacing (m)

Table 2-3. Description and ratings for the lithology permeability index (LPI) [53]

Lithology	Hydraulic conductivity (m/s)				Range of rating	Suggested rating
	Reference [54]	Reference [55].	Reference [56]	$K_{average}$		
Sandstone	10^{-6}–10^{-9}	10^{-7}–10^{-9}	10^{-7}–10^{-9}	$10^{-7.5}$	0.8–1.0	1.00
Silty sandstone (SS)	-	-	-	-	0.9–1.0	0.95
Argillaceous sandstone	-	-	-	-	0.8–0.9	0.85
SS interbedded with some shale	-	-	-	-	0.7–0.8	0.75
Alternations of SS and shale	-	-	-	-	0.6–0.7	0.65
Shale interbedded with some SS	-	-	-	-	0.5–0.7	0.60
Alternations of SS and mudstone	-	-	-	-	0.5–0.6	0.55
Dolomite	10^{-6}–$10^{-10.5}$	10^{-7}–$10^{-10.5}$	10^{-9}–10^{-10}	10^{-8}	0.6–0.8	0.70
Limestone	10^{-6}–$10^{-10.5}$	10^{-7}–10^{-9}	10^{-9}–10^{-10}	10^{-8}	0.6–0.8	0.70
Shale	10^{-10}–10^{-12}	10^{-10}–10^{-13}	-	$10^{-10.5}$	0.4–0.6	0.50
Sandy shale	-	-	-	-	0.5–0.6	0.60
Siltstone	10^{-10}–10^{-12}	-	-	10^{-11}	0.2–0.4	0.30
Sandy siltstone	-	-	-	-	0.3–0.4	0.40
Argillaceous siltstone	-	-	-	-	0.2–0.3	0.20
Claystone	-	10^{-9}–10^{-13}	-	10^{-11}	0.2–0.4	0.30
Mudstone	-	-	-	-	0.2–0.4	0.20
Sandy mudstone	-	-	-	-	0.3–0.4	0.40
Silty mudstone	-	-	-	-	0.2–0.3	0.30
Granite	-	-	10^{-11}–10^{-12}	$10^{-11.5}$	0.1–0.2	0.15
Basalt	10^{-6}–$10^{-10.5}$	10^{-10}–10^{-13}	-	$10^{-11.5}$	0.1–0.2	0.15

The HC index (equation (2-6)) can be used to predict hydraulic conductivity (*K*):

$$K = 2.93 \times 10^{-6}\,(HC)^{1.380}\ \ (R^2 = 0.866) \qquad (2\text{-}6)$$

Equations for the relationship between rock mass geological indices and hydraulic conductivity are summarized in Table 2-4.

Table 2-4. Existing equations for hydraulic conductivity of a rock mass using rock mass geological indices

Equation	Reference	Parameters	Type of rock
$$uL = \exp\left[\left(5.5 + \left(\frac{16.5\,JCond - 165}{RQD}\right)\right) - 1\right]$$	Öge [11]	uL, Lugeon value for hydraulic conductivity (uL).	Agglomeratic, basaltic, andesitic, siltstone, clay stone, marl
$$K_a = 0.01382 - 0.003\ln RQD$$	Qureshi et al. [12]	K_a, apparent hydraulic conductivity (cm/s); RQD, rock quality designation (%).	Sedimentary rocks (mainly in sandstone and limestone)
$$K = 177.45\exp(-0.0361 \times RQD)$$ $$K = 5 \times 10^6 \exp(-0.1923 \times RMR)$$	El-Naqa [13] For borehole data	K, hydraulic conductivity in Lugeon (uL); RQD, rock quality designator (%); RMR, rock mass rating.	Cambrian sandstone
$$K = 890.9\exp(-0.0559 \times RQD)$$ $$K = 3166.1\exp(-0.0755 \times RMR)$$	El-Naqa [13] For field mapping		
$$K = 0.4892\exp(-0.0543 \times RQD)$$	Jiang et al. [15]	K, hydraulic conductivity (m/s); RQD, rock quality designator (%).	Monzonitic granite, quartz monzonite, and quartz syenite
$$K = 2.93 \times 10^{-6} \times (HC)^{1.38}$$ $$HC = (1 - RQD)\,(DI)\,(1 - GCD)\,(LPI)$$	Ku et al. [53]	RQD, rock quality designation (%); DI, depth index; GCD, gouge content designation; LPI, lithology permeability index.	Highly disturbed clastic sedimentary rocks

In this section, we have highlighted the most important empirical approaches developed to extract the relationships between hydraulic conductivity and other geological parameters. Most developed equations rely on the depth-*K* relationship; in addition, empirical equations predict hydraulic conductivity using rock mass geological indices, such as the *RQD* and *RMR.* There is general agreement that the hydraulic conductivity of a rock mass decreases with depth and that the geological characteristics of a rock mass affect K. The variation of the hydraulic conductivity of the rock mass with depth is due to the increase of stress because of the overburden load. Normally, the stress would reduce the aperture and decrease the permeability, but the type of stress (shear or normal) is not taken into account; in contrast, the effect of stress is extensively studied in the analytical and numerical methods (sections 2.5 and 2.6). These existing equations for *K*-depth relations remain valid only for rock masses sharing highly similar geological and morphological characteristics. They do not consider the key parameters affecting the hydraulic conductivity

of the rock mass, such as the aperture or the spacing and orientation of fractures. Furthermore, as geological indices of rock mass are adopted mainly to characterize rock mass mechanics, the indices may not be entirely applicable to hydraulic behaviour. Neither the *RQD* nor the *HC* index [53] includes the major parameters affecting rock mass hydraulic conductivity (aperture, spacing, orientation, etc.). However, as the existing empirical equations are based on the field data, they are more reliable than the other methods and hence, the results of other methods have to be compatible with empirical equations. To increase the comprehensiveness of empirical methods, further studies and the discretization of associated parameters are needed to ensure more accurate predictions of the hydraulic behaviour of a rock mass.

2.5 ANALYTICAL MODELLING

For determining hydraulic conductivity, analytical modelling aims at establishing a relationship between the characteristics of rock mass (discontinuities, depth and excavation geometries) and permeability. To illustrate this goal, in this section we discuss two approaches: first we describe the classical means of estimating rock mass permeability whereby the geometrical characteristics of the discontinuities are established. Second, we summarize the existing analytical equations for estimating the water inflow rate into tunnels. These estimates depend on the depth, geometry, and water conditions of the underground excavation.

2.5.1 Analytical formulation of hydraulic conductivity

An analytical approach can be used to determine the hydraulic behaviour of a rock mass [25, 32, 57]. The classic formulation for the hydraulic conductivity tensor of the rock mass was developed by Snow [19], Kiraly [58], Oda [20], and later by Zhou et al. [21]. Analytical models have also included the key parameters into their formulations, such as normal stress [59], shear stress [25, 60], and joint set orientation [30, 59].

Darcy's law [61] is one of the fundamental components of the analytical approach:

$$Q = -KA\frac{h_L}{L} \ \ or \ Q = -KA\frac{dh}{dl} \qquad\qquad (2\text{-}7)$$

where Q is the discharge rate (m³/s), K is the hydraulic conductivity (m/s), and *dh/dl* is the hydraulic gradient (m/m). The negative sign is required because fluid flows from high pressure to low pressure. For a 3D fluid flow through a cross-sectional area, Darcy's equation is modified as:

$$\begin{bmatrix} q_{xx} & q_{xy} & q_{xz} \\ q_{yx} & q_{yy} & q_{yz} \\ q_{zx} & q_{zy} & q_{zz} \end{bmatrix} = - \begin{bmatrix} K_{xx} & K_{xy} & K_{xz} \\ K_{yx} & K_{yy} & K_{yz} \\ K_{zx} & K_{zy} & K_{zz} \end{bmatrix} \times \begin{bmatrix} J_x & 0 & 0 \\ 0 & J_y & 0 \\ 0 & 0 & J_z \end{bmatrix} \qquad (2\text{-}8)$$

where q_{ij} is the flow in direction *i* as a result of hydraulic conductivity in direction *j*, K_{ij} is the hydraulic conductivity in the direction *i* as a result of the hydraulic gradient in direction *j*, and J_i is the hydraulic gradient in direction *i*. Analytical methods propose equations for determining each element of the hydraulic conductivity tensor. As the intact rock is regarded as impermeable [62, 63], the fluid passes through the rock mass via discontinuities, and rock mass permeability is governed by fracture permeability defined by cubic law [64, 65]. Most analytical models of hydraulic conductivity of a rock mass are based on Darcy and cubic laws. According to cubic law, in the case of laminar flow and assuming parallel plates instead of fracture walls, hydraulic conductivity of a fracture having an aperture *b* is given by:

$$K_f = \frac{\rho g b^2}{12\mu} \qquad (2\text{-}9)$$

where K_f is the hydraulic conductivity of the fracture, *b* is the fracture aperture, μ is the dynamic viscosity, ρ is fluid density, and *g* is the acceleration of gravity. In one of the first and most important works formulating the hydraulic conductivity of a fractured network, Snow [19] developed a model for a single parallel plate opening that considered an inclined fracture against a hydraulic gradient. Snow then developed a new equation (equation (2-10)) by extending the initial model to sets of parallel plate openings and included a dispersed orientation for the sets and the distribution of apertures (Fig 2-4).
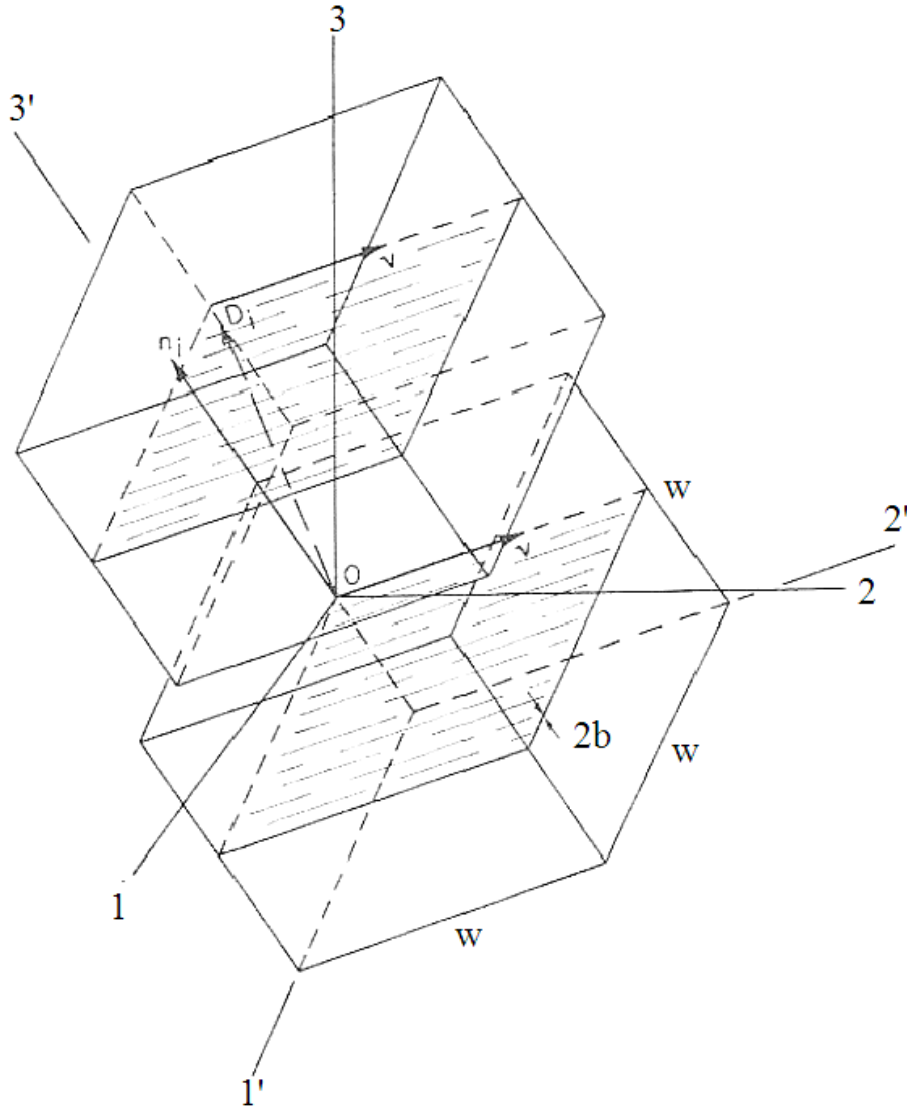
Fig 2-4. A joint conductor having normal n_i and its image, distant D_i, the sampling length [19].

$$k_{ij} = \frac{2}{3} \sum \frac{b^3}{|n_i D_i|} (\delta_{ij} - m_{ij}) \qquad \text{(2-10)}$$

where, according to Fig 2-4, b is the half fracture aperture, n_i is the unit vector in the direction of hydraulic gradient, n_j is normal to discontinuity plane cosines in a 123 system, $m_{ij}=n_i.n_j$, δ_{ij} is the Kronecker delta that vanishes when $i \neq j$ and unity when $i = j$, and D_i is the oblique distance (oblique spacing) between fractures of the ith joint set. In equation (2-10), k_{ij} is the permeability of the rock mass that illustrates the ability of the media to transmit fluid. Permeability is an intrinsic property of the formation, and fluid properties are not included, defined as equation (2-11) [66]:

$$k_{ij} = \frac{K_{ij}\mu}{\rho g} \ (m^2) \qquad\qquad (2\text{-}11)$$

where K_{ij} is hydraulic conductivity. Assuming an impermeable rock matrix, the analysis of geometric fracture patterns provides an estimate of anisotropic permeability tensors. In this model, the effect of joint aperture, spacing and orientation are considered. Using similar assumptions as Snow for deriving the permeability tensor of the rock mass, Kiraly [58] estimated the permeability tensor (k_{ij}) for N joint sets where each set has parallel discontinuities via equation (2-12):

$$k_{ij} = \frac{g}{12\mu}\sum_{i=1}^{N} f_i e_i^3 [M] \qquad\qquad (2\text{-}12)$$

where g is gravity acceleration, μ is kinematic viscosity of water, N is total number of discontinuities sets, f is average frequency of the ith set of discontinuities, e_i is average hydraulic aperture of the ith set of discontinuities [67], and [M] is the conversion matrix that is defined as:

$$[M] = [I] - \{n\}\{n\}^T = \begin{bmatrix} 1-n_1^{\ 2} & -n_1 n_2 & -n_1 n_3 \\ -n_2 n_1 & 1-n_2^{\ 2} & -n_2 n_3 \\ -n_3 n_1 & -n_3 n_2 & 1-n_3^{\ 2} \end{bmatrix} = \left(\delta_{ij} - m_{ij}\right) \qquad\qquad (2\text{-}13)$$

where in equation (2-13), n is the normal vector to discontinuity, and n_1, n_2, n_3 denote the direction cosines of the unit vector normal to the discontinuity in the direction of axes x, y, and z, respectively. In another study, Oda [20] concluded that for deriving the permeability tensor, the crack tensor (P_{ij}), which depends only on the geometry of the related cracks (aperture size and orientation), should be included:

$$P_{ij} = \frac{\pi\rho}{4}\int_0^{\infty}\int_0^{\infty}\int_{\Omega} r^2 t^3\, n_i\, n_j E(n,r,t)\, d\Omega dr dt \qquad\qquad (2\text{-}14)$$

where it is assumed that cracks are disks of diameter r and aperture t, their orientation indicated by its normal vector n that is oriented over the entire solid angle Ω corresponding to the surface of a unit sphere; n_i are components of n projected on the orthogonal reference axes x_i (i = 1, 2, 3), n_j is the unit vector in the direction of the hydraulic gradient, $E(n,r,t)$ is probability density function for (n,r,t) cracks (where $\int_0^{\infty}\int_0^{\infty}\int_{\Omega} E(n,r,t)\, d\Omega dr dt = 1$), ρ is the density of the crack centres, and P_{ij} is the crack tensor. Crack tensor is a symmetric, second-rank tensor related only to crack geometry, i.e., to the crack shape, size,

aperture, and orientation, and its value is obtained by statistically treating the crack orientation data−presented via a stereographic projection, together with the detailed mapping of crack traces visible on rock exposures.

By defining crack tensor, Oda [20] defined the permeability tensor as:

$$k_{ij} = \lambda \left(P_{kk} \delta_{ij} - P_{ij} \right) \qquad (2\text{-}15)$$

where λ is the dimensionless scalar adopted to penalize the permeability of real fractures with roughness and asperities, P_{kk} is mean permeability ($P_{kk} = P_{11} + P_{22} + P_{33}$), while the deviatory part P_{ij} is the anisotropic permeability.

Analytical approaches also incorporate the influence of fracture stress and connectivity on rock mass permeability [21, 59]. Zhou et al. [21] developed an analytical equation using the concept of energy dissipation through fractures by assuming each fracture as the jth discontinuity of an ith set that is a disc of radius r_{ij}. Their estimate of the permeability tensor (equation (2-16)) uses the correlation between energy dissipation, hydraulic conductivity, and joint interconnection to provide a more comprehensive formulation.

$$[\bar{K}] = [\bar{K}]_r + \frac{g\pi}{12\mu V_P} \sum_{i=1}^{n} \sum_{j=1}^{m_i} W_{ij} f^3(\beta_{ij}) r_{ij}^2 b_{0ij}^3 [M]_{ij} \qquad (2\text{-}16)$$

where $[\bar{K}]$ is the permeability tensor for the fractured rock mass, $[\bar{K}]_r$ denotes the permeability tensor for the rock matrix, V_p is the rock mass volume, $W_{ij} = \xi_{ij}/\bar{\xi}_i$ (ξ_{ij} is a stochastic variable denoting the number of discontinuities intersected by the jth discontinuity belonging to the ith set, and ξ_i denotes the maximum number of discontinuities cut by the ith set of discontinuities that demonstrate the influence of the interconnectivity of the joint sets. $f(\beta)$ is a function used to demonstrate the coupling effect between the fracture aperture and deformation, b_0 is initial aperture, and $[M]$ is the conversion matrix as defined in equation (2-13). This approach thus considers the impact of the interconnection, hydraulic aperture, and stress—both shear and normal stresses—on the permeability tensor of the rock mass.

Zoorabadi et al. [68] also consider the impact of the interconnectivity of the joint sets on the permeability tensor by using the influence of the interconnectivity coefficient (C_i) [69, 70] on the apparent

flow velocity. They developed an analytical formulation for permeability in an objective volume of radius R around the tunnel of radius r. In the case of $r = 0$ and $C_i = 1$, their equation reduces to the Snow model (equation (2-10)).

Shear stress increases the permeability of the rock mass. The occurrence of this effect in a rock mass, known as dilation and first published by Reynolds [71], can modify fracture aperture and thus alter the hydrological behavior of the discontinuity network [72-77]. The mechanism of fracture aperture opening during dilation is schematically illustrated in Fig 2-5.

$a_s = U_s tan(\varphi_{dil})$,
U_s = shear displacement
a_s = stimulated aperture
a_0 = initial aperture
φ_{dil} = dilation angle
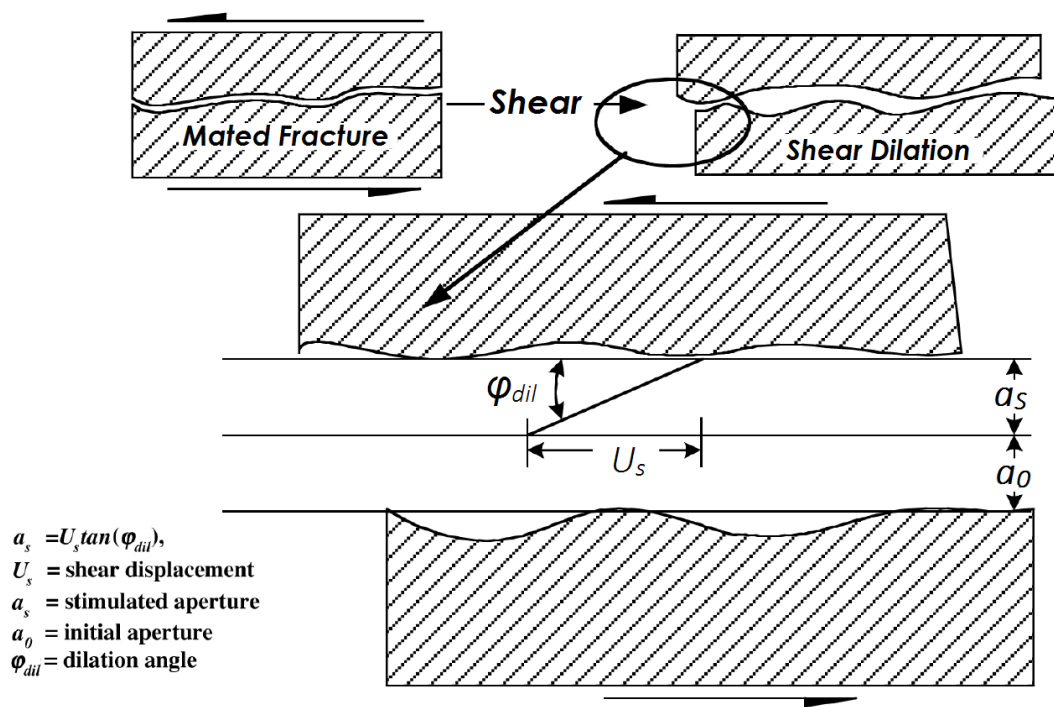
Fig 2-5. Increase of fracture aperture by shear dilation [78]

Through dilation, the hydraulic conductivity of the fracture increases [25, 60] due to the increase of the fracture aperture. However, estimating shear dilation in a rock mass is also possible by applying a defined level of horizontal-to-vertical normal stresses ratio [25] (based on Mohr–Coulomb criteria [79], as increasing the ratio of normal stress heightens the resulting shear stress).

To evaluate the effect of joint orientation on the permeability of a rock mass, Bear [56] demonstrated that permeability k'_{pq} in an x'_p system can be measured by knowing the permeability components k_{ij} in an x_i coordinate system. The components are obtained by:

$$k'_{pq} = k_{ij}\, \alpha_{pi}\, \alpha_{qj} \qquad\qquad (2\text{-}17)$$

where α_{mn} is the direction cosine between axes x'_m and x_n (m and n could be p/q and i/j respectively). Thus, by defining the hydraulic conductivity in the direction of the fracture surface, permeability in other directions is defined by equation (2-17). Multiple authors have performed analytical studies of directional hydraulic conductivity and the effect of joint set orientation [30, 59].

If we suppose that the hydraulic conductivity of a fracture i having an aperture b is equal to K_i, then according to equation (2-17), the hydraulic conductivity in a direction that has an angle α in the direction of the fracture is equal to $K_i\, cos^2\alpha$. Given the aperture and spacing of the joint set, equation (2-17) reduces to:

$$K_N = \sum_{i=1}^{n} \frac{b_i}{s_i}\, K_i\, \cos^2 \alpha_i \qquad\qquad (2\text{-}18)$$

where K_N is the hydraulic conductivity in the direction of N, K_i is the hydraulic conductivity of the ith joint set and is defined by cubic law, b is the aperture, s is the spacing, and α_i is the angle between direction N and the ith joint set. As a derivation of equation (2-18), for a formation that is hydraulically conductive only in direction x ($K_{yy} = K_{zz} = K_{xy} = K_{xz} = K_{yz} = 0$), the hydraulic conductivity in any other direction (Fig 2-6a) is given by:

$$K_d = K_{xx}\, \cos^2 \alpha \qquad\qquad (2\text{-}19)$$

where α is the rotation angle. Accordingly, for a network having three sets of fractures of variable orientation, fixed aperture, and spacing (Fig 2-6b), equation (2-17) reduces to [59]:

$$\frac{K_N}{K_1} = \cos^2 \alpha_1 + \cos^2(\theta_1 - \alpha_1) + \cos^2(\theta_2 - \alpha_1) \qquad\qquad (2\text{-}20)$$

where α_1 is the angle between the selected direction N and the first (horizontal) set, θ_1 and θ_2 are the angles between the joint sets, K_N is hydraulic conductivity in the direction of N, and K_1 is the hydraulic conductivity in each joint set.
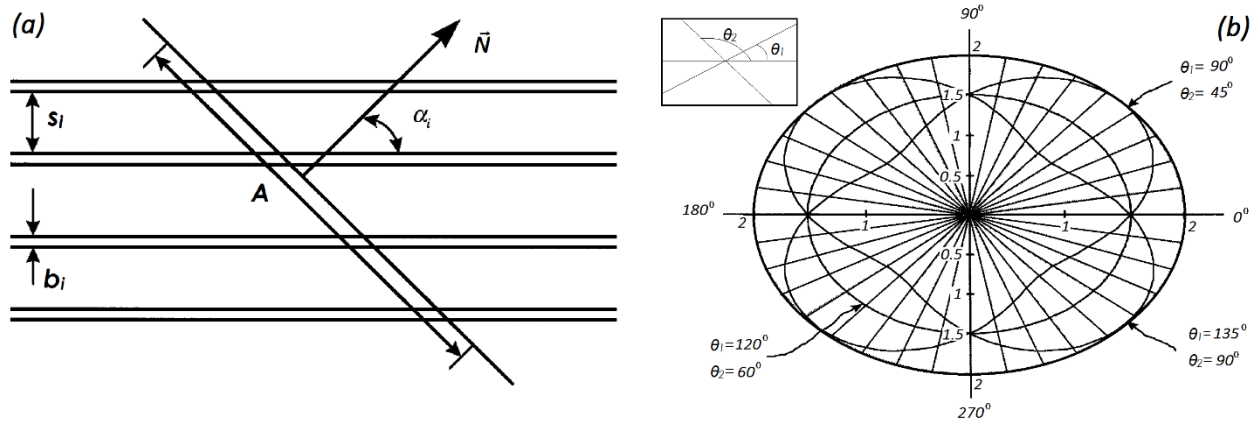
Fig 2-6. (a) Hydraulic conductivity in direction N in a joint set (b) Variation of directional hydraulic conductivity in the presence of three joint sets [59]

In this section, the developed equations and models to determine the permeability of a rock mass incorporate the characteristics of rock mass discontinuities, e.g., aperture, orientation, spacing. Analytical equations and models present some limitations in terms of their application. For example, the permeability of the rock matrix is rarely included in the development of the equations. Not all parameters affecting rock mass permeability are considered by the analytical models, such as joint infillings, joint persistence or joint termination. Analytical models are developed for deterministic conditions but do not take into account any uncertainties in the value of each parameters. Future research could focus on improving the accuracy of analytical methods by considering a greater number of parameters that affect rock permeability. Despite these limitations, analytical solutions can be very useful because they allow a first good approximation to predict the permeability of rock mass. Indeed, such solutions are useful in direct applications or in the validation and verification of numerical models, keeping in mind the assumptions they involve. Analytical approaches can be preferred by practitioners because of the relatively low investments required (time and money) compared to numerical approaches. Furthermore, the uncertainties inherent in the field of hydrogeology can affect the results and consequently do not necessarily make numerical approaches more accurate than analytical approaches.

In the following section, we list the types of analytically developed models for evaluating the fluid inflow rate into underground tunnels. In contrast with the analytical approaches mentioned previously, these next equations assume a homogenous and isotropic rock mass having a constant value for hydraulic conductivity, and discontinuity characteristics are not considered.

2.5.2 Inflow rate into underground excavations

Proper evaluation of water seepage into tunnels excavated below the water table within a rock mass is essential for designing tunnel drainage systems and reducing the risk of rock failure in these tunnels. As well, drainage into underground excavations can have an environmental impact by altering the groundwater regime and causing the settling of surface structures [80]. Seepage decreases rock mass stability around a tunnel, adding pressure on temporary and permanent support systems and decreasing the excavation rate [81]. The importance of inflow into underground excavations has led to multiple analytical studies focused on predicting flow rates into these underground spaces; however, comparing the various studies is difficult as each relies on specific and differing notations, boundary conditions, ground disturbance levels around excavation sites, and potential solutions. Nonetheless, all these analytical formulations rely on the Laplace equation under a 2D steady-state condition assuming different boundary conditions for the ground surface and the tunnel circumference.

Polubarinova and Kochina [82] undertook one of earliest and most comprehensive analytical studies (Table 2-5) of steady flow into a horizontal tunnel within a fully saturated, semi-infinite homogeneous formation. Thereafter, Goodman et al. [17] reviewed the equation of Polubarinova and Kochina and presented solutions for cases of transient flow. As Goodman et al.'s equation greatly overestimated the predicted inflow relative to the actual inflow [81, 83], Heuer [83] added a coefficient to Goodman's equation that decreased estimates to 1/8 of the initial estimate; Heuer also published a new method for estimating tunnel inflow rate using a Lugeon test (Fig 2-7).
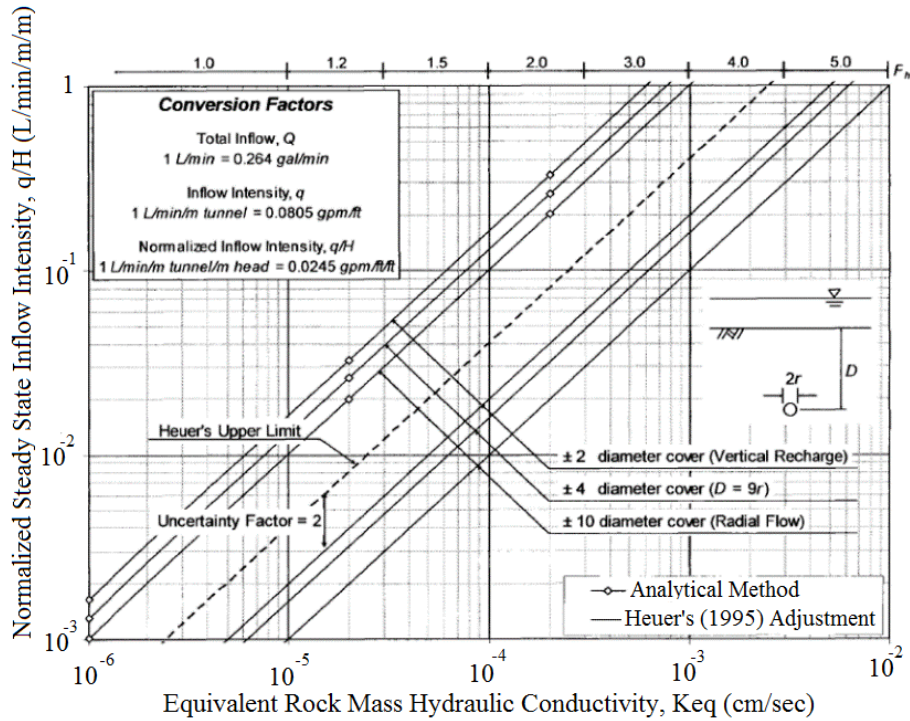
Fig 2-7. The Heuer abacus empirical method for estimating tunnel inflow rate with the Lugeon test [83]

Later, El Tani [5, 84] published equations for square sections, elliptical sections, pairs of identical circular tunnels, and circular section tunnels within an anisotropic aquifer. Karlsrud [80] evaluated water seepage into tunnels under urban areas (soft clay deposits) to back-calculate permeability and predict the settlement of the building structures. Most recently, Kolymbas and Wagner [85] and Park et al. [18] developed more accurate equations for tunnels having a circular cross-section in a soil or rocks having differing boundary conditions (Fig 2-8).
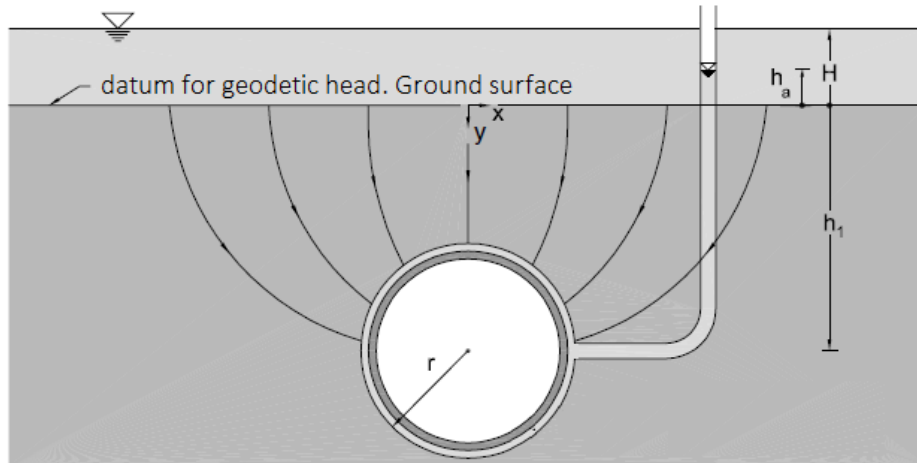
Fig 2-8. The Kolymbas and Wagner [85] model for deriving an analytical equation for a circular cross-section tunnel

Analytical formulas for predicting water seepage into underground joined tunnels are generally valid for homogeneous and isotropic formations [81]; nonetheless, they tend to overestimate the tunnel inflow rate, especially in discontinuous rock masses. Hydraulic conductivity is also assumed to be constant throughout the formation even though the actual permeability varies greatly in the damage zone around a tunnel [43, 86] due to variations in stress patterns [87, 88]. Tunnels are usually considered as having a circular cross-section, but in actual excavation spaces, the cross-section deviates from this assumed circular shape. Tunnel geometry that differs from the assumptions coupled with variable environmental situations likely alter the amount of estimated seepage [81]. Finally, the assumption of a constant hydraulic head above the tunnel is rarely observed in actual settings as the underground water levels vary over time. Overall, the assumptions of analytical formulas related to the rock mass formation, boundary conditions, and tunnel geometry limit the real-world applicability of tunnel inflow rates calculated using the analytical method.

Table 2-5. Existing equations for estimating water seepage into underground joined tunnels per unit length of tunnel

Equation	Reference	Parameters	Assumptions
$Q = 2\pi K \dfrac{h}{\ln\left(\frac{2h}{r}\right)}$	Muskat and Meres [16]	K, hydraulic conductivity of homogeneous and isotropic rock mass; h, water head above the tunnel; r, tunnel radius.	Steady-state inflow along tunnel length; Saturated, homogeneous, and isotropic formations.

34

Equation	Reference	Variables	Conditions
$Q = \dfrac{2\pi K(d - \varphi_0)}{\ln\left(\dfrac{2D}{r}\right)}$	Polubarinova and Kochina [82]	K, hydraulic conductivity; r, tunnel's radius; D, depth of the tunnel centreline; φ_0, hydraulic head at the tunnel perimeter; d, aboveground water depth.	Fully saturated, semi-infinite homogeneous media. For $D \gg r$.
$Q = \dfrac{2\pi K h}{\ln\left(\dfrac{2D}{r}\right)}$	Goodman et al. [17]	K, hydraulic conductivity of homogeneous and isotropic rock mass; h, water head above the tunnel; D, depth of the tunnel; r, tunnel radius.	Steady-state inflow along tunnel length; Saturated, homogeneous, and isotropic formations; Applicable to deep tunnels ($L \approx D$).
$Q = \dfrac{2\pi K(d + P_a - \varphi)}{\ln\left[\dfrac{D}{r} + \sqrt{\left(\dfrac{D}{r}\right)^2 - 1}\right]}$	Lei [57]	K, hydraulic conductivity; r, tunnel radius; D, depth of the tunnel centreline; d, aboveground water depth; φ, hydraulic head; P_a, atmospheric pressure head	Fully saturated, homogeneous, isotropic, and semi-infinite aquifers; Constant total head along the tunnel circumference; Deep tunnels.
$Q = 2\pi K h \dfrac{1 - 3\left(\dfrac{r}{2h}\right)^2}{\left[1 - \left(\dfrac{r}{2h}\right)^2\right]\ln\dfrac{2h}{r} - \left(\dfrac{r}{2h}\right)^2}$	El Tani [5]	K, hydraulic conductivity; r, tunnel radius; h, tunnel depth below the water table.	Water level as the elevation reference datum; Constant total head (ha) along the tunnel circumference; Semi-infinite isotropic and homogeneous aquifers drained by a circular tunnel.
$Q = 2\pi k \dfrac{h}{\ln\left(\dfrac{2h}{r} - 1\right)}$	Karlsrud [80]	k, permeability of homogeneous and isotropic rock mass; h, tunnel depth below the water table; r, equivalent tunnel radius.	Homogenous media having constant permeability in all directions; Tunnel is deeply embedded ($h/r \geq$ 3–4); Groundwater table is not influenced by the leakage.
$Q = \dfrac{2\pi K(H - h_a)}{\log\dfrac{r}{h_1 - \sqrt{h_1^2 - r^2}}}$	Kolymbas and Wagner [85]	K, hydraulic conductivity of homogeneous and isotropic rock mass; r, tunnel radius; H, water depth at the upper boundary; h_1, tunnel depth from the reference datum; h_a, total head at the tunnel circumference.	For deep and shallow tunnels; Ground surface as the elevation reference datum; Variable water heads at the tunnel circumference and ground surface; Homogeneous and isotropic permeability; Steady flow.
$Q = K\dfrac{2\pi}{\ln\left(\dfrac{h}{r} + \sqrt{\dfrac{h^2}{r^2} - 1}\right)}(A + H)$	Park et al. [18]	h, tunnel depth; r, tunnel radius; K, hydraulic conductivity;	Ground surface is used as the elevation reference datum; Water table is above the

		H, water depth at the upper boundary. $A = h\dfrac{(1 - \alpha^2)}{(1 + \alpha^2)}$ $\alpha = \dfrac{1}{r}\left[h - \sqrt{h^2 - r^2}\right]$	ground surface ($H = 0$, and h is groundwater depth for the water table below the ground surface); Steady-state groundwater inflow into a drained circular tunnel.

2.6 NUMERICAL MODELLING

Numerical models for assessing permeability aim to evaluate the quantity of fluid flowing through a rock mass. A rock body can be considered as permeable [89, 90] or impermeable [91, 92]. These numerical models can include the characteristics of discontinuities [93], their correlation [94, 95], and their distribution [96, 97] to reduce error. These characteristics include discontinuity size [98-100], spacing [101], aperture [102, 103], location [104], and orientation [105].

Numerous studies use a numerical method to evaluate the permeability of a rock mass [106-108]. Table 2-6 summarizes the numerical techniques that are frequently used for studying the hydro-geomechanical behaviour of the rock mass.

Table 2-6. Numerical techniques used for studying the hydro-geomechanical behavior of the rock mass depending on the characteristics of the developed numerical models

Type of model	Numerical technique	Model characteristics	References
Continuum/extended-continuum models	Finite element method (FEM)	The rock mass is considered as a continuous body, the overall characteristics of the rock body and the properties of discontinuities are defined in the continuum model	Rutqvist et al. [109] Oda et al. [110] Kobayashi et al. [111] Gan and Elsworth [112] [113]
	Finite difference method (FDM)		
Block system discontinuum models	Distinct element method (DEM)	The rock mass is composed of discrete elements and discontinuities are their boundaries	Zhang and Sanderson [114] Lin and Lee [30] Fernandez and Moon [24] Rouainia et al [115]
	Discontinuous deformation analysis (DDA)	DEM is based on an explicit time-marching scheme, while DDA is based on an implicit time-marching scheme	
Particle-based discontinuum models	Particle flow method (PFM)	The movement of particles and blocks is defined by solving Newton's second law through an explicit time-marching scheme	[116] Kozicki and Donze [117] [118]
Hybrid finite-discrete element models (FDEM or FEMDEM) (Discontinuous)	Hybrid finite-discrete element method (FEMDEM)	The FEM solver calculates inter-block stress-strain, while intra-blocks interaction are analysed by the DEM method.	[119] Munjiza [120]

A large variety of commercial codes make it possible to build numerical models based on the numerical techniques exposed in Table 2-6, such as UDEC, 3DEC, Hydrogeosphere and Comsol, to name a few. Other than the numerical methods described in Table 2-6, the most frequently applied model is the Universal Distinct Element Code (UDEC) [121] that provides a 2D evaluation of permeability and allows for extrapolating the results into 3D [122, 123]. UDEC considers rock as a series of impermeable blocks separated by discontinuities (faults, joints, etc.). It can reproduce fully coupled hydromechanical behaviours and satisfy the conservation of momentum and energy in its dynamic simulations. Fluid flow calculations are derived from Darcy's law. Computations using codes such as UDEC are limited by their practical application restricted to either detailed small-scale (<50 m) studies, 2D fracture networks [124, 125], or stochastic representations of larger-scale models [126]. UDEC can be used to simulate stress effects on hydraulic conductivity [33, 114], to evaluate seepage from dams [3] and around tunnels [24, 30], and to

define the REV (Representative elementary volume) of a rock mass formation [22, 25]. New codes such as FLAC are also currently being applied to calculate the groundwater inflow into underground excavations [127] and to simulate hydro-geomechanical behaviour of the rock mass [113, 128].

Generally, the numerical simulation of the hydromechanical behaviour of a rock mass follows four main steps [36]:

1) Modelling elastic/elastoplastic response of the rock mass to stress;

2) Evaluating the nonlinear response of fractures to stress;

3) Determining expected fracture propagation under stress;

4) Coupling the geomechanical model to hydrological solvers.

Nine parameters may significantly affect DFN permeability: fracture length distribution, aperture distribution, fracture surface roughness, fracture dead-end (connectivity), number of intersections, hydraulic gradient, boundary stress, anisotropy, and scale [100]. Stress is the most frequently considered parameter when studying the hydromechanical behaviour of a rock mass, as in-depth permeability needs to be established and in situ stress increases with depth [23, 30, 31]. Studies considering stress may be divided into two categories. The first assumes that only normal stress exists [25, 31, 32], whereas the second considers both shear stress and normal stress [25, 33]. In both cases, pore pressure and its influence on the effective stress must be taken into account [129].

In addition to numerical experiments, laboratory investigations of single rock fractures have shown that the normal closure and shear dilation [130], as well as fracture infillings and effective flow area [21], can markedly alter fracture permeability. Thermal stress impacts on permeability may also being included in researches. Takatoshi et al. [107] concluded that cooling provokes a shrinkage of the rock that leads to the opening of fracture apertures and, thus, an increase in permeability.

Numerical modelling of a sensitivity analysis of the effect of normal stress illustrates that as normal stress increases, the flow rate (permeability) decreases (Fig 2-9).
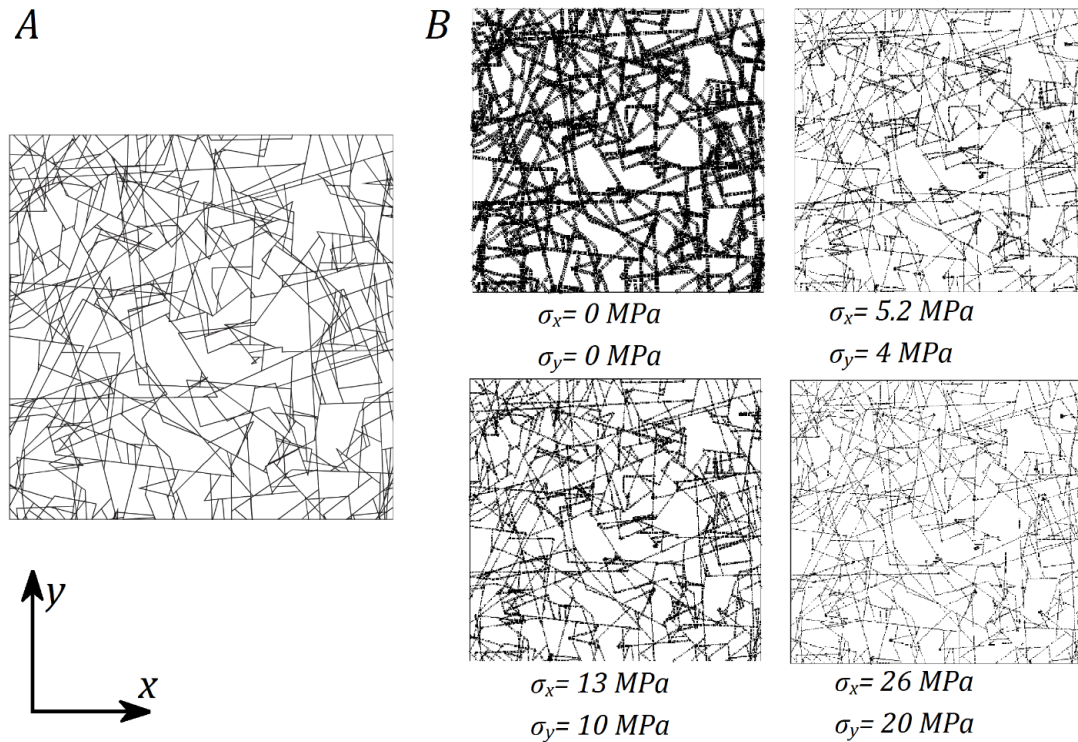
Fig 2-9. (A) Geometry of initial fractures in a DFN model of UDEC simulation and (B) change of flow rate with increasing stress for a fixed k = σ$_v$/σ$_h$ ratio of 1.3. Line thickness indicates the magnitude of flow [25]

This effect has been validated analytically via equation (2-16). As opposed to numerical and analytical validation and following cubic law, an increase in normal stress will decrease joint aperture and, as a result, decrease overall hydraulic conductivity. By combining shear and normal stress, shear dilation (Fig 2-5) modifies the mechanical aperture and alters permeability. During shear processes, a three-stage evolution of hydraulic aperture/permeability takes place [131]: (1) a declining stage due to less dilation (contraction) of fractures; (2) a fast-growth stage, during which the hydraulic aperture increases almost linearly with the shear-induced dilation; and (3) a gentle-growth stage, where the hydraulic aperture continues to increase but at a much slower and decreasing rate. This effect is studied further numerically by modelling the presence of shear and normal stresses. However, as a rock mass represents a pattern of populated discontinuities, it is impossible in physical experimentation to define specific shear stress values for each fracture. The approach is therefore to apply an incremental normal stresses ratio (σ_x/σ_y) until shear dilation

initiates (Fig 2-10) [25, 26]. Use of the normal stresses ratio does not always initiate dilation; in simple models having orthogonal sets of fractures, dilation occurs solely by applying shear stress in the presence of the orthogonal normal stress. A combination of fracture dilation and larger fractures−having higher aperture values−that remained open after applying normal stresses, increases the permeability of the overall fracture network in the particular direction defined by the shear stress component [33, 34].
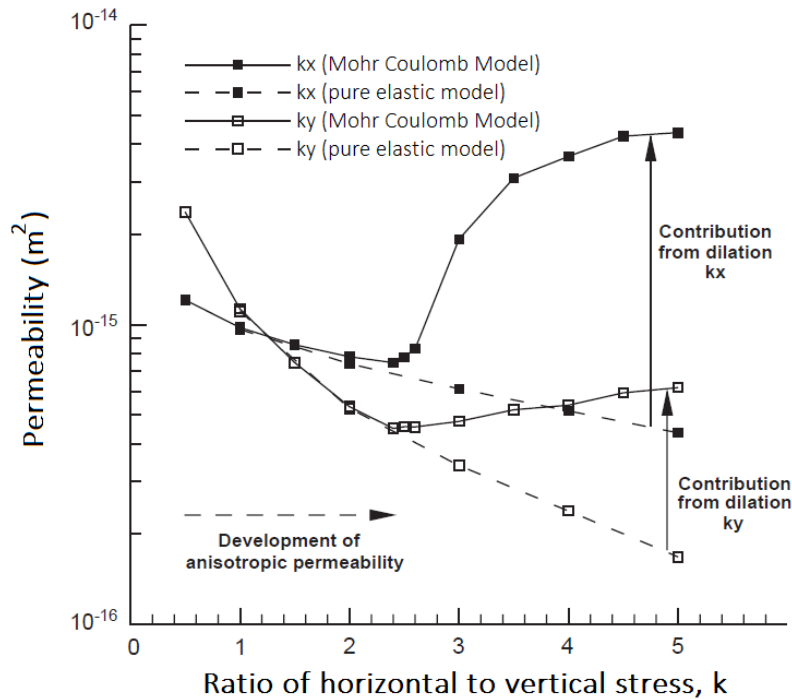
Fig 2-10. The effect of dilation as a result of incremental normal stress on permeability [25]

In Fig 2-10, the dilation begins at a horizontal (σ_x) to vertical (σ_y) stress ratio of approximately 2.5. Beyond this ratio, the contribution of dilation in the *x*-direction is higher than in the *y*-direction; this is due to the impact of the direction of the higher stress value and shows that in such cases most change in permeability occurs in the direction of the highest stress value. For drawing k_x, both the upper and lower boundaries of the model are assumed to be impermeable for k_y. Application of the orthogonal normal stresses to DFN could also alter the direction of the maximum and minimum permeability [27]. The direction of maximum permeability of the DFN tends to be oriented parallel to the direction of maximum stress (Fig 2-11).
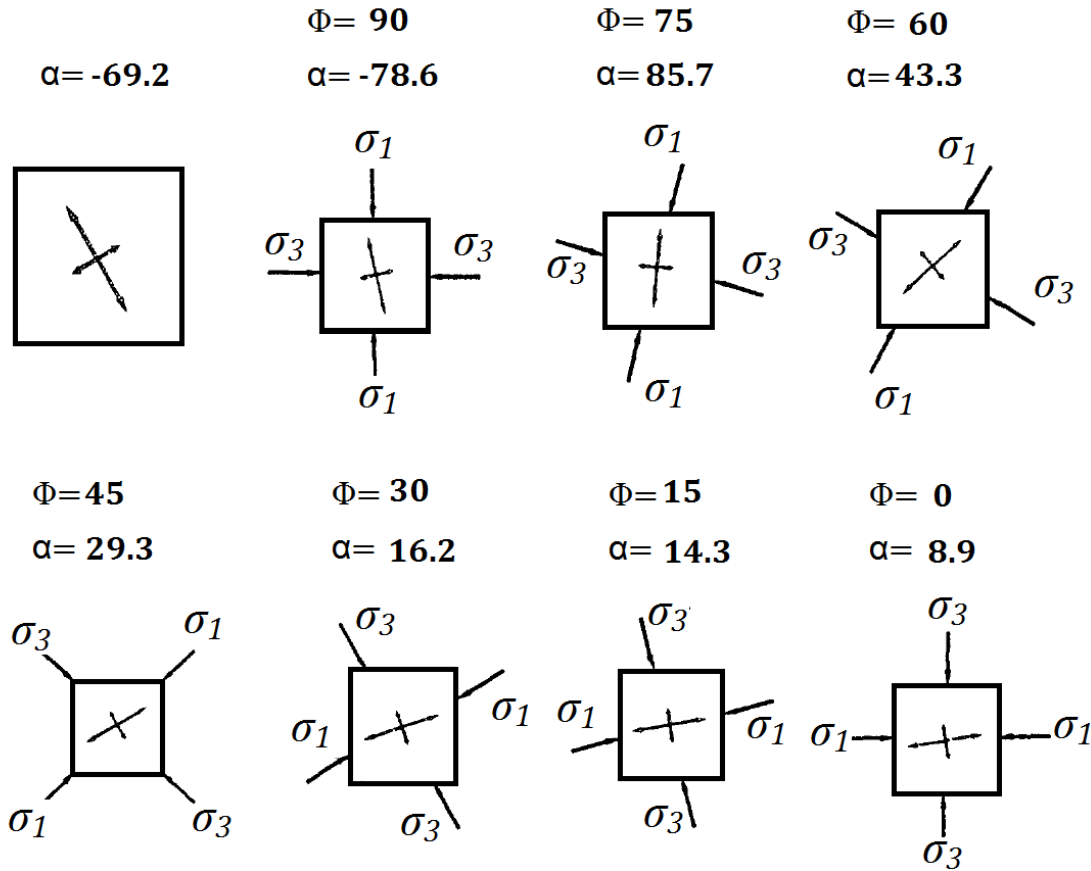
Fig 2-11. The direction of the major principal component of permeability corresponds approximately to the direction of the major stress [27]

In addition to the abovementioned effects, when applying and increasing stress, there is an increased tendency for brittle failure and crack propagation (mostly in hydraulically inactive fractures), and the permeability of fractured rocks becomes markedly higher [108, 132, 133] as new fractures are produced and generate a greater number of interconnections.

After resolving the existing analytical models to evaluate the inflow rate into underground excavations (Section 2.5.2) and to ensure more precise evaluations, numerical models are used to estimate the inflow rate of groundwater into underground excavations and evaluate how this rate varies with depth. Fig 2-12a presents a numerical model for an underground tunnel, and Fig 2-12b provides the results of simulation for the effect of depth on the hydrological behaviour of the rock mass. The field data show reasonable consistency with the numerical model output and identify the overall decrease of inflow rate with increased depth. Both field data and UDEC results show a moderate variation of water flow with depth in the first

50 m, and this variation decreases rapidly at depths beyond 50 m. In contrast to Fig 2-1, Fig 2-12b is not consistent with the empirical results of the variation of permeability with depth, which shows a rapid change of the permeability at shallower depths followed by a declining rate of change for permeability with increasing depth.
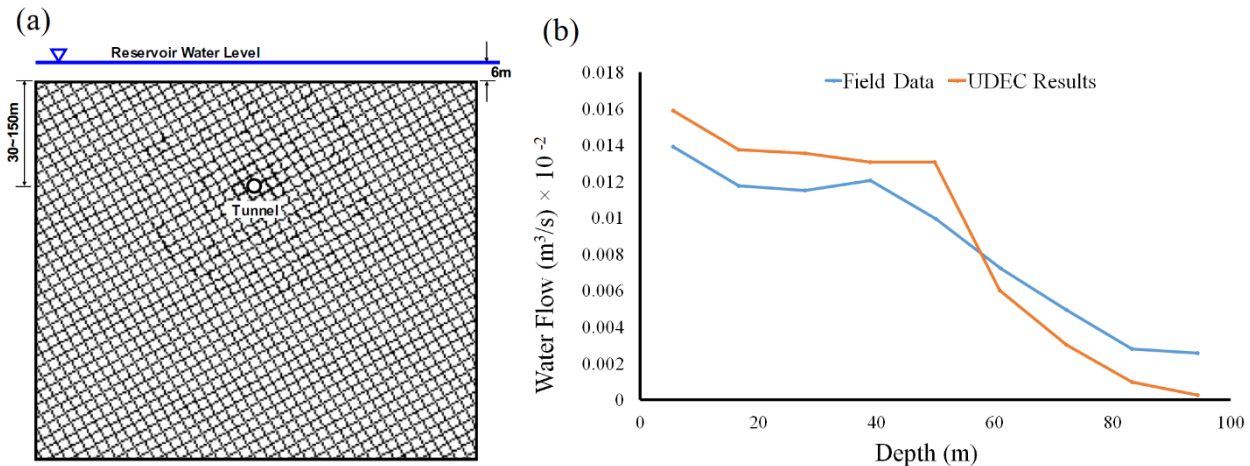
Fig 2-12. (a) Numerical model of a tunnel [24]; (b) Results of in situ data and UDEC results for tunnel inflow rate [23]

As evidenced in the above figures, depth is one of the most important parameters for evaluating underground excavations given its importance for estimating the permeability of a rock mass and inflow rates into the underground excavations; hence, depth is often considered in numerical studies [22, 23, 30].

The presence of a lining-like zone around an underground excavation can be detected using numerical models [24]. This zone is less permeable relative to other zones along the excavation walls and could restrict water inflow into the excavated space. This zone can expand by increasing the geometry of the underground excavation [24]. Despite some studies showing the decreased permeability within these lining-like zones [24], others demonstrate that permeability increases in a tangential direction and decreases in a radial direction from the tunnel [30, 43, 59] Permeability also increases in this lining-like zone [4]. Generally, numerical and analytical modelling as well as the empirical formulations of the variability of permeability with depth produce very similar trends, whereas a nonlinear relationship between normal stress and fracture closure shows that permeability is more sensitive to stress at shallower depths [25, 134],

as illustrated in Fig 2-1. Permeability is more sensitive to depth in a rock mass having larger joint spacing [30] because of the lack of available stress concentration zones.

Based on cubic law, among all parameters, joint aperture has the greatest impact on the hydrological behaviour of a rock mass, because it influences fracture permeability and flow rate. Joint aperture is very often included in studies, and the results of numerical models are consistent with in situ and analytical formulations regarding its impact on permeability [22, 23, 30].
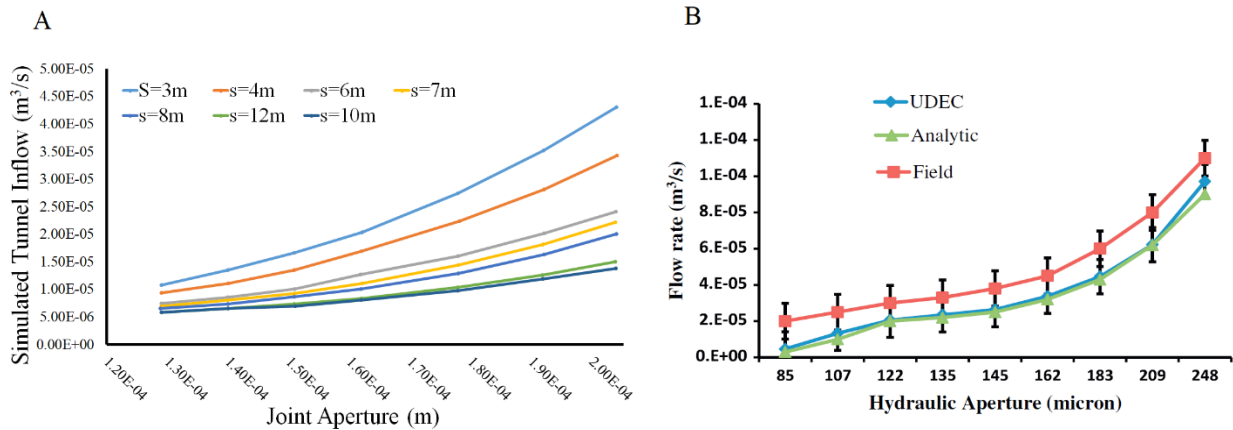
Fig 2-13. (A) Relationship between tunnel inflow rate and joint aperture [22]. (B) Validation of the numerical and analytical methods using in situ data [23]

As illustrated in Fig 2-13A and B, flow rate (permeability) increases with an increased mechanical (Fig 2-13A) or hydraulic (Fig 2-13B) aperture. The mechanical aperture is the physical measurement of the joint aperture, and the hydraulic aperture is the effective aperture under ideal conditions. Joint physical characteristics include roughness, tortuosity, irregularity, and other flow-inhibiting parameters that cause the hydraulic aperture to be smaller than the mechanical aperture. As hydraulic aperture is one of the input data for numerical models and mechanical aperture is the only aperture measurable by physical surveying, finding a correlation between mechanical and hydraulic apertures has been the focus of multiple studies (Table 2-7).

Table 2-7. Relationship between hydraulic (b) and mechanical (b) apertures*

Reference	Equation	Remarks
Lomize [135]	$b^* = b\left[1 + 6\left(\dfrac{e}{b}\right)^{1.5}\right]^{-1/3}$	e, absolute asperity height
Louis [136]	$b^* = b\left[1 + 8.8\left(\dfrac{e_m}{D_H}\right)^{1.5}\right]^{-1/3}$	e_m, the average asperity height; D_H, the hydraulic radius
Patir and Cheng [137]	$b^* = b\left(1 - 0.9\exp\left(-\dfrac{0.56}{C_v}\right)\right)^{1/3}$	C_v, variation coefficient of the mechanical aperture
Barton et al. [67]	$b^* = b^2 JRC^{-2.5}$	JRC, joint roughness coefficient
Olsson and Barton [130]	$b^* = \dfrac{b^2}{JRC_0{}^{2.5}}$ for $u_s \leq 0.75u_{sp}$ $b^* = \sqrt{b}\,JRC_{mob}$ for $u_s \geq u_{sp}$	JRC_0, the initial value of JRC; JRC_{mob}, the mobilized JRC; u_s, the shear displacement; u_{sp} the peak shear displacement
Walsh [138]	$b^{*3} = b^3\dfrac{1+C}{1-C}$	C, constant
Hakami [139]	$b^{*2} = \dfrac{b^2}{C}$	$1.1 \leq C \leq 1.7$ and for $100 \leq b \leq 500$ μm
Renshaw [140]	$b^* = b\left(1 + \dfrac{\sigma_b^2}{b^2}\right)^{-\frac{1}{2}}$	σ_b, the standard deviation of the mechanical aperture
Rasouli and Hoseinian [141]	$b^* = b\left(1 - 2.25\dfrac{\sigma_b}{b}\right)^{\frac{1}{3}}$	σ_b, the standard deviation of the mechanical aperture
Xie et al [142]	$b^{*3} = b^3\left(0.94 - 5.0\dfrac{\sigma_{bs}^2}{b^2}\right)$	σ_{bs}, the standard deviation of b during shear

Sensitivity analysis shows that aperture increases until the flow changes from a linear [61] to a nonlinear regime [143]. Beyond this point, Darcy's law is no longer applicable [124]. As the fracture aperture varies only in the presence of stress, and since the correlation between fracture aperture and normal stress is nonlinear, the larger the initial fracture aperture, the greater the variation in hydraulic conductivity stemming from the application of stress [30].

Baghbanan and Olson [28, 144] studied the effect of fracture length on permeability. Longer fractures are likely to be more conductive even though they may be fewer in number than shorter fractures [145], as they have a larger aperture. With the increment of fracture length and density, both the connectivity and permeability of fracture networks increase [146]. In the case of correlation between fracture length and aperture, the overall permeability is greater than the situation where no correlations exist [28].

The influence of joint spacing on the permeability and flow rate of the rock mass has also been assessed. Analytical methods and various numerical models [22-24] have been applied to studies of the

effect of joint spacing on the flow rate and permeability of underground excavations. Joint frequency, which is inversely related to joint spacing, is also considered in numerical models. With increased joint spacing (decreasing joint frequency), flow rate/permeability would decrease, as illustrated in Fig 2-14.
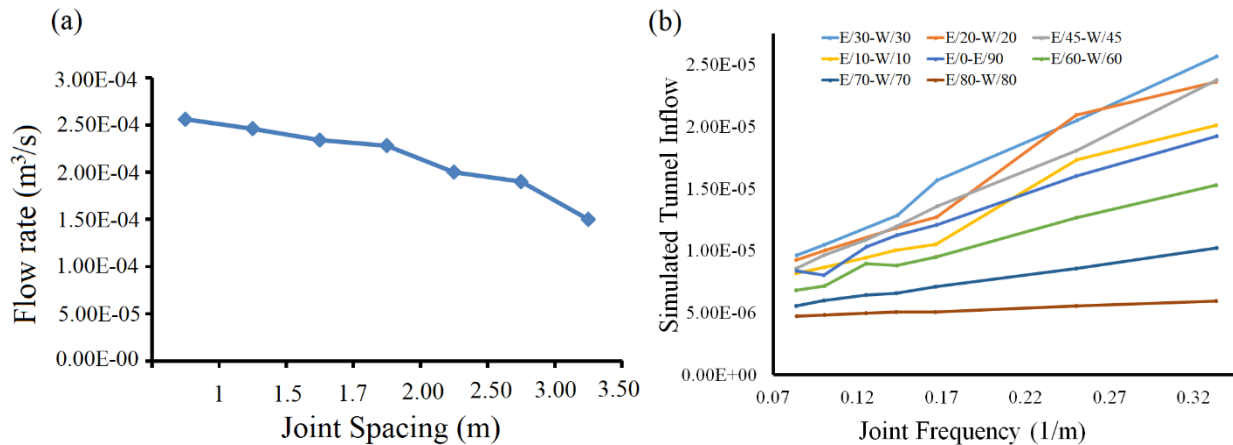
Fig 2-14. Increase of flow rate as a result of (a) a decrease in joint spacing [23] and (b) an increase in joint frequency [22] for a constant joint aperture

Furthermore, Fernandez et al. and Lin et al. [24, 30] point out that at higher values of joint spacing and in the presence of the stress, the reduction in stress concentration centres causes the effective normal stress to increase and therefore results in permeability decreasing more rapidly than in the lower joint spacing.

Numerical models are often used to study the effect of the joint set orientation on permeability and flow rate. Joint set orientation is defined by in situ surveys via DIP. The effect of joint set orientation on the hydrological behaviour of the rock mass can be assessed by analytical models (equations (2-10), (2-12), (2-14) and (2-16); however in the case of inflow rate, numerical models (Fig 2-15a) do not show an obvious trend for a variation of flow rate with joint orientation [127]. As most numerical models consider the presence of two or more joint sets (Fig 2-15b), the effect of the interconnection interferes with flow direction and disorganizes the initial flow and permeability direction [22, 30, 31].
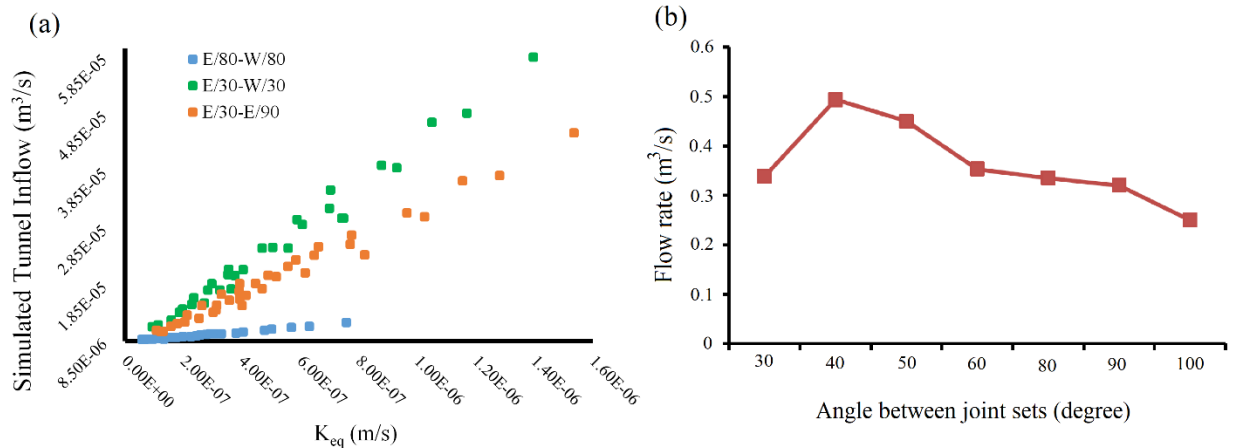
Fig 2-15. (a) Flow rate at different joint set orientations [22]. (b) The effect of the angle between joint sets on flow rate [23]

Furthermore, in the presence of the stress, the orientation of the joint plays a key role in establishing the direction of permeability. Barton et al. [147] illustrate that horizontal preferential flow occurs along fractures that are oriented orthogonal to the minimum principal stress direction or inclined around 30° to the maximum principal stress direction. Generally, fractures that are either perpendicular to normal stress or parallel to shear stress are oriented in the most sensitive directions for affecting permeability. The fracture aperture decreases with perpendicular normal stress [31] and increases with parallel shear stress [25]. As a result, flow channels tend to align along the direction of maximum principal stress [114]. Without this stress, the orientation of the joint set is the main determinant of the direction of maximum permeability. Furthermore, if the angle between joint sets is very small, total permeability is rather small due to the low connectivity ratio of the fractured rock [27].

The physical and mechanical properties of the joints are parameters that also affect fluid flow in a rock mass [31, 60, 148]. Although some authors [149, 150] argue that the influence of joint normal stiffness on the permeability of the rock mass is negligible, analytical [32] and numerical [24] approaches demonstrate that fracture compressibility controls the variation of the permeability of the fracture network when stress is applied, as illustrated in Fig 2-16a.
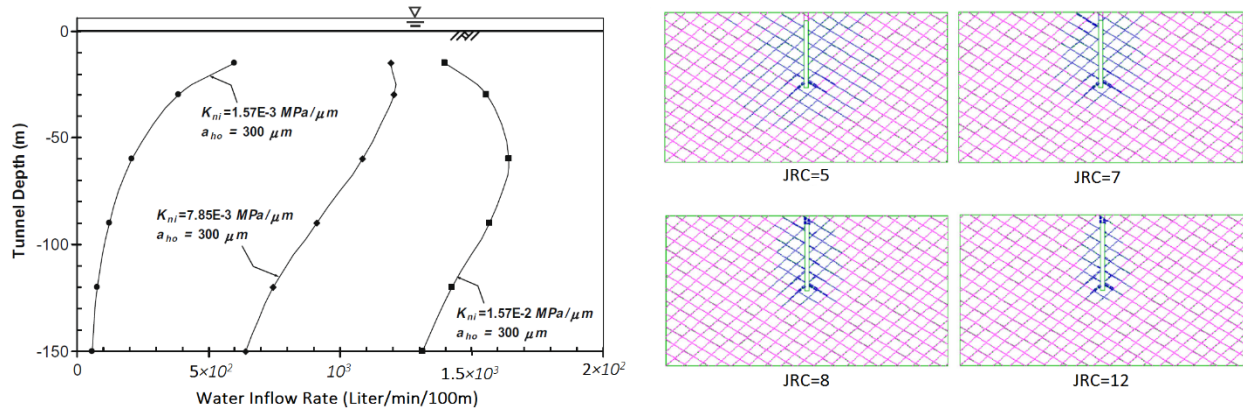
Fig 2-16. (a) Numerical modelling (UDEC) of the effect of depth on water inflow rate into a tunnel, considering different initial joint stiffness values (k_{ni}) [24]. (b) Decreasing penetration length by an increase in JRC, as simulated using a constant joint aperture of UDEC [23]

From Fig 2-16a, as joint stiffness increases−due to the resistance of apertures to closure and the increasing hydraulic head with depth−inflow rate initially increases and then decreases [24]. Furthermore, as joint stiffness varies with the level of stress, permeability is more sensitive to stress at low stress levels than at high stress levels [25, 33] due to the stiffening of the fracture.

The effect of the joint roughness coefficient (JRC) on permeability is illustrated in Fig 2-16b. Fracture roughness can reduce flow rates from those predicted by a smooth parallel plate model in two ways: first, by increasing frictional resistance along the separated fracture surfaces [23] and second, by creating points or areas of direct contact between the fracture surfaces to produce tortuous flow pathways or channels having an increased streamlined length and therefore a reduced hydraulic gradient and flow rate. Fracture roughness, on the other hand, can increase the permeability of the fracture subjected to active shear stress by increasing the amount of dilation [25, 30, 148].

For evaluating the permeability of the fracture network, it is necessary to ensure that the selected volume of the DFN is representative of the hydraulic properties of the entire network and that permeability has tensor characteristics. Therefore, the scale effect in rock mass permeability is studied by determining the REV of the fracture networks. Although REVs do not always exist in naturally fractured rocks [151], the variability of the calculated permeability components is reduced and permeability increases [152] as model size increases; permeability values maintain a constant range beyond a certain size, indicating the size of

the REV [28, 29]. Other parameters may also affect the size of the REV; for example, REV increases if fracture aperture correlates with length or if the apertures are more widely distributed [28]. Generally, actual REV size may be much larger than the numerically determined values [28].

To verify whether the calculated permeability has a tensor quality at a certain scale, one series of the DFN models are rotated at an interval of α^0 in the clockwise direction to calculate the directional hydraulic conductivity values of the DFN models using the same generic boundary conditions. Whether the size of the DFN is equal or greater to the REV−and, as a result, hydraulic conductivity is a tensor form−can be verified by ensuring that the directional values of hydraulic conductivity $\left(1/\sqrt{K}\right)$ are in an ellipse or ellipsoid form [28, 29] (Fig 2-17).
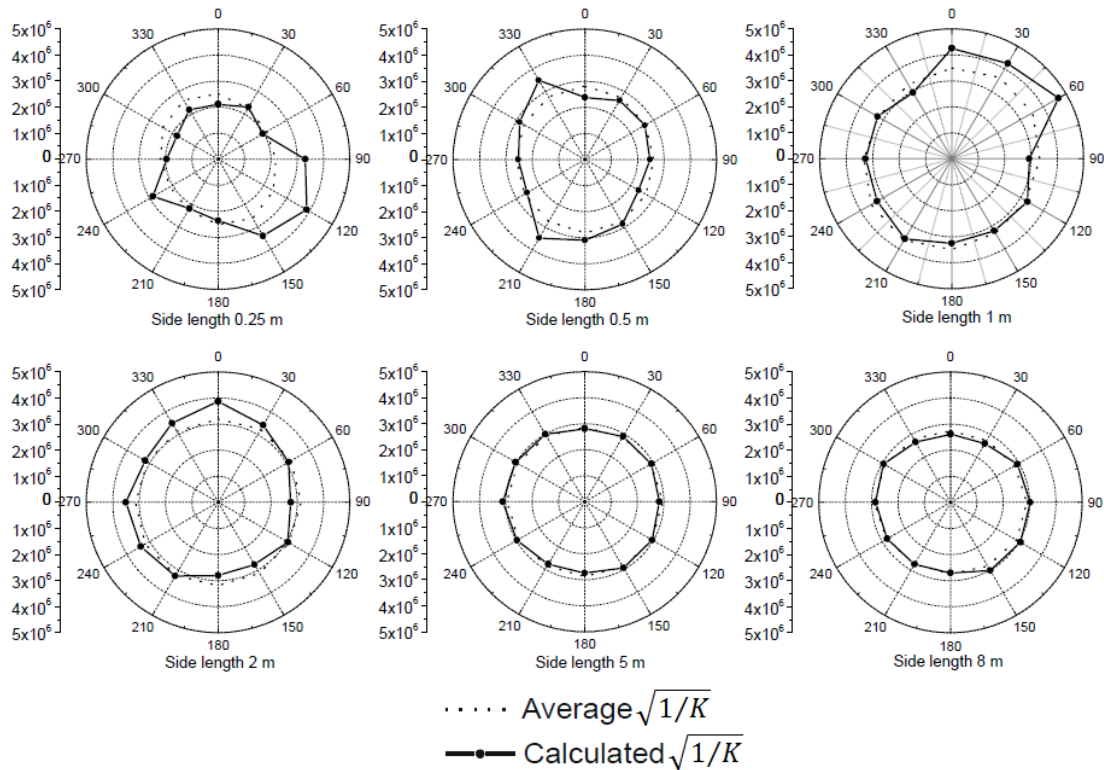
Fig 2-17. Approximation of equivalent hydraulic conductivity tensor with increasing model size [153]

The shape of the permeability ellipse is greatly affected by the fracture's geometry, such as density, length, orientation, spacing and interconnectivity of the fractures [154]. More precisely, fracture orientation is the main controlling factor of the overall shape of the ellipse [27, 155]. For instance, in the presence of

two fracture sets, by increasing the angle between them until π/2, the shape of the permeability ellipse varies from a bean-like form to a circle [105].

2.7 SUMMARY AND DISCUSSION

The three main approaches for investigating rock mass permeability are empirical formulations, analytical modelling and numerical simulation. Based on the assumptions used by each method, we will discuss the applicability of the various equations and methods outlined above.

Empirical relationships and their derived equations are based mainly on how permeability changes with depth. The resulting depth-permeability empirical equations do not consider the geometrical parameters of the studied rock mass, and the applicability of each existing empirical formulation is limited to the specific rock formation from which the experimental data were obtained. Therefore, although permeability generally decreases with depth, changing the rock formation—and thus the rock type and its geometrical characteristics—makes an existing equation invalid in a new location. Despite the existence of several relationships that link geological parameters (*RMR*, *RQD*, and *GSI*) to permeability, the geometrical characteristics of the discontinuities have the greatest effect on rock mass permeability; therefore, the suggested relationships should be revised to include these key parameters. Developing such a comprehensive empirical method requires extensive amounts of in situ data to derive a reliable relationship for prediction of the permeability; and, as geological formations are not identical, developing an empirical method that would be applicable to all geological formations appears extremely unlikely.

Analytical studies mainly apply cubic law, Darcy's law, and other mechanical formulas as the core constituents of the developed equations to evaluate the hydraulic behaviour of a rock mass. Most of these analytical equations incorporate the effect of stress (strain), fracture orientation, aperture, spacing, and geomechanical characteristics. However, other important parameters, such as infillings, joint persistence, joint termination, etc., are not considered by this approach. Neither is the variability of the abovementioned parameters incorporated into the equations. In situ surveys of outcrops or boreholes illustrate that there is much uncertainty regarding the orientation of joint sets, and this parameter does not have a unique value in either fractures or joint sets. This issue is equally applicable to the spacing and aperture of the

discontinuities. This occurs despite the fact that in analytical models, the abovementioned parameters are always assumed to be constant and hence, overestimation or underestimation is expected. Furthermore, in the analytical models developed to estimate underground tunnel inflow rate, assumptions include the rock mass as an isotropic and homogeneous formation, the tunnel having a circular, square, or regular geometric cross-section, and boundary conditions to be constant at the interfaces. From these assumptions, errors in predicting the water inflow rate to tunnels should be expected, as has been reported in multiple works. Despite these limitations, one of the main advantages of the analytical method remains the possibility of undertaking an immediate, rough estimate of permeability. However, none of the existing analytical methods for determining permeability consider all the important rock mass parameters.

Much of the variation in the geometrical parameters of a rock mass, e.g., aperture, spacing, length, and orientation distribution, and the correlation between these parameters are incorporated into DFN models. Using a fracture network model that matches the in-situ data, more realistic results are obtained. Through numerical modelling of the permeability of the rock mass, the impact of each parameter on the overall permeability of the fracture network can be assessed, and the existing analytical/empirical models can also be validated. Normal and shear stress, geometrical properties of fractures and directional permeability are studied extensively using numerical modelling, and the effect of each parameter on permeability can be determined. Directional permeability also helps define the hydrogeological REV of the fracture network. As numerical models run mostly in a 2D state, care should be taken to avoid errors produced when extrapolating 2D results to a 3D network.

All methods discussed and reviewed in this paper rely on a set of assumptions, boundary conditions, and solving methods that assume ideal conditions for the hydrologic properties of the rock mass. Although these methods greatly assist in conceptualizing the hydrological behaviour of the rock mass, the manipulation of a more applicable method (empirical, analytical, numerical or a combination of them) is most helpful for studying underground excavations and the related water seepage issues. It is feasible to take advantage of all of these in order to arrive at a more accurate result by harnessing the advantages of all three categories of approaches. It is possible to imagine a comprehensive approach based on: the actual results of the empirical methods; the exact logical relationship between the various parameters obtained

from analytical models, and; the greater scope of variables in numerical simulations. An optimized approach would ideally combine these specific elements of the methods. It would also be possible to use the empirical method to calibrate the numerical or analytical models and also integrate the numerical and analytical approaches to achieve a more accurate model.

2.8 CONCLUSION

The various approaches for estimating rock mass permeability each have their advantages and limitations. An empirical method is applicable only to a specific geological condition, thereby limiting the use of the developed equations in other geological settings. The analytical approach relies on several simplifying assumptions that can lead to errors in the estimated permeability, and numerical models are used mainly for sensitivity analysis or assessment of the equivalent permeability of a specific fracture network. Overall, a comprehensive method is lacking that would make it possible to evaluate the hydraulic behaviour of a rock mass; no single approach incorporates all the main geological and geomechanical parameters of a rock mass. Nonetheless, such a comprehensive method could be developed by drawing from the specific advantages of the existing methods by combining approaches to ensure more accurate estimates of permeability.

2.9 DECLARATIONS OF INTEREST

The authors declare that there is no conflict of interest associated with this publication.

CHAPTER 3

Article 2: A new combined analytical-numerical method for evaluating the inflow rate into a tunnel excavated in a fractured rock mass

Alireza Shahbazi*, Romain Chesnaux, Ali Saeidi

Université du Québec à Chicoutimi, 555 boulevard de l'Université, Chicoutimi, Québec G7H 2B1, Canada

*Email: alireza.shahbazi1@uqac.ca

3.1 ABSTRACT

A new method combining analytical and numerical tools is developed for evaluating the inflow rate to an underground tunnel that is excavated in a fractured rock mass. The method is comprised of a series of analytical formulas based on Darcy's and Cubic laws and assumes the rock mass to be impermeable except for the discontinuities which are considered to be the main pathways for groundwater flow. The geometrical and spatial characteristics of the discontinuities, the depth of the tunnel below the water table and the dimension and orientation of the tunnel are the effective parameters for calculating the groundwater inflow rate. The proposed method includes a new semi-numerical equation developed to determine the hydraulic gradient at the wall of the tunnel, using empirical input parameters derived from numerical simulations. The inflow rate to the tunnel is calculated from the general expression of Darcy's law, using the hydraulic conductivity calculated using the Cubic law and factoring the hydraulic gradient defined by a newly developed equation, taking into account the pertinent flow surface. In order to determine the inflow rate using this proposed method, the data required are the orientation, hydraulic aperture and spacing of the joint sets, the level of the water table, and the depth and diameter of the tunnel.

Keywords: Analytical model; tunnel; Fractured rock mass; Vertical hydraulic gradient; Inflow rate

3.2 INTRODUCTION

Prior to excavating a tunnel, the ability to predict the probable inflow rate to the tunnel could effectively help to first evaluate the stability of the cavity walls, and second, to evaluate the possible means of evacuating seeped water from the excavation area [156-158]. Assessing the inflow rate to

the tunnel also makes it possible to anticipate the environmental impacts on water resources and human activities as a result of underground water level and settlement of the aboveground buildings [159, 160]. In addition, seepage could produce extra pressure on temporary and permanent support systems in the tunnel, leading to a slowdown of the excavation rate [81]. In order to assess the inflow rate to tunnels, analytical models were developed by solving the Laplace equation under 2D steady-state conditions [17, 161, 162]. So far, the assumption of homogeneous and isotropic conditions of the fractured rock have been required for solving the existing analytical models developed to calculate the groundwater inflow rate in tunnels. The difference between various analytical models used to calculate the inflow rate to tunnels resides in the solving method and boundary conditions that are considered by each model.

The earliest analytical model for calculating the inflow rate to a tunnel was developed by Muskat and Meres [16, 163] for a homogeneous and isotropic formation in which a circular tunnel is excavated below the water table. The model calculated the inflow rate based on the hydraulic conductivity of the formation (K), tunnel radius (r) and water head above the tunnel (h). Polubarinova and Kochina [82] analytically calculated the inflow rate using a model considering a fully saturated, semi-infinite homogeneous formation. Afterwards, Goodman et al. [17] revised and modified the Polubarinova and Kochina model to apply it to cases of transient fluid flow. To take into account the overestimation of the inflow rate resulting from Goodman's equation , Heuer [83, 164] corrected the overestimation by a factor of 1/8 and published a new method for estimating tunnel inflow rate. Thereafter, El Tani [5, 84] developed a set of equations for various sections of a tunnel considering the assumption of anisotropic soils. Subsequently, Karlsrud [80], referring to the amount of water flowing into tunnels that had been excavated under cities, back-calculated the permeability and predicted the aboveground structures settlement. More recently, Kolymbas and Wagner [85] and Park et al. [18] developed an analytical model for calculating inflow rate to circular tunnels in homogeneous and isotropic formations and variable boundary conditions (Fig 3-1).
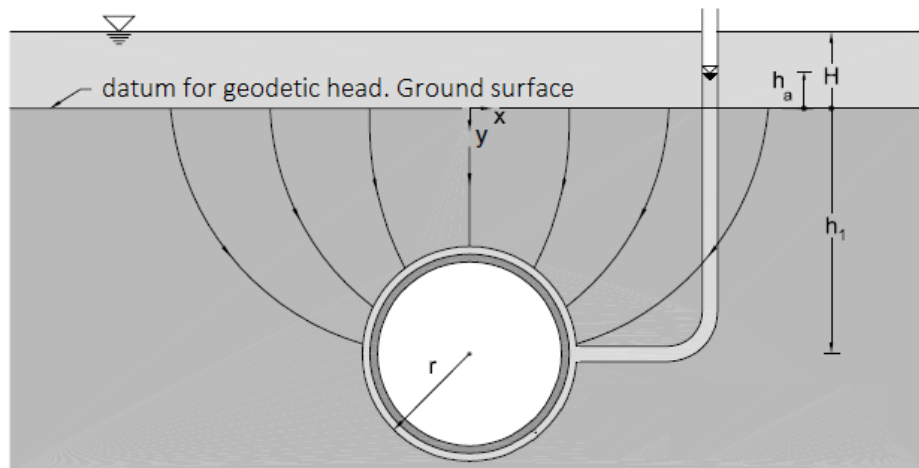
Fig 3-1. Kolymbas and Wagner's simplified conceptual model [85] used to establish an analytical equation to calculate the inflow rate to a cylindrical and horizontal tunnel in an isotropic and homogeneous formation

Table 3-1 summarizes the existing analytical solutions, including the parameters and assumptions they use to calculate the inflow rate to an underground tunnel excavated in different types of formations. The chronological sequence of the development of the equations is representative in Table 3-1 of the evolution of the parameters that were considered in each method.

Table 3-1. Existing equations for estimating inflow rate into underground tunnels per unit length of tunnel [165]

Equation	Reference	Parameters	Assumptions
$Q = 2\pi K \dfrac{h}{\ln\left(\dfrac{2h}{r}\right)}$	Muskat and Meres [16]	K, hydraulic conductivity of homogeneous and isotropic formation; h, water head above the tunnel; r, tunnel radius.	Steady-state inflow along tunnel length; Saturated, homogeneous, and isotropic formations.
$Q = \dfrac{2\pi K(d - \varphi_0)}{\ln\left(\dfrac{2D}{r}\right)}$	Polubarinova and Kochina [82]	K, hydraulic conductivity; r, tunnel's radius; D, depth of the tunnel centreline; φ_0, hydraulic head at the tunnel perimeter; d, water head above reference level.	Fully saturated, semi-infinite homogeneous media. For $D>>r$.
$Q = \dfrac{2\pi Kh}{\ln\left(\dfrac{2D}{r}\right)}$	Goodman et al. [17]	K, hydraulic conductivity of homogeneous and isotropic formation; h, water head above the tunnel; D, depth of the tunnel centre; r, tunnel radius.	Steady-state inflow along tunnel length; Saturated, homogeneous, and isotropic formations; Applicable to deep tunnels ($L\approx D$).
$Q = \dfrac{2\pi K(d + P_a - \varphi)}{\ln\left[\dfrac{D}{r} + \sqrt{\left(\dfrac{D}{r}\right)^2 - 1}\right]}$	Lei [57]	K, hydraulic conductivity; r, tunnel radius; D, depth of the tunnel centreline; d, aboveground water depth; φ, hydraulic head; P_a, atmospheric pressure head	Fully saturated, homogeneous, isotropic, and semi-infinite aquifers; Constant total head along the tunnel circumference; Deep tunnels.
$Q = 2\pi Kh \dfrac{1 - 3\left(\dfrac{r}{2h}\right)^2}{\left[1 - \left(\dfrac{r}{2h}\right)^2\right]\ln\dfrac{2h}{r} - \left(\dfrac{r}{2h}\right)^2}$	El Tani [5]	K, hydraulic conductivity; r, tunnel radius; h, depth of the tunnel centre below the water table.	Water level as the elevation reference datum; Constant total head (ha) along the tunnel circumference; Semi-infinite isotropic and homogeneous aquifers drained by a circular tunnel.
$Q = 2\pi k \dfrac{h}{\ln\left(\dfrac{2h}{r} - 1\right)}$	Karlsrud [80]	k, permeability of homogeneous and isotropic rock mass; h, depth of the tunnel centre below the water table; r, equivalent tunnel radius.	Homogenous media having constant permeability in all directions; Tunnel is deeply embedded ($h/r \geq 3$–4); Groundwater table is not influenced by the leakage.

$$Q = \dfrac{2\pi K(H - h_a)}{\log\dfrac{r}{h_1 - \sqrt{h_1^2 - r^2}}}$$	Kolymbas and Wagner [85]	K, hydraulic conductivity of homogeneous and isotropic rock mass; r, tunnel radius; H, water depth at the upper boundary; h_1, depth of the tunnel centre below the reference datum; h_a, total head at the tunnel circumference.	For deep and shallow tunnels; Ground surface as the elevation reference datum; Variable water heads at the tunnel circumference and ground surface; Homogeneous and isotropic permeability; Steady flow.
$$Q = K\dfrac{2\pi}{\ln\left(\dfrac{h}{r} + \sqrt{\dfrac{h^2}{r^2} - 1}\right)}(A + H)$$	Park et al. [18]	h, tunnel centre depth; r, tunnel radius; K, hydraulic conductivity; H, water depth at the elevation reference datum. $A = h\dfrac{(1 - \alpha^2)}{(1 + \alpha^2)}$ $\alpha = \dfrac{1}{r}\left[h - \sqrt{h^2 - r^2}\right]$	Ground surface is used as the elevation reference datum; Water table is above the ground surface ($H = 0$, and h is groundwater depth for the water table below the ground surface); Steady-state groundwater inflow into a drained circular tunnel.

According to the analytical methods listed in this table, calculations of fluid flow into tunnels have mostly assumed homogeneous and isotropic formations [43, 165]. Simplified models assume an ideal geometry of the tunnel and may not represent variable environmental situations; these limitations likely alter the accuracy of the inflow rate estimated by these analytical solutions [165, 166]. Although water table levels are assumed to be constant in the analytical models, in reality they may vary over time. Up to now, analytical models have generally considered restrictive assumptions to evaluate the inflow rate in a tunnel; these assumptions may no longer be valid when the tunnel is excavated in a fractured rock mass. These models (Table 3-1) cannot be applied for discontinuous media presenting heterogeneous and anisotropic conditions of permeability. Thus, new specific analytical or semi-analytical models would be of interest to make it possible to calculate the inflow rate from discontinuous media such as fractured rock into a tunnel.

The development of new analytical models for fractured rock conditions would thus require the definition of new assumptions. In this study, the intact rock is assumed to be an impermeable mass through which fluid may flow solely through the discontinuities (impermeable matrix containing a permeable discrete fracture network). This assumption implies that no inflow through the rock matrix

could occur into the tunnel. Such conditions would be representative of the majority of rock types and especially of crystalline fractured rock. In this study, the opening of the discontinuities is designated as hydraulic aperture, signifying the opening of the fractures, taking into account the physical characteristics of the discontinuities [130, 167]. The persistence of all joint sets is assumed to be 100%; this means that all joint sets will be terminated at the boundaries of the model. The tunnel excavated in the rock is represented by a cylinder and consequently has a circular cross-section. Note that no assumption is made in regards to the water table, which may not be horizontal in reality. The hydraulic conductivity tensor of the rock mass is used to develop the new model. Accordingly, the inflow rate (the principal result of this study) is calculated based on the knowledge of the orientation and features of the fractures (structural data). An important feature of the new proposed model concerns the determination of the vertical hydraulic gradient at the wall of an underground excavation. Previous models considered only the hydraulic head at the wall of the tunnel, but this new proposed model will consider the hydraulic gradient along the tunnel walls. Through this study, a numerical approach is proposed to determine and calculate this hydraulic gradient, as well.

The proposed equations to calculate the inflow rate in an underground tunnel will be especially useful for geotechnical and geological engineers working on mining as well as tunnelling projects. The continuity of excavation processes of the tunnel depends on the evacuation of groundwater flowing into the tunnel. Furthermore, the geomechanical stability and tunnel lining design [168] depend directly on hydraulic parameters, which are among the main concerns of geological engineers. These parameters may be solved through knowledge of the inflow rate into the tunnel as well as the hydraulic gradient at the wall of the tunnel. The advantage of using semi-analytical equations combining closed-from solutions and numerical modelling resides in their usefulness in direct applications, keeping in mind the assumptions they involve. These equations are preferred by practitioners in the field of engineering geology because of the relatively minor time and cost investments required. It is hoped that the results of the current study may assist geological engineers working on tunnel projects in solving the inflow-rate and hydraulic gradient problems.

3.3 MODEL DEVELOPMENT

When excavating a circular tunnel in a rock mass, traces of the embedded fracture network are revealed on the tunnel walls; these depend both on the orientation of the tunnel and the discontinuities within the rock. If the intact rock is considered as impermeable, only the fracture network will contribute to the fluid flow into the tunnel. By this manner and according to Darcy's law, the aperture of fractures, their frequency and apparent surface area perpendicular to the fluid flow direction, and the existing hydraulic gradient in the fracture around the tunnel wall are the effective parameters that control the inflow rate to the tunnel. On this basis, in the next section, the general form of the model is developed using the above-mentioned parameters. Since the hydraulic gradient in the wall of the tunnel is needed to calculate the inflow rate, an empirical-numerical equation has been derived for this purpose and is presented in section 3.3.2.

3.3.1 Inflow rate into underground excavations

In order to evaluate the water inflow rate to the underground tunnel that has been excavated in a fractured rock mass below the water table, Darcy's law [61] is applied to calculate the inflow rate using Eq. (3-1):

$$q = -K\,i\,A \qquad\qquad (3\text{-}1)$$

Where q is the discharge rate (m^3/s), K is the hydraulic conductivity tensor (m/s) of the fractured rock, i is the hydraulic gradient (m/m) and A is the surface area of the formation perpendicular to the direction of the flow (m^2). However, Pudasaini [169] proposed a physics-based generalized Darcy expression for fluid velocity that could describe the fluid flow dynamics considered here, as well. In the proposed model, as with models proposed by [47, 170], the matrix (intact rock) is regarded as impermeable and the fluid flows only through the fracture network. The overall fractured rock permeability is governed by the permeability of fractures which can be expressed by the cubic law [64, 65, 171]. According to the cubic law, in the case of laminar flow and assuming parallel plates for simulating the fracture walls, the hydraulic conductivity of a fracture having an aperture b is given by Eq. (3-2):

$$K_f = \frac{\rho g b^2}{12\mu} \qquad \text{(3-2)}$$

Where K_f is the hydraulic conductivity of the fracture (m/s), b is the aperture of the fracture (m), μ is the water dynamic viscosity (kg/m.s), ρ is the fluid density (kg/m³) and g is the acceleration of gravity (m/s²). Combining Eq. (3-2) and Eq. (3-1), yields Eq. (3-3) that determines the inflow rate of the fluid that flows through a fracture.

$$q = -\frac{\rho g b^2}{12\mu} \, i \, A \qquad \text{(3-3)}$$

As mentioned earlier, it is assumed by the proposed model that the fluid flows only through the fractures. Therefore, in order to determine the total inflow rate to the tunnel, the inflow rates through all fractures that intercept the wall of the tunnel will have to be added together. In order to define the inflow rate that takes place through the jth fracture of the ith set (or fracture ij), Eq. (3-3) transforms to Eq. (3-4)

$$q_{ij} = -\frac{\rho g b_{ij}^2}{12\mu} \, i_{ij} \, A_{ij} \qquad \text{(3-4)}$$

Index of ij points out the relevant characteristics of jth fracture of ith set. In developing the model, each parameter of Eq. (3-4) will be substituted by its relevant equation.

A_{ij} in Eq. (3-4) refers to the surface area in the fracture that is perpendicular to the fluid flow direction (m²). When excavating a tunnel in a rock mass formation, each fracture will be crossed by the tunnel and the traces of the fractures on the wall of the tunnel depend on the directions of both the tunnel and the fractures. As illustrated in Fig 3-2, in the particular case of a perpendicular intersection between the fracture plane and the tunnel direction, the trace takes the shape of a circle, whereas when the intersection is oblique, then the trace takes the shape of an ellipse. It should be considered that the fluid flows into the tunnel only via these traces.
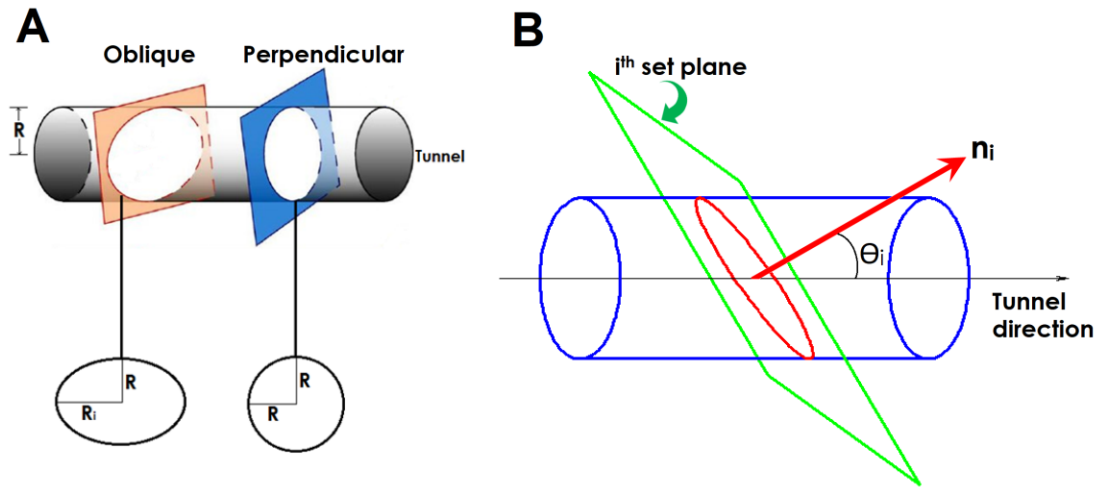
Fig 3-2. (A) Trace of a fracture on the tunnel wall when the fracture plane is perpendicular or oblique to the tunnel direction (B) the angle between the tunnel direction and the normal to the plane direction of the ith set

If the trace is generally assumed to be an ellipse (a circular trace is a specific case of ellipse), its larger radius is calculated by Eq. (3-5)

$$R_i = R \times \frac{1}{\cos \theta_i} \qquad (3\text{-}5)$$

Where θ_i is the angle between the tunnel direction and direction of the normal to joint set i (n_i) and R is the tunnel radius (m). Accordingly, the flow surface A_{ij} is defined by Eq. (3-6).

$$A_{ij} = P_i \times b_{ij} \qquad (3\text{-}6)$$

Where P_i is the perimeter of the ellipse (m). Considering Eq. (3-5), P_i will be defined using Eq. (3-7)

$$P_i = 2\pi \sqrt{\frac{R^2 + R_i^2}{2}} = 2\pi R \sqrt{\frac{2 + \tan^2 \theta_i}{2}} \qquad (3\text{-}7)$$

The inflow rate of the fluid that flows through the fractures into the tunnel increases with the apparent frequency of joints in the tunnel wall. However, the apparent frequency of the ith set (f^*_i) may be equal to or smaller than the real frequency (f_i). Knowing that the frequency is the inverse of spacing ($f_i = 1/S_i$) and considering Fig 3-3, f^*_i could be determined using Eq. (3-8).

$$f_i^* = f_i \times \cos \theta_i \qquad (3\text{-}8)$$
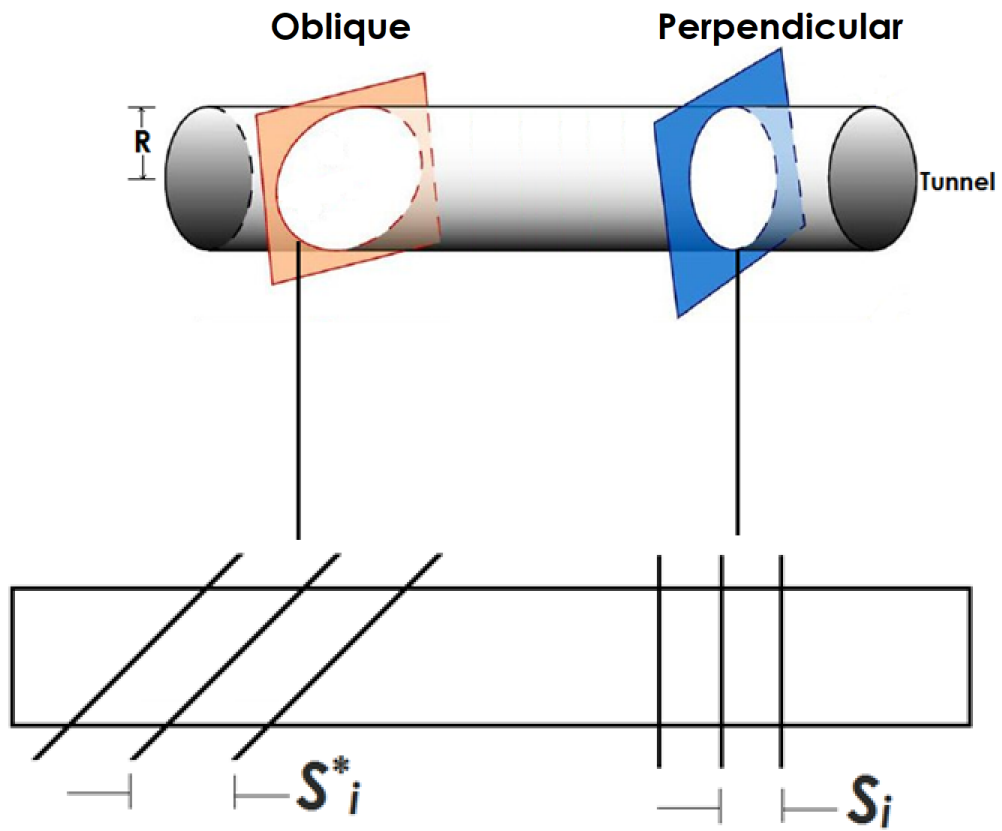
Fig 3-3. Apparent and real spacing of the joint set on the wall of the tunnel

In Eq. (3-4), i_{ij} refers to the hydraulic gradient that exists in the plane of the fracture ij. In order to determine i_{ij}, it is assumed that the overall hydraulic gradient that exists in a formation with the presence of a tunnel, could be represented by a vector, as i.
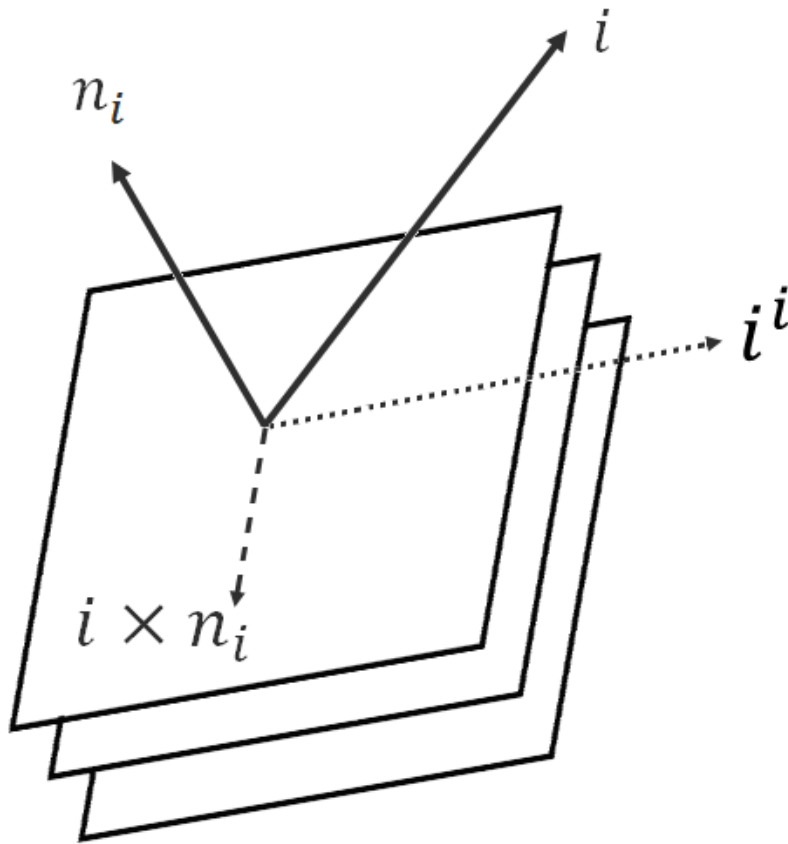
Fig 3-4. ith fracture set and the hydraulic gradient in the plane of the fractures

As illustrated in Fig 3-4, the normal to joint set i could be represented by the n_i vector. The cross product of i and n_i is a vector that is perpendicular to both the i and n_i vectors and is placed in the plane of discontinuity. This vector is shown by a dashed line in Fig 3-4. Finally, the projection of the hydraulic gradient i in the plane of set i (dotted line in Fig 3-4) could be defined as i_i and calculated according to Eq. (3-9).

$$\vec{i}_i = \vec{n}_i \times (\vec{i} \times \vec{n}_i) \qquad (3\text{-}9)$$

The vector i_i is the projection of the overall hydraulic gradient i in the plane of joint set i, and as all fractures in a joint set are parallel, it is equal to the hydraulic gradient that exists in the jth fracture of ith set, as well; i.e., $i_{ij} = i_i$. Based on Eq. (3-9), i_i could simply be defined by knowing the overall hydraulic gradient i and trend and plunge of the joint set. As i is a vector with the elements in x, y, and z direction and considering Fig 3-5, each of its elements could be defined by Eq. (3-10)

$$i_x = \frac{\Delta h_x}{\Delta x}$$

water table   water table $i_y = \frac{\Delta h_y}{\Delta y}$

$h = h_z$

d

$h = h_{atm}$

$$i_z = \lim_{d \to 0} \frac{h_z - h_{atm}}{d}$$
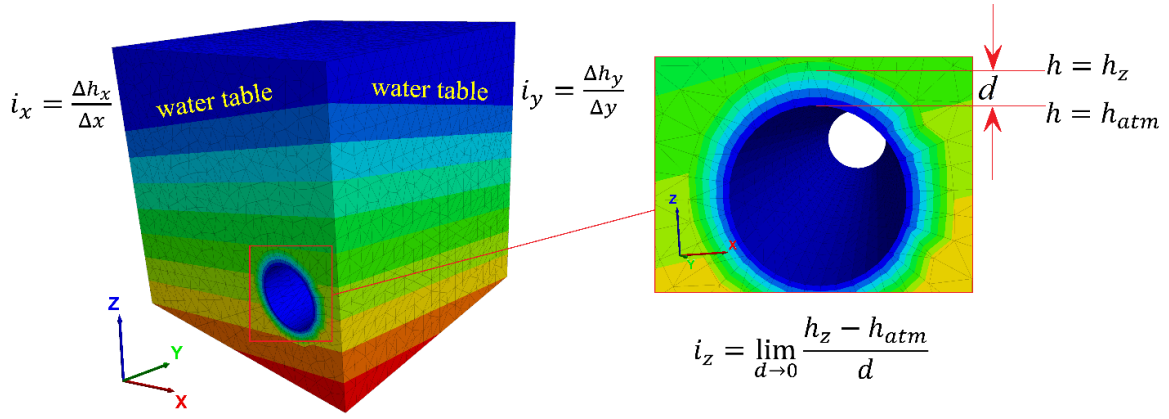
Fig 3-5. Overall hydraulic gradient in the presence of the underground tunnel

$$i_x = \frac{\Delta h_x}{\Delta x}$$

$$i_y = \frac{\Delta h_y}{\Delta y} \qquad\qquad (3\text{-}10)$$

$$i_z = \lim_{d \to 0} \frac{\partial h_z}{d}$$

Where Δh_x, Δh_y and ∂h_z are the variations of the hydraulic head isolines in the *x*, *y* and *z* directions, respectively. In Eq.(3-10), the limit is used for vertical hydraulic gradient as the variation of the hydraulic head is large in zones near the tunnel and small in zones far from the tunnel. Considering an inclined water table, the Δh_x is the decrease of the water table level in the *x*-direction per meter of length and accordingly, Δh_y is the decrease of the water table level in *y*-direction per meter of length. i_x and i_y could easily be determined by excavation and monitoring of observation wells installed in the vicinity of the tunnel. Theoretically, i_z could be determined by applying a series of piezometers above the tunnel in the vertical direction, although this would not be feasible in practice. Because the determination of the value of i_z is not as simple as are the other elements in this method (since it varies with the depth of the tunnel below the water table), this parameter will be discussed in detail in section 3.3.2.

The calculation of the water inflow rate through the *j*th fracture of the *i*th set could be performed by inserting Eqs. (3-6), (3-7) and (3-9) into Eq. (3-4).

$$q_{ij} = -K_{ij}.i_i.A_{ij} = -\frac{\rho g b_{ij}^2}{12\mu} \times \left(\vec{n}_i \times (\vec{i} \times \vec{n}_i) \right) \times \left(b_{ij} \times 2\pi R \sqrt{\frac{2 + \tan^2 \theta_i}{2}} \right) \qquad (3\text{-}11)$$

63

For the inflow rate through the ith set, by considering Eq. (3-8), Eq. (3-11) changes to Eq. (3-12)

$$q_i = f_i^* \sum_j q_{ij} = \sum_j -\frac{\rho g \pi R b_{ij}^3}{6\mu} \left(\vec{n}_i \times (\vec{\imath} \times \vec{n}_i)\right)(f_i \cos \theta_i) \sqrt{\frac{2 + \tan^2 \theta_i}{2}} \qquad (3\text{-}12)$$

Finally, the inflow rate per unit length of tunnel via all the fracture apertures is calculated by Eq. (3-13)

$$q_{total} = \sum_i \sum_j \left| -\frac{\rho g \pi R f_i b_{ij}^3}{6\mu} \left(\vec{n}_i \times (\vec{\imath} \times \vec{n}_i)\right) \cos \theta_i \sqrt{\frac{2 + \tan^2 \theta_i}{2}} \right| \qquad (3\text{-}13)$$

As the fluid flow in any direction seeps into the tunnel, the absolute value of the flow rate is considered for each fracture. Eq.(3-13) is the resultant relationship between the inflow rate to the tunnel (q_{total}) and other parameters such as discontinuity characteristics, hydrological state of the formation and the tunnel's geometrical characteristics. All right-side parameters of Eq.(3-13) may be defined from field surveying, except the hydraulic gradient (i) which is determined by a method explained in section 3.3.2. It should be mentioned that Eq.(3-13) is valid for all cases except one: when the normal to the joint set is perpendicular to the tunnel direction. In that specific case, the value of the term A_{ij} is different from its value in Eq. (3-11). Re-writing this equation results in Eq.(3-14).

$$q_{ij} = -K_{ij} . i_i . A_{ij} = -\frac{\rho g b_{ij}^2}{12\mu} \times \left(\vec{n}_i \times (\vec{\imath} \times \vec{n}_i)\right) \times 2 \times (2R \times f_i) \qquad (3\text{-}14)$$

If the joint set plane is parallel to the tunnel direction, the trace of the joint set on the wall of the tunnel will be fully in the direction of the tunnel. The number of the fractures in a set that crosses the tunnel could be determined by [2R×f_i]. If each cross of the fracture and tunnel results in two traces at the tunnel wall, then the total number of the fracture traces at the wall of the tunnel could be defined by 2× [2R×f_i]. Finally, Eq.(3-13) will change to Eq. (3-15) for this specific case. Section 3 describes a numerical simulation used to validate and verify the accuracy of Eq.(3-13).

$$q_{total} = \sum_i \sum_j \left| -\frac{\rho g b_{ij}^3}{6\mu} \left(\vec{n}_i \times (\vec{\imath} \times \vec{n}_i)\right) \times [2R \times f_i] \right| \qquad (3\text{-}15)$$

Where [] is the function to calculate the round of a decimal value. It should be noted that b_{ij} in Eq.(3-13) and (3-15) is the hydraulic aperture and could be predicted either by surveying the joint sets in the ground surface [25, 172] or by measuring them at the wall of the tunnel. In order to estimate the in-depth hydraulic aperture from knowledge of the ground surface hydraulic aperture, Chen and Zhao [173] proposed Eq.(3-16) below for the calculation of the in-depth hydraulic aperture (b_{ij}):

$$b_{ij} = E_{ij} - \Delta V_{ij} \qquad (3\text{-}16)$$

Where, E_{ij} is the joint hydraulic aperture of the jth fracture of the ith set at ground surface (mm) and ΔV_{ij} is the reduction of the aperture because of the overburden load. Bandis et al [172] showed that ΔV_{ij} could be calculated according to Eq.(3-17):

$$\Delta V_{ij} = \frac{\sigma_n V_{mij}}{K_{ni} V_{mij} + \sigma_n} \qquad (3\text{-}17)$$

Where V_{mij} is the average maximum closure of the aperture (mm), σ_n is the normal stress (Mpa) and the K_{ni} is the initial joint stiffness (GPa/m). As Eq.(3-17) is an empirical equation, the resultant dimensions in the left and right side of the equation are not necessarily the same. Finally, Bandis et al [172], proposed Eq.(3-18) to define the V_{mij}:

$$V_{mij} = A_1 + B_1 \left(JRC_{ij} \right) + C_1 \left(\frac{JCS_{ij}}{E_{ij}} \right)^{D_1} \qquad (3\text{-}18)$$

Where A_1, B_1, C_1 and D_1 are constants, JRC_{ij} is the joint roughness coefficient of set i, JCS_{ij} is the joint wall compressive strength (Mpa).

Based on the above-mentioned explanations, without access to the tunnel wall and prior to the excavation of the tunnel, it is possible to predict the hydraulic aperture at the wall of the tunnel by knowing the geometrical and geo-mechanical characteristics of the joint set.

3.3.2 Hydraulic gradient at the wall of the tunnel

According to Darcy's law, the hydraulic gradient is an effective parameter that controls the flow rate and its direction through a formation. Accordingly, in order to determine the inflow rate to the tunnel, the existing hydraulic gradient in the vicinity of the wall of the tunnel must be defined. Determination of the hydraulic gradient at the tunnel wall has rarely been considered by researchers; instead, the water head above the tunnel has been used to calculate the inflow rate. Previous investigations regarding the determination of the hydraulic gradient were mostly conducted with the aim of evaluating the variation of the hydraulic head across the lining-like zone around the tunnel [6, 158, 174]. In a research study conducted by Shin et al [175], the variation of the hydraulic gradient in the vertical direction in the presence of a circular tunnel with lining was determined according to Eq. (3-19) (Fig 3-6).
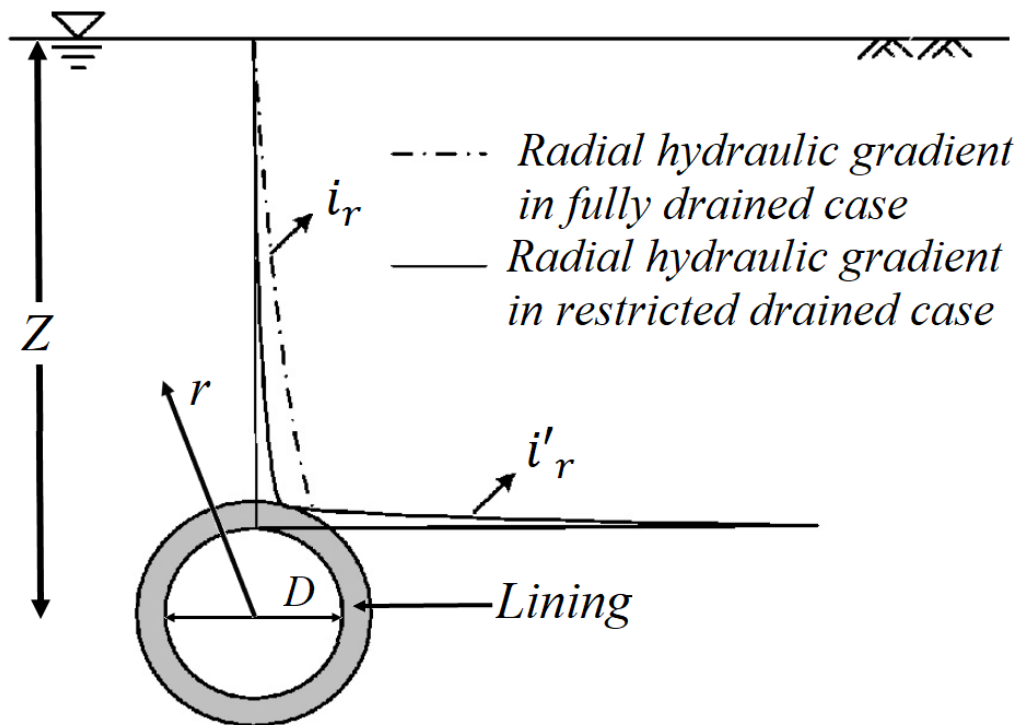
Fig 3-6. The variation of the hydraulic gradient in the vertical direction above the tunnel [175]

$$\frac{i_r}{Z^2} = 0.0012 \left(\frac{r}{D_T}\right)^{-1.0346} \qquad\qquad (3\text{-}19)$$

Where, i_r is the radial component of the hydraulic gradient, Z is the depth of the tunnel centre below the groundwater table in meters, D_T is the diameter of the tunnel (m) and r is the distance from the centre of the tunnel (m). Eq. (3-19) transforms to Eq. (3-20) that determines the hydraulic gradient at the wall of the tunnel (where $r=D_T/2$) as a function of the depth Z of the centre of the tunnel below the groundwater table.

$$i_{\left(r=D_T/_2\right)} = (2.458 \times 10^{-3})\, Z^2 \qquad (3\text{-}20)$$

The relation of dependence between the hydraulic gradient and the depth of the centre point of an underground excavation is quite clear, as demonstrated in Eq. (3-20). However, it is likely that the hydraulic characteristics of the formation (considered in the model as isotropic and homogeneous) could affect the hydraulic gradient. In this section, the interdependency between the hydraulic gradient at the wall of the tunnel and various other parameters is numerically investigated and accordingly, a new and more comprehensive equation has been developed. A set of numerical simulations using *RS2* software [176] has been performed to assess several parameters: 1) the variation of the vertical hydraulic gradient (i_z) with the change of depth (Z, the depth below water table); 2) the ratio between the principal sub-vertical (K_{2y}) and sub-horizontal (K_{1x}) hydraulic conductivities ($a=K_{2y}/K_{1x}$); 3) the directions of the fractures (α, the angle between K_{1x} and x axis). Here, the principal hydraulic conductivity that is closer to x-axis is named K_{1x} and the hydraulic conductivity closer to y-axis is similarly named K_{2y}. The principal hydraulic conductivities are named in this manner as their relevant vectors are not essentially in the direction of the original axis; furthermore, the deviation of the principal hydraulic conductivities is one of the parameters that is used to define the vertical hydraulic gradient at the wall of the tunnel. The definition of these parameters aims to make the Laplace equation concordant with homogeneous and isotropic conditions. The Laplace equation for homogeneous and anisotropic aquifers in a steady state condition could be written as Eq. (3-21) [66]:

$$k_{1x}\frac{\partial^2 h}{\partial x^2} + k_{2y}\frac{\partial^2 h}{\partial y^2} = 0 \qquad (3\text{-}21)$$

Where h is the hydraulic head and x and y are the coordinate axes. In another form, this equation could be rewritten as Eq. (3-22)

$$\frac{\partial^2 h}{\partial x^2} + \frac{1}{\left(k_{1x}\big/k_{2y}\right)}\frac{\partial^2 h}{\partial y^2} = 0 \qquad (3\text{-}22)$$

According to Eq. (3-22), for anisotropic aquifers, the ratio between hydraulic conductivities could affect the hydraulic head. On the other hand, the orientations of the hydraulic conductivities will affect the (K_{1x}/K_{2y}) ratio. Therefore, these two parameters, as well as the depth of the centre below the water table, were used to develop the hydraulic gradient determinant equation.

The numerical model consists of a cylindrical tunnel with a radius of 2 m that is excavated in a homogeneous formation, whose horizontal hydraulic conductivity is 1×10^{-6} m/s and the water table has been set at 100m above the tunnel. This is a 2-dimensional model and its dimensions are 50 m×150 m as illustrated in Fig 3-7.
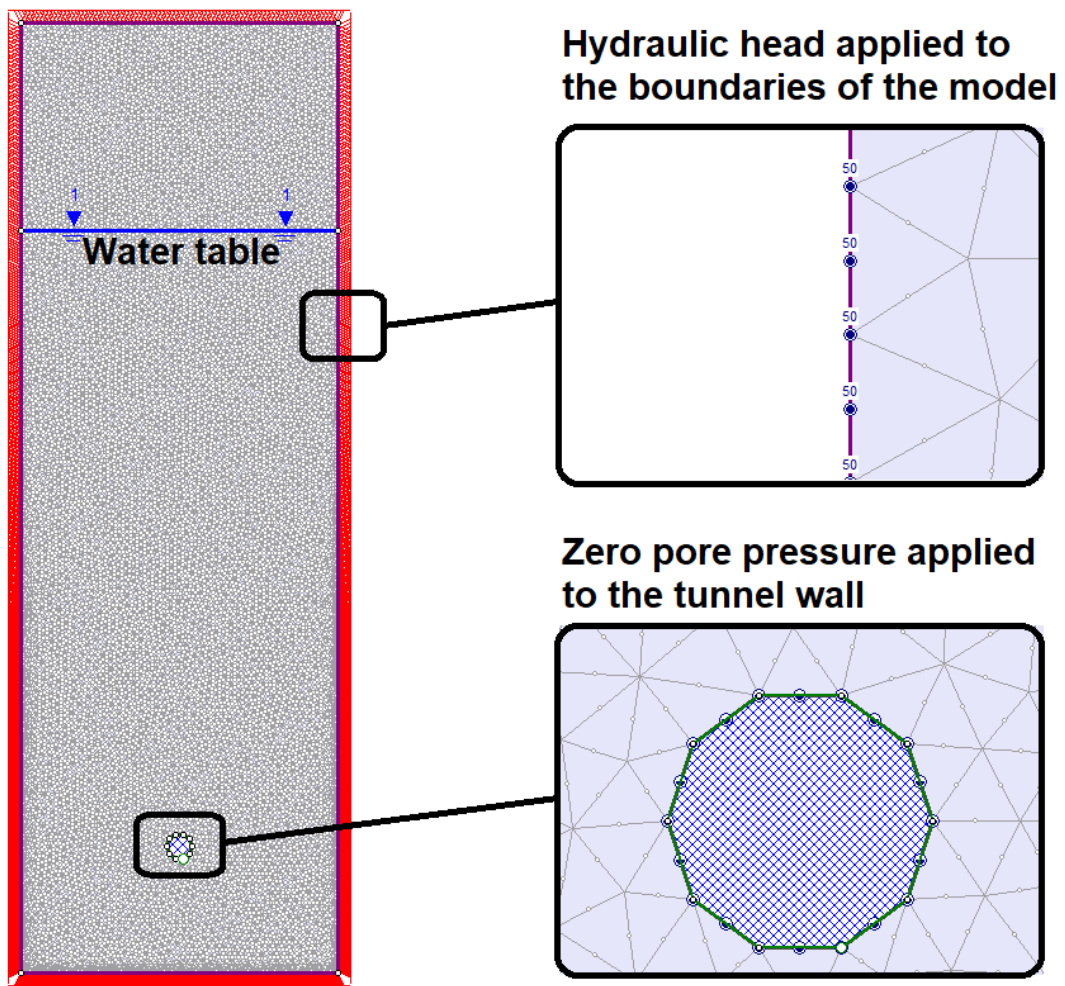
Fig 3-7. Numerical model and relevant settings for studying the hydraulic gradient at the wall of the tunnel

In the first step, the variations of i_z with Z for different ratios of hydraulic conductivities (*a*) are calculated for 4 orientations of the hydraulic conductivities (*α=0, 20, 30, 45*). In Fig 3-8, the relevant diagram is presented for the case of α=*30º.*

$$i_z = AZ + B$$
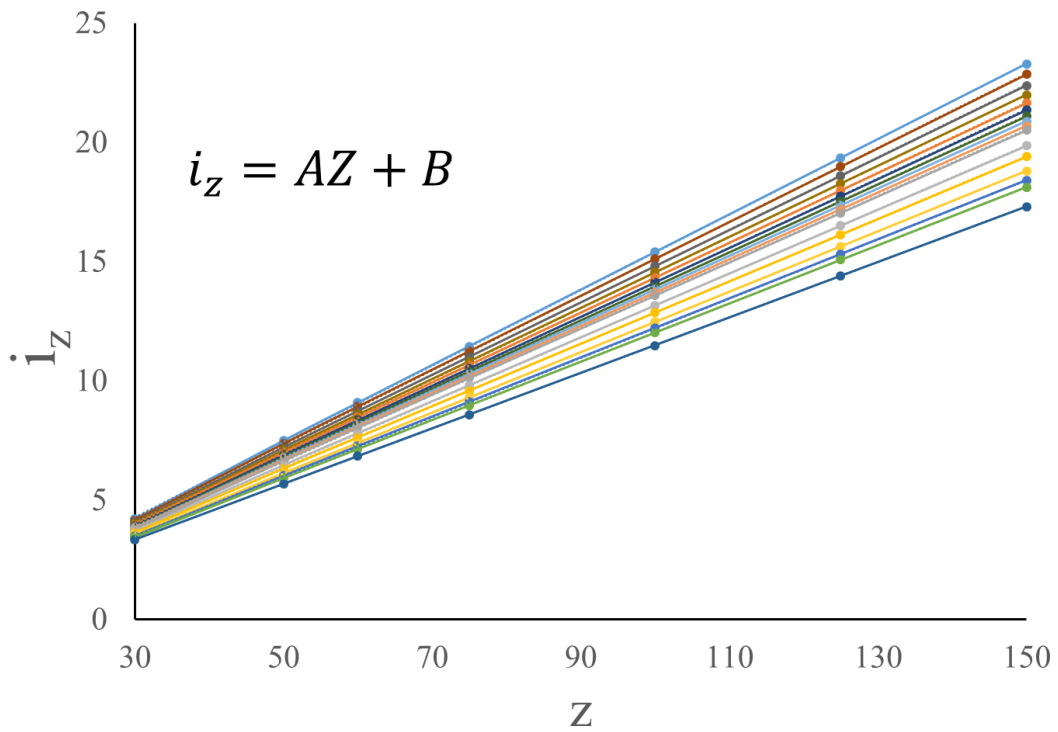
Fig 3-8. The variation of i_z with depth of the tunnel below the water table in various ratios of hydraulic conductivities (a) for the case of α=30º- each line color demonstrates a specific ratio of hydraulic conductivities from a=1 to a=100

The dependency of *A* and *B* coefficients of Fig 3-8 to *a*, is demonstrated in Fig 3-9.
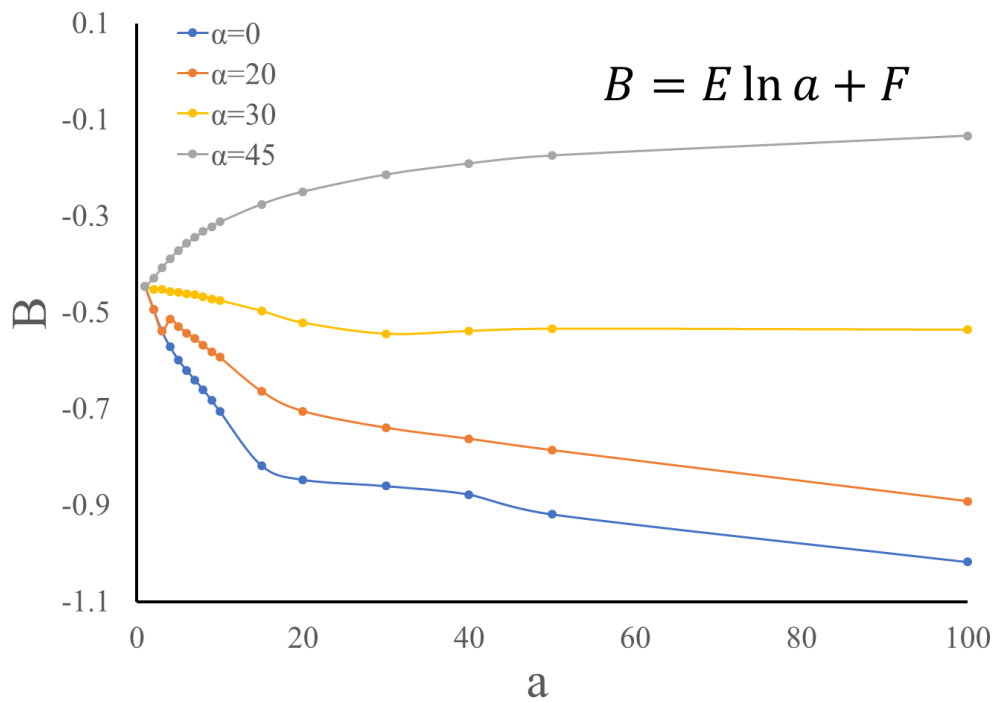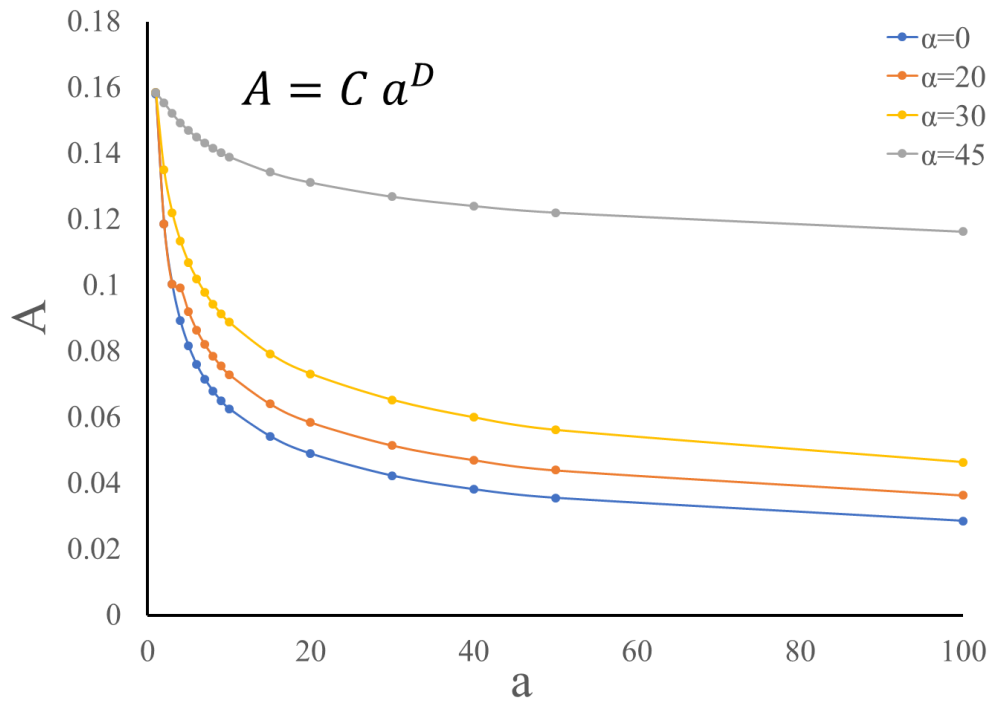
Fig 3-9. Variation of the A and B coefficients with ratio of hydraulic conductivities (a) for different orientations of hydraulic conductivities (α). Each line color refers to one level of orientation

Based on Fig 3-8 and Fig 3-9, the variation of the hydraulic gradient with *z*, *a* and *α* could be empirically represented by Eq.(3-23)

$$i_z = AZ + B = (C\,a^D)Z + (E \ln a + F)$$ (3-23)

Where the coefficients *C*, *D*, *E* and *F* for different angles *α* are given in Table 3-2.

Table 3-2. Constants in Eq.(3-23) given for different values of the angle (α)

Angle to the x axis (α)	C	D	E	F	R^2
0	0.1636	-0.073	-0.133	-0.4028	0.998
20	0.1640	-0.271	-0.098	-0.3954	0.996
30	0.1508	-0.314	-0.027	-0.4236	0.995
45	0.1502	-0.371	0.076	-0.4817	0.996

The result obtained by Eq.(3-23) corresponding to the vertical hydraulic gradient is then integrated into Eq.(3-13) to determine the inflow rate per unit length of tunnel.

3.4 MODEL VALIDATION

In order to validate the proposed semi-analytical model for calculating the inflow rate to the tunnel (Eq.(3-13)), the results of the proposed model must be compared against the output of a numerical simulation (RS2 Rocscience), considering the same characteristics and boundary conditions for both models. For the semi-analytical model, specific joint set characteristics (dip, dip direction, joint aperture and spacing) and a circular tunnel that is excavated in a specific orientation and depth are assumed. A constant level of the water table is also assumed for the semi-analytical calculations and then, the hydraulic gradient at the wall of the tunnel is defined by Eq.(3-23), accordingly. Finally, the inflow rate is calculated using Eq.(3-13). In order to obtain the result of the numerical simulation, the same model is introduced into the RS2 software with the same conditions for the tunnel and water table level. Finally, the results of the numerical and semi-analytical methods are compared. A rock mass with specific characteristics of joint sets is considered according to Table 3-3.

Table 3-3. Joint set characteristics assumed for comparison

Strike	Dip	Hydraulic aperture (m)	Frequency
130	80	10^{-04}	2
180	40	10^{-04}	2
290	55	10^{-04}	2

The tunnel direction is assumed to be in N41W/86 direction (trend/plunge). According to the joint set characteristics presented in Table 3-3 and in order to define the hydraulic conductivity matrix, the equation of Kiraly [44, 58] (Eq. (3-24)) was used.

$$K_{ij} = \frac{\rho g}{12\mu} \sum_{i=1}^{N} f_i e_i^3 [M] \qquad (3\text{-}24)$$

here N is total number of sets of discontinuities, f is average frequency of the ith set of discontinuities, e_i is average hydraulic aperture of the ith set of discontinuities, and $[M]$ is the conversion matrix that is defined as:

$$[M] = \begin{bmatrix} 1 - n_1^2 & -n_1 n_2 & -n_1 n_3 \\ -n_2 n_1 & 1 - n_2^2 & -n_2 n_3 \\ -n_3 n_1 & -n_3 n_2 & 1 - n_3^2 \end{bmatrix} \qquad (3\text{-}25)$$

Where n is the normal vector to discontinuity, and n_1, n_2, n_3 denote the direction cosines of the unit vector normal to the discontinuity in the direction of axes x, y, and z, respectively. By this method, the matrix of hydraulic conductivities of the joint sets of Table 3-3 is defined according to Eq. (3-26)

$$[K] = \begin{bmatrix} 3.43288 \times 10^{-6} & -1.1291 \times 10^{-6} & 7.19327 \times 10^{-7} \\ -1.1291 \times 10^{-6} & 2.99431 \times 10^{-6} & -5.05758 \times 10^{-7} \\ 7.19327 \times 10^{-7} & -5.0576 \times 10^{-7} & 3.34561 \times 10^{-7} \end{bmatrix} \qquad (3\text{-}26)$$

Accordingly, the matrix of the principal hydraulic conductivities could be calculated according to Eq. (3-27)

$$[K_p] = \begin{bmatrix} 2.05863 \times 10^{-6} & 0 & 0 \\ 0 & 2.84522 \times 10^{-6} & 0 \\ 0 & 0 & 4.86894 \times 10^{-6} \end{bmatrix} \qquad (3\text{-}27)$$

Based on the principal hydraulic conductivities of Eq.(3-27) and the tunnel direction, the angle between the principal sub-horizontal hydraulic conductivity (4.86894×10⁻⁶ m/s) and x direction is approximately 43°. In order to use equation (3-23) with certainty, the angle between K_{1x} and x axis

73

should be exactly one of the four levels that has been defined (α = 0°, 20°, 30° or 45°). If the value of α is not equal to what was stated in Table 3-2, the vertical hydraulic gradient (i_z) should be calculated using the closest value of α in that table. As 43° is close to 45° and a specific equation for the vertical hydraulic gradient was not developed for 43°, the equation of 45° is used instead. It is evident that this will constitute one of the sources of error in the results of the model. Firstly, the vertical hydraulic gradient (i_z) as a result of 100 m of water head above the tunnel is calculated according to Eq.(3-23) and Table 3-2 to be approximately 15.22. According to the proposed method (Eq. (3-13)), the calculated inflow rate to the tunnel for the assumed case is approximately 49.48 (m³/day) for each meter of tunnel length.

Using the principal hydraulic conductivities of Eq.(3-27), a numerical model is prepared using *RS2* software [176] in the case of a tunnel that is excavated under a water table located 100 meters above the tunnel centreline (Fig 3-10). As illustrated in Fig 3-10, due to the limitation of the RS2 software for configuration of the circular discharge section, the tunnel is assumed to have the shape of a decagon (composed of 10 straight sides) and the total inflow rate has been calculated by adding the sum of all the inflow rates from each side. The hydraulic conductivity for the model is defined according to Eq.(3-28)

$$K_{eq} = \sqrt[3]{K_1 K_2 K_3} \qquad (3\text{-}28)$$

Where K_1, K_2 and K_3 are the principal hydraulic conductivities of the rock mass that have been previously calculated in Eq.(3-27). For the above-mentioned principal hydraulic conductivities, K_{eq}=3.0552×10⁻⁶ m/s. Using this value for the hydraulic conductivity and above-mentioned criteria, the inflow rate to the tunnel is given as 55.82 m³/day for each meter of tunnel length (Fig 3-10). Comparing with the result of the proposed model (49.48 m³/day), the difference is approximately 11%; this shows the efficacy of the new proposed semi-analytical approach. In the same manner, several simulations were carried out by varying the assumed joint set characteristics, for different values of parameters. The comparative results obtained by the semi-analytical model and the numerical simulations are briefly presented in Table 3-4.

Table 3-4. Comparison of tunnel inflow rate values predicted by the new proposed semi-analytical model and a numerical simulation used as a control method

Discontinuities & tunnel characteristics	Depth below water table (m)	Inflow rate by new proposed semi-analytical model ((m³/day)/m)	Inflow rate by numerical model ((m³/day)/m)	Difference between numerical and semi-analytical results (%)
Joint sets (strike/dip): (100/40), (200/25), (45/10) Aperture (m): 10^{-6} Frequency: 8 Tunnel direction (trend/plunge): N31W,15	120	1.82×10^{-4}	2.16×10^{-4}	16
Joint sets (strike/dip): (130/80), (180/40), (290/55) Aperture (m): 10^{-4} Frequency: 2 Tunnel direction (trend/plunge): N41W,86	100	49.48	55.82	11
Joint sets (strike/dip): (120/10), (95/15), (220/20) Aperture (m): 10^{-5}, 10^{-4} and 10^{-4} respectively Frequency: 3, 2 and 4 respectively Tunnel direction (trend/plunge): N70E,12	90	26.9	31.1	13.5
Joint sets (strike/dip): (10/45), (20/70), (300/20) Aperture (m): 10^{-4}, 10^{-4} and 10^{-5} respectively Frequency: 5, 7 and 5 respectively Tunnel direction (trend/plunge): N70E, 30	160	129.4	104.2	19
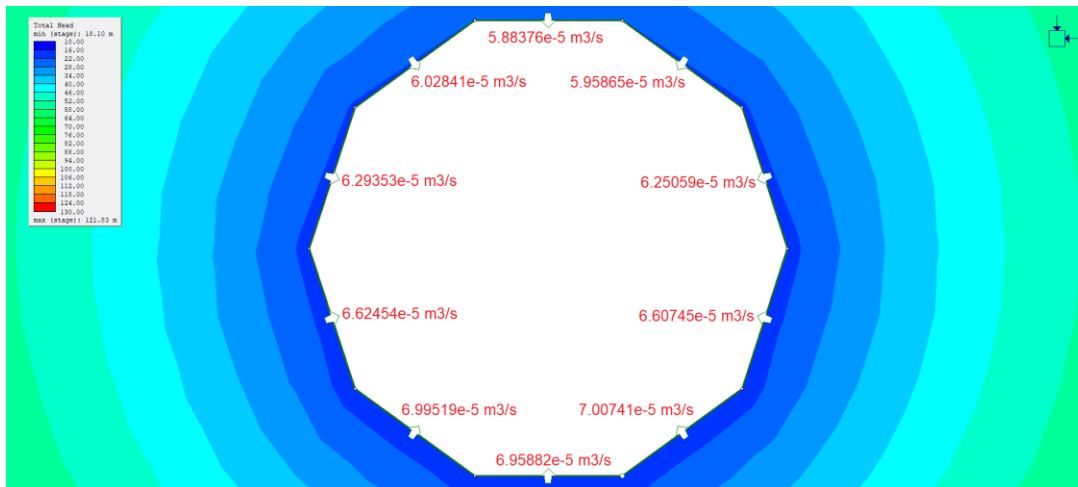
Fig 3-10. Inflow rate for each of the 10 sides of the tunnel; their sum is equal to 55.82 ((m³/day)/m)

3.5 SUMMARY AND DISCUSSION

This study proposes an enhanced semi-analytical approach to calculate the water inflow rate to a tunnel excavated in a rock mass. It considers a number of key effective parameters: orientation of the tunnel against the joint sets, fracture aperture and spacing, tunnel dimensions and tunnel depth below the water table, as well as the number of joint sets.

The inflow rate from each meter of tunnel length reaches its maximum value when the tunnel direction tends to be perpendicular to the normal to joint set; when the joint set deviates from this direction, the inflow rate will be diminished. In other words, the number of fracture traces in the tunnel wall will be increased when normal to joint set and tunnel direction approach the perpendicularity. The right side of Eq.(3-13) (after $cos\ \theta_i$) will be equal to 1 in the case of a perpendicular relative position and accordingly, q_{total} will be minimum if $\theta_i=0$. Based on Eq.(3-13), any increase in tunnel diameter, fracture aperture and/or fracture frequency will increase the inflow rate. The impact of hydraulic gradient on the inflow rate is obvious according to Darcy's law, as an increase in hydraulic gradient will increase the inflow rate accordingly. Concerning the effect of depth on inflow rate, it should be mentioned that two contrary phenomena operate at depth. On one hand, the hydraulic gradient will increase with the depth of excavation, as will the pressure head above tunnel crown. On the other hand, fracture apertures diminish as depth increases based on Eq.(3-16), thus reducing the inflow rate. Each parameter that shows the greater effect on the inflow rate will determine the increase or decrease of the inflow rate. Depending on the mechanical behaviour of the fracture at depth, as well as the surface characteristics being considered in the present model [167], the results will show that up to a specific depth, which will be defined by mechanical and geometrical characteristics of the fracture, the tunnel inflow rate increases and then decreases. As demonstrated in Fig 3-11, this is compatible with previous results [177] for the variation of the tunnel inflow rate as a function of depth.
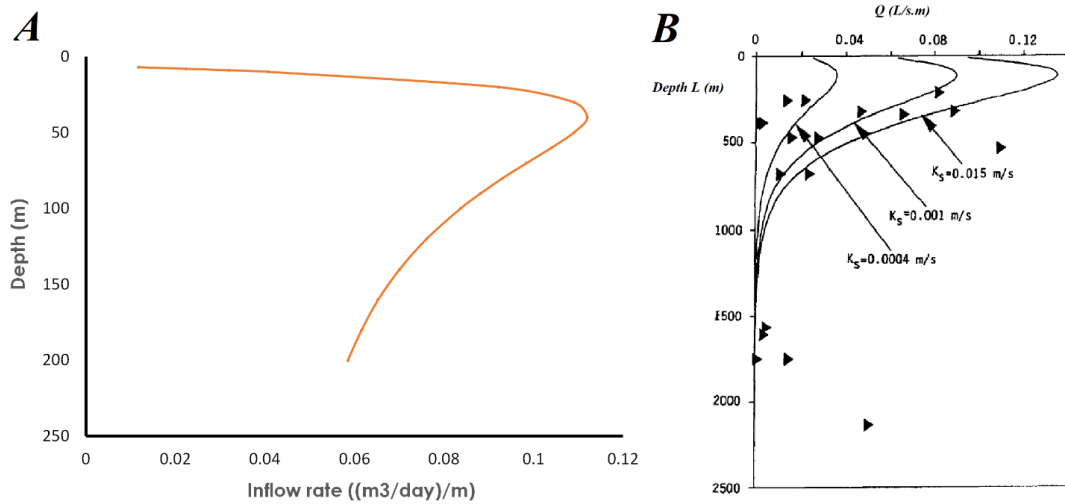
Fig 3-11. The variation of inflow rate into a tunnel with depth obtained from (A) the proposed semi-analytical model for a tunnel with a 1.5m radius and in a 45/45 direction. The water table is at 6m below the ground surface and rock mass includes 3 orthogonal joint sets with JRC=9, JCS=100MPa, aperture of 1e-4 m and spacing about 0.3m.(B) previous studies [177]

Eq. (3-13) considers the value of hydraulic aperture that exists in the wall of the tunnel. In order to define this parameter based on the measured mechanical aperture, several equations have been published [165]. The surface characteristics of the fracture is the parameter that mostly defines the relationship between hydraulic and mechanical aperture [67]. Therefore, in order to utilize the proposed method, it is necessary to define the joint characteristics, especially joint roughness coefficient (JRC), by in-situ tests, e.g., core logging, to define the hydraulic fracture aperture.

The most distinctive difference between the new proposed method and previously developed models is the way in which the hydraulic characteristics of the formation are considered. In our proposed model, the rock mass is regarded as a discontinuous body and in this regard, it is different from the formerly developed models (Table 2-5). These require an equivalent hydraulic conductivity of the formation in order to calculate the inflow rate, and therefore also require a pre packer/Lugeon test. In a rocky formation, the equivalent permeability that is measured from borehole testing is strongly affected by the orientation of the borehole and the location where the test is performed. To counter this limitation, in the new proposed model, the geometrical characteristics of the discontinuities were used to define the permeability of the rock mass by assuming the average value for aperture, spacing and orientation of each joint set. These data could be gained by surveying the discontinuities and using statistical methods to define the mean values of each parameter.

Considering the fractures as the sole conveying route for the flow of fluid into the tunnel makes their orientation a determining parameter in the calculation of the tunnel inflow rate. Therefore, it is expected that a maximum inflow rate occurs for a certain orientation of the tunnel, and using the proposed model, it is possible to find this direction as well as the direction having the minimum inflow rate.

When a tunnel is excavated, the existing hydraulic gradient is modified to a new condition: its direction will be mostly vertical. The projection of the overall hydraulic gradient in the plane of the fracture, on the other hand, will depend on the orientation of the fracture. Furthermore, the overall hydraulic gradient that is produced after excavation of the tunnel depends on the tunnel depth, ratio between hydraulic gradients and their orientations. Fig 3-8 illustrates that the variation of vertical hydraulic gradient at the wall of the tunnel by depth is linear, and more importantly, it does not depend on the hydraulic conductivity of the formation. This means that the vertical hydraulic gradient at the wall of an underground excavation is the same for the all formations, independently of their hydraulic conductivity. In Fig 3-12, the variation of i_z by Z and a at various α has been illustrated using surface diagrams.
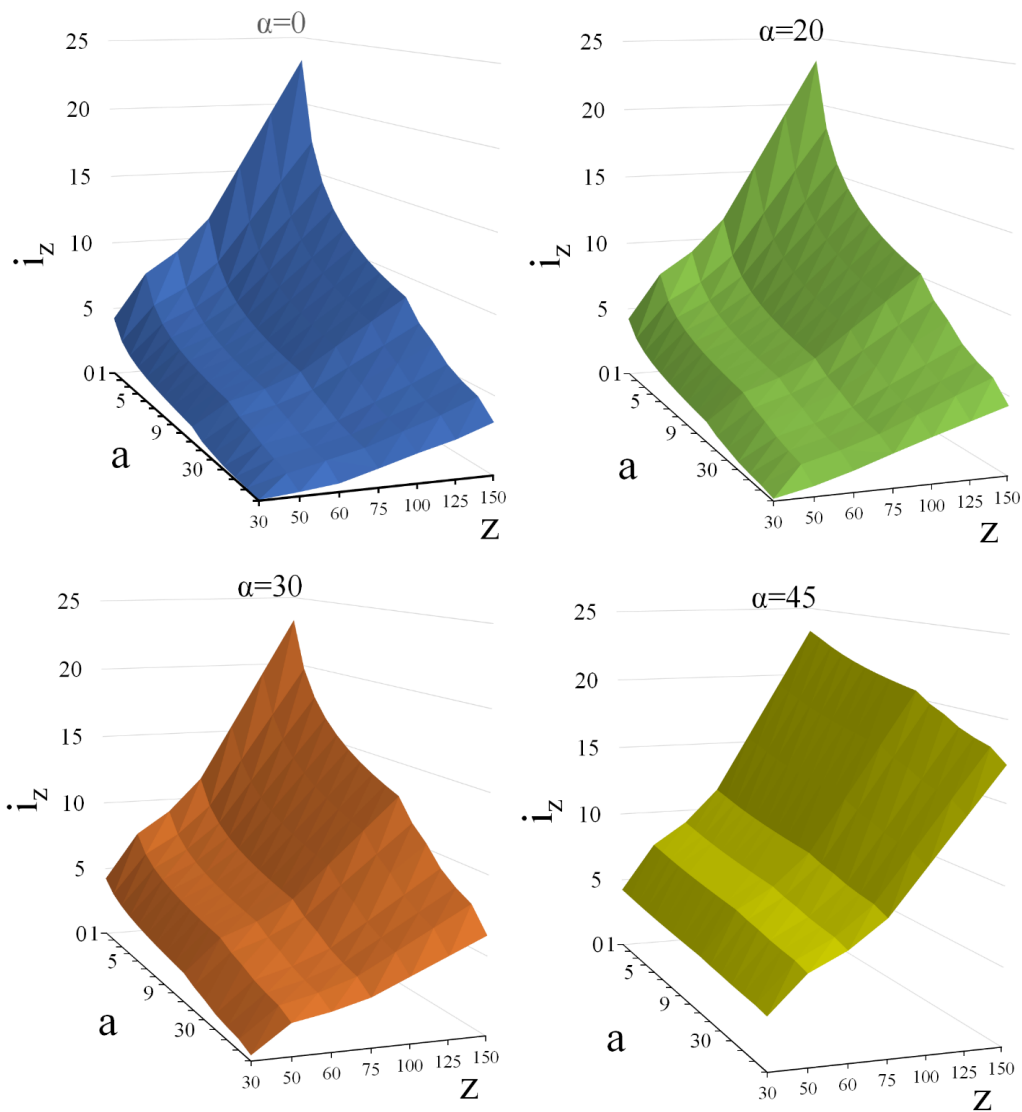
Fig 3-12. The variation of hydraulic gradient with depth (Z) and ratio of hydraulic conductivities (a) at different orientations (α)

According to Fig 3-12, the hydraulic gradient increases with the increase in depth and the decrease in *a*. Its variation is more sensitive to depth than to *a* in a constant *α*. Deviation of *α* from the horizontal direction will mostly affect the variation of i_z with depth rather than *a*. The minimum i_z is gained in shallow depths, high value of *a* and low value of *α*, and the maximum i_z will be gained in the opposite conditions. Therefore, the inflow rate is expected to reach its highest value in a homogeneous (minimum *a*) formation when its hydraulic conductivity is horizontally aligned (*α=0*). This condition will be satisfied in a rock mass with horizontal and/or vertical joint sets in which a tunnel is excavated horizontally.

Determination of the hydraulic gradient at the wall of an underground excavation is important because according to Darcy's law, it is not possible to define the inflow rate without knowing this parameter. In previously developed analytical methods, the hydraulic gradient was substituted in the equations by water head above the tunnel (h) that varies only with the variation of depth below water table and does not depend on the anisotropy of the hydraulic conductivity. The hydraulic conductivity that is defined by the proposed method is a dependent variable, as well. As a result, it is expected that the estimated inflow rate to the tunnel by this method may be more reliable than previously developed equations for rock mass formations.

3.6 CONCLUSION

A new semi-analytical model is developed to calculate the water inflow rate to a tunnel excavated below the water table. Unlike previously developed models, this proposed model is capable of measuring the inflow rate without pre-evaluation of the equivalent hydraulic conductivity of the formation by means of a Lugeon or packer test. However, it requires the definition of joint set characteristics (dip, dip direction, aperture and spacing) and water table level to measure the inflow rate to the tunnel. Hence, this proposed method considers the rock mass as a heterogeneous and/or anisotropic formation.

Furthermore, a numerical equation is developed to calculate the vertical hydraulic gradient in the wall of the tunnel; this value is meant to be inputted into the analytical series of equations that make up the new proposed method. Generally, in the case of underground excavations (and it is also true in the present study) the horizontal hydraulic gradient (i_x and i_y) is neglected as it is assumed that the water table is almost horizontal. It is deduced that the vertical hydraulic gradient at the wall of the tunnel (i_z), that is the determining factor of the inflow rate, is dependent on the depth of the tunnel (z), the ratio between principal hydraulic conductivities (a) and their orientation (α). Finally, for each orientation and using curve fitting, an equation is proposed for determination of the i_z. It should be noted that determination of the hydraulic gradient was not a focus of previous research works where models were based on presuming a homogeneous and isotropic formation and solving the Laplace equation.

3.7 CONFLICT OF INTEREST

The authors declare that there is no conflict of interest associated with this publication.

CHAPTER 4

Article 3: The specific length of an underground tunnel and the effects of rock block characteristics on the inflow rate

Alireza Shahbazi[*], Ali Saeidi, Romain Chesnaux, Alain Rouleau

Université du Québec à Chicoutimi, 555 boulevard de l'Université, Chicoutimi, Québec G7H 2B1, Canada

*Email: alireza.shahbazi1@uqac.ca

4.1 ABSTRACT

The specific length of a tunnel (STL) and a new analytical model for calculating the block surface area of the rock mass are introduced. First, a method for determining the appropriate length of a tunnel for numerical simulation is described. The length is then used to examine the correlation between the inflow rate to the tunnel and the block volume, the block surface area, and the fracture intensity (P_{32}) through analytical and numerical modelling. The results indicate that the length of the tunnel should minimally be equal to the least common multiple (LCM) of the apparent spacings of the joint sets at the wall of the tunnel to obtain the more reliable and immediate results for the inflow rate to a tunnel that is excavated in a fractured rock mass. A new analytical model was developed to calculate the block surface area and determine the essential joint set parameters, which include the dip, dip direction, and spacing. The determination of the rock block characteristics through numerical modelling requires considering the intact block for calculations. The results indicated that the inflow rate to the tunnel increased with increase in fracture intensity and decrease in block volume and surface area. The STL and the analytical model used for calculating the block surface area are validated through numerical simulations with 3DEC software version 7.0.

Keywords: Specific Tunnel Length, Block Surface, Analytical method, 3DEC, Rock mass, Inflow rate, Block volume

4.2 INTRODUCTION

Quality information on the inflow rate to an underground excavation is useful in a wide range of civil works. Taking into account the project requirements on the control of groundwater inflow during tunnelling [178], assessment of the stability of the rock blocks at the wall of the tunnel [179], tunnel lining design [180], probable damage to the tunnel support structure and lowering the tunnel excavation rate [181], and settlement of the aboveground buildings [182, 183] are some of the risks that relate directly to the rate of inflow to a tunnel and emphasize the significance of estimating the inflow rate. The inflow rate is also effectively a determining parameter for the cost of a civil and mining engineering project. Previous studies that aimed to estimate the inflow rate to a tunnel were developed through empirical, analytical, and numerical methods.

Many of the empirical equations that have been developed for estimating the inflow rate to a tunnel consider increasing depth, which results in the permeability of the rock mass decreasing and the hydraulic gradient at the wall of the tunnel increasing [9, 22, 184]. The developed empirical equations are based on data obtained from the double packer [6] or Lugeon tests [185] for the hydraulic conductivity of the rock mass. Several investigations have also been conducted for adjusting the relationships between the permeability of the rock mass and its geological indices [186, 187], e.g. RQD, RMR, and GSI.

The proposed analytical models for estimating the inflow rate to tunnels were developed with the assumptions of substituting the fractured or porous media through equivalent homogeneous and isotropic formations. The application of various boundary conditions and solving the Laplace equation then allowed the development of a set of equations for the calculation of the inflow rate to a tunnel [17, 188]. These equations could be applied to any tunnel excavated in a fractured rock mass using pre-determined values of its equivalent hydraulic conductivity using Packer or Lugeon tests. However, a minority of analytical methods that have been developed are not necessary for equivalent permeability [189], and thus, conducting a field test is essential before the application of the analytical models.

A wide range of studies has also focused on the determination of the inflow rate to a tunnel using numerical simulations. In this regard, the effects of geometrical characteristics of the rock mass, i.e., joint spacing, aperture, and orientation [190], as well as the overburden load/stress [191] on the inflow rate to the tunnel have been considered using a two-dimensional [23, 192] or three-dimensional [193, 194] model. Although the inflow rate increases by increasing the fracture aperture and decreasing the spacing, the effects of joint set orientation on inflow rate remains unclear. Furthermore, by increasing normal stress on a fracture plane, the fracture aperture decreases and any shear displacement results in a lower increase in fracture transmissivity and inflow rate. Among the above-mentioned parameters, the effects of the block characteristics on the inflow rate to a tunnel have not been well studied. In addition, no criterion has been determined for the length of the tunnel to be considered in the numerical simulations of the inflow rate.

In this study, the relationship between the inflow rate to a tunnel and rock block characteristics including block volume, block surface area, and volumetric fracture intensity (P_{32}) have been investigated using Itasca 3DEC version 7.00 software. 3DEC is a three-dimensional command-driven numerical program based on the distinct element method for discontinuum modelling. It is used to evaluate the response of the fractured media to the static or dynamic forces, and to carry out hydromechanical coupling simulations. Because the actual geometry of a rock mass is usually too complex for being simulated, similar to all other numerical models for this purpose, several simplifying assumptions are considered in this study. For a rock mass that includes less than three joint sets, randomly generated joints define the block volume; if more than three joint sets are present, only the three prominent sets are considered to determine the block volume [195]. Thus, it is assumed that the rock mass includes three joint sets with different orientations and spacings, but each set has a fixed value of these parameters. The length of the tunnel is defined by a newly proposed analytical method, called the Specific Tunnel Length (STL), which is adapted to a three-dimensional model as used in the current study, and yields more reliable results. The STL represents the minimal length of a tunnel that is representative of its entire length regarding its hydraulic characteristics. The STL is introduced as an important parameter because in all of the 3D numerical simulations, the length of the tunnel is a critical input parameter that strongly affects the value of the inflow rate. The length of the tunnel smaller than the STL value has been proven to mostly produce an error in the value of the

inflow rate because it is not representative of the complete hydraulic conditions observed along the tunnel. In contrast, the tunnel length larger than the STL will effectively increase the processing time of the numerical modelling without bringing more information. The optimum length of the tunnel for the numerical simulations in relation to hydraulic characteristics has been demonstrated to be equal to STL. The existence of the STL is supported by numerical simulations using 3DEC version 7.00 software. The last section of this paper focuses on the evaluation of the relationship between the tunnel inflow rate and three other parameters, which include block volume, block surface area, and volumetric fracture intensity. For this purpose, a series of numerical simulations have been conducted based on the already introduced specific length of the tunnel. In addition, an analytical model is developed for the calculation of the block surface area that is created by the intersection of three joint sets. Having the values of the inflow rate on the one hand and numerically and analytically calculated block volume, block surface area, and P_{32}, on the other hand, allows the investigation the effects of each parameter on the inflow rate.

4.3 SPECIFIC TUNNEL LENGTH

In all numerical models, the first and the most important concern is to determine the minimum reliable size of the model that is representative of its unlimited sizes. For the rock mass, this size was addressed in the literature as Representative Elementary Volume (REV), which could be defined for the mechanical properties [196] or hydraulic characteristics [197]. As a general rule, to gain reliable results from the numerical simulations, the model has to be equal or greater than the REV of the rock mass. However, in the case of excavating a tunnel in a fractured rock mass, the predefined REV is not appropriate for use in the calculation of the inflow rate to the tunnel. Thus, for a better understanding of the problem, Fig 4-1 shows a rock mass that includes three joint sets. It is assumed that the intact rock is impermeable and the fluid flows only through the fractures. Fig 4-1A shows the predefined dimension of the REV and the horizontal tunnels excavated in two different directions in Fig 4-1B and Fig 4-1C.

Joint set No.	Dip	Dip Direction	Spacing (m)
1	90	90	0.5
2	45	0	0.4
3	20	270	0.6
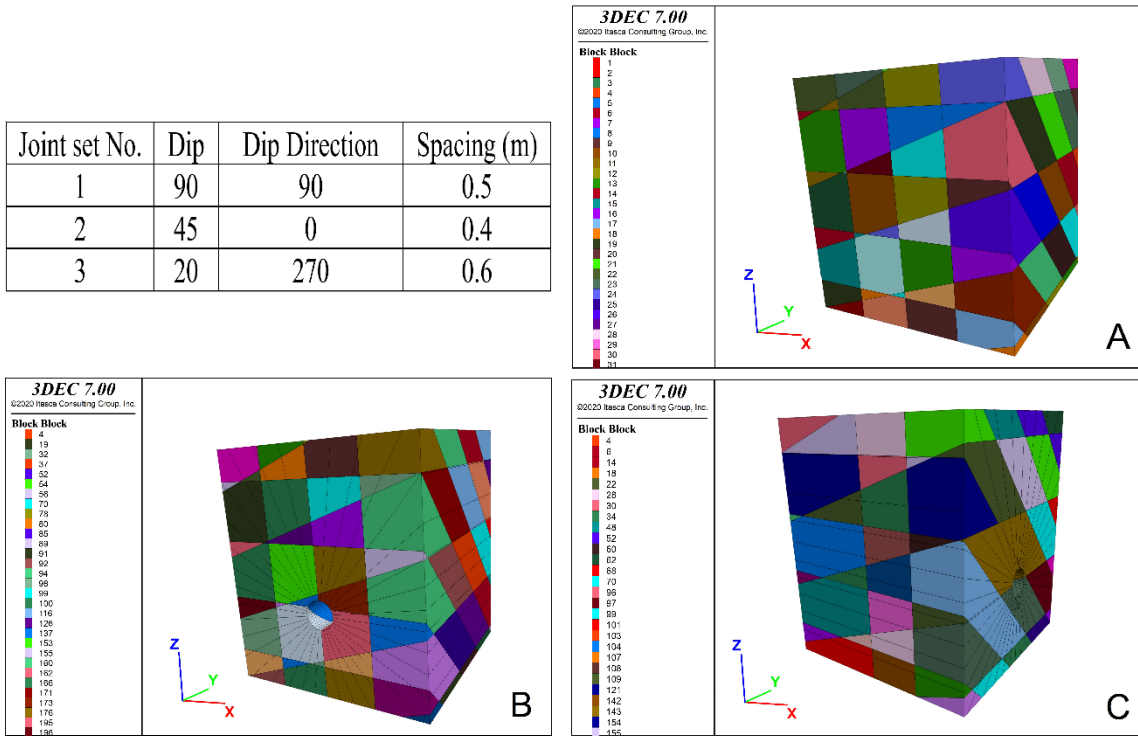
Fig 4-1. Modes of excavation of the tunnel in a fractured rock mass, (A) predetermined REV of the rock mass, (B) excavation of a horizontal tunnel in the y-direction of model A, (C) excavation of the horizontal tunnel in the x-direction

Based on Fig 4-1, the tunnel can be excavated in any direction in a REV of a rock mass. Despite the requirement that the REV of a specific formation should yield a unique hydraulic behaviour, Fig 4-2 shows that the number and total length of the fractures that cross the tunnel vary by changing their direction. Because the intact rock is presumed to be impermeable and if a fixed level of the water table is set for both models of Fig 4-2C and D, by variation of the trace length of the fractures at the wall of the tunnel (Fig 4-2A and B), the inflow rate to the tunnel will differ for the same length of the tunnel.
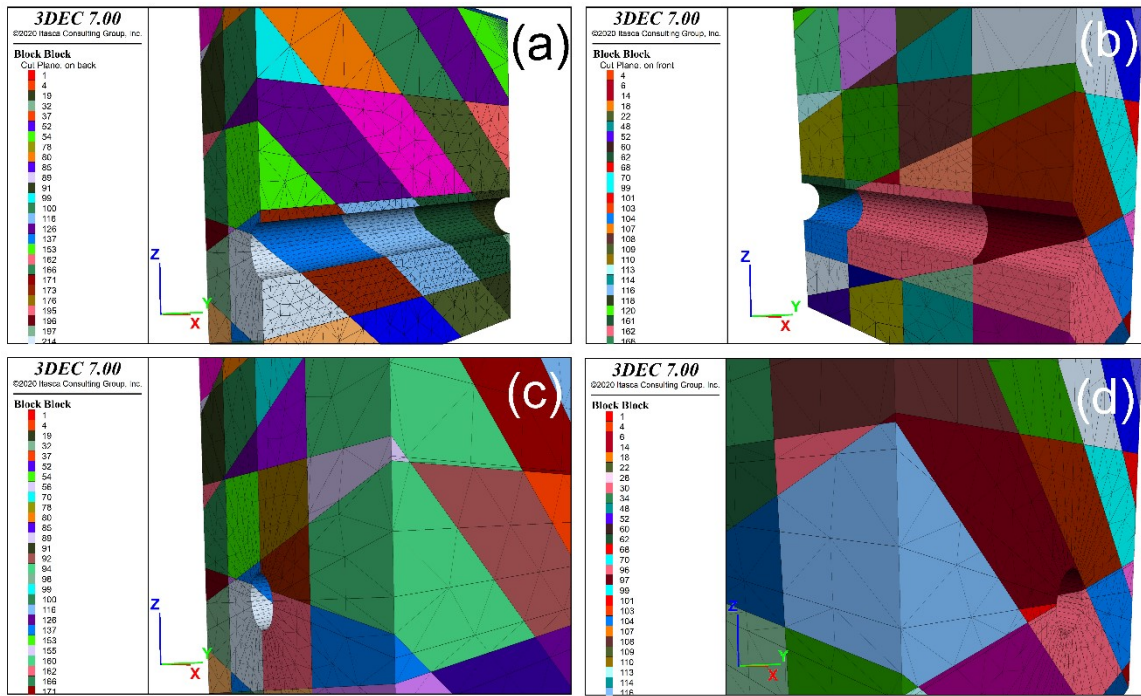
Fig 4-2. Longitudinal cross-section of the tunnel that is excavated in (a) x-direction, (b) y-direction, (c), and (d) original tunnel of the case (a) and (b), respectively

The differences observed in Fig 4-1 and Fig 4-2 illustrate the necessity of revising the concept of the hydraulic REV for the cases that a tunnel excavated in the rock mass. For this purpose, the hydraulic REV of a tunnel can be defined as the shortest length of the tunnel for which the inflow rate is representative of a unit inflow rate obtained from all hydraulic expressions of the fracture sets. This length is called the specific tunnel length or STL in this paper. In other words, the STL is the shortest length of the tunnel that integrates the flow rate contribution of the entire fracture sets (inflow rate per each meter of the tunnel length). Multiplying the inflow rate provided by the fractures along with the STL value by the total length of the tunnel divided by the STL value yields the total inflow rate through the tunnel. For a specific formation, different STL values exist for each direction of the tunnel and accordingly, the length of the tunnel in the numerical simulations should be equal to an integer multiplication of the STL to attain reliable results. In section 4.3.1 the method for defining the STL is described and the STL is validated in section 4.3.2.

4.3.1 Determination of the STL

To determine the STL, the joint sets are assumed to be persistent, the intact rock is impermeable, and fluid flows only through the fractures. Furthermore, the values of the spacing,

aperture, and orientation of the joint sets are fixed. Fig 4-3 shows the cross-section of the tunnel excavated in a rock mass having three joint sets. The apparent spacing that can be seen at the wall of the tunnel will always be equal or greater than the true spacing and the difference between the apparent and true spacings depends on the angle between the joint set and tunnel directions. As a reminder, true spacing refers to the shortest distance between two adjacent fractures of a joint set and apparent spacing refers to the observed spacing in any direction that is not essentially perpendicular to the plane of the joint set.
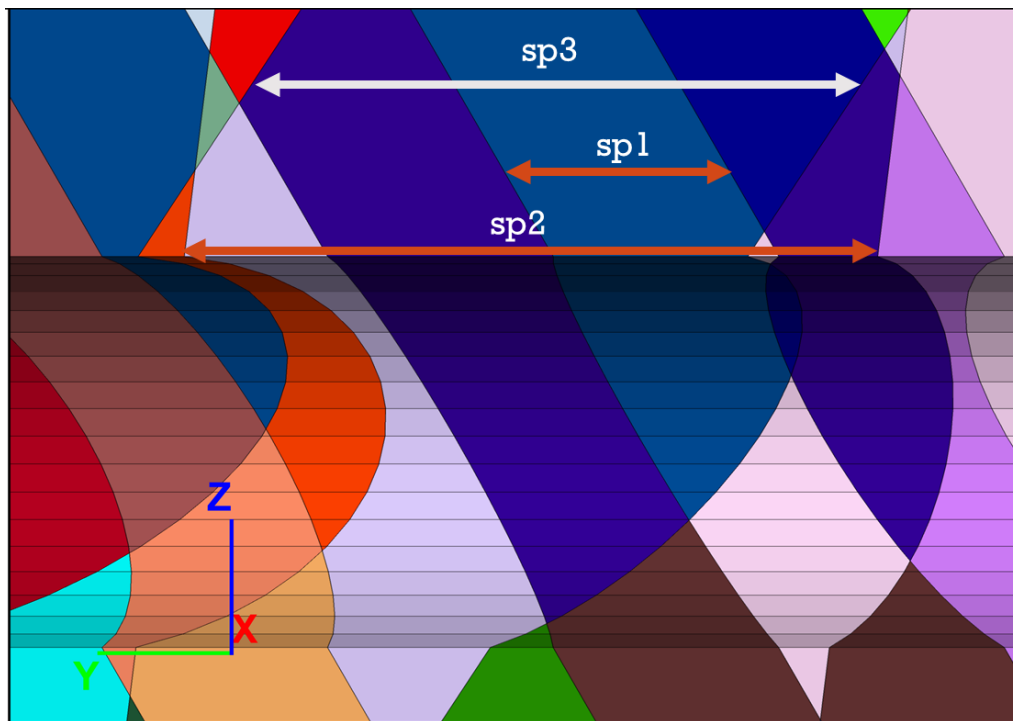
Fig 4-3. Apparent spacings of each joint set at the wall of the tunnel- sp1, sp2, and sp3 are the apparent spacings of the joint set 1, joint set 2, and joint set 3, respectively.

The fractures are assumed to be the sole channels for water flowing into the tunnel, and thus, to define the STL, the minimum length of the tunnel whose arrangement of the joint sets repeats at any multiple of STL (i.e., 1STL, 2STL, …, nSTL) should be defined. In this regard, Fig 4-4 illustrates the locations of the traces of each joint set at the wall of the tunnel. For simplicity, it is assumed that at the first point (zero points), the traces of all joint sets are overlapped. Thus, the same results for the value of the STL might be observed if the traces do not overlap at the initial point. As the apparent spacing of set 1 is 1, then it will be repeated at each multiple of 1, and similarly, joint sets 2 and 3 are repeated at each multiple of 1.5 and 2, respectively. According to the arrangement of the traces, all

traces overlapped again at points 6, 12, and 18. Furthermore, the sequences of the traces from point 1 to 6 are repeated in the ranges between 7 to 12 and 13 to 18.
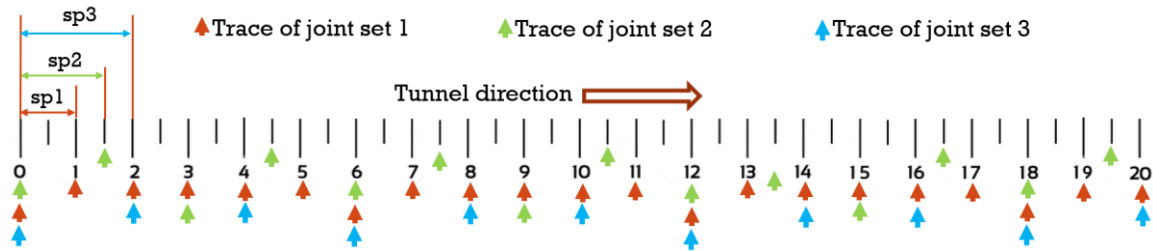
Fig 4-4. Locations of the traces of joint sets at the wall of the tunnel excavated in a rock mass and includes three joint sets- sp1, sp2, and sp3 are the apparent spacings of joint set 1, joint set 2, and joint set 3, respectively

By considering the repetition points (6,12, and 18), the first repetition point is found as the least common multiple (LCM) of the apparent spacings of joint sets at the wall of the tunnel, as in Fig 4-4, 6 is the LCM of 1, 1.5, and 2. Furthermore, the second and third repetition points are the integer multiples of the LCM. Therefore, the STL is equal to LCM of the apparent spacings of joint sets at the wall of the tunnel. The existence of the STL is demonstrated graphically in Fig 4-5. In this figure, the rock mass includes three joint sets with apparent spacings equal to 0.1, 1, and 6 meters. It is also evident that in each case, the sequence of the fractures in all spans along the tunnel direction with length equal to the STL is repeated in all next spans with the length equal to STL.
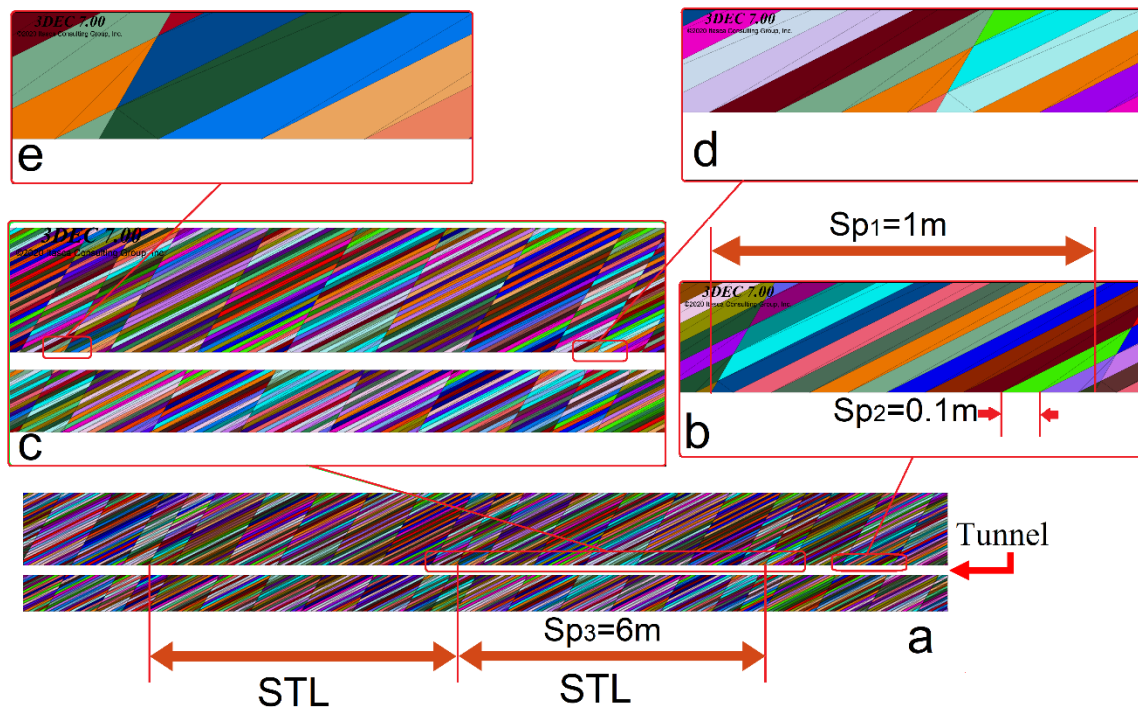
Fig 4-5. A rock mass including three joint sets with apparent spacings equal to 0.1, 1, and 6 meters, (a) cross-section of the tunnel along its direction showing the repeating pattern of the discontinuities in the direction of the tunnel and 3rd set's apparent spacing (6$_m$), (b) apparent spacings of 1st and 2nd joint sets, (c) close up of the section of the tunnel that includes STL, (d) and (e) close up of the beginning and end of the STL showing the existence of an analogous pattern at both ends

Before specifying the STL, the apparent spacings of each joint set at the wall of the tunnel should be determined. Based on Fig 4-6, the cross-section of the intersection of the cylinder (tunnel) and fracture plane is a circle perpendicular and ellipse in an oblique cross. The apparent spacing will increase accordingly by deviating from the perpendicular cross.
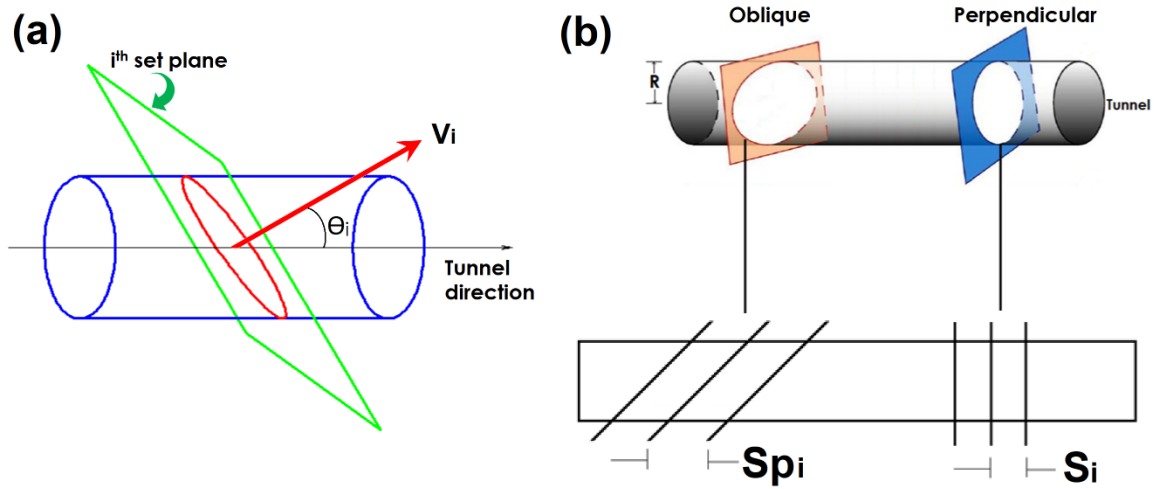
Fig 4-6. Specifying the apparent spacing of a joint set at the wall of the tunnel (a) Θ_i is the angle between normal to joint set and direction of the tunnel, (b) variation of the joint spacing by deviation from the perpendicular cross of the tunnel and fracture plane

The true and apparent spacings of set i are named as S_i and Sp_i, respectively, and the angle between normal to joint set i and tunnel direction is called Θ_i. Eq.4-1 expresses the relationship between apparent and true spacings.

$$Sp_i = \frac{S_i}{\cos\theta_i} \qquad \text{4-1}$$

The angle between normal to joint set and tunnel direction Θ_i could be specified by identifying the dip/dip direction of the joint set and direction of the tunnel. Components of the unit normal vector to the joint set i (direction cosines of V_i in Fig 4-6) can be specified according to Eq.4-2.

$$l_i = \sin(DD_i)\sin(D_i)$$
$$m_i = \cos(DD_i)\sin(D_i) \qquad \text{4-2}$$
$$n_i = -\cos(D_i)$$

where D_i and DD_i are the dip and dip direction of set i, respectively. Therefore,

$$\vec{V}_i = (l_i\vec{\imath}, m_i\vec{\jmath}, n_i\vec{k}) \qquad \text{4-3}$$

Furthermore, by identifying trend (T_T) and plunge (P_T) of the tunnel centreline, the components of the unit vector of the tunnel direction (V_T) are shown as Eq.4-4:

91

$$l_T = \sin(T_T)\cos(P_T)$$

$$m_T = \cos(T_T)\cos(P_T) \qquad \text{4-4}$$

$$n_T = -\sin(P_T)$$

The same could be defined for the unit vector of the tunnel direction:

$$\vec{V}_T = \left(l_T \vec{\imath}, m_T \vec{\jmath}, n_T \vec{k}\right) \qquad \text{4-5}$$

Meanwhile, the angle Θ_i will be specified using the inner product of vectors V_T and V_i as

$$\vec{V}_T.\vec{V}_i = |\vec{V}_T| \times |\vec{V}_i| \times \cos\theta_i \xrightarrow{|\vec{V}_T|=|\vec{V}_i|=1} \cos\theta_i = \vec{V}_T.\vec{V}_i \qquad \text{4-6}$$

Combining Eqs.4-2, 4-3, 4-4, and 4-5 with Eq.4-6 yields the following:

$$\begin{aligned}
\cos\theta_i = \vec{V}_T.\vec{V}_i &= \left(l_T\vec{\imath}, m_T\vec{\jmath}, n_T\vec{k}\right).\left(l_i\vec{\imath}, m_i\vec{\jmath}, n_i\vec{k}\right) = l_T l_i + m_T m_i + n_T n_i \\
&= [\sin(T_T)\cos(P_T) \times \sin(DD_i)\sin(D_i)] \\
&\quad + [\cos(T_T)\cos(P_T) \times \cos(DD_i)\sin(D_i)] + [\sin(P_T) \times \cos(D_i)]
\end{aligned} \qquad \text{4-7}$$

Finally, for a rock mass that includes three joint sets, the STL could be specified using Eq.4-8:

$$STL = LCM(Sp_1, Sp_2, Sp_3) = LCM\left(\frac{S_1}{\cos\theta_1}, \frac{S_2}{\cos\theta_2}, \frac{S_3}{\cos\theta_3}\right) \qquad \text{4-8}$$

where Sp_1, Sp_2, and Sp_3 are the apparent spacings and S_1, S_2, and S_3 are the true spacings of joint sets 1, 2, and 3, respectively. Furthermore, Θ_1, Θ_2, and Θ_3 are the angles between tunnel direction and normal to each joint set.

4.3.2 Validation of the STL

The existence of the STL in a rock mass that includes three joint sets is investigated and validated using the numerical simulation by 3DEC version 7.00 software. It should be emphasized that the rock mass could contain more than three joint sets and, in this case, the same method is applicable for defining the STL. Numerical models with various values of the apparent spacings (Sp_i in Eq.4-1) were prepared to evaluate the existence of the STL. Afterward, the inflow rates to the tunnels with a length of half STL, 1STL, 1.5STL, 2STL, and 3STL have been calculated. Fig 4-7 shows the models used for the numerical simulations. The x and z dimensions of the models are kept constant and only the y dimension varies to create the tunnels with different lengths.
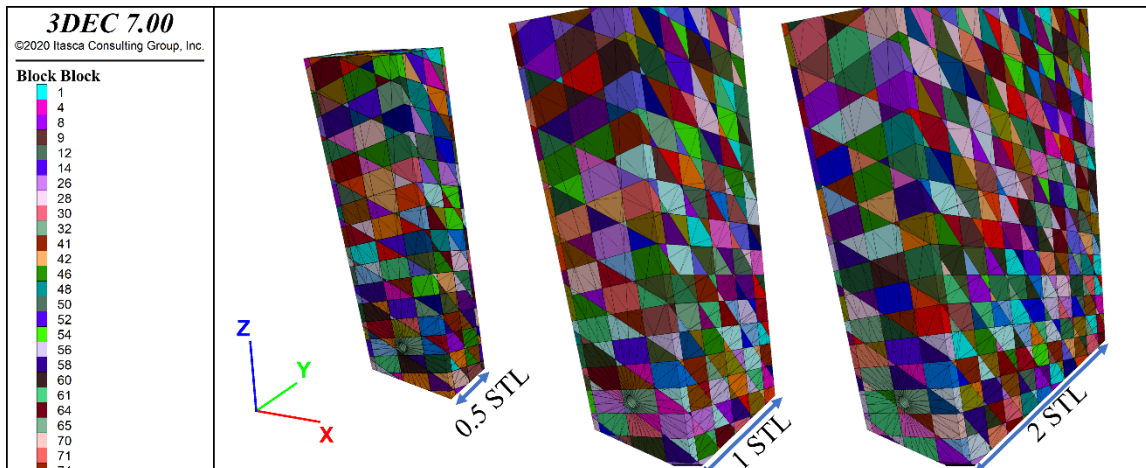
Fig 4-7. Numerical models for validation of the existence of the STL using 3DEC software- the tunnel in all cases is excavated in the y-direction (S-N)

Fig 4-8 illustrates the boundary conditions and the applied method for calculations of the inflow rate to the tunnel. As shown in Fig 4-8a, a fixed level of the water table is adjusted at the top of the model, and the pore pressure at sides of the model parallel to the *y-z* plane is set to be equal to its initial values during the numerical calculations. The pore pressure at the wall of the tunnel is set to be zero to simulate the inflow to the tunnel as shown in Fig 4-8b. Because the inflow rate decreases by moving from the tunnel wall toward the boundaries of the model, the area close to the wall of the tunnel is selected for the calculation of the inflow rate as shown in Fig 4-8c. Fig 4-8 shows that the spatial discretization must increase where hydraulic gradients are higher, as is the case when we get closer to the tunnel to decrease the time of the calculation and to maintain the accuracy of the results.
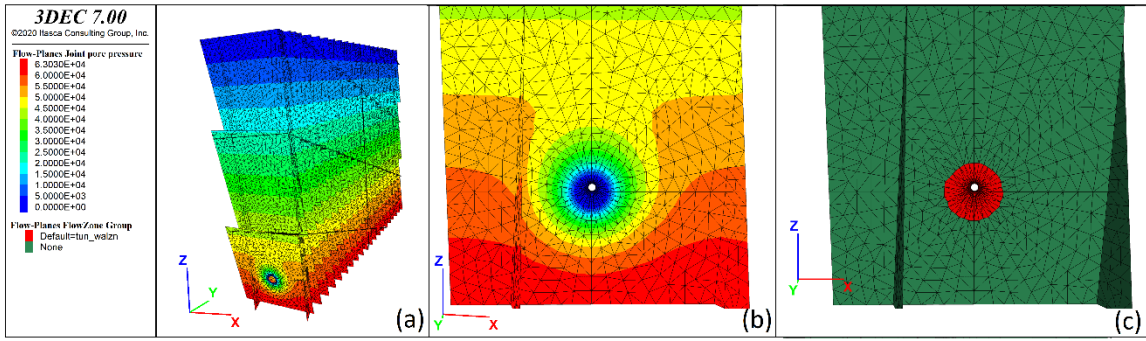
Fig 4-8. Boundary conditions and calculation methods applied in numerical simulations (a) flow planes or the planes of the fractures, (b) pore pressure around the tunnel in a flow plane, (c) flow plane zones selected for calculation of the inflow rate to the tunnel

In Fig 4-8, the flow plane is the planar polygon corresponding to face-to-face contact between solid blocks, the flow plane zone is a triangular discretization element of the flow plane, and the flowknot is the vertices of a flow plane zone that generally correspond to a sub-contact between solid blocks. To ensure that the model is in steady-state conditions, the variation of the pore pressure with cycling steps is recorded at four points around the tunnel circumference (the nearest flowknot to the wall of the tunnel at 3, 6, 9, and 12 o'clock positions). The model reaches the steady-state condition when the pore pressure at all points does not vary anymore.

Based on the results of the numerical simulations, it is observed that in all cases, the average inflow rate (inflow rate per meter of tunnel length) in 1STL, 2STL, and 3STL is equal and differs from what was calculated for 0.5STL and 1.5STL. In this study, the direction of the tunnel is always in S-N and the hydraulic apertures of all joint sets are set to be equal. However, it could be simply proved that the different hydraulic apertures of joint sets and tunnel direction do not affect the length and existence of the STL.

For this purpose, the STL is evaluated for five different cases according to Table 4-1.

Table 4-1. Joint set characteristics considered in the numerical models for assessment of the STL (DIP, DD, and S are the dip, dip direction, and true spacings of the joint sets, respectively)

Case No.	Joint set 1			Joint set 2			Joint set 3		
	DIP 1	DD 1	S1 (cm)	DIP 2	DD 2	S2 (cm)	DIP 3	DD 3	S3 (cm)
1	22	25	205.2	21	342	205.2	80	0	9.8
2	81	5	39.4	73	25	519.6	82	354	98.5
3	86	9	590.9	67	340	8.7	80	0	590.9

4	84	8	590.9	86	351	590.9	80	0	590.9
5	61	8	8.7	21	342	13.7	80	2	9.8

The hydraulic aperture and tunnel diameter in all cases were set to be equal to 1×10^{-4} (cm) and 20 cm, respectively to simplify the models and speed up the time of calculations. The level of the water table is fixed to 5 meters above the centreline of the tunnel in all cases. The apparent spacings relevant to Table 4-1 and unit inflow rate to the tunnel for each model are listed in Table 4-2.

Table 4-2. The apparent spacings (Sp1, Sp2, and Sp3) at the wall of the tunnel for each model, STL, and the value of the inflow rate to the tunnel for the tunnel length of 0.5STL, 1STL, 1.5 STL, 2STL and 3STL

				Inflow rate (m³/s) per meter of tunnel length				
Case No.	Sp1 (m)	Sp2 (m)	Sp3 (m)	STL (m)	0.5 STL	1.0 STL	1.5 STL	2.0 STL	3.0 STL
1	6	6	0.1	6	2.15E-08	9.35E-10	1.02E-08	9.35E-10	9.35E-10
2	0.4	6	1	6	7.15E-10	3.58E-10	9.41E-10	3.58E-10	3.58E-10
3	6	0.1	6	6	1.28E-08	1.51E-08	1.36E-08	1.51E-08	1.52E-08
4	6	6	6	6	5.96E-10	8.98E-10	1.50E-09	8.98E-10	8.98E-10
5	0.1	0.4	0.1	0.4	7.15E-10	8.28E-10	5.96E-09	8.28E-10	5.96E-10

Fig 4-9 is drawn based on the data provided in Table 4-2 and illustrates the equal inflow rate in 1STL, 2STL, and 3STL (and generally nSTL where n is an integer) as well as the different values for 0.5STL and 1.5STL. Regarding this figure and the spacings listed in Table 4-2, it is worth considering that the case numbers 1 to 5 are created by different arrangements of three apparent joint spacings, including 0.1, 0.4, and 6 m. It shows that the various values of the inflow rates may be obtained in different orientations of the tunnel. Furthermore, Fig 4-9 confirms that the value of the average inflow rate to each integer multiplication of the STL is equal to the average inflow rate to 1 STL and accordingly, it is equal to the infinite length of the tunnel. The deviation of the inflow rate for 0.5 STL and 1.5 STL with 1 STL is also decreased, indicating that the deviation will tend to zero by increasing the length of the tunnel when the length is not equal to the n×STL.
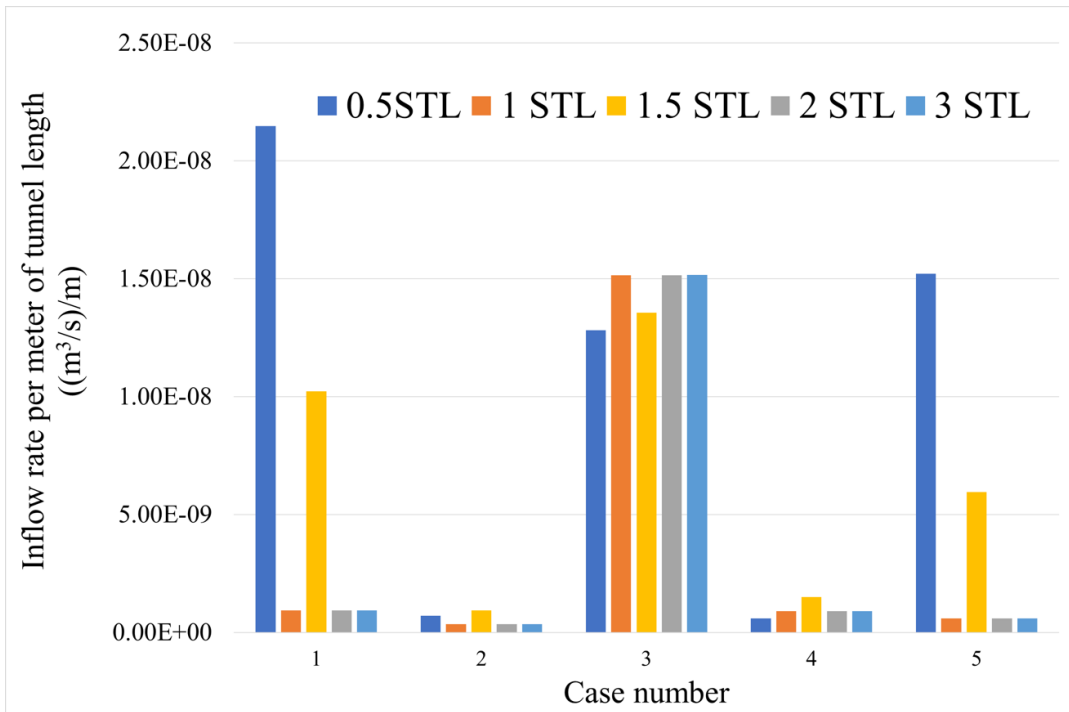
Fig 4-9. Average inflow rate to the tunnel for half STL (0.5STL), 1STL, 1.5 STL, 2STL, and 3STL-the diagram shows that the average inflow rate is equal for the tunnels with 1STL, 2STL, and 3STL but differs for the 0.5STL and 1.5STL

4.4 EVALUATION OF THE EFFECTS OF BLOCK CHARACTERISTICS ON THE INFLOW RATE

Using the concept of STL, which is explained and validated in section 4.3, a series of numerical simulations are designed to study the relationship between geometrical characteristics of the rock block, i.e., rock block volume, block surface area, and volumetric fracture intensity on the one hand and the inflow rate to the tunnel on the other hand. This section aims to define the parameter with the most important impact on the inflow rate to the tunnel. That parameter could be an efficient representation of the geometrical characteristics of the rock mass, e.g., spacing, dip, and dip direction of the joint sets [198, 199].

In this regard, numerical models comprised three joint sets with various spacings, dip, and dip directions. The tunnel is always excavated in the N-S direction and a fixed level of the water table is applied to the model. Because the orientations and spacings of the joint sets vary, the trace length of the fractures at the wall of the tunnel change, and the inflow rate will vary. Using a FISH function in the 3DEC commands, the block characteristics, as well as the inflow rate to the tunnel, are calculated numerically. The block volume and surface are calculated analytically using a formerly developed

analytical equation for block volume specification [195, 198, 200] and an analytical equation developed in this study for the block surface computation. Rather than a comparison of the results of the numerical and analytical block volume and block surfaces, a discussion on the reliability of the block volume and surface calculation is presented at the end of this section.

4.4.1 Analytical calculation of the block volume and surface area

For the evaluation of the effects of one parameter on the output of a model, it is mostly assumed that all variables are in their ideal conditions. For the case of a fractured rock mass, it is assumed that each joint set has a constant value of the spacing, orientation, and aperture, and that the persistence of the fractures is always 1, i.e., all the fractures cross the boundaries of the model. In the current study, it is assumed that the rock mass includes three persistent joint sets with fixed values of the spacings, dip, and dip direction for each joint set. In addition, the model does not contain random joints and the blocks are formed by the joint sets only. Based on the previous studies and the above-mentioned assumptions, [195, 198, 200] the volume of the block created by the cross of three joint sets could be calculated using Eq.4-9:

$$V_b^A = \frac{S_1 \times S_2 \times S_3}{\sin \gamma_1 \times \sin \gamma_2 \times \sin \gamma_3} \qquad \text{4-9}$$

where V_b^A is the analytically calculated block volume, S_1, S_2, and S_3 are the true spacings of joint sets, and γ_1, γ_2, and γ_3 are the angles between joint sets. For calculation of the surface area of a rock block created by three joint sets, an equation is mathematically developed using the methodology described briefly in Fig 4-10.
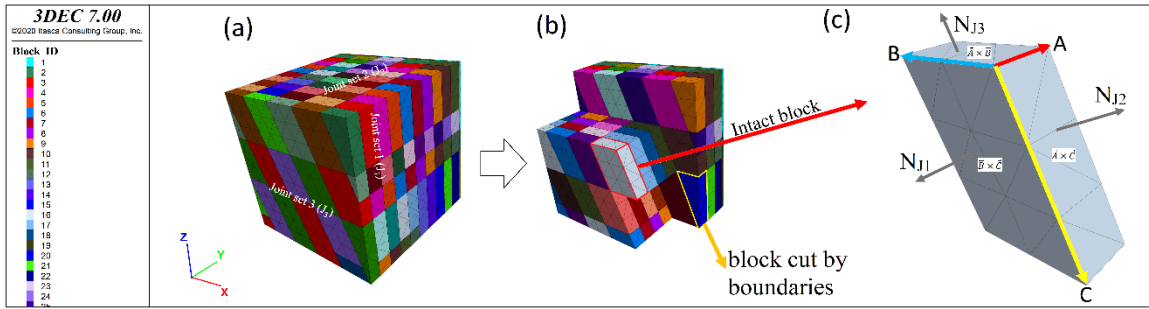
Fig 4-10. Methodology used for analytical calculation of the block surface area. (a) a model comprising of three joint sets, (b) selected block not cut by the boundaries of the model, (c) edge vectors and surface area of each side of the selected block

Except for the blocks cut by the boundaries of the model, the other blocks' geometries are identical. An intact block is selected for model development as illustrated in Fig 4-10b. Assuming that each edge of the block could be shown by a vector (A, B, and C in Fig 4-10c), the surface area of each face of the block can be determined by the cross product of each pair of vectors A, B, and C. The surface area of each frontside faces of the block are equal because all fractures in a joint set are parallel. Accordingly, the surface area of the block could be calculated by Eq.4-10:

$$S_b^A = 2 \times \left(|\vec{A} \times \vec{B}| + |\vec{A} \times \vec{C}| + |\vec{B} \times \vec{C}| \right) \qquad \text{4-10}$$

where S_b^A is the analytically calculated block surface and A, B and C are the edge vectors of the intact block. Each edge vector has a direction and a magnitude. The direction of a vector could be specified by a unit vector and for this specific case, it could be defined by Eq.4-11:

$$\vec{u_A} = \frac{\overrightarrow{N_{J2}} \times \overrightarrow{N_{J3}}}{|\overrightarrow{N_{J2}} \times \overrightarrow{N_{J3}}|}$$

$$\vec{u_B} = \frac{\overrightarrow{N_{J1}} \times \overrightarrow{N_{J3}}}{|\overrightarrow{N_{J1}} \times \overrightarrow{N_{J3}}|} \qquad \text{4-11}$$

$$\vec{u_C} = \frac{\overrightarrow{N_{J1}} \times \overrightarrow{N_{J2}}}{|\overrightarrow{N_{J1}} \times \overrightarrow{N_{J2}}|}$$

where N_{J1}, N_{J2}, and N_{J3} are the normal to joint set J_1, J_2, and J_3, and u_A, u_B, and u_C are the unit vectors of A, B, and C, respectively. On the other hand, by considering Fig 4-11, the magnitude of edge vectors is determined by Eq.4-12.

$$|\vec{A}| = \frac{S_1}{\cos\theta_1}$$

$$|\vec{B}| = \frac{S_2}{\cos\theta_2} \qquad \text{4-12}$$

$$|\vec{C}| = \frac{S_3}{\cos\theta_3}$$

where |A|, |B|, and |C| are the magnitude of each edge vectors, S_1, S_2, and S_3 are the spacings, and θ_1, θ_2, and θ_3 are the angles between normal to joint sets and direction of the edge vectors. These parameters are illustrated in Fig 4-11. The directions of the spacings S_1, S_2, and S_3 are parallel to N_{J1}, N_{J2}, and N_{J3}, respectively.
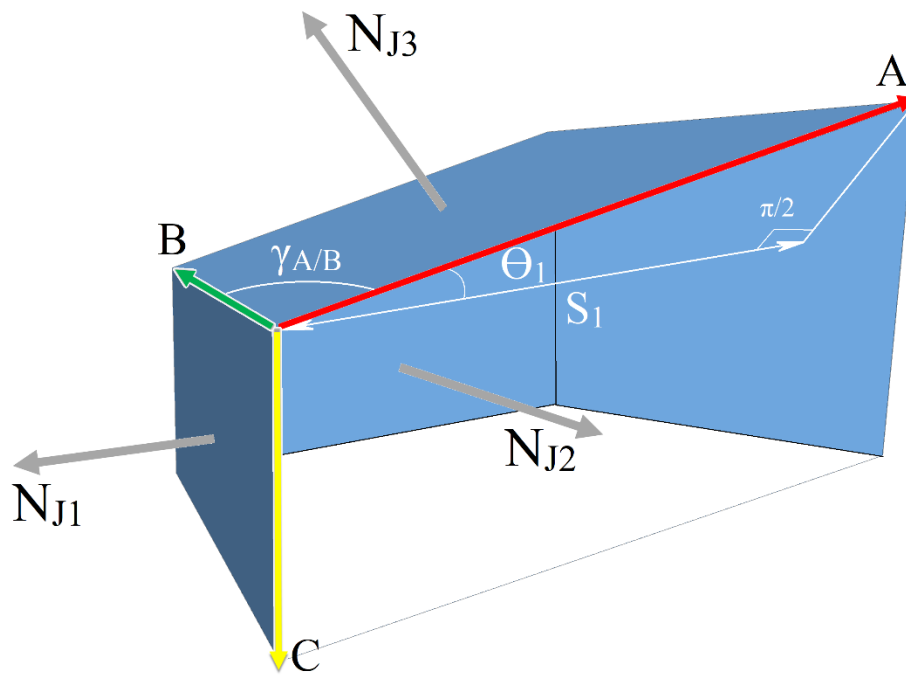
Fig 4-11. Inner view of an intact block. Edge vectors of the block and the angles between the true spacing of joint set 1 and direction of the edge vector A (θ_1). θ_2 and θ_3 could be specified with the same method. $\gamma_{A/B}$, $\gamma_{A/C}$, and $\gamma_{B/C}$ are the angles between edge vectors A&B, A&C, and B&C, respectively.

Based on Eq.4-12, to specify the magnitude of the edge vectors, θ_i should be determined. According to Fig 4-11, θ_i can be calculated by Eq.4-13:

$$\vec{u_A}.\vec{N_{J1}} = |\vec{u_A}| \times |\vec{N_{J1}}| \times \cos\theta_1$$

$$\vec{u_B}.\vec{N_{J2}} = |\vec{u_B}| \times |\vec{N_{J2}}| \times \cos\theta_2 \qquad \text{4-13}$$

$$\vec{u_C}.\vec{N_{J3}} = |\vec{u_C}| \times |\vec{N_{J3}}| \times \cos\theta_3$$

Given that u_A, u_B, u_C, and N_{J1}, N_{J2} and N_{J3} are unit vectors and their absolute values are 1, by combining Eq.4-11 and Eq.4-13, we can obtain the following:

$$\cos\theta_1 = \left(\frac{\vec{N_{J2}} \times \vec{N_{J3}}}{|\vec{N_{J2}} \times \vec{N_{J3}}|}\right).\vec{N_{J1}}$$

$$\cos\theta_2 = \left(\frac{\vec{N_{J1}} \times \vec{N_{J3}}}{|\vec{N_{J1}} \times \vec{N_{J3}}|}\right).\vec{N_{J2}} \qquad \text{4-14}$$

$$\cos\theta_3 = \left(\frac{\vec{N_{J1}} \times \vec{N_{J2}}}{|\vec{N_{J1}} \times \vec{N_{J2}}|}\right).\vec{N_{J3}}$$

Considering Eq.4-11, Eq.4-12, and Eq.4-14, vectors A, B, and C could be specified by Eq.4-15.

$$\vec{A} = |\vec{A}| \times \vec{u_A} = \frac{S_1}{(\vec{N_{J2}} \times \vec{N_{J3}}).\vec{N_{J1}}} \times (\vec{N_{J2}} \times \vec{N_{J3}})$$

$$\vec{B} = |\vec{B}| \times \vec{u_B} = \frac{S_2}{(\vec{N_{J1}} \times \vec{N_{J3}}).\vec{N_{J2}}} \times (\vec{N_{J1}} \times \vec{N_{J3}}) \qquad \text{4-15}$$

$$\vec{C} = |\vec{C}| \times \vec{u_C} = \frac{S_3}{(\vec{N_{J1}} \times \vec{N_{J2}}).\vec{N_{J3}}} \times (\vec{N_{J1}} \times \vec{N_{J2}})$$

It should be mentioned that the unit normal vector to joint sets (N_{J1}, N_{J2}, and N_{J3}) could be determined knowing the dip and dip direction of the joint sets, according to Eq.4-16.

$$\vec{N_{J1}} = (\sin DD_1 . \sin D_1)\vec{\imath}, (\cos DD_1 . \sin D_1)\vec{\jmath}, (-\cos D_1)\vec{k}$$

$$\vec{N_{J2}} = (\sin DD_2 . \sin D_2)\vec{\imath}, (\cos DD_2 . \sin D_2)\vec{\jmath}, (-\cos D_2)\vec{k} \qquad \text{4-16}$$

$$\vec{N_{J3}} = (\sin DD_3 . \sin D_3)\vec{\imath}, (\cos DD_3 . \sin D_3)\vec{\jmath}, (-\cos D_3)\vec{k}$$

where DD_1, DD_2, and DD_3 are the dip directions and D_1, D_2 and D_3 are dip of the joint set 1, 2, and 3, respectively. Finally, the surface area of the blocks could be specified by incorporating Eq.4-16 and Eq.4-15 into Eq.4-10. For calculation of the block surface using Eq.4-10, an excel sheet is prepared and attached to this paper.

4.4.2 Validation and comparison of the analytical models

As it is explained in section 4.4.1, the analytical method for calculation of the block volume was previously developed by Eq.4-9 and a new analytical model is developed in this article for calculation of the block surface according to Eq.4-10. In this section, the outputs of the analytical models for 13 cases that are listed in Table 4-3 are compared with the results of the numerical simulations using the 3DEC version 7.0.

Table 4-3. Characteristics of the discontinuities used for comparison of analytical and numerical calculation of the block volume and block surface and also assessing the effects of the block characteristics on the inflow rate to the tunnel

Case	Joint set 1			Joint set 2			Joint set 3		
	DIP 1	DD 1	Spacing 1 (m)	DIP 2	DD 2	Spacing 2 (m)	DIP 3	DD 3	Spacing 3 (m)
1	23	30	0.34	20	10	2.05	27	320	0.14
2	90	350	0.39	20	352	0.14	90	10	0.39
3	73	25	0.35	61	352	0.35	84	8	5.91
4	22	25	0.34	90	350	0.98	60	0	0.35
5	90	350	0.39	90	10	0.39	32	50	2.05
6	90	350	5.91	90	70	0.14	90	30	5.2
7	20	350	0.34	22	25	1.37	61	354	5.2
8	54	65	0.34	90	350	0.98	90	30	0.35
9	80	0	5.91	90	70	0.14	66	292	0.34
10	60	0	3.46	67	340	5.2	90	30	0.87
11	90	30	3.46	54	295	1.37	80	0	3.94
12	90	70	0.34	43	300	1.37	73	25	5.2
13	43	60	0.14	73	335	5.2	90	10	0.39

Based on the data listed in Table 4-3, a numerical model was prepared for the calculation of the representative block volume and surface for each case. For this reason, the volume and surface of the intact block, as illustrated in Fig 4-10c, should be specified. The most important point is to be certain that at least one intact block exists in the model. On the one hand, this block is representative

of all blocks of the model when the dimension of the model is unlimited and on the other hand, the intact block is created and its number increase by extending the size of the numerical model. From now on, the RBL, RBLV, and RBLS will be used in this article for referring to the representative block, representative block volume, and representative block surface, respectively. It should also be emphasized that the RBL is the intact block shown in Fig 4-10c. In Table 4-4, the results of the analytical and numerical calculations of RBLS and RBLV for the 13 cases of Table 4-3 are listed.

Table 4-4. Comparison of the analytical and numerical calculation of the block volume (RBLV) and block surface (RBLS) for the cases of Table 4-3. N/A means that the parameter is unmeasurable.

	Block surface (RBLS) (m^2)		Block volume (RBLV) (m^3)	
Case	Analytical (This study)	Numerical (3DEC)	Analytical [195]	Numerical (3DEC)
1	320.2	320.2	4.31	15.14
2	1.63	1.63	0.07	0.07
3	54.15	54.16	8.55	4.6
4	49.73	49.71	0.36	3.65
5	12.08	12.07	1.03	1.08
6	N/A	N/A	10.57	N/A
7	131.54	131.53	24.90	17.02
8	4.21	4.20	0.25	0.31
9	21.35	21.35	0.45	1.04
10	278.38	278.39	89.33	85.36
11	317.93	318.04	39.91	124.94
12	54.75	54.75	3.80	7.09
13	10.15	10.14	0.53	0.51

Based on Table 4-4, the analytical model for RBLS is in good accordance with the results of the numerical models; however, a remarkable discrepancy exists between the numerical and analytical calculations of the RBLV. Furthermore, for case number 6, the analytical and numerical model for RBLS and the numerical model for RBLV could not specify any value for these parameters because the constructed blocks are columnar and stretched in the *z*-direction (all dips are 90° with various dip directions). Therefore, by increasing the size of the numerical model, the RBLS and RBLV increase, and hence, the numerical RBLS and RBLV depend fully on the size of the numerical model. However, for such a case, the analytical model defines 10.57 m^3 for RBLV. Because of this

discrepancy and the existence of noticeable differences between numerical and analytical calculations of the RBLV, this method needs to be revised.

4.4.3 Evaluation of the effect of block characteristics on the inflow rate

The average inflow rate to the tunnel that is excavated in the *y*-direction (S-N) of a rock mass is calculated using 3DEC version 7 software for the 13 cases of Table 4-3.To simplify the model and place more focus on the effects of the block characteristics on the inflow rate, the hydraulic aperture is assumed to be constant for all joint sets, and a fixed level of the water table is applied to all of the models.

The variations on the unit inflow rate to the tunnel with the numerical and analytical RBLV for the cases of Table 4-3 and Table 4-4 are shown in Fig 4-12 in the logarithmic scale of the block volume. The inflow rate decreases with the increase in the volume of rock blocks. However, this dependency is a little more relevant for the numerically calculated RBLV than the analytical ones (based on the R^2 of the trendlines). The reason is probably because of the accuracy of the numerical models for calculation of the block volume compared with the analytical model. However, as a general rule, the inflow rate to the tunnel is expected to decrease by increasing the block volume.
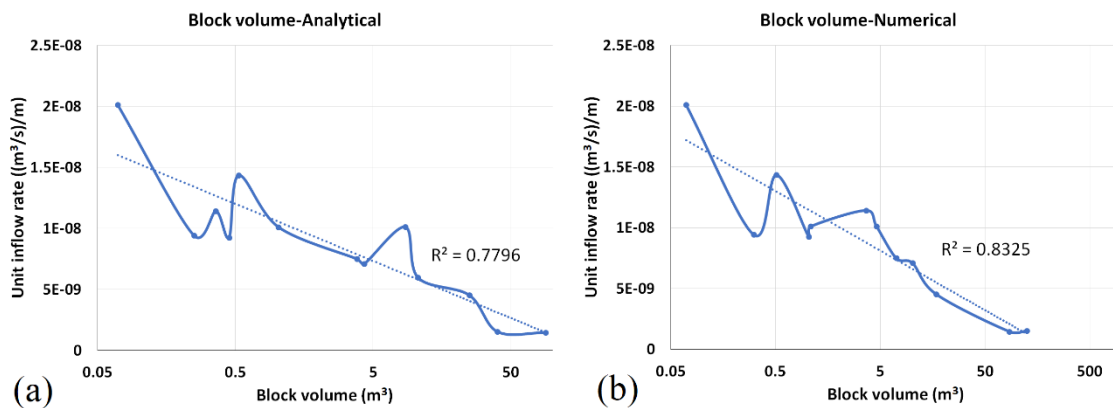
Fig 4-12. Relationship between inflow rate to the tunnel and logarithm of RBLV that is calculated using (a) analytical and (b) numerical methods

The relation between the logarithm of RBLS and inflow rate to the tunnel is illustrated in Fig 4-13. As the results of numerical and analytical models are almost the same, the diagrams in Fig 4-13 are identical. However, similar to Fig 4-12, the inflow rate to the tunnel decreases by increasing the

surface of the block although the relationship between RBLV and inflow rate seems to be more relevant than the RBLS and inflow rate.

(a)

(b)
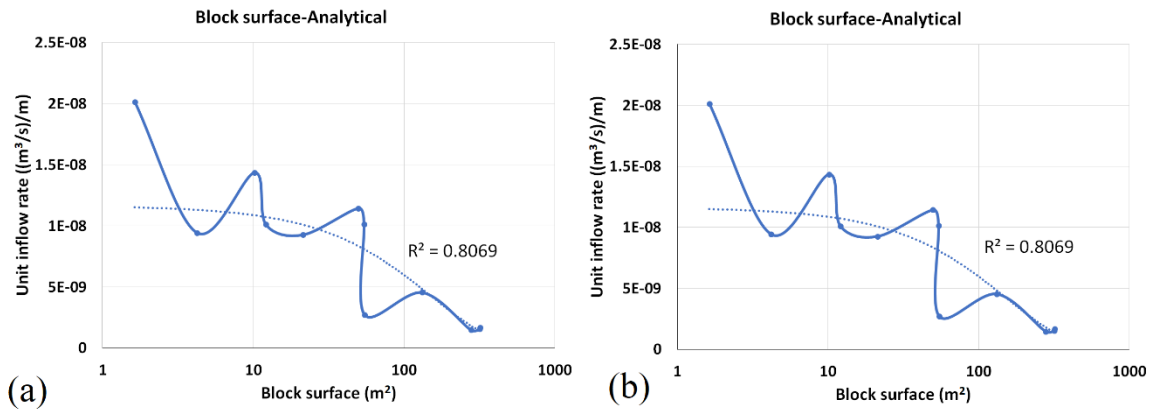
Fig 4-13. Relationship between the inflow rate and logarithm of RBLS calculated using (a) analytical and (b) numerical methods

Another block characteristic assessed in this study is the 3D volumetric fracture intensity or P_{32}, which is defined by Eq.4-17. The P_{32} represents the fracture area per unit volume of the block.

$$P_{32} = \frac{RBLS}{RBLV} \qquad 4\text{-}17$$

where P_{32} is the 3D volumetric fracture intensity. Based on the data presented in Fig 4-12 and Fig 4-13, the relationship between the inflow rate to the tunnel and P_{32} is illustrated in Fig 4-14. From analytical calculation of the block volume and surface, no logical relationship exists between the P_{32} and the inflow rate to the tunnel. However, the inflow rate to the tunnel increases by increasing the numerically calculated fracture intensity.
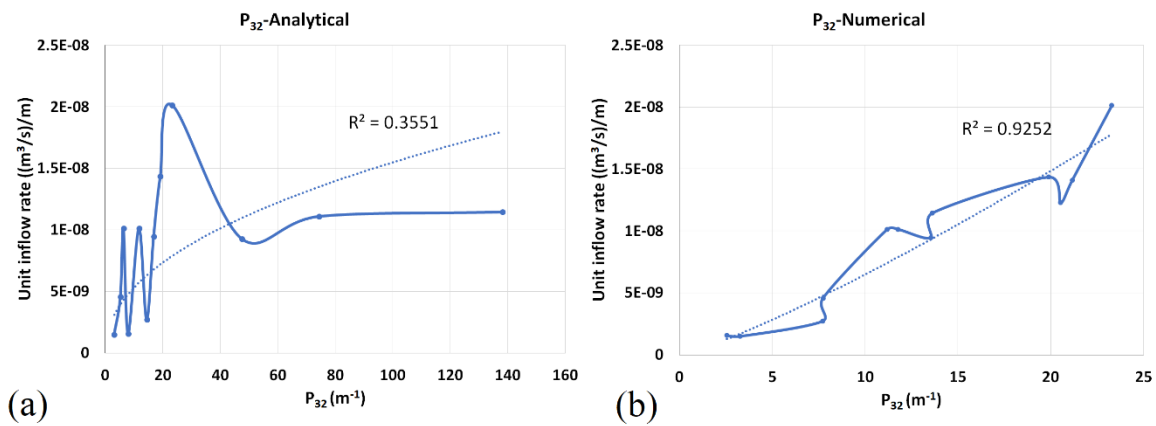
Fig 4-14. Relationship between the inflow rate and the 3D fracture intensity (P_{32}) that is calculated (a) analytically and (b) numerically

4.5 SUMMARY AND DISCUSSION

In all geomechanical and hydrogeological studies of the rock mass, the first step is to determine the reliable dimension of the rock mass that is representative of its unlimited size. In the case of excavation of a circular tunnel in a rock mass and for evaluation of the inflow rate, as the flow takes place through the fractures at the wall of the tunnel, the length of the fractures per surface area of the tunnel is the determining factor in this regard. Meanwhile, the surface area is defined by the tunnel radius and length, and since the radius is assumed to be constant all over the tunnel, the length of the tunnel is the parameter that its variation affects the inflow rate. With this approach, STL is the shortest length of the tunnel that integrates the flow rate contribution of the entire fracture sets, and hence, the inflow rate per meter of the tunnel length to the STL is equal to the average inflow rate to an unlimited length of the tunnel. As illustrated in Fig 4-15, the inflow rate to 1STL is equal to 7STL and generally, it will be equal to n×STL. As a result, the STL is the minimum length of the tunnel that could represent the hydrogeologic characteristics of the tunnel with unlimited length.

To specify the STL and simplify the numerical simulations, it was assumed that the hydraulic apertures of all joint sets are equal. However, different values of the hydraulic aperture do not affect the validity of the STL because that arrangement that exists in each STL, repeats at the subsequent multiple of STL and as a result, the inflow rate will be again equal for all next lengths equal to STL.
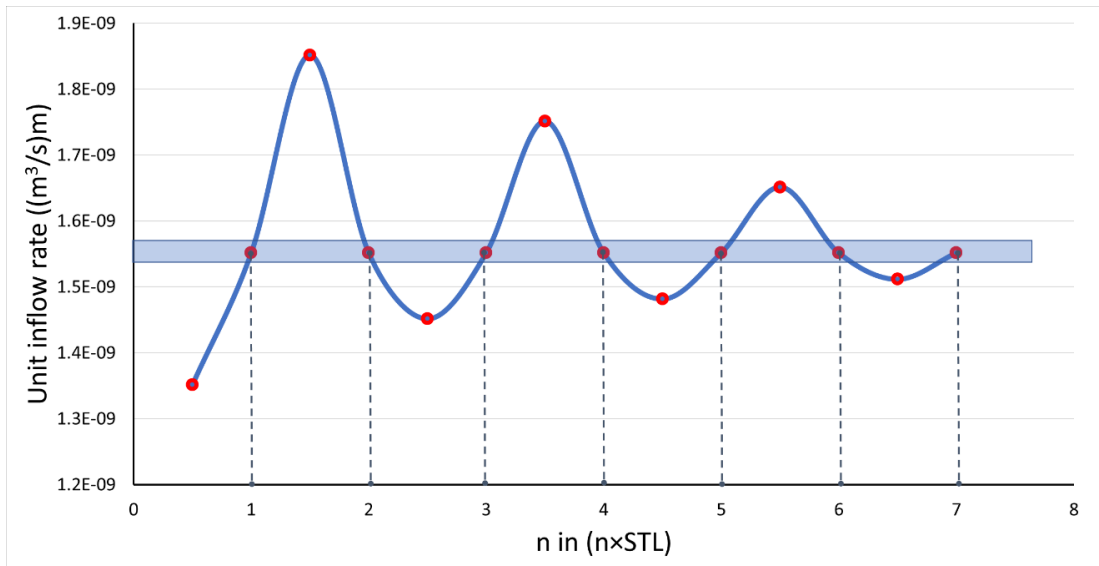
Fig 4-15. Variations of the inflow rate with the tunnel length as the multiple of STL for case number 10 of Table 4-3. The inflow rate to the tunnel with a length equal to 1STL is the same as that for the length of tunnel equal to n×STL.

All the apparent spacings at the wall of the tunnel are assumed to be integers to simplify the validation process of STL in section 4.3.2. However, the apparent spacings are mostly decimal values in nature. For example, if the apparent spacings of the three joint sets are 1.3, 0.4, and 2.7 meters, the LCM of the spacings or STL is 140.4. However, through a small variation of spacings to 1.5, 0.5, and 2.5 meters, the STL is 7.5 meters. In cases such as this, if the 7.5 m considered as the STL, the inflow rate varies in 2STL, 3STL, etc. comparing with STL. However, the variations of the inflow rate for 2STL and 3STL compared to STL is small enough to be neglected and the domain of variation decreases with the increase of n. Therefore, in such cases, the inflow rate to 1STL could provide an acceptable estimation of the inflow rate to nSTL and hence, it is recommended that the STL (or LCW) should be calculated by rounding the apparent spacings to an acceptable value.

STL is an important parameter for the evaluation of the inflow rate to the tunnel and is the minimum length of the tunnel that should be considered in the studies. Its importance is much more in three-dimensional numerical simulations because it is possible to excavate a tunnel in various directions in a rock mass and according to the direction, the probability of intersecting discontinuities by the tunnel will be different. As a result, the STL and inflow rate vary according to the tunnel direction, and hence, to simulate the inflow rate numerically, a specific STL should be defined for each direction of the tunnel. As the only joint sets that are parallel to the tunnel direction (when normal

106

to joint set is perpendicular to tunnel direction) are considered in 2-dimensional numerical simulations, in such cases, any length of the tunnel could be considered as STL, and as a result, the absence of the STL is one of the major weak points of 2-D modelling. In practical works and to design seeped water evacuating systems, consideration of the STL could be effectively useful for an acceptable estimation of the inflow rate to the tunnel.

An analytical method is developed for the calculation of the RBLS that is created by the 3 persistent joint sets, knowing their dip/dip directions and true spacings. This model accurately defines the unlimited surface area for the blocks that are created by 3 vertical joint sets having different values of dip directions. However, analytically calculated RBLV for such cases is not unlimited and thus, Eq.4-9 is not sufficiently comprehensive at all. Furthermore, the results of the developed model for the calculation of the RBLS are validated by numerical simulations using 3DEC software. It is although the results of the previously developed model for specifying the RBLV (Eq.4-9) have a debatable difference with the 3DEC software results (Table 4-4).

To numerically specify RBLV and RBLS, the size of the numerical model increases until at least one block among all blocks of the model reaches its maximum possible size. If the block characteristics are in interest, in such a state, the model is not in its representative size. In this regard, the size of the model should be increased until the average block size tends to the RBLV. This size maybe not equal to the representative size of the model when the other parameters of the rock mass such as spacing, aperture, etc. are in interest. Therefore, it is essential to define a separate REV for each interesting characteristic of the rock mass and discontinuities, the same as what was defined for STL in section 4.3.

The block volume and surface that are defined by the numerical simulations should be evaluated carefully before being used in the studies, as the average and maximum block size and surface area that is defined might be different for one specific model with various sizes. Furthermore, these characteristics are highly affected by the arrangement of the discontinuities, i.e., the start point for the generation of the joint sets in numerical models. For avoiding this error, either the size of the numerical model should be large enough to include mostly the RBLs, or just the analytically calculated block volume/surface should be used.

107

Based on Fig 4-12, Fig 4-13, and Fig 4-14, it is specified that a relevant relationship exists between the inflow rate to the tunnel on the one hand and numerical RBLV, numerical and analytical RBLS, and numerical P_{32} on the other hand. According to the coefficients of determination (R^2) of each diagram, it could be concluded that the relationship between P_{32} and inflow rate is more relevant than the other parameters and hence, P_{32} could be used for the prediction of the inflow rate to the tunnel that is excavated in a rock mass. The advantage of using block characteristics for estimation of the inflow rate is that the RBLV, RBLS, and P_{32} could be representative of spacing, dip, and dip direction of joint sets and in this regard, various interesting parameters in the studies could be summarized in one parameter.

4.6 CONCLUSION

Before the calculation of the inflow rate, it is necessary to determine the minimum length of a tunnel that should be considered to obtain representative values of the inflow rate for the entire tunnel length. This STL is equal to the LCM of the apparent spacings of the joint sets at the wall of the tunnel. Using numerical simulation with 3DEC version 7.0 software, the unit inflow rate (inflow rate per each meter of the tunnel length) has been shown to be constant for any subsequent integer multiple of the STL (n×STL). Accordingly, the STL is also verified to be the representative length of the tunnel for hydrologic purposes. In developing the STL, the discontinuities are assumed to be persistent and the joint sets are in their ideal states, i.e., with fixed values of spacing, aperture, and orientation. Hence, the STL is recommended to be considered as the representative length of a tunnel to gain immediate and reliable results in all numerical studies relating to the evaluation of the inflow rate to a tunnel, especially in three-dimensional numerical simulations. In addition, more reliable estimates of the inflow rate could be obtained by considering STL in underground works, such as excavation of an underground tunnel. The STL value can be estimated when the dip, dip direction, and spacing of the joint sets are known and is independent of the hydraulic aperture.

Block surface area is an important parameter in the geomechanical and hydrological investigations of a rock mass. An analytical model is developed for calculating the block surface area when the orientations and spacings of the joint sets are known. The accuracy of the model is supported using the results of the simulation using the 3DEC software. The block surface area

measured by the numerical models are shown to be possibly misleading because of the boundary effects as several blocks are often cut along the model boundaries. This error can be reduced by considering a simulation domain large enough to include a larger number of RBLS.

An analytical model that was previously developed for the calculation of the block volume for the case of three joint sets is used in this article. This model needs to be revised because a comparison of the results of the model with the output of the numerical simulation shows a significant difference. Block size is a very important parameter and is widely used for predicting the geomechanical and hydrological behaviours of the rock mass. Therefore, the acceptable accuracy of this parameter could guarantee the reliability of all other dependent parameters.

The relationship between the inflow rate to the tunnel and the RBLV, RBLS, and P_{32} are investigated. We observed that the inflow rate to the tunnel decreases by increasing the RBLV. Almost similar but weaker relationships can be observed between the RBLS and the inflow rate to the tunnel. Furthermore, the inflow rate increases by increasing the volumetric fracture intensity (P_{32}), and this relationship is more relevant than the relationship between the RBLV, RBLS, and inflow rate. As a result, RBLV, RBLS, and P_{32} could be representatives of several geometrical characteristics of the rock mass, e.g., joint set orientations and spacings. Hence, new relationships could be developed for the calculation of the inflow rate to the tunnel as a function of block characteristics. From a practical point of view, the rock block characteristics could be used in the estimation of the inflow rate to a tunnel. As a general rule, a higher inflow rate should occur in a tunnel excavated in a rock mass with smaller blocks.

4.7 CREDIT AUTHORSHIP CONTRIBUTION STATEMENT

Alireza Shahbazi: Methodology, Software, Validation, Writing - original draft; Ali Saeidi: Supervision, Writing - review & editing; Romain Chesnaux: Supervision, Writing - review & editing; Alain Rouleau: Supervision, Writing - review & editing

4.8 DECLARATION OF COMPETING INTEREST

The authors declare that there is no conflict of interest associated with this publication.

4.9 ACKNOWLEDGMENTS

CHAPTER 5

Article 4: Effects of fracture system geometrical parameters on the inflow rate into a tunnel in rock: a numerical modelling experiment

Alireza Shahbazi[*], Ali Saeidi, Romain Chesnaux, Alain Rouleau

[1]Université du Québec à Chicoutimi, 555 boulevard de l'Université, Chicoutimi, Québec G7H 2B1, Canada

*Email: alireza.shahbazi1@uqac.ca

5.1 HIGHLIGHTS

- ☐ Individual and interactional effect of parameters on the inflow rate is determined

- ☐ An empirical-numerical model is developed to calculate the inflow rate to the tunnel

- ☐ Response surface methodology is used for designing the numerical simulations.

- ☐ Hydraulic aperture is the most effective parameter on controlling the inflow rate

- ☐ The tunnel radius has limited impact on the unit inflow rate to the tunnel

5.2 ABSTRACT

The relationship between the inflow rate to a tunnel excavated in a fractured rock mass and the effective parameters controlling the inflow rate, such as hydraulic aperture, spacing, orientation, tunnel radius, and water head above the tunnel, is investigated through numerical modelling. Response surface methodology is adopted to optimize the number of numerical simulations and their meaningful interpretation, and Design-Expert version 11 software is used for this purpose. Consequently, numerical simulations are performed using 3DEC version 7 software for 88 scenarios based on different values of parameters related to fracture system geometry and boundary conditions. Accordingly, the relations between the inflow rate to the tunnel and the effective parameters as well as their interaction are determined and presented in the form of empirical equations. In addition, the mean value of each parameter is used to develop another equation for calculating the inflow rate to the tunnel. Specifically, the hydraulic aperture and spacing, as well as the interaction between the two parameters and other effective parameters, have the most important impacts on the value of the inflow rate. In addition, the impact of tunnel radius on the unit inflow rate

is negligible. In this regard, using numerical simulations, two empirical equations, which are directly available for practitioners, have been developed for the calculation of unit inflow rate values to the tunnel: one for exact values of parameters and another for their mean values.

Keywords: Tunnel inflow rate, Rock mass, Response Surface Methodology (RSM), 3DEC, Empirical equations

5.3 INTRODUCTION

One of the main concerns in underground excavations, especially tunnelling and subsea tunnels, is the amount of water flowing into the tunnel [201]. The excavation of a tunnel at a depth below the water table has impacts on hydrology, ecology, and the environment [202]. An accurate estimation of the inflow rate to a tunnel is crucial considering the economical and safety aspects of the underground excavations. The overestimation of the inflow rate may result in over-design of the water evacuation system [203], while an underestimation may hinder or stop the excavation progression by causing geomechanical instability [157], mud and water inrush [204], and environmental impacts [205]. Accurate estimation of the inflow rate has a high degree of importance in assessing the safety requirements of special excavations, such as subsea tunnels [206], where specific equations are developed for defining the inflow rate. The evaluation of the inflow rate to the tunnel is generally conducted using three main categories of methods: empirical, analytical, and numerical. However, combinations of these categories have also been developed [189, 207].

Empirical methods for inflow rate estimation are mainly based on data obtained from the field or experiments and are mostly based on hydrogeological and geotechnical information. On this basis, site groundwater rating (SGR) [208] and tunnel inflow classification (TIC) [209] have also been proposed to determine water inflow into tunnels. In this regard, SGR is a tunnel rating method in the groundwater hazard viewpoint, and TIC is a method used to evaluate the tunnel underwater inflow in various complicated geological conditions. In addition, Gattinoni [22] and Heuer [83] empirically corrected the Goodman equation [17] for inflow rate estimation by adding a corrective coefficient and modifying analytical equations.

Most prediction methods for inflow rate to a tunnel use analytical modelling, which is mainly based on the fundamental fluid flow equations (i.e., Laplace equation, Darcy and Cubic laws). Based on these equations, analytical models are developed for fractured, porous, homogeneous, and heterogeneous formations, wherein a tunnel with different cross-sections, linings, and grouting is excavated. Considering different solving methods for obtaining the inflow rate equation (flow in the fractured network instead of porous media) and by application of various boundary conditions, a series of analytical equations were developed for calculating the inflow rate [189, 210] with the assumption of laminar fluid flow. However, other studies also considered a turbulent fluid flow (nonlinear flow) in the development of the analytical models [211, 212]. The weakness of the analytical models lies in their possible oversimplification of the reality by focusing on various simplifying assumptions; for example, considering that the excavated tunnel is perfectly horizontal and drilled within a homogeneous and isotropic aquifer with steady-state flow conditions.

The inflow rate to a tunnel could also be evaluated using numerical tools. However, contrary to empirical and analytical models, numerical modelling is not applied for the development of specific equations, allowing the prediction of the inflow rate to a tunnel. Meanwhile, numerical methods are mainly used for two-dimensional modelling of inflow rate [190] and sensitivity analysis for measuring the impacts of input parameters [213] or lining [181] on the inflow rate by using continuous [164] or discontinuous approach [214]. The accuracy of the predicted inflow rate could be highly improved by using three-dimensional numerical simulation methods and considering the effective parameters. In conjunction with experiment design, numerical simulations could also facilitate a possible definition of the interactional effect of parameters on the inflow rate and assign an equation for the inflow rate calculation by the input parameters. The objectives of this article are defined on this basis.

This article proposes a new approach for calculating the inflow rate to a tunnel excavated in a fractured rock mass that includes three persistent joint sets. This approach is developed by running a series of numerical simulations that are designed by response surface methodology (RSM). The RSM is a useful statistical and mathematical method for modelling a process, in which a relationship exists between the response and various variables, by designing the number and types of the required experiments. First, the effective parameters for the inflow rate are selected on the basis of

the literature review; these parameters include aperture, spacing and orientation of joint sets, water head above tunnel, and tunnel radius. Notably, the angle between the normal to a joint set and the tunnel direction has been considered in this article instead of the orientation of joint set; thus, instead of two parameters (dip & dip direction), a single angle parameter is considered in the simulations. Second, by defining the variation range of each parameter according to the existing classifications (ISRM classification, RMR table), the type and number of the required numerical simulations for defining the relationship between inflow rate and effective parameters are specified by Design-Expert software. Consequently, an equation showing the relationship between the inflow rate and the effective parameters is defined and compared with the results of a previously developed analytical model. This equation might be long and complicated to use. Thus, another equation is introduced for the relationship between the inflow rate and the mean value of each parameter. Notably, no similar investigation has been reported thus far for predicting the inflow rate using the results of 3D numerical simulation. In addition, the individual effect of each parameter and the interaction between them on the inflow rate to the tunnel are investigated by using the RSM. From a practical viewpoint, the proposed equations could be helpful for the geological engineers to estimate the inflow rate by identifying the effective parameters through fracture surveying. In addition, a reasonable estimation of the inflow rate before excavation is possible and will help plan preventive measures against the potentially destructive effects of unexpected high inflow rate to the tunnel. Therefore, the inflow rate could be estimated using the defined equation by determining the orientation, spacing, and aperture of the joint sets, as well as the depth and radius of the tunnel.

5.4 METHODOLOGY

5.4.1 Selection of the effective parameters controlling the inflow rate to a tunnel

Water possibly flows into the tunnel when excavated in a fractured rock mass at a depth below the water table. The inflow to the tunnel occurs either via the body of the rock (matrix) or through the fractures or both. Tunnels are dug in a wide range of rock mass types from soft to hard rock. The permeability of intact rock is negligible in most cases, especially in crystalline rocks [215]. The impermeability of the rock matrix is assumed in this article; hence, fluid flows only through the fractures with laminar flow mode. With these explanations, the geometrical characteristics of the

discontinuities play an important role in controlling the hydraulic behaviour of the rock mass. The Cubic law [64] indicates that the fracture aperture has a significant effect on the inflow that occurs through the area between the fracture planes. Furthermore, a series of publications have been dedicated to studying the effect of joint spacing on the flow rate [216], and the inflow rate to the tunnel generally decreases by increasing the joint spacing. The orientation of joint sets and its effect on the inflow rate and the rock mass permeability is frequently considered in the studies [59, 197]. In the case of a tunnel or a borehole, the previous studies mostly focused on the two-dimensional evaluation of the impact of fracture orientation on the inflow rate [22, 23] and finally reminded that further investigations are essential to define the impact of joint orientation on the inflow rate in real cases (three-dimensional cases). In addition to the above-mentioned parameters, the height of water head above the tunnel is an effective parameter for the inflow rate to the tunnel using either empirical [217], analytical [189], or numerical methods [192]. The depth of the tunnel also has a dual impact on the inflow rate. On the one hand, the overburden load increases, and the stress induced by depth closes the fractures and decreases the permeability due to the increasing tunnel depth [172, 218]. On the other hand, the pressure head on the tunnel increases by raising the depth; consequently, the inflow rate to the tunnel increases [180].

In addition to the parameters listed above, a series of other parameters show a secondary impact on the inflow rate. For example, the effect of joint roughness coefficient (JRC) on the inflow rate to the tunnel could be considered via the hydraulic aperture [219] because hydraulic aperture decreases by increasing JRC. In addition, the impact of the tunnel depth could be represented by the in-depth mechanical aperture at the tunnel wall because the mechanical aperture decreases by increasing the tunnel depth [172]. The stress and its effect on the inflow rate could be considered via the variation of the joint aperture by the varying load.

The effects of hydraulic aperture, spacing, angle between joint sets and tunnel direction, water head above the tunnel, and tunnel radius on the inflow rate to the tunnel are considered in this article. The angle between the normal to a joint set and the tunnel direction has been considered instead of the dip and the dip direction of joint set to reduce the number of parameters and simplify the design of experiments. Such a consideration is a reasonable and effective assumption because the trace of

the discontinuities at the tunnel wall is the only way for fluid to enter the tunnel. By contrast, the trace length is directly related to the angle between the tunnel and normal to the joint set; consequently, this angle is considered to be a valid substitute to the dip/dip direction of joint sets. In addition, the rock mass is assumed to include three persistent joint sets with fixed values of dip, dip direction, and spacing and aperture for each set; a circular tunnel is always excavated in the S-N direction to simplify the model. All calculations of the inflow rate are performed in steady-state conditions in the presence of a fixed water table level. In addition, the specific length of the tunnel (STL) is considered in this study as the representative length of the tunnel to ascertain the representativeness of the model dimensions [220]. Therefore, the type and number of the required numerical experiments are defined in Section 5.4.3.

5.4.2 Selection of the level of parameters

As mentioned in Section 5.3, the main scope of this article is to propose an equation representing the relationship between the inflow rate to the tunnel and the effective parameters described in Section 5.4.1. Considering the effects of interaction between parameters, the experiments are designed using the response surface methodology (RSM) to achieve this goal. RSM is a method that uses statistical quantitative data from experiments to perform the regression model equations. It is a series of mathematical and statistical methods for modelling and analysing the influence of several variables on the response of the model. The randomized optimal RSM is considered in this study, that is a flexible design structure to accommodate custom models when the levels of parameters are defined manually.

The variation range of each parameter must be specified by defining levels that represent expected real values of the parameter to use the RSM methodology, adequately. Parameters in the experiment are controlled and set to levels prescribed by the design. These levels could be either defined by the RSM method or selected on the basis of existing categorizations. The levels of effective parameters are selected on the basis of the classifications defined by the previous studies as listed in Table 5-1.

Table 5-1. The range of variation of the effective parameters on the inflow rate to the tunnel

| | Levels | | | | | | | Reference |
	1	2	3	4	5	6	7	
Spacing (m)	Extremely close (<0.02)	Very close (0.02-0.06)	Close (0.06-0.2)	Moderate (0.2-0.6)	Wide (0.6-2)	Very wide (2.0-6.0)	Extremely wide (>6.0)	[221]
Hydraulic aperture (m)	Very tight (<0.0001)	Tight (0.0001-0.001)	Open (0.001-0.005)	Very open (>0.005)				[222]
Angle between normal to joint set and tunnel (degree)	0-20	20-45	45-90					[223]
Water head above tunnel (m)	10	40	100					…
Tunnel radius (m)	1	2	4					…

5.4.3 Design of the experiments

Table 5-1 shows that the spacing is classified by the ISRM [221] in seven levels based on the distribution of spacing obtained from real field data. However, the first three levels of spacing are sufficiently small to be considered as a crushed rock mass. In addition, a rock mass with fracture spacing higher than 6 m is uncommon [221]. Consequently, levels 4 to 6 are considered to be the levels of spacing for designing the experiments. Levels 1 to 3 are selected for the values of hydraulic aperture. Finally, the selected levels of the parameters for designing the experiments are presented in Table 5-2.

Table 5-2. The selected levels of parameters for designing the experiments that are required for calculation of the inflow rate to the tunnel

| | Levels | | |
	1	2	3
Spacing (m)	0.4	1	4
Hydraulic aperture (m)	5.00E-05	5.00E-04	2.00E-03
Angle between normal to joint set and tunnel (degree)	10	30	70
Water head (m)	10	40	100
Tunnel radius (m)	1	2	4

The statistical software package Design-Expert (Stat-Ease, Inc., Minneapolis, USA) is used to design the experiments and define the number and types of required numerical simulation based on considered levels of parameters according to Table 5-2. On this basis, the Design-Expert software defined that 88 numerical simulations are required for performing the regression analysis and

obtaining experimental data to fit the developed equations and plot the response surface, as listed in Table 5-3. ANOVA is used to estimate the statistical parameters. Analysis of Variance (ANOVA) is a statistical formula used to compare variances across the means (or average) of different groups.

Table 5-3. Number and arrangement of the numerical experiments that are defined by Design-Expert software in order to evaluate the inflow rate as a function of spacing, orientation, aperture, water head and tunnel radius. As the original table has 88 rows and for summarizing its content, rows 6 to 87 are not showed in this table.

	Spacing (m)			Angle between tunnel and normal to joint set (°)			Hydraulic aperture (m)			Water head above tunnel (m)	Tunnel radius (m)
	J1	J2	J3	J1	J2	J3	J1	J2	J3		
1	1	1	0.4	10	30	30	0.002	0.00005	0.002	40	4
2	4	0.4	4	10	30	10	0.002	0.002	0.0005	10	1
3	4	4	4	10	70	70	0.0005	0.002	0.0005	10	4
4	1	4	4	10	10	10	0.00005	0.002	0.002	10	4
5	1	4	4	70	30	30	0.0005	0.00005	0.002	40	2
…	…	…	…	…	…	…	…	…	…	…	…
88	88	0.4	0.4	30	70	10	0.00005	0.002	0.00005	10	1

It should be noted that Table 5-3 shows only selected results of the experiments. However, the complete version of this table showing the results of all the 88 experiments is given as Table A1 of appendix.

5.4.4 Model creation and numerical simulation

The Itasca 3DEC version 7.00 software is used to simulate and calculate numerically the inflow rate to the tunnel excavated in a fractured rock mass. 3DEC is a three-dimensional command-driven numerical program based on the distinct element method for discrete fracture network modelling. This software is mostly used to evaluate the response of the fracture network to the static or dynamic loads and perform hydromechanical coupling simulations under laminar flow mode. Simplifying assumptions is considered in this study because the real geometry of a rock mass is generally complex for modelling. In addition to several individual or random joints, a rock mass includes one to three prominent joint sets and one or more minor sets in most cases [224]. This study assumed that the rock mass includes three joint sets with various values of dip, dip direction, spacing, and aperture, but each set has a fixed value of these parameters. The length of the tunnel is defined by a recently

developed analytical method, namely the specific tunnel length (STL). This method, which is adapted to a three-dimensional model, has been proven to yield reliable results for 3D numerical simulation of inflow rate to the tunnel excavated in a fractured rock mass [220].

Fig 5-1 illustrates the results of the numerical modelling and boundary conditions for the determination of the inflow rate to a tunnel by 3DEC software. A fixed water table level is applied at the top of the model, and the pore pressure at the sides of the model parallel to the *y-z* plane is fixed to its initial values during the numerical calculations, as illustrated in Fig 5-1a. In addition, the pore pressure at the tunnel wall is zero. Fig 5-1b indicates that the inflow rate decreases because water is flowing from the model boundaries toward the tunnel wall. Consequently, the area that is close to the wall of the tunnel is considered for the calculation of the inflow rate to the tunnel. The spatial discretization of the numerical model must be refined; hydraulic gradients are high when water gets close to the tunnel. This refinement allows effective convergence of the simulations and improved accuracy of the results, as demonstrated in Fig 5-1.
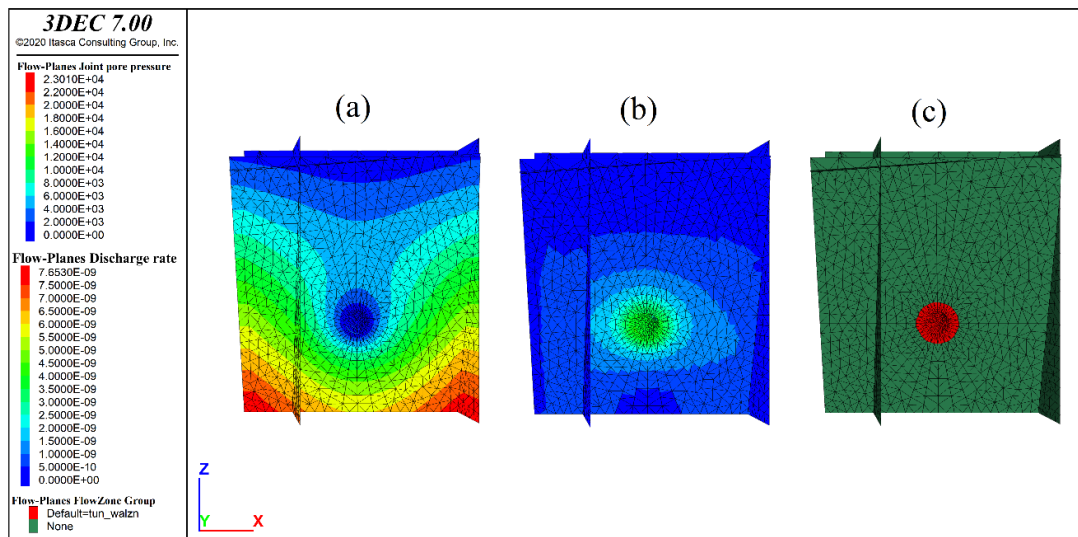
Fig 5-1. Boundary conditions and calculation methods applied in numerical simulations. (a) pore pressure around the tunnel in a flow plane and applied boundary conditions, (b) discharge rate in flow planes (c) flow plane zones selected for calculation of the inflow rate to the tunnel

In Fig 5-1, the Flow Plane is the planar polygon corresponding to face-to-face contact between solid blocks, the Flow Plane Zone is a triangular discretization element of the flow plane, and the Flowknot is the vertices of a flow plane zone that generally correspond to a sub-contact between solid

blocks [225]. In this study, the inflow rate to the tunnel is calculated when the model reaches steady-state conditions. In order to ensure that steady-state conditions are reached, the variation of the pore pressure with cycling steps is recorded around the tunnel circumference. As soon as the pore pressure at all nodes do not vary with time anymore, then it means that the simulation has reached steady-state conditions. Finally, the inflow rate calculations in this study has been performed by using a FISH function that is available in the 3DEC command lines.

5.5 RESULTS AND DISCUSSION

The relationship between the unit inflow rate to the tunnel and the effective parameters based on the numerical simulation results for the cases listed in Table 5-3 is presented in Section 5.5.1. In addition, the individual and interaction effects of parameters on the unit inflow rate are presented in Sections 5.5.2 and 5.5.3, respectively. Furthermore, the mean values of the parameters of Table 5-3 are considered to provide a simple equation for calculating the unit inflow rate to the tunnel and show a perceptible individual and interactional effect of parameters on the inflow rate. Notably, the average flow into the tunnel for each square meter of the tunnel wall is considered in this article as the unit inflow rate to minimize the impact of the tunnel radius on the inflow rate. However, the STL, which is a measure of inflow rate per meter of tunnel length, is used in this article to specify the minimum representative length of the tunnel.

5.5.1 Inflow rate

As listed in Table 5-3, 88 numerical simulations using the 3DEC version 7 software are performed, and a sample of the results is given in Table 5-4. However, the complete table is provided in the supplementary material. Notably, the inflow rate is measured as the flow rate that occurs in a unit area of the tunnel wall or unit inflow rate; hence, its unit is ($(m^3/s)/m^2$) or (m/s) in this study.

Table 5-4. Results of the numerical simulation for calculation of the inflow rate for the cases of Table 5-3

Run	1	2	3	4	5	…	88
Unit Inflow rate (($m3/s)/m^2$)	2.24585	0.518672	0.099508	0.155529	0.188979	…	0.405854

In the next section, the relationships between unit inflow rate and the effective parameters as well as the mean values of parameters are studied by using the Design-Expert software.

5.5.1.1 Regression model equation

The optimal design was used to develop the correlation between the inflow rate to the tunnel and the effective parameters, including aperture, spacing, orientation, tunnel radius, and water head above the tunnel. The model was selected on the basis of the highest-order polynomial regression; in the model, the additional terms were significant, and the model was not aliased. A quadratic model is selected for the inflow rate based on the sequential model sum of squares, as proposed by the software. The regression analysis is conducted to fit the inflow rate to the tunnel as the response function of aperture, spacing and orientation of joint sets, tunnel radius and water head above the tunnel. The model expressed by Eq.(5-1), where the variables take their coded values, represents the decimal logarithm of the unit inflow rate as a function of: 1 - spacing of joint set 1 (A), joint set 2 (B), and joint set 3 (C); 2 - the angle between the tunnel and normal to joint set 1 (D), normal to joint set 2 (E), and normal to joint set 3 (F); 3 - the hydraulic aperture of joint set 1 (G), joint set 2 (H), and joint set 3 (I); 4 - the water head above the tunnel (J); 5 - the tunnel radius (K). The final empirical equation considering coded factors after excluding the insignificant parameters for unit inflow rate to the tunnel is given as follows:

Log_{10} (Unit inflow rate) = -3.51083 -1.08328 (A) -0.090386 (B) + 0.0762999 (C) -0.0083711 (D) -0.00130131 (E) + 0.017995 (F) + 2712.76 (G) + 1719.03 (H) + 2008.14 (I) + 0.00259443 (J) -0.182086 (K) + 0.0222344 (AB) -0.0557452 (AC) -0.00173015 (AF) + 72.5935 (AI) + 0.0190945 (BC) - 0.00131037 (BD) -61.2519 (BH) + 0.00104241 (CD) -0.00215562 (CF) - (5-1) 86.9808 (CI) -0.000133722 (DF) + 2.41614 (DG) -4.16163 (DH) + 2.46503 (EH) -3.93298 (EI) + 4.27762e-05 (EJ) -3.7148 (FG) -429057 (GH) -452172 (GI) -371223 (HI) -75.9181 (HK) + 4.16784 (IJ) + 0.219485 (A^2) + 0.000272018 (D^2) -559064 (G^2) -287575 (I^2) + 0.0522276 (K^2)

A positive sign in front of the terms indicates a synergistic impact on the inflow rate, whereas a negative sign indicates an antagonistic effect. The coefficients of the parameters of Eq.(5-1) are estimated using the multiple regression analysis techniques included in the RSM. Fit quality of the models is judged from their coefficients of correlation and determination, as respectively illustrated in Table 5-6 and Table 5-7.

The regression model of Eq.(5-1) is compared with a recently developed analytical model [189] for the inflow rate, in order to verify the equation. For this purpose, the root means square error (RMSE) of the results is calculated and shows that there is a satisfying match between the analytical model and Eq.(5-1). Table 5-5 shows the analytical and numerical (Eq.(5-1)) results for the inflow rate to the tunnel and the associated errors and RMSE. However, the complete list of square errors and analytical model results are presented in supplementary material A of this document.

Table 5-5. Comparison of the results of Eq.(5-1) and an analytical model for calculation of the inflow rate to the tunnel

Run No.	Eq.(5-1)	Analytical model [189]	Squares of errors
1	2.241	2.411	0.027275
2	0.519	0.451	0.004716
3	0.099	0.091	7.24E-05
4	0.156	0.083	0.005332
5	0.189	0.089	0.009967
…	…	…	…
88	0.406	0.428	0.000491
		RMSE	0.966

The coefficients of parameters in Eq.(5-1) could be considered to evaluate the effect of each parameter on the unit inflow rate to the tunnel. Three coefficients for spacing, orientation, and hydraulic aperture are used in this equation (because 3 joint sets exist), and one coefficient is used for the water head above the tunnel and tunnel radius. The overall sign of the coefficients regarding the spacing is negative; hence, the spacing has a negative effect on the inflow rate. The effect of the angle between the tunnel and the normal to joint sets on the inflow rate is shown by D, E, and F in Eq.(5-1), and the overall coefficient of this parameter has a positive sign. Therefore, the inflow rate to the tunnel increases by raising the angle (deviation from the perpendicular cross of the tunnel and joint set). The hydraulic aperture always has a positive effect on the inflow rate because the coefficients G, H, and I always have positive values. An increase in the water head results in an increase in the inflow rate. However, an increase in tunnel radius will imply a decrease in the unit inflow rate to the tunnel because the coefficient of K is negative in Eq.(5-1). This effect is logical because a slight decrease occurs in the water head above the tunnel wall as the tunnel radius increases, and the inflow rate subsequently decreases. Despite the above-mentioned effects of parameters on the unit inflow rate to the tunnel, Eq.(5-1) indicates that the effect of interaction

between parameters is as important as the individual effect of parameters. Hence, the impact of a specific parameter should be considered by individual and interaction effects of parameters. This issue is further discussed in Section 5.5.3.

Eq.(5-1) also demonstrates the weight factor of each parameter on the inflow rate to the tunnel. On this basis, the hydraulic aperture is the weightiest parameter because its variation will intensely affect the inflow rate to the tunnel. With a weight factor far less than the hydraulic aperture, the variation of the spacing affects the inflow rate at the second level of importance. The angle between the tunnel and normal to joint sets, water head above the tunnel, and tunnel radius have remarkably significant weight factors on the inflow rate. However, a definite conclusion on the weight of parameters on the inflow rate could be made by considering the individual effects and their interactions, and these results are presented in Sections 5.5.2 and 5.5.3.

Eq.(5-1) is a complicated approach for the calculation of the inflow rate. Thus, the historical data design is used to develop a simple equation for the relation between the mean value of the parameters and the inflow rate. A quadratic model is applied to the data presented in Table A3. The regression analysis for the model is illustrated by Eq.(5-2), where the variables take their coded values and represent the decimal logarithm of the unit inflow rate as a function of average spacing (A), average angle between the tunnel and normal to joint set (B), average hydraulic aperture of joint sets (C), water head above the tunnel (D), and the tunnel radius (E). The final empirical equation considering coded factors after excluding the insignificant parameters for unit inflow rate to the tunnel is as follows:

$$\text{Log}_{10}(\text{Unit inflow rate}) = -2.71924 - 0.372363\,(A) + 0.007064\,(B) + 4728.60779\,(C) + 0.002522\,(D) - 0.372733\,(E) + 5.81715\,(CD) - 0.00147609\,(DE) - 1.68318\times10^6\,C^2 + 0.079285E^2 \qquad (5\text{-}2)$$

Eq.(5-2) validates the relative influences of the weight factors of the parameters on the inflow rate. This issue is further discussed in section 5.5.3.

5.5.1.2   Statistical analysis

The reliability of the models of Eq.(5-1) and Eq.(5-2) is assessed on the basis of the correlation coefficient values. Table 5-6 shows that the value of the coefficient of determination (R^2) for Eq.(5-1) is 0.9885. Thus, 98.85% of the total variation in the inflow rate to the tunnel is attributed to the considered experimental variables. The standard deviation for the model is 0.1707 for Eq.(5-1). A close value of the R^2 to unity and a low standard deviation facilitates precise prediction by the model, in which the values are close to the actual values of the response (inflow rate).

Table 5-6. Fit statistics of Eq.(5-1). The Predicted R² of 0.9618 is in reasonable agreement with the Adjusted R² of 0.9796; i.e. the difference is less than 0.2. Adeq Precision measures the signal to noise ratio and is desirable if it is greater than 4. The ratio of 53.498 indicates an adequate signal. This model can be used to navigate the design space.

Std. Dev.	0.1707	R²	0.9885
Mean	-0.4938	Adjusted R²	0.9796
C.V. %	34.56	Predicted R²	0.9618
		Adeq Precision	53.4983

The analysis of variances (ANOVA) is used to justify the adequacy of the model. Table 5-7 gives the ANOVA results for the reduced quadratic model for the inflow rate to the tunnel according to Eq.(5-1). The F-value of 111.10 implies that the model is significant. In this model, all values of spacings (A, B, and C), angles between joint set 1 and tunnel direction (D), all the values of hydraulic apertures (G, H, and J), and water head above the tunnel (K) are significant model terms. The obtained statistical results demonstrate that the proposed model of Eq.(5-1) is adequate to predict the inflow rate to the tunnel with the considered variables.

Table 5-7. ANOVA for Reduced Quadratic model of Unit Inflow rate to the tunnel based on Eq.(5-1)

Source	Sum of Squares	df	Mean Square	F-value	P-value	
Model	122.97	38	3.24	111.10	< 0.0001	significant
A-Spacing 1	4.92	1	4.92	168.86	< 0.0001	
B-Spacing 2	2.36	1	2.36	80.91	< 0.0001	
C-Spacing 3	3.21	1	3.21	110.22	< 0.0001	
D-Angle 1	1.48	1	1.48	50.78	< 0.0001	
E-Angle 2	0.0106	1	0.0106	0.3627	0.5498	
F-Angle 3	0.0040	1	0.0040	0.1365	0.7134	
G-App 1	15.27	1	15.27	524.16	< 0.0001	
H-App 2	12.66	1	12.66	434.78	< 0.0001	
J-App 3	16.23	1	16.23	557.15	< 0.0001	
K-hw	6.93	1	6.93	237.94	< 0.0001	
L-Tr	0.0002	1	0.0002	0.0058	0.9395	

AB	0.2301	1	0.2301	7.90	0.0071	
AC	1.33	1	1.33	45.65	< 0.0001	
AF	0.3330	1	0.3330	11.43	0.0014	
AJ	0.6965	1	0.6965	23.91	< 0.0001	
BC	0.1685	1	0.1685	5.78	0.0200	
BD	0.1862	1	0.1862	6.39	0.0147	
BH	0.4682	1	0.4682	16.07	0.0002	
CD	0.1498	1	0.1498	5.14	0.0278	
CF	0.6164	1	0.6164	21.16	< 0.0001	
CJ	1.04	1	1.04	35.83	< 0.0001	
DF	0.5360	1	0.5360	18.40	< 0.0001	
DG	0.2012	1	0.2012	6.91	0.0114	
DH	0.6281	1	0.6281	21.56	< 0.0001	
EH	0.2043	1	0.2043	7.01	0.0108	
EJ	0.5261	1	0.5261	18.06	< 0.0001	
EK	0.1128	1	0.1128	3.87	0.0548	
FG	0.4868	1	0.4868	16.71	0.0002	
GH	6.51	1	6.51	223.36	< 0.0001	
GJ	8.00	1	8.00	274.49	< 0.0001	
HJ	4.62	1	4.62	158.70	< 0.0001	
HL	0.4648	1	0.4648	15.96	0.0002	
JK	1.38	1	1.38	47.47	< 0.0001	
A²	1.88	1	1.88	64.62	< 0.0001	
D²	0.5904	1	0.5904	20.27	< 0.0001	
G²	1.53	1	1.53	52.64	< 0.0001	
J²	0.4675	1	0.4675	16.05	0.0002	
L²	0.1311	1	0.1311	4.50	0.0390	
Residual	1.43	49	0.0291			
Lack of Fit	1.25	44	0.0284	0.8058	0.6936	Not significant
Pure Error	0.1764	5	0.0353			
Cor Total	124.40	87				

In addition, Table 5-8 shows that the R^2 value for Eq.(5-2) is 0.902. that is, 90.2% of the total variation in the inflow rate to the tunnel is attributed to the considered experimental variables: i.e., the mean values of the aperture, spacing and the angle between normal to joint sets and tunnel direction, and the exact values of tunnel radius and water head above the tunnel. Notably, the standard deviation for the model of Eq.(5-2) is approximately 0.376.

Table 5-8. Fit statistics of the Eq.(5-2). The Predicted R² is in reasonable agreement with the Adjusted R². In addition, Adeq precision is in desirable range and hence, model could be used for design.

Std. Dev.	0.3760	R²	0.9021
Mean	-0.4781	Adjusted R²	0.8922
C.V. %	78.65	Predicted R²	0.8741
		Adeq Precision	42.7308

Table 5-9 gives the ANOVA results for the reduced quadratic model for the inflow rate to the tunnel according to Eq.(5-2). The F-value of 91.02 shows that the model is significant. In this model, the values of the average spacing (A), average hydraulic aperture (C), and the water head above the tunnel (D) are significant model terms. In addition, the proposed model is sufficiently accurate to predict the inflow rate to the tunnel with the studied variables.

Table 5-9. ANOVA for Reduced Quadratic model of Unit Inflow rate to the tunnel based on Eq.(5-2)

Source	Sum of Squares	df	Mean Square	F-value	P-value	
Model	102.94	8	12.87	91.02	< 0.0001	significant
A-Spacing	10.21	1	10.21	72.23	< 0.0001	
B-Angle	1.02	1	1.02	7.23	0.0087	
C-Aperture	49.08	1	49.08	347.18	< 0.0001	
D-Water head	9.41	1	9.41	66.54	< 0.0001	
E-Tunnel radius	0.0773	1	0.0773	0.5469	0.4618	
CD	1.13	1	1.13	7.98	0.0060	
C²	17.76	1	17.76	125.61	< 0.0001	
E²	0.4048	1	0.4048	2.86	0.0946	
Residual	11.17	79	0.1414			
Lack of Fit	10.99	74	0.1485	4.21	0.0553	Not significant
Pure Error	0.1764	5	0.0353			
Cor Total	114.11	87				

5.5.2 Individual effects of parameters

In all phenomena in which the output is attributed to several effective parameters, in addition to the individual effect of each parameter on the response of the model, the interaction between the parameters may also have a significant impact on the model output. Therefore, the individual effects are demonstrated in this section, and the interaction effects are presented in Section 5.5.3.

Joint set hydraulic aperture, spacing, orientation, water head above the tunnel, and tunnel radius are the parameters considered for defining the inflow rate to the tunnel. Considering the characteristics of any one of the joint sets alone might be misleading in the sensitivity analysis because the rock mass is assumed to contain three joint sets. Consequently, the average value of the parameters is considered for this purpose; for example, a single average spacing value for all three joint sets combined.

Fig 5-2 illustrates the variation of the unit inflow rate to the tunnel by the mean values of the parameters obtained from numerical and analytical models. Increasing the hydraulic aperture results

in a rapid increase in the unit inflow rate (Fig. 2a) due to the remarkably high slope of the diagram. The effect of spacing is opposite to that of the aperture (Fig. 2b) because the inflow rate decreases by increasing the average spacing. However, the rate of variation of the inflow rate by spacing is substantially lower than that by the aperture. Fig 5-2c shows that the radius of the tunnel has a limited impact on the inflow rate; the variation of inflow rate is almost negligible by changing the radius of the tunnel from 1 m to 4 m. Fig 5-2d shows that the unit inflow rate increases by raising the average angle between the tunnel and normal to joint sets. The rate of variation of the unit inflow rate with the angle value is uniform but higher than the variation with tunnel radius (Fig 5-2c) and lower than the effect of aperture (Fig 5-2a). The inflow rate also increases by raising the water head, as illustrated in Fig 5-2e.
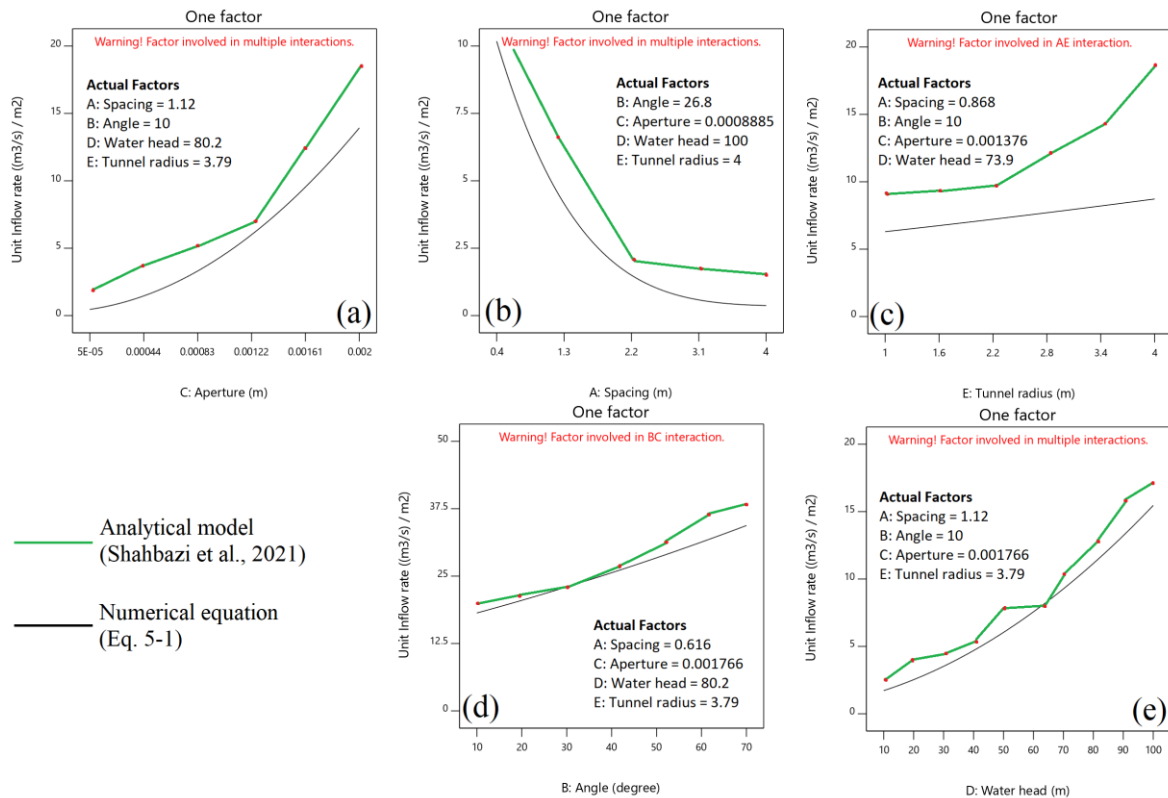
Fig 5-2. Individual effect of the parameters on the unit inflow rate to the tunnel for (a)hydraulic aperture, (b)Spacing, (c)Tunnel radius, (d)the angle between normal to joint set and tunnel and (e)water head above the tunnel; the green line shows the relevant inflow rate by analytical

The impact of each parameter on the unit inflow rate is illustrated in Fig 5-2. However, all parameters are involved in the interaction with the other parameters regarding the effect on unit inflow rate. This effect is investigated and discussed in Section 5.5.3.

5.5.3 Effect of interaction between parameters

Fig 5-2 illustrates all the parameters involved in interaction effects. Therefore, the effect of every parameter considered is compounded by the effects of interactions between parameters. Some of these effects are presented in this section, and the rest can be found in the supplementary material.

Fig 5-3 shows the effect of the interaction between water head above the tunnel, and the angle between the tunnel and normal to joint set on the inflow rate. Increasing the water head raises the inflow rate for all angle values. However, the effect of this increase is substantial at large angles. Similar behavior is shown with an increasing angle. Thus, the maximum inflow rate is obtained when the cross-section of the tunnel and joint sets deviates from the perpendicular contact.
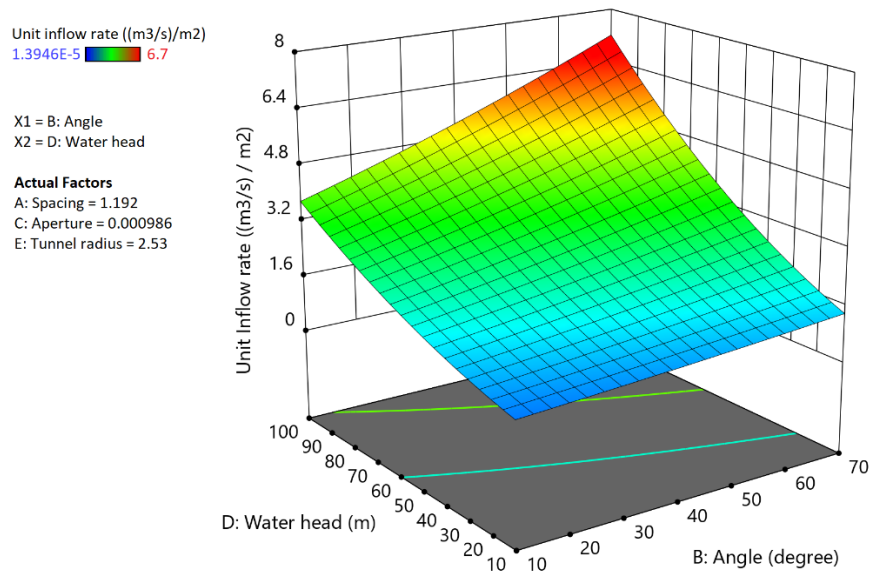
Fig 5-3. The effect on the inflow rate to the tunnel of the interaction between the water head above the tunnel, and the angle between tunnel and the normal to joint set

The effect of interaction between tunnel radius and water head on the inflow rate is illustrated in Fig 5-4. The inflow rate generally increases by raising the water head above the tunnel. A high unit inflow rate in a large tunnel radius is observed as expected, but this impact is limited. The minimal inflow rate is observed with the lowest water head and the small tunnel radius.
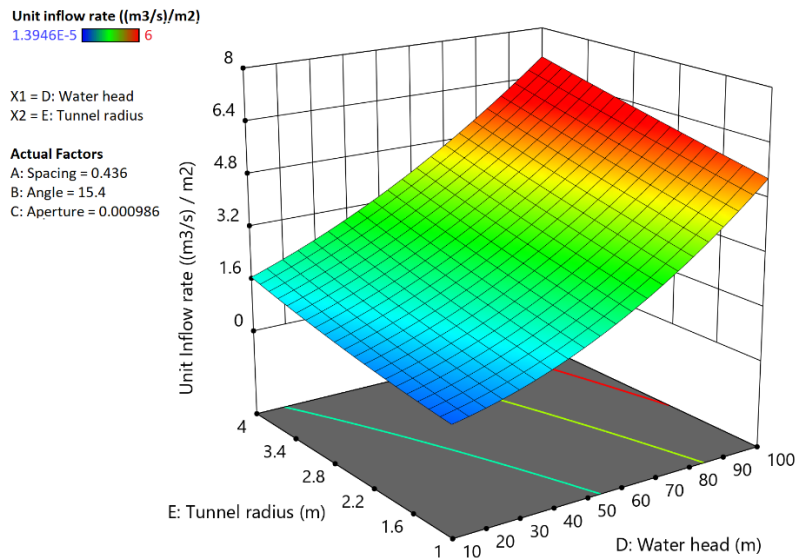
Fig 5-4. The effect of interaction between water head above the tunnel and tunnel radius on the unit inflow rate

Similar to that in Fig 5-3 and Fig 5-4, the impacts of interactions between the other parameters have been investigated. Therefore, the interactions between each pair of parameters are summarized below.

☐ Hydraulic aperture/angle between the tunnel and normal to joint set: the effect of aperture on the inflow rate is more important by deviating from the perpendicular cross of joint set and tunnel. In addition, the orientation of the joint set is effective on the inflow rate at wide apertures.

☐ Tunnel radius/angle between the tunnel and normal to joint set: the effect of tunnel radius on the inflow rate is less in the nearly perpendicular crossing of joint set and tunnel.

☐ Spacing/angle between the tunnel and normal to joint set: the angle has a negligible effect on the inflow rate at large spacings. By contrast, the impact of spacing on the inflow rate increases by deviating from the perpendicular cross of joint set and tunnel.

☐ Aperture/tunnel radius: the effect of tunnel radius on the inflow rate is insignificant in close apertures. The impact of aperture on inflow rate is also significant in large tunnel radiuses.

☐ Aperture/water head above tunnel: the effect of aperture on the inflow rate is less in low water heads. In addition, the impact of the water head on the inflow rate is negligible in the close apertures.

☐ Spacing/aperture: the effect of aperture and spacing on the inflow rate is negligible in wide spacings and close apertures, respectively.

☐ Spacing/tunnel radius: the effect of tunnel radius on inflow rate is insignificant in wide spacings. However, the effect of spacing on the inflow rate is sensible in a large radius of the tunnel.

☐ Spacing/water head: the effect of water head and spacing on the inflow rate is negligible in wide spacings and low water head, respectively.

5.6 DISCUSSION AND CONCLUSION

The unit inflow rate to a tunnel excavated in a fractured rock mass is investigated in this article. The rock mass is assumed to contain three persistent joint sets with various orientations, spacings, and hydraulic apertures. However, the values of each parameter are fixed in each joint set. In addition, the tunnel is assumed to be excavated in the S-N direction and has a circular cross-section. Some conclusions can be summarized below based on the analysis of numerical simulation results with RSM.

Two empirical–numerical equations are developed for the calculation of unit inflow rate to the tunnel, that is, the inflow rate per unit area of the tunnel wall. The first equation (Eq.(5-1)) is developed by separately considering the characteristics of each joint set. By contrast, the second equation (Eq.(5-2)) considers the mean values of the spacing, aperture, and orientation. The coefficient of determination (R^2) of Eq.(5-1) shows its superior accuracy to Eq.(5-2); however, Eq.(5-2) is easy to apply due to its simplicity. Both equations are useful for estimating the probable inflow rate to a tunnel by determining the geometry of the discontinuities around the tunnel and the groundwater level. These equations may be preferred by practitioners in the engineering geology field due to their easy application and minimal time and cost investments. The output of this study may be helpful for geological engineers working on the tunnel and underground projects in solving inflow rate problems.

In most of the interactional effects between parameters, the radius of the tunnel has a negligible impact on the value of the unit inflow rate to the tunnel. The unit inflow rate considered in this article is the inflow rate per surface area of the tunnel wall. Thus, the tunnel radius will have a substantial effect on the unit inflow rate when the unit inflow rate from the length of the tunnel is considered.

Based on the individual and interactional effect of parameters on the inflow rate, the lowest unit inflow rate to the tunnel occurs in perpendicular crossing of joint sets to the tunnel, and by deviation from perpendicular crossing, the inflow rate increases accordingly. However, this rate is highly affected by the value of spacing and hydraulic aperture.

Among all parameters considered in this study, aperture, spacing, and orientation have the most important impacts on the unit inflow rate to the tunnel. However, the impact of the hydraulic aperture is not comparable with other parameters because a minor variation of the aperture will strongly affect the inflow rate according to Cubic law. As a general rule, the effect of a specific parameter could be intense in different values of other parameters, a point that is regarded in Section 5.5.3 of this article.

5.7 CREDIT AUTHORSHIP CONTRIBUTION

Alireza Shahbazi: Conceptualization, Resources, Data curation, Software, validation, Methodology, Writing-original draft; Ali Saeidi: Conceptualization, Supervision, Investigation, Methodology, Project administration, Writing-review & editing; Romain Chesnaux: Supervision, Writing-review & editing; Alain Rouleau: Conceptualization, Supervision, Writing-review & editing

5.8 DECLARATION OF COMPETING INTEREST

The authors declare that there is no conflict of interest associated with this publication.

5.9 ACKNOWLEDGEMENTS

CHAPTER 6

Article 5: Rock block volume calculation by analytical method for geological engineering applications

Aboubacar Sidiki Koulibaly[1], Alireza Shahbazi[1*], Ali Saeidi[1], Alain Rouleau[1], Marco Quirion[2], Romain Chesnaux[1],

[1]Université du Québec à Chicoutimi, 555 boulevard de l'Université, Chicoutimi, Québec G7H 2B1, Canada

[2]Hydro-Québec Production Unité Expertise en barrages, 75 boulevard René-Lévesque Ouest, Montréal, Québec, H2Z 1A4, Canada

*Email: alireza.shahbazi1@uqac.ca

6.1 HIGHLIGHTS

- A new vectoral method for calculating block volume has been developed for a rock mass consisting of 3 sets persistent joint sets.
- Previously developed models produce noticeable errors in calculating block volume.
- The spacings and orientations of the joint sets are the main influential parameters in calculating the volume of the block.
- The error of previous methods in calculating block volume has been calculated for a series of field data.

6.2 ABSTRACT

The size of rock block is an important parameter to maintain the stability of underground and open structures in a rock mass, especially in determining the risk of erosion in dam spillways. A new method based on vector operations is developed and compared with formerly proposed models for the calculation of the volume of the block formed by cross-cutting joint sets. The rock mass is assumed to include three persistent joint sets with various values of spacing and orientation. The volume of the resulting rock blocks is calculated through the multiplication of the block's edge vector. The results of the developed model are validated with the output of the numerical simulations using 3DEC version 7.0 software. A real database of field data for block volume is compared with the results

of the proposed and previously developed methods. The degree of accuracy for each method is determined.

Keywords: Block volume, Rock mass, Analytical method, Vectoral multiplication

6.3 INTRODUCTION

Hydraulic erosion of the flow channels in uncoated spillways is one of the present-day concerns of hydropower industries. This phenomenon occurs when the hydraulic power of the water in a spillway is greater than the strength of the rock mass, and the rock mass erodes by the dynamic displacement of rock blocks. The erodibility of the rock mass directly depends on its mechanical properties, most of which are defined by the discontinuity system of the rock mass [224]. The most important geomechanical parameters affecting the rock mass strength are the uniaxial compressive strength (UCS), the inter-block shear strength (J_r/J_a), block size (V_b), the opening of the joints (J_o), and the arrangement of the joints in relation to the flow direction (J_s and E_{doa}). In this regard, the block size plays an important role in the stability of underground and surface structures [198, 224, 226]. Several methods for calculating the block volume have been proposed [198, 200, 224, 227-230], and various equations have been developed (Table 6-1). Nevertheless, calculated block volumes mostly deviate from actual field values. For example, based on data from discontinuity survey from 11 limestone quarries in Karaburn Peninsula (Izmir in Turkey), Elci and Turk [229] calculated the block volume (V_b) using the average spacing of the discontinuities (S_a), their real spacing (S), and the number of volumetric joints (J_v). The calculated V_b values showed significant differences with the real values of the block volume.

Table 6-1: Methods for calculation of the block volume of a fractured rock mass

Reference	Equation	Parameters	Types of measurement	Method
[230]	$V_b = RQD/J_n$	RQD: Rock Quality Designator J_n: number of joint sets	1D measurement on the drill core direction	B
[227]	$V_b = \dfrac{\beta \times J_v^{-3}}{\sin \gamma_1 \times \sin \gamma_2 \times \sin \gamma_3}$	J_v: joint set number β: block shape factor	3D indirect measurement on a rock surface	C

[228]	$V_b = \dfrac{S_1 \times S_2 \times S_3}{\sin\gamma_1 \times \sin\gamma_2 \times \sin\gamma_3}$	S_i: average spacing of set i γ_i: angle between a pair of joint sets	3D direct measurement on a rock surface	D
[228]	$V_b = S_a^3$	S_a: average spacing of all joint sets (m)	3D direct measurement on a rock surface	E
[228]	$V_b = \dfrac{\beta \times wJd^{-3}}{\sin\gamma_1 \times \sin\gamma_2 \times \sin\gamma_3}$	wJd: weighted joint density β: block shape factor	1D or 2D indirect measurement on a rock surface or on drill core	F
[231]	$V_b = \dfrac{S_1 \times S_2 \times S_3}{\sin\gamma_1 \sin\gamma_2 \sin\gamma_3 \sqrt[3]{P_1 P_2 P_3}}$	S_i: average spacing of set i γ_i: angle between pair of joint sets P_i: Persistence of joint set i	3D direct measurement on rock surface	G
[232]	$V_b = 36 \times (S_a/2)^3$	S_a: average spacing of all joint sets (m)	3D direct measurement on a rock surface or 1D in drill cores.	H
[227] [232]	$V_b = \dfrac{1}{\sin\gamma_1 \times \sin\gamma_2 \times \sin\gamma_3 \times (S_a/2)^3}$	S_a: average spacing of all joint sets (m)	If assumed $J_v = 2/S$ 3D indirect measurement on a rock surface	I

Rock mass classification systems, such as Q-system [230] and excavation index [233], include the ratio of (RQD/J_n), which represents the block size. However, the limitation of this quotient in estimating block size has been frequently criticized by Bieniawiski [234], Edelbro [235], Grenon and Hadjigeorgiou [236], Palmström [198], and Pells [237]. Hence, this quotient is not considered in this article. Palmström [198] considered that the 3D determination of block volume helps characterize the geomechanical behaviour of a fractured rock mass. On this basis, he proposed a series of equations to estimate the volume of the block (V_b) and in this regard, Eq. 6-1 is developed as the first equation, as follows:

$$V_b = S_a^3 \qquad\qquad\qquad 6\text{-}1$$

where S_a is the average spacing of all joint sets and could be determined by Eq. 6-2, as follows:

$$S_a = \frac{\sum_1^n S_i}{n} \qquad\qquad\qquad 6\text{-}2$$

where S_i is the spacing of joint set i, and n is the number of joint sets. This equation is only applicable when the average spacing of at least three or more joint sets is known. If the rock mass includes three persistent joint sets and the angle between each pair of sets is known, then the

following Eq. 6-3, which was developed by Palmström [228], can be used to calculate the block volume:

$$V_b = \frac{S_1 \times S_2 \times S_3}{\sin \gamma_1 \times \sin \gamma_2 \times \sin \gamma_3} \qquad \text{6-3}$$

where γ_1, γ_2, and γ_3 are the angles between each pair of joint sets. If all joint sets are perpendicular to one another, Eq. 6-3 is simplified to Eq. 6-4, as follows:

$$V_b = S_1 \times S_2 \times S_3 \qquad \text{6-4}$$

Eqs. 6-3 and 6-4 are applicable only if the blocks are formed by the assembly of three joint sets. However, in many cases, either the blocks are formed by random joints or some of the discontinuity sets do not appear in a rock exposure. Such a phenomenon occurs when a rock mass includes less than three joint sets or the joint spacings are large [198]. For such cases, Palmström proposed the use of Eqs. 6-5 and 6-6 to empirically calculate the block volume, as follows:

$$V_b \approx S_1 \times 5S_1 \times 5S_1 = 25S_1^3 \qquad \text{if one set is detectable} \qquad \text{6-5}$$
$$V_b \approx S_1 \times S_2 \times 5S_1 = 5S_1^2 \times S_2 \qquad \text{if two sets are detectable} \qquad \text{6-6}$$

The volumetric joint count (J_v) is also used for block volume calculation. J_v is the number of joints cutting a volume of 1 m^3 of rock and can be calculated by using Eq. 6-7 [238], as follows:

$$J_v = \sum_{1}^{n} \frac{1}{S_i} \qquad \text{6-7}$$

where S_i is the average spacing of set i. To consider the effect of random joints, Palmström [227] modified Eq. 6-7 to Eq. 6-8, as follows:

$$J_V = \frac{1}{s_1} + \frac{1}{s_2} + \frac{1}{s_3} + \cdots + \frac{Nr}{5(\sqrt{A})} \qquad \text{6-8}$$

where N_r is the number of random joints that exist in a square meter of the surveying area. Subsequently, the correlation between the volumetric joint count (J_v) and the block volume (V_b) is defined by Eq. 6-9 [195], as follows:

$$V_b = \beta \times J_v^{-3} \frac{1}{\sin \gamma_1 \times \sin \gamma_2 \times \sin \gamma_3} \qquad \text{6-9}$$

where β is the shape factor of blocks and represents the ratio of spacings in a rock mass. In the case of three joint sets, β could be defined by Eq. 6-10, as follows:

$$\beta = \frac{(\alpha_2 + \alpha_2 \times \alpha_3 + \alpha_3)^3}{(\alpha_2 \times \alpha_3)^2} \qquad \text{6-10}$$

where $\alpha_2 = S_2/S_1$ and $\alpha_3 = S_3/S_1$; S_1 are the minimum spacings, whereas S_3 is the maximum spacing. For blocks with irregular shapes (more than 6 faces), β can be roughly estimated using Eq. 6-11, as follows:

$$\beta = 20 + 7a_3/a_1 \qquad \text{6-11}$$

where a_1 and a_3 represent the longest and shortest dimensions of the block, respectively. In addition, J_v could be measured using other surveying methods, i.e., by borehole or surface scanning and by defining the weighted joint density (wJd). wJd is a representative index used to illustrate the angle between joint set and survey direction (core log) or plane (outcrop or ground surveying) and could be estimated by using Eqs. 6-12 and 6-13, as follows:

$$wJd = \frac{1}{\sqrt{A}} \Sigma f_i \qquad \text{For surface survey} \qquad \text{6-12}$$

$$wJd = \frac{1}{L} \Sigma f_i \qquad \text{For core logging} \qquad \text{6-13}$$

where A is the surface area of the survey, L is the length of the drill core, and f_i is the interval factor that could be defined by the angle between joint set and core logging direction or the surface area of the survey. The value of the wJd is almost equal to the volumetric joint count. According to Latham [232], wJd is an extension of J_v and is used because of the feasibility of the measurements, even if it is potentially less precise than J_v.

The impact of joint persistence on the block volume calculation by Eq. 6-3 was investigated by Cai [200]. Persistence is a term used to describe the ratio between the size of the discontinuity and rock mass dimension. If l_i is the accumulated joint length of set i in a sampling plan, and L is the characteristic length of the rock mass, then the joint persistence of set i (P_i) can be specified by Eq. 6-14, as follows:

$$P_i = \begin{cases} \dfrac{\bar{l_i}}{L} & if\ l_i < L \\ 1 & if\ l_i \geq L \end{cases}$$
6-14

Accordingly, the block volume in the case of non-persistent joints could be calculated by using Eq. 6-15, as follows:

$$V_b = \frac{S_1 S_2 S_3}{\sin \gamma_1 \sin \gamma_2 \sin \gamma_3 \sqrt[3]{P_1 P_2 P_3}}$$
6-15

Given that the direction of core logging regarding the joint set orientation is not often recorded in borehole logs, Latham [232] developed an approach to estimate the volume of blocks in this case, as shown in the following Eq. 6-16:

$$V_i = 36 \times (S_a/2)^3$$
6-16

where S_a is the average joint spacing measured along the drill core.

Based on the above-mentioned review of the common methods for block volume calculation, and because the different models are already developed for this purpose, the accuracy and applicability of each model for block volume calculation should be evaluated via comparison with a more reliable method. For this purpose, a new analytical method to calculate block volume is developed on the basis of vectoral calculation and is validated by 3D numerical modelling. This method is named as method "A" in this article. To calculate the volume of the block, the rock mass is assumed to include three persistent joint sets. The volume of the block that is created by the cross of the joint sets is determined by the vectoral multiplication of the block's edge vectors. Generally, the block in this case will be a parallelepiped with six faces, and each pair of frontside faces is identical. The block volume calculation with method "A" is fully compatible with the results of the numerical simulation. Also, the block volume for a series of field data calculated by each method is compared

138

with that calculated by method "A", and the relevant error is evaluated. The previous methods for block volume calculation that have been considered in this article are summarized in Table 6-1. In Section 6.4, the method "A" is developed and validated by numerical simulation. In Section 6.5, the block volume calculations by all models for a specific series of field data are compared.

6.4 DEVELOPMENT OF AN ANALYTICAL MODEL FOR CALCULATION OF THE BLOCK VOLUME

Considering the common methods for block volume calculation reviewed in Section 6.3, and despite that Eq. 6-3 is widely used for this purpose [195, 198, 200], a noticeable error is found among the results of this model and real data. Thus, the block volume for 10 cases of rock mass, including three joint sets, has been calculated using Eq. 6-3 and compared with the result of 3DEC software in Table 6-2.

Table 6-2. block volume calculation for a rock mass that includes three joint sets by Eq.6-3 and 3DEC software

	Dip/dip direction			Spacing			Block volume (m3)	
	J_1	J_2	J_3	J_1	J_2	J_3	Eq.6-3	3DEC
1	0/20	50/120	10/300	2	1	3	26.54	23.39
2	30/20	10/100	80/300	4	1	0.5	4.14	4.52
3	10/20	50/200	10/300	1	5	0.5	21.7	23.57
4	0/0	30/130	20/27	2	2	7	260.13	167.64
5	39/44	10/130	20/340	1	2	0.5	5.73	3.70
6	0/10	30/45	40/340	1	2	2	20.70	13.73
7	60/10	25/60	55/300	0.5	4	1	57.58	77.65
8	70/20	45/70	40/240	2	3.5	2.5	24.14	25.30
9	0/10	60/100	70/20	1	3	6	23.28	22.46
10	55/60	20/95	90/180	2	3	2	20.57	25.47

Based on Table 6-2, a considerable difference exists between the block volume calculation obtained using a previously developed model (Eq. 6-3) and the output of numerical simulation. As a result, a new model that can be used to calculate the volume of the block created by three persistent joint sets is developed in the following section. Initially, the significant rock mass parameters needed for block volume calculation are identified. Then, a vectoral model is developed to calculate the block volume in the case of three persistent joint sets. The model is validated by 3D numerical modelling using 3DEC software [225].

6.4.1 Selection of the significant parameters for block size calculation

Rock mass consists of an intact rock and a system of discontinuities. Joint set is a family of parallel and evenly spaced planar discontinuities that can be characterized by dip, dip direction, spacing, and others. Fig 6-1 shows the most significant parameters of a fractured rock mass. The mechanical properties of a rock mass depend largely on the characteristics of the system of discontinuities and the strength of the intact rock [198].
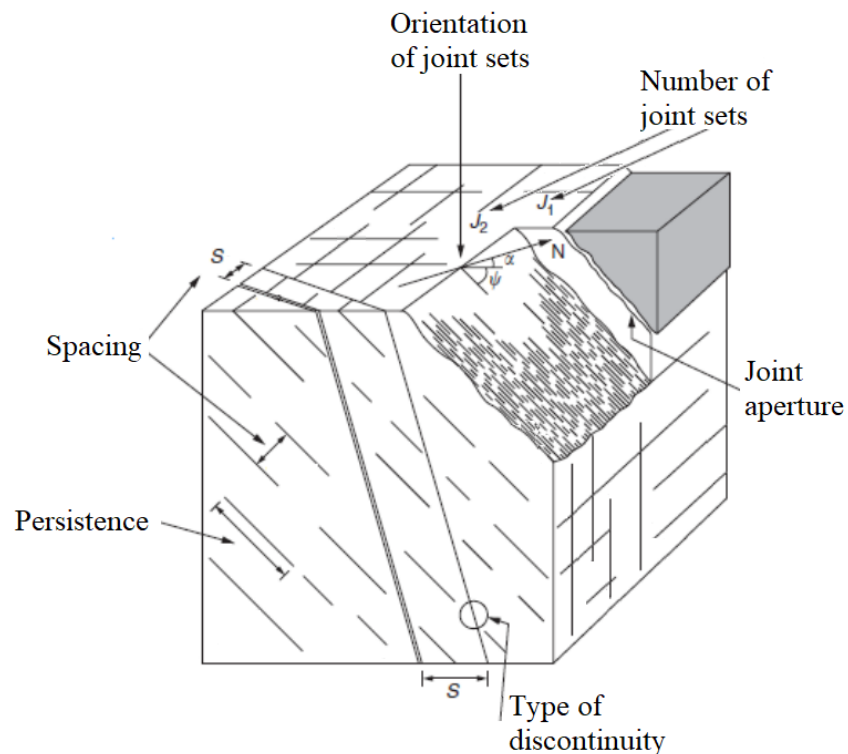
Fig 6-1. The structural characteristics of a rock mass

Based on Fig 6-1, a rock mass is an assembly of blocks superimposed on top of one another. Blocks are formed because of the presence of a system of discontinuities in the rock. Block shape and dimensions are defined by geometrical characteristics of joint sets, i.e., number of joint sets, spacing, dip, dip direction, and persistence. However, other geometrical properties of the rock mass, such as aperture and surface profile, do not affect the block size. An analytical approach is used in this article. Hence, an ideal condition of the discontinuities is assumed for the development of the model. A series of simplifying assumptions are considered, e.g., all joint sets are fully persistent and have fixed values of spacing and orientation. As a result, dip, dip direction, and spacing are assumed

to be the only parameters that define block volume. In addition, according to Palmström [195], for a rock mass that includes less than three joint sets, the random joints define the block volume. For more than three joint sets, the block volume could be determined by considering a rock mass with three joint sets instead. Based on this statement and according to Table 6-1, the rock mass is assumed to include three joint sets.

6.4.2 Model development

Fig 6-2a illustrates the rock mass that is created by cross of three joint sets considering the simplifying assumptions described in Section 6.4.1. However, by creating a model, the boundary blocks are mostly cut by the boundaries of the model, and only a couple of inner blocks remained intact, as shown in Fig 6-2b and c. The outcomes of all previously developed and current models are used to calculate the volume of the intact blocks, i.e., the blocks shown in Fig 6-2c.
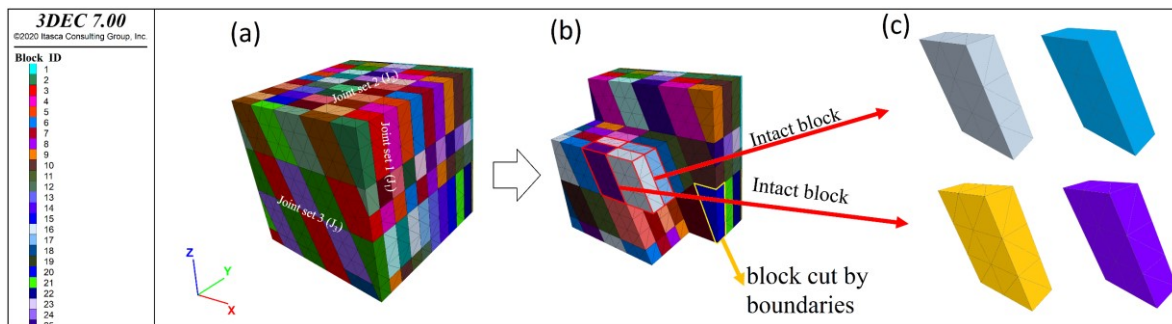
Fig 6-2. The methodology used for the analytical calculation of the block volume. (a) a model comprising three joint sets, (b) the selected block is not cut by the boundaries of the model, (c) all the intact blocks are identical in dimension and volume.

Except for the boundary blocks, the geometries of the all other blocks are identical, as illustrated in Fig 6-2c. To develop the model, one of the intact blocks of Fig 6-2c is selected and analysed in Fig 6-3.
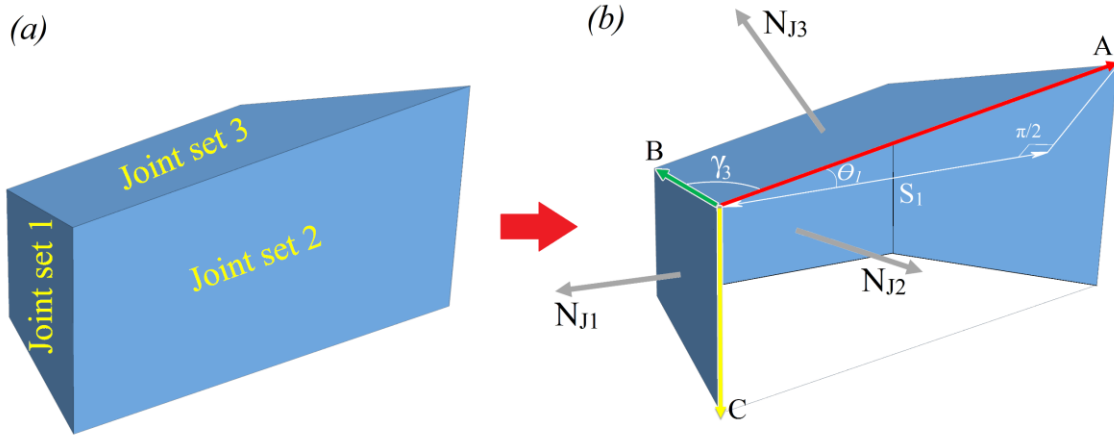
Fig 6-3. Block volume calculation models, (a) an intact block that produced by three joint sets. (b) normal to joint set (N_{J1}, N_{J2} and N_{J3}), edge vectors (A, B, and C) and true spacing of joint set 1 (S_1) as well as the angle between A and S_1 (θ_1) and the angle between joint set 1 and 2 (γ_3)

According to Fig 6-3a, each couple of parallel sides of the parallelepiped belongs to one joint set. On this basis, the edge vectors (A, B, and C) and normal vectors to joint set planes (N_{J1}, N_{J2}, and N_{J3}) are presented in Fig 6-3b. The volume of the parallelepiped could be defined by Eq. 6-17, as follows:

$$V_b^A = \left|(\vec{A} \times \vec{B}).\vec{C}\right|$$

6-17

where V_b^A is the analytically calculated block volume, and A, B, and C are the block's edge vectors. In this equation, the multiplication sign (×) demonstrates the cross product, and the point (.) shows the inner product of a pair of vectors. Each vector and an edge vector have a direction and a magnitude. The direction of a vector can be specified by a unit vector, and for the case of edge vectors, the unit vectors could be defined by Eq. 6-18, as follows:

$$\vec{u_A} = \frac{\vec{N_{J2}} \times \vec{N_{J3}}}{\left|\vec{N_{J2}} \times \vec{N_{J3}}\right|}$$

$$\vec{u_B} = \frac{\vec{N_{J1}} \times \vec{N_{J3}}}{\left|\vec{N_{J1}} \times \vec{N_{J3}}\right|}$$

6-18

$$\vec{u_C} = \frac{\vec{N_{J1}} \times \vec{N_{J2}}}{\left|\vec{N_{J1}} \times \vec{N_{J2}}\right|}$$

where N_{J1}, N_{J2}, and N_{J3} are the normal vectors to joint set J_1, J_2, and J_3, and u_A, u_B, and u_C are the unit vectors of A, B, and C, respectively. According to Fig 6-3, the magnitude of edge vectors could be determined by Eq. 6-19, as follows:

$$|\vec{A}| = \frac{S_1}{\cos \theta_1}$$

$$|\vec{B}| = \frac{S_2}{\cos \theta_2} \qquad\qquad \text{6-19}$$

$$|\vec{C}| = \frac{S_3}{\cos \theta_3}$$

where IAI, IBI, and ICI are the magnitudes of each edge vectors; S_1, S_2, and S_3 are the true spacing of joint sets 1, 2, and 3, respectively; and θ_1, θ_2, and θ_3 are the angles between normal to joint sets and the direction of the edge vectors. These parameters are illustrated in Fig 6-3b. γ (or γ₁ in Fig 6-3b) is the angle considered by the previous studies [195, 198, 200] for the development of Eq. 6-3.

Based on Eq. 6-19, to specify the magnitude of edge vectors, it is essential to determine θ_i. According to Fig 6-3b, the angle θ could be defined by considering the inner product of normal to joint set vectors (N_J) and the unit edge vectors (u) according to Eq. 6-20, as follows:

$$\overrightarrow{u_A}.\overrightarrow{N_{J1}} = |\overrightarrow{u_A}| \times |\overrightarrow{N_{J1}}| \times \cos \theta_1$$

$$\overrightarrow{u_B}.\overrightarrow{N_{J2}} = |\overrightarrow{u_B}| \times |\overrightarrow{N_{J2}}| \times \cos \theta_2 \qquad\qquad \text{6-20}$$

$$\overrightarrow{u_C}.\overrightarrow{N_{J3}} = |\overrightarrow{u_C}| \times |\overrightarrow{N_{J3}}| \times \cos \theta_3$$

Given that u_A, u_B, and u_C and N_{J1}, N_{J2}, and N_{J3} are unit vectors, their absolute values are equal to 1 by combining Eq. 6-18 and Eq. 6-20, as follows:

$$\cos \theta_1 = \left(\frac{\overrightarrow{N_{J2}} \times \overrightarrow{N_{J3}}}{|\overrightarrow{N_{J2}} \times \overrightarrow{N_{J3}}|} \right).\overrightarrow{N_{J1}} \qquad\qquad \text{6-21}$$

143

$$\cos\theta_2 = \left(\frac{\overrightarrow{N_{J1}} \times \overrightarrow{N_{J3}}}{\left|\overrightarrow{N_{J1}} \times \overrightarrow{N_{J3}}\right|}\right) . \overrightarrow{N_{J2}}$$

$$\cos\theta_3 = \left(\frac{\overrightarrow{N_{J1}} \times \overrightarrow{N_{J2}}}{\left|\overrightarrow{N_{J1}} \times \overrightarrow{N_{J2}}\right|}\right) . \overrightarrow{N_{J3}}$$

Considering Eq. 6-18, Eq. 6-19, and Eq. 6-21, the vectors A, B, and C could be determined by Eq. 6-22, as follows:

$$\vec{A} = \left|\vec{A}\right| \times \overrightarrow{u_A} = \frac{S_1}{\left(\overrightarrow{N_{J2}} \times \overrightarrow{N_{J3}}\right) . \overrightarrow{N_{J1}}} \times \left(\overrightarrow{N_{J2}} \times \overrightarrow{N_{J3}}\right)$$

$$\vec{B} = \left|\vec{B}\right| \times \overrightarrow{u_B} = \frac{S_2}{\left(\overrightarrow{N_{J1}} \times \overrightarrow{N_{J3}}\right) . \overrightarrow{N_{J2}}} \times \left(\overrightarrow{N_{J1}} \times \overrightarrow{N_{J3}}\right) \qquad \text{6-22}$$

$$\vec{C} = \left|\vec{C}\right| \times \overrightarrow{u_C} = \frac{S_3}{\left(\overrightarrow{N_{J1}} \times \overrightarrow{N_{J2}}\right) . \overrightarrow{N_{J3}}} \times \left(\overrightarrow{N_{J1}} \times \overrightarrow{N_{J2}}\right)$$

The normal vector to joint sets (N_{J1}, N_{J2}, and N_{J3}) could be defined by Eq. 6-23, as follows:

$$\overrightarrow{N_{J1}} = (\sin DD_1 . \sin D_1)\vec{\imath}, (\cos DD_1 . \sin D_1)\vec{\jmath}, (-\cos D_1)\vec{k}$$

$$\overrightarrow{N_{J2}} = (\sin DD_2 . \sin D_2)\vec{\imath}, (\cos DD_2 . \sin D_2)\vec{\jmath}, (-\cos D_2)\vec{k} \qquad \text{6-23}$$

$$\overrightarrow{N_{J3}} = (\sin DD_3 . \sin D_3)\vec{\imath}, (\cos DD_3 . \sin D_3)\vec{\jmath}, (-\cos D_3)\vec{k}$$

where DD_1, DD_2, and DD_3 are dip directions, and D_1, D_2, and D_3 are dip of the joint sets 1, 2 and 3, respectively. Finally, block volume could be specified through the incorporation of Eq. 6-23 and Eq. 6-22 into Eq. 6-17. By obtaining the information on the dip, dip direction, and true spacing of the three joint sets, the volume of the intact blocks could be determined by Eq. 6-17. For easier use of Eq. 6-17, an excel spreadsheet for calculating the block volume has been attached to this article.

6.4.3 Model validation

The result of the proposed method for the calculation of the block volume with Eq. 6-17 is compared with the output of the numerical simulations using 3DEC version 7 software [225]. A series

of 13 cases with various arrangements of dip, dip direction, and spacing are considered. Accordingly, the results of each method are listed in Table 6-3. The volume calculated in Table 6-2 and Table 6-3 belongs to the intact block, as shown in Fig 6-2b and c.

Table 6-3. Discontinuity's characteristics used for comparison of block volume calculation by analytical and numerical methods

Cas e	Joint set 1			Joint set 2			Joint set 3			Block volume (m^3)	
	DIP 1	DD 1	Spacing 1 (m)	DIP 2	DD 2	Spacing 2 (m)	DIP 3	DD 3	Spacing 3 (m)	3DEC	Eq.6-1 7
1	23	30	0.34	20	10	2.05	27	320	0.14	15.14	15.14
2	90	350	0.39	20	352	0.14	90	10	0.39	0.07	0.07
3	73	25	0.35	61	352	0.35	84	8	5.91	4.60	4.60
4	22	25	0.34	90	350	0.98	60	0	0.35	3.65	3.65
5	90	350	0.39	90	10	0.39	32	50	2.05	1.08	1.08
6	90	350	5.91	90	70	0.14	90	30	5.2	N/A	N/A
7	20	350	0.34	22	25	1.37	61	354	5.2	17.02	17.02
8	54	65	0.34	90	350	0.98	90	30	0.35	0.31	0.31
9	80	0	5.91	90	70	0.14	66	292	0.34	1.04	1.04
10	60	0	3.46	67	340	5.2	90	30	0.87	85.36	85.35
11	90	30	3.46	54	295	1.37	80	0	3.94	124.94	124.90
12	90	70	0.34	43	300	1.37	73	25	5.2	7.09	7.09
13	43	60	0.14	73	335	5.2	90	10	0.39	0.51	0.51

To numerically calculate the volume of the intact block with 3DEC software, a FISH function is embedded in the command lines to define the maximum block size of the model. The numerical model should be large enough to contain at least one intact block. The maximum block size did not change with further increase of the model size.

In addition, according to Table 6-2, in most of the cases, a major difference exists among the results of the previously developed model [195] and the output of the numerical simulations. However, the calculation of the block volume with the developed model is completely in accordance with the results of 3DEC, as shown in Table 6-3. Furthermore, in case number 6 of Table 6-3, the block volume is defined to be unlimited by numerical simulations and by Eq. 6-17. However, Eq. 6-3 specifies a real value for the block volume that is calculated by this method (10.57 m^3).

A series of analytical models are already developed to calculate the volume of blocks formed by the cross of three joint sets in a rock mass, as listed in Table 6-1. In all models, all joint sets can be assumed to be persistent, and the orientations and spacing of the discontinuities are constant. As the results of these methods are not sufficiently accurate, a more efficient model is developed in the

current study. This developed method calculates the block volume by determining the dip, dip direction, and spacing of the joint sets.

Based on Eq. 6-17, the block volume is defined by inner and cross products of parallelepiped edge vectors. If all edge vectors (A, B, and C) are perpendicular to each other, the volume of the formed block is equal to multiply of the edge's values. This case is correctly calculated by considering $\Theta_1 = \Theta_2 = \Theta_3 = \pi/2$ in Eq. 6-21 and Eq. 6-22. Accordingly, the block volume is defined by $V_b^A = |A| \times |B| \times |C|$. However, the volume of the case number 6 in Table 6-3 is defined as 10.57 m³ by Eq. 6-3 despite the fact that Eq. 6-17 and the numerical model calculate the infinite block volume for this case. For better comprehension of the case, a 3D model of case number 6 with different values of spacing is illustrated in Fig 6-4. The spacing is selected to be different from case number 6 for better block visualization. However, it does not affect the whole issue.
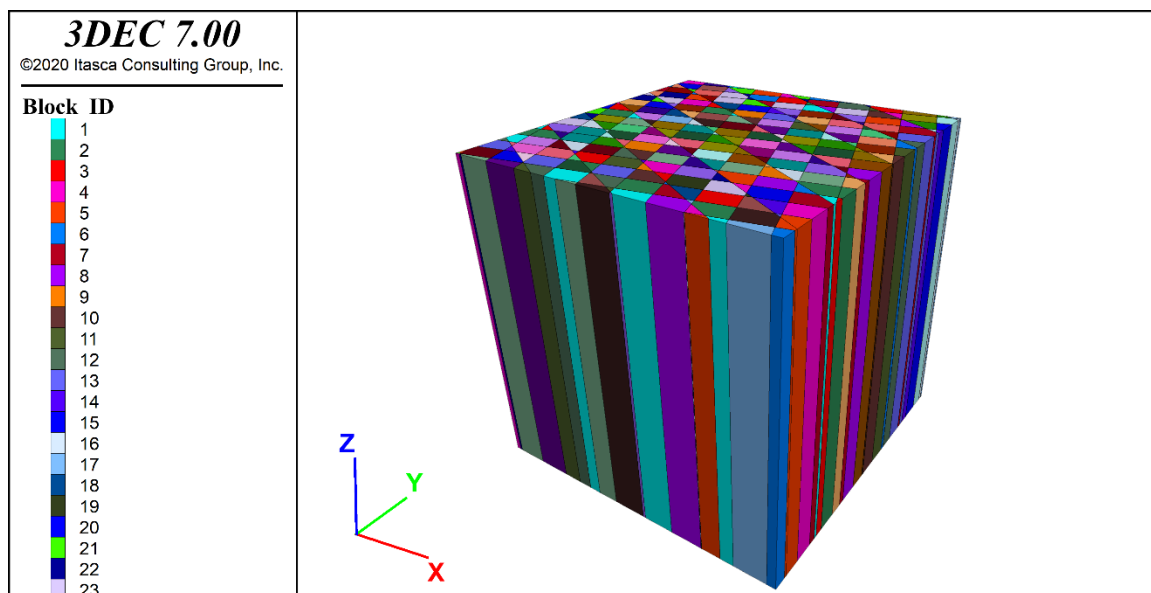
Fig 6-4. A 20x20 m rock mass that includes three joint sets with dip/dip direction according to case number 6 in Table 6-3, but with different spacings (2, 3, and 4 meters for joint sets 1, 2, and 3, respectively).

According to Fig 6-4, all formed blocks are stretched vertically. Hence, by increasing the size of the model, the blocks expand in an unlimited manner. The output obtained using the developed model is in accordance with the results of the numerical simulations, and both are different from the output obtained using the previously developed model (Eq. 6-3).

146

6.5 COMPARISON OF THE METHODS FOR BLOCK VOLUME CALCULATION

6.5.1 Preparation of the database

The Pells database [239] was used to compare previously developed models with the one presented in this article (method "A"). This database was made up of field data collected from more than 100 real case studies conducted on the uncoated flow channels of the spillways in Australia and South Africa. In addition, it summarizes all the relevant geomechanical parameters, i.e., dip, dip direction of joints, and spacings. To adjust the compatibility between this database and the methods listed in Table 6-1, the cases that include only three persistent joint sets and do not comprise columnar blocks, as shown in Fig 6-4, are selected in this study and listed in Table 6-4.

Table 6-4. Characteristic data of the database summarizing the case studies

	Dip/Dip direction			Joint spacing (m)				Angle between joint sets (°)			
	Joint Set 1	Joint Set 2	Joint Set 3	Joint Set 1	Joint Set 2	Joint Set 3	Average (S$_a$)	Angle 1-2	Angle 1-3	Angle 2-3	Average
1	25/110	30/230	20/220	0.75	1	1.5	1.08	47	36	11	31
2	10/50	90/192	90/50	0.35	2.5	6	2.95	97	80	142	106
3	05/50	35/50	90/120	0.35	6	4	3.45	30	88	78	65
4	10/50	80/130	90/65	1.5	4.5	0.06	2.02	78	80	65	74
5	10/50	30/350	90/50	1.2	0.75	10	3.98	26	80	75	60
6	05/50	90/140	90/80	1.75	0.4	0.7	0.95	90	85	60	78
7	5/200	80/250	80/225	1.5	1.75	10	4.42	76	75	24	58
8	5/200	80/250	80/225	1.5	3	10	4.83	76	75	24	58
9	5/200	80/225	80/140	0.65	6.5	0.65	2.60	75	77	83	78
10	5/200	80/225	80/140	0.65	6.5	0.65	2.60	75	77	83	78
11	57/150	80/243	19/165	0.4	1.1	1.35	0.95	87	38	76	67
12	57/150	80/243	19/165	0.4	1.1	1.35	0.95	87	38	76	67
13	57/150	80/243	19/165	0.4	1.1	1.35	0.95	87	38	76	67
14	70/77	80/335	35/335	0.22	0.3	0.4	0.31	97	80	45	74
15	20/74	80/335	80/290	0.8	0.55	1.6	0.98	83	96	44	74
16	20/63	80/316	75/5	0.8	0.55	0.55	0.63	86	65	48	66
17	41/193	72/244	80/337	0.8	0.8	0.8	0.80	51	113	89	84
18	85/280	76/51	27/208	0.65	1.5	0.8	0.98	128	77	101	102
19	90/98	90/192	0/100	0.7	0.7	0.5	0.63	94	90	90	91
20	50/160	90/255	35/155	0.9	0.4	1.15	0.82	71	15	79	55
21	9/105	90/237	90/170	0.4	8	20	9.47	96	86	67	83
22	9/105	90/237	90/170	0.4	8	20	9.47	96	86	67	83
23	9/105	90/237	90/170	0.4	8	15	7.80	96	86	67	83
24	9/105	90/237	90/170	0.4	8	15	7.80	96	86	67	83
25	0/150	90/75	90/202	0.6	0.075	0.2	0.29	90	90	127	102
26	12/150	90/75	90/202	0.6	0.075	0.2	0.29	87	82	127	99
27	10/65	62/75	90/310	0.35	1	0.5	0.62	52	94	120	89
28	35/200	90/202	90/310	0.35	0.2	0.5	0.35	55	101	108	88
29	22/228	75/172	77/246	0.15	0.1	0.15	0.13	64	56	71	64
30	80/278	80/130	35/280	10	0.3	0.55	3.62	142	45	110	99
31	75/278	80/130	58/200	10	1	0.4	3.80	101	56	67	75
32	90/220	86/103	9/133	0.8	3	0.45	1.42	116	89	78	94
33	80/231	65/162	15/250	1.25	0.2	0.45	0.63	66	65	65	65
34	62/243	83/144	34/130	0.19	0.45	0.45	0.36	94	78	50	74
35	25/150	35/340	85/250	0.4	2	0.4	0.93	59	89	86	78
36	25/150	35/340	85/250	0.4	2	0.4	0.93	59	89	86	78

	Dip/Dip direction			Joint spacing (m)				Angle between joint sets (°)			
	Joint Set 1	Joint Set 2	Joint Set 3	Joint Set 1	Joint Set 2	Joint Set 3	Average (S$_a$)	Angle 1-2	Angle 1-3	Angle 2-3	Average
37	65/250	85/190	55/350	0.4	0.13	0.4	0.31	60	83	135	93
38	65/250	85/190	55/350	0.4	0.06	0.4	0.29	60	83	135	93
39	25/110	90/90	90/0	0.4	1.3	1.3	1.00	66	98	90	85
40	25/110	90/90	90/0	0.4	1.3	1.3	1.00	66	98	90	85
41	25/110	90/90	90/0	0.4	1.3	1.3	1.00	66	98	90	85
42	25/110	90/90	60/0	0.4	1.3	1.3	1.00	66	70	90	75
43	25/110	90/90	60/0	0.4	1.3	1.3	1.00	66	70	90	75
44	45/55	57/235	75/0	0.06	0.06	0.06	0.06	102	55	109	89
45	45/55	57/235	75/0	0.06	0.06	0.06	0.06	102	55	109	89
46	45/55	57/235	75/0	0.06	0.06	0.06	0.06	102	55	109	89
47	45/55	57/235	75/0	0.06	0.06	0.06	0.06	102	55	109	89
48	25/0	60/220	63/145	0.4	0.06	1.3	0.59	80	84	64	76
49	25/0	60/220	63/145	0.4	1.3	1.3	1.00	80	84	64	76
50	25/0	60/220	63/145	0.4	1.3	1.3	1.00	80	84	64	76
51	20/270	72/180	85/0	1.3	1.3	1.3	1.30	73	85	157	105
52	20/270	72/180	85/0	1.3	1.3	1.3	1.30	73	85	157	105
53	20/270	72/180	85/0	0.4	0.4	0.4	0.40	73	85	157	105
54	20/270	72/180	85/0	0.4	0.4	0.4	0.40	73	85	157	105
55	20/270	72/180	85/0	0.4	0.13	0.4	0.31	73	85	157	105
56	15/150	80/250	80/90	1.3	1.3	0.4	1.00	82	72	151	102
57	15/150	80/250	80/90	1.3	1.3	0.4	1.00	82	72	151	102
58	15/150	80/250	80/90	1.3	1.3	0.4	1.00	82	72	151	102
59	15/150	80/250	80/90	1.3	1.3	0.4	1.00	82	72	151	102
60	15/150	80/250	80/90	1.3	1.3	0.4	1.00	82	72	151	102
61	0/0	90/10	80/290	1.3	1.3	1.3	1.30	90	80	80	83
62	0/0	90/10	80/290	0.4	1.3	0.4	0.70	90	80	80	83
63	0/0	90/10	80/290	1.3	1.3	1.3	1.30	90	80	80	83
64	0/0	90/10	80/290	1.3	1.3	1.3	1.30	90	80	80	83
65	0/0	90/10	80/290	0.4	0.4	0.4	0.40	90	80	80	83
66	0/0	90/10	80/290	1.3	1.3	1.3	1.30	90	80	80	83
67	0/0	90/10	80/290	0.4	0.4	0.4	0.40	90	80	80	83
68	30/12	90/105	80/195	0.4	0.4	0.13	0.31	91	110	90	97
69	30/12	90/105	80/195	0.4	0.4	0.13	0.31	91	110	90	97
70	30/12	90/105	80/195	0.4	0.4	0.13	0.31	91	110	90	97
71	30/12	90/105	80/195	0.4	0.4	0.13	0.31	91	110	90	97
72	30/12	90/105	80/195	0.4	0.4	0.13	0.31	91	110	90	97

1

2

6.5.2 Block volume calculation

The block volume is calculated using the previously developed methods listed in Table 6-1 and the method developed in this study (Eq. 6-17- method "A"), and the results are presented in Fig 6-5.
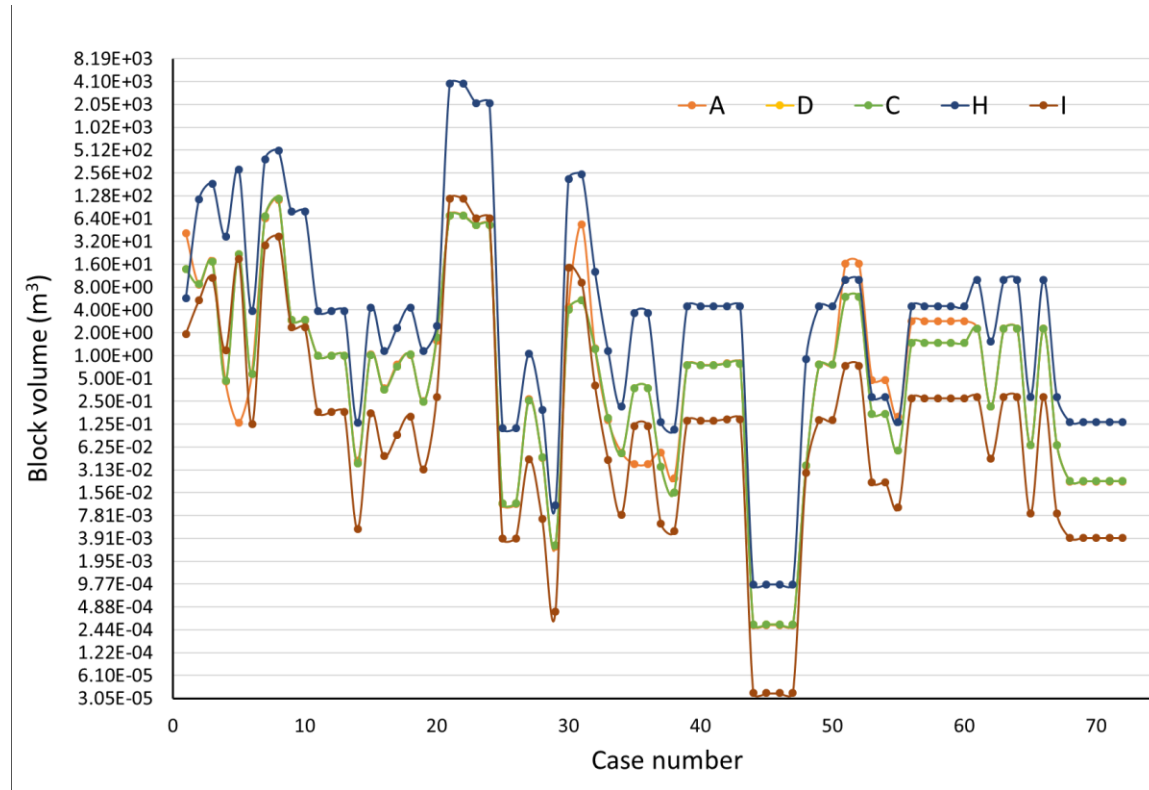
Fig 6-5. Graphical representation of the block volumes for the cases presented in Table 6-4, that are calculated by models of Table 6-1 and the method that is developed in this article (method "A")

According to Fig 6-5, the results of the models are compatible in some ranges and incompatible in other ranges. Most of the differences exist in the range of case numbers 1 to 11, 20 to 25, 29 to 32, 44 to 47, and 67 to 72. Method A (Eq. 6-17) can calculate the block volume accurately. Thus, whether the method overestimates or underestimates the block volume was determined. Comparison result of the graphs of other methods with method A shows that methods H, D, and C mostly overestimate, whereas method I greatly underestimates block volume in some ranges.

From Fig 6-5 and according to Elci and Turk [229], a noticeable difference exists between the actual value of the block volume and that obtained using previously developed methods. To better evaluate the

differences, the Root Mean Square Error (RMSE) of the methods for block volume calculation of the cases in Fig 6-5 is explained in detail in Section 6.5.3.

6.5.3 Root Mean Square Error (RMSE) calculation

RMSE measures the difference between the actual and expected values of a specific parameter. The lower the RMSE value, the more accuracy is expected. For block volume calculation, RMSE is calculated by comparing results obtained using the previously developed models with method A (Eq. 6-17), as the accuracy of this method is already validated in Section 6.4.3. The RMSE values of each method are listed in Table 6-5.

Table 6-5. RMSE of block volume calculation results obtained by previously developed methods compared with the method developed in this study (Eq. 6-17) for the cases in Fig 6-5

Method	Equation	Reference value	RMSE
D	$V_b = \dfrac{S_1 \times S_2 \times S_3}{\sin \gamma_1 \times \sin \gamma_2 \times \sin \gamma_3}$		7
E	$V_b = S_a^3$		148
C	$V_b = \dfrac{\beta \times J_v^{-3}}{\sin \gamma_1 \times \sin \gamma_2 \times \sin \gamma_3}$	$V_b^A = \left|(\vec{A} \times \vec{B}).\vec{C}\right|$	7
I	$V_b = \dfrac{1}{\sin \gamma_1 \times \sin \gamma_2 \times \sin \gamma_3} \times (S_a/2)^3$		15
H	$V_b = 36 \times (S_a/2)^3$		20

Based on Table 6-5, the accuracy of most of the previously developed models is questioned. The RMSE varies from 7 to 148 and shows a noticeable deviation between the actual and the calculated values. The source of the error is discussed in Section 6.6 to identify block characteristics that affect the accuracy of block size values.

6.6 DISCUSSION

Geomechanical and geometrical characteristics of the joints have an indisputable impact on the mechanical properties of the rock mass. The block volume is a geometrical parameter that has a significant

impact on the mechanical properties of the fractured rock mass. Commonly used methods for calculating block size in a fractured rock mass were developed based on measurements of spacings and the orientation of the joint sets. For better discussion of the various methods, all joint sets in a rock mass are assumed to be persistent. Eq. 6-3 is one of the most widely used equations and comprises the spacings of the joint sets and the angle between them. This equation comprises 3 parts ($S_i/\sin\gamma_i$), and as a result, the author estimated $\sin\gamma_i$ by $\cos\theta_i$; i.e., $\sin\gamma_i \approx \cos\theta_i$, where θ_i is the angle between apparent and true spacing of joint sets, as illustrated in Fig 6-3. Therefore, $S_i/\sin\gamma_i \approx Sp_i$, where Sp_i is the apparent spacing of joint set i. By these assumptions, Eq. 6-3 calculates the block volume by the multiplication of three apparent spacings. Almost the same logic is behind the development of the other equations for the calculation of the block volume. However, two major criticisms of the utilization of these methods exist. First of all, approximation of the volume of a parallelepiped block by multiplication of the apparent spacings by itself is accompanied with error; it is a reminder of the right method for calculation of the parallelepiped volume. The second source of the error belongs to the estimation of the apparent spacings by true spacing and the angle between joint sets. The apparent spacing is accurately calculated using the $Sp_i = S_i/\cos\theta_i$ relation. However, approximation of $\sin\gamma_i$ by $\cos\theta_i$ is fundamentally accompanied by the error in calculation of the block volume. This phenomenon occurs despite the fact that the angle θ_i is considered for the development of Eq. 6-17.

Table 6-5 lists the errors produced by each method compared with the block volume calculated by Eq. 6-17. However, the error values differ from one model to another. At first glance, the accuracy of the method that has the least difference with method A, i.e., methods D and C in Table 6-5, is more than that of the other models. However, the type of data and geometrical characteristics of the rock mass that are used to determine the error has a direct impact on the error value. To systematically evaluate the error of each method for calculation of the block volume, the error function should be specified in the range of variation of the effective parameters. By doing this, specifying the ranges of reliability for each model becomes possible. However, the error values listed in Table 6-5 are a sample of the field data for calculation of the block volume and could represent the overall accuracy of each model.

6.7 CONCLUSION

An analytical model based on vectoral multiplication has been developed to calculate the block volume for the case of three persistent joint sets with constant values of spacing and orientation. The accuracy of the model is validated by the numerical simulation. The results of the developed model are more reliable than those of the previously developed ones. The method could be applied using the vectoral multiplication (an excel spreadsheet is attached to this article) by knowing dip, dip direction, and spacings of joint sets.

The accuracy of each method in block volume calculation is evaluated using a series of field data in Table 6-5. Despite that the error values differ from one model to another, a range of variation for each parameter could be specified, so that the accuracy level of the model can be acceptable. This issue is the subject of future research, and the relevant results will be published in the next reports.

6.8 DECLARATIONS

6.8.1 Declaration of Competing Interest

The authors declare that there is no conflict of interest associated with this publication.

6.8.2 Code availability

The Itasca 3DEC version 7.0 software with license number 215-001-0266-00001 under the IEP loan program has been used in this research.

6.8.3 Authors' Contribution

Aboubacar Sidiki Koulibaly: Resources, Formal analysis, Investigation, Writing-original draft; Alireza Shahbazi: Conceptualization, Resources, Data curation, Software, validation, Methodology, Writing-original draft; Ali Saeidi: Conceptualization, Supervision, Investigation, Methodology, Project administration, Writing-review & editing; Romain Chesnaux: Supervision, Writing-review & editing; Alain Rouleau: Conceptualization, Supervision, Writing-review & editing; Marco Quirion: Funding acquisition,

6.9 ACKNOWLEDGMENT

CHAPTER 7

Article 6: Development of a practical method for calculation of the block volume and block surface in a fractured rock mass

7.1 HIGHLIGHTS

- ☐ A method is developed for calculation of block volume by using the stereonet

- ☐ Spacing and orientation of joints are determinant parameters of block dimension

- ☐ Error source of previous models for block volume calculation is identified

- ☐ Volumetric fracture intensity and Surface area of blocks are analytically calculated

7.2 ABSTRACT

A practical method based on the geometrical characteristics of three persistent joint set is proposed for calculation of the volume and surface area of the blocks that are created by cross of three persistent joint sets in a fractured rock mass. It is illustrated that the block volume and surface area relate to the true spacings of the joint sets as well as the angle between edge vectors and normal to joint sets. Knowing the values of the spacings, the method for determining the required angles is presented using the stereographic projections of joint sets. In order to validate the equations, the output of proposed models is validated using 3DEC version 7.0 software. In addition, by using the response surface methodology (RSM), the effect of each parameter on block volume and surface calculation is shown. Furthermore, the error that is produced by previously developed models for calculation of the block volume is analysed and the range of reliability of each method is identified. Design-Expert version 11 has been used for this purpose. It is clear that by dividing the block surface by block volume, the volumetric fracture intensity (P_{32}) could be analytically determined by using the stereographic projection.

Keywords: Block volume, Block surface, 3DEC, Rock mass, RSM

7.3 INTRODUCTION

Shape and size of blocks in a fractured rock mass have a significant role in rock mechanics and rock engineering, and could be considered as an important indicator of rock mass quality. Stability, permeability,

erodibility and reinforcement of the underground excavations are significantly affected by the size of rock blocks. Over the years, different methods have been developed for calculation of block volume. Most of investigations for this purpose have been accomplished by Palmström between 1974 to 2005. He developed a series of equations by assuming various hypothesizes. As one of the first and let say, the fundamental to many other models in this regard, Palmström [228] developed Eq.7-1 for calculation of the block volume for the case that the rock mass includes three persistent joint sets and the angle between each pair of sets are known.

$$V_b = \frac{S_1 \times S_2 \times S_3}{\sin \gamma_1 \times \sin \gamma_2 \times \sin \gamma_3} \qquad \text{7-1}$$

Where S_1, S_2 and S_3 are the spacings of joint sets 1, 2 and 3, respectively and γ_1, γ_2 and γ_3 are the angles between each pair of joint sets. In Eq.7-1, the impact of all affecting parameters in block volume calculations were considered, except the persistence, which was also considered later by Cai [200]. As a result, the volume of the blocks in the case of non-persistent joints could be calculated using Eq.7-2:

$$V_b = \frac{S_1 S_2 S_3}{\sin \gamma_1 \sin \gamma_2 \sin \gamma_3 \sqrt[3]{P_1 P_2 P_3}} \qquad \text{7-2}$$

Where P_1, P_2 and P_3 are the persistence of joint sets 1, 2 and 3, respectively. Taking into account various assumptions and methods, several equations were formerly developed for calculation of the block volume and in this regard, a summary of them have been listed in Table 7-1.

Table 7-1. Existing methods for calculation of the volume of the blocks that formed by cross of joint sets

Reference	Equation	Parameters	Assumptions
Barton [230]	$V_b = RQD/J_n$	RQD: Rock Quality Designator J_n: Joint set number	The block volume could be estimated by the first two parameters of Q-system
Palmström [227]	$V_b = \dfrac{\beta \times J_v^{-3}}{\sin \gamma_1 \times \sin \gamma_2 \times \sin \gamma_3}$	J_v: Volumetric joint count β: Block shape factor	the block volume as a function of volumetric joint count
Palmström [228]	$V_b = \dfrac{S_1 \times S_2 \times S_3}{\sin \gamma_1 \times \sin \gamma_2 \times \sin \gamma_3}$	S_i: average spacing of set i γ_i: angle between pair of joint sets	3 persistent joint sets with known spacing and orientation
Palmström [228]	$V_b = \dfrac{\beta \times wJd^{-3}}{\sin \gamma_1 \times \sin \gamma_2 \times \sin \gamma_3}$	wJd: weighted joint density β: block shape factor	the block volume as a function of weighted joint density

Cai [200]	$V_b = \dfrac{S_1 \times S_2 \times S_3}{\sin\gamma_1 \sin\gamma_2 \sin\gamma_3 \sqrt[3]{P_1 P_2 P_3}}$	S_i: average spacing of set i γ_i: angle between pair of joint sets P_i: persistence of set i	3 non-persistent joint sets with known spacing and orientations
Latham [232]	$V_b = 36 \times (S_a/2)^3$	S_a: average spacing measured along the drilling direction (m)	$\beta=36$, there are many sub-vertical joints noted in the core logs, bedding is known to be typically at 35°

The mechanical behaviour of the rock mass is affected by a series of geomechanical characteristics including uniaxial compressive strength (UCS), the inter-block shear strength (J_r/J_a), block size (V_b) and the opening of the joints (J_o). Among these parameters, block geometry is doubly important in the stability of underground and aboveground structures [198, 224, 226]. In this regard, various analytical models for calculation of the block volume have been developed [198, 200, 224, 227-230], as they are listed in Table 7-1. However, block volume that is calculated by these methods mostly have deviation from real field data. As an example, Elci and Turk [229] mentioned that the calculated the block volume (V_b) using the analytical methods and by having the average spacing of the discontinuities (S_a), their real spacing (S), and the number of volumetric joints (J_v) showed a significant differences with its real values.

In this study, on the basis of vectoral model for calculation of the block volume [240], an analytical model is developed for this purpose by using the stereographic projection of joint sets. The accuracy of the model is validated by the numerical simulation using 3DEC version 7 software [225]. This is despite the fact that there is a noticeable discrepancy exist between the output of this method (or numerical simulation) and all methods that are listed in Table 7-1. In addition, an analytical equation has been developed for block surface calculation on the basis of formerly developed vectoral model [220, 241] and validated using numerical simulation. Since no analytical model is yet developed for block surface calculation, the comparison of this method with other models could not been performed. The stereographic method for calculation of the block volume and surface has been explained, as well. Finally, by using the response surface methodology (RSM), the impact of the affecting parameters on the error of each method that are listed in Table 7-1 are discussed.

Since the accurate calculation of the block volume will have a significant impact on acceptable estimation of mechanical and hydrological characteristics of the rock mass, the output of this study will have

a considerable impact on the past and future works in these fields. There is exist a couple of geomechanical characteristics of the rock mass that were formerly defined by using the block volume [198, 200], and by considering this investigation, they need to profoundly being revised, as almost all previously developed equation for calculation of the block volume include a significant amount of error in their equations. In addition, the block surface area was never being formulated formerly and hence, this article is the first investigation that introduces an analytical method for block surface calculation. Consequently, the volumetric fracture intensity (P_{32}) could be analytically calculated using the equations of block volume and surface. Totally, the engineers, practitioners and professionals in the field of rock mechanics and geology will experience a more reliable and accurate value of the block volume by using the equation that is introduced by this study. Despite there are a number of assumptions used for developing these models, e.g., the existence of three persistent joint sets in a rock mass, however, the comprehensiveness of the model could be improved by including more affecting parameters in the model, such as joint persistence and number of joint sets.

7.4 MODEL DEVELOPMENT

Based on the existing equations for calculation of the block volume that is provided in Table 7-1 and in spite of widespread application of Eq.7-1 for this purpose [195], a significant discrepancy already exists between the results of this model and field data. Accordingly, new models are developed in section 7.4.2 for calculation of the volume and surface of the block that is created by three persistent joint sets by knowing dip, dip direction and spacing of joints and using the stereographic projection method. Therefore, signification parameters that affect the volume and surface of the block are discussed in section 7.4.1. In addition, the output of the models is validated using the results of 3DEC version 7 software in section 7.4.3.

7.4.1 Selection of the parameters

The mechanical characteristics of a rock mass mostly depend on the properties of the rock matrix and the fracture networks [198]. Fracture networks consist of joint sets; i.e., a family of parallel, evenly spaced discontinuities that can be specified by orientation (dip, dip direction), spacing, etc. Fig 7-1 shows the most significant parameters of a fractured rock mass.
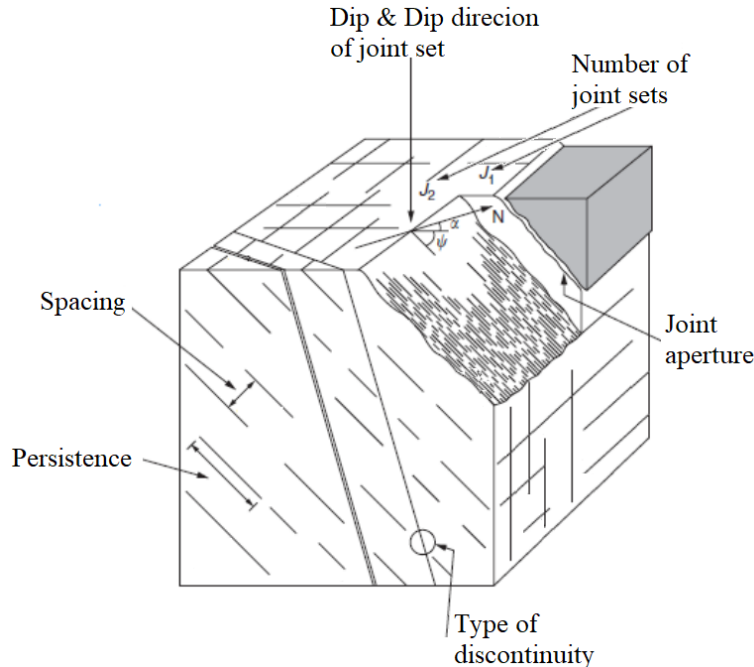
Fig 7-1. The structural characteristics of a rock mass

Basically, blocks are produced due to the existence of a system of discontinuities in rock mass, that its size and shape are defined by geometrical characteristics of joint sets, such as spacing, orientation, joint set number and persistence. In this article, the analytical method is used for determination of the block volume and surface and for this purpose, the ideal conditions of the discontinuities are considered. In this regard, it is assumed that joint sets are persistent and the values of spacing and orientation are fixed in a joint set. On this basis, it is assumed that the volume and surface area of the block could be determined by knowing the dip, dip direction and spacing of joint sets, and the persistence is not included for development of this model. In addition, if the rock mass contains less than three joint sets, the random joints are defining the block volume and for more than three joint sets, the block volume could be determined by considering a rock mass with three joint sets, instead [195]. On this basis, it is assumed that the rock mass comprises of three joint sets. It is a reasonable assumption since most of the models that are listed in Table 7-1 were developed on the basis of this hypothesis. Therefore, the parameters that have been considered for development of the models are the spacing and orientation of joint sets.

7.4.2 Development of the model

Based on the vectoral model that was formerly developed for calculation of the block volume and surface of a fractured rock mass [220, 240, 241], the surface area and volume of the blocks that are formed by cross of three persistent joint sets, could be calculated using Eqs.7-3 and 7-4.

$$S_b^A = 2 \times \left(\left| \vec{A} \times \vec{B} \right| + \left| \vec{A} \times \vec{C} \right| + \left| \vec{B} \times \vec{C} \right| \right) \qquad \text{7-3}$$

$$V_b^A = \left| (\vec{A} \times \vec{B}).\vec{C} \right| \qquad \text{7-4}$$

Where S_b^A and V_b^A are the vectorially calculated block surface area and block volume, respectively, and A, B and C are the edge vectors of the block, as it is illustrated in Fig 7-2.
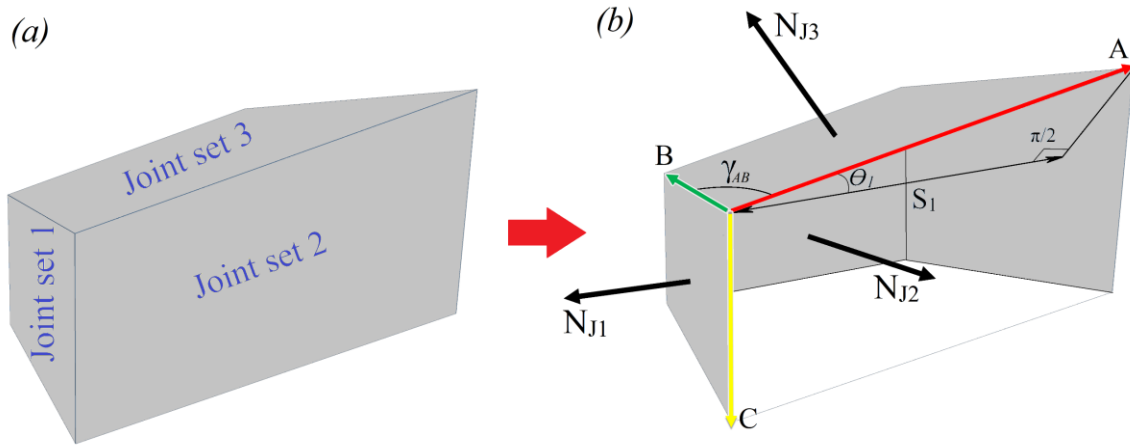
Fig 7-2. The block that is created by the cross of joint sets 1, 2 and 3 for development of the model (a) the produced intact block as a result of three persistent joint sets. (b) Inner view of an intact block. Edge vectors (A, B and C), normal to joint set (N_{J1}, N_{J2} and N_{J3}) and true spacing of joint set 1 (S_1) as well as the angle between edge vector A and S_1 (θ_1) and the angle between edge vector A and B (γ_{AB}).

In order to make Eqs.7-3 and 7-4 simpler and more compatible to be used in field work applications, the vectoral multiplication of edge vectors should be performed for finding the volume and surface area of the block. For this purpose, and according to Fig 7-2, edge vectors could be determined using Eqs.7-5.

$$\vec{A} = \left| \vec{A} \right| \times \overrightarrow{u_A} = \frac{S_1}{\cos \theta_1} \times \overrightarrow{u_A}$$

$$\vec{B} = \left| \vec{B} \right| \times \overrightarrow{u_B} = \frac{S_2}{\cos \theta_2} \times \overrightarrow{u_B} \qquad \text{7-5}$$

$$\vec{C} = |\vec{C}| \times \overrightarrow{u_C} = \frac{S_3}{\cos\theta_3} \times \overrightarrow{u_C}$$

Where S_1, S_2 and S_3 are the true spacings of joint sets 1, 2 and 3, respectively; u_A, u_B and u_C are the unit edge vectors A, B and C, and θ_1, θ_2 and θ_3 are the angle between edge vectors and direction of true spacings measurement (or normal to joint sets). Also, N_{J1}, N_{J2} and N_{J3} are the unit vectors of normal to joint sets. From Eq.7-5 and knowing that $\vec{u}_A \times \vec{u}_B = \vec{N}_{j3}$ (Fig 7-2), the cross product of vectors A and B will be:

$$\vec{A} \times \vec{B} = |\vec{A}| \times |\vec{B}| \times \sin\gamma_{AB} \times \overrightarrow{N_{J3}} = \frac{S_1}{\cos\theta_1} \times \frac{S_2}{\cos\theta_2} \times \sin\gamma_{AB} \times \overrightarrow{N_{J3}} \qquad \text{7-6}$$

Where γ_{AB} is the angle between edge vectors A and B, as illustrated in Fig 7-2. For finding the volume of the blocks, Eq.7-4, Eq.7-5 and Eq.7-6 should be combined. Then:

$$(\vec{A} \times \vec{B}).\vec{C} = \left[\left(\frac{S_1}{\cos\theta_1} \times \frac{S_2}{\cos\theta_2} \times \sin\gamma_{AB}\right) \times \overrightarrow{N_{J3}}\right].\left(\frac{S_3}{\cos\theta_3} \times \overrightarrow{u_C}\right) \qquad \text{7-7}$$

Given that the angle between N_{J3} and u_C is equal to θ_3, Eq.7-7 converts to Eq.7-8.

$$(\vec{A} \times \vec{B}).\vec{C} = \left[\left(\frac{S_1}{\cos\theta_1} \times \frac{S_2}{\cos\theta_2} \times \sin\gamma_{AB}\right) \times \left(\frac{S_3}{\cos\theta_3}\right) \times \cos\theta_3\right] \times (\overrightarrow{N_{J3}} \times \overrightarrow{u_C}) \qquad \text{7-8}$$

Since N_{J3} and u_C are unit vectors, their cross products will be a unit vector, as well. As a result, the volume of the block could be calculated by Eq.7-9

$$V_b^A = |(\vec{A} \times \vec{B}).\vec{C}| = \frac{S_1 \times S_2 \times S_3}{\cos\theta_1 \cos\theta_2} \times \sin\gamma_{AB} \qquad \text{7-9}$$

With the same method that is used for block volume calculation, the block surface could be specified by Eq.7-10.

$$S_b^A = \frac{2S_1 S_2}{\cos\theta_1 \cos\theta_2}\sin\gamma_{AB} + \frac{2S_1 S_3}{\cos\theta_1 \cos\theta_3}\sin\gamma_{AC} + \frac{2S_2 S_3}{\cos\theta_2 \cos\theta_3}\sin\gamma_{BC} \qquad \text{7-10}$$

Where γ_{AB}, γ_{AC} and γ_{BC} are the angles between each pairs of edge vectors; i.e., A and B, A and C and B and C, respectively. The volumetric fracture intensity (P^A_{32}) is another useful parameter that could be calculated by dividing Eq.7-10 by Eq.7-9 and the result will be as Eq.7-11.

$$P^A_{32} = \frac{2 \sin \gamma_{AB}}{S_3} + \frac{2 \cos \theta_2 \sin \gamma_{AC}}{S_2 \cos \theta_3} + \frac{2 \cos \theta_1 \sin \gamma_{BC}}{S_1 \cos \theta_3} \qquad 7\text{-}11$$

7.4.3 Models validation

In this section, the accuracy of the analytical equations that are developed for calculation of the block volume (Eq.7-9) and surface (Eq.7-10) are validated by using the numerical simulation method. It is clear that by validating the block volume and surface model, the model for volumetric fracture intensity (P_{32}-Eq.7-11) will be automatically validated. In this regard, the block volume and surface that analytically calculated for 20 cases of fractured rock mass are compared with the results of the numerical simulations using the 3DEC version 7.0 software. For this purpose, the fractured rock mass includes three persistent joint sets and by variation of the spacing and orientations, different values of block volume and surface area will be obtained. Table 7-2 lists the rock mass cases that are used for comparison.

Table 7-2. Discontinuities characteristics that used for comparing the analytical (Eq.7-9 and Eq.7-10) and numerical methods for calculation of the block volume and block surface

Case	Joint set 1			Joint set 2			Joint set 3		
	DIP 1	DD 1	Spacing 1 (m)	DIP 2	DD 2	Spacing 2 (m)	DIP 3	DD 3	Spacing 3 (m)
1	90	350	0.98	61.57	10	0.87	81.96	29	0.35
2	90	10	3.94	67.16	340	0.35	90	350	3.94
3	90	10	3.94	90	70	1.37	43.16	300	1.37
4	80	0	0.98	90	10	3.94	90	350	3.94
5	43.16	60	0.34	67.16	20	3.46	67.16	340	3.46
6	90	10	0.39	90	30	0.87	67.16	340	3.46
7	43.16	60	0.34	60	0	3.46	23.26	330	0.14
8	20.32	10	0.34	90	70	0.34	67.16	340	3.46
9	21.34	340	0.34	80	0	0.98	43.16	60	0.34
10	90	30	0.87	90	350	0.98	80	0	3.94
11	80	0	0.98	67.16	340	0.87	60	0	0.87
12	90	10	0.98	61.57	350	3.46	43.16	60	0.14
13	90	10	0.39	90	350	0.39	43.16	60	0.14
14	80	0	0.39	43.16	60	0.14	90	350	0.39
15	67.16	20	0.87	90	70	0.14	21.34	340	0.34
16	67.16	20	0.87	43.16	60	1.37	90	350	0.39
17	90	350	0.98	90	10	0.98	43.16	60	1.37
18	43.16	60	0.14	90	10	0.39	90	350	0.39

| 19 | 90 | 30 | 0.35 | 90 | 350 | 3.94 | 90 | 10 | 0.98 |
| 20 | 90 | 10 | 3.94 | 90 | 350 | 3.94 | 60 | 0 | 0.35 |

The numerical model for calculation of the volume and surface area of the block was created based on the joint sets arrangements that are listed in Table 7-2. In order to do the comparison between Eq.7-9 and Eq.7-10 with the numerical model, the volume and surface are of the intact block that are illustrated in Fig 7-3b, should be specified.
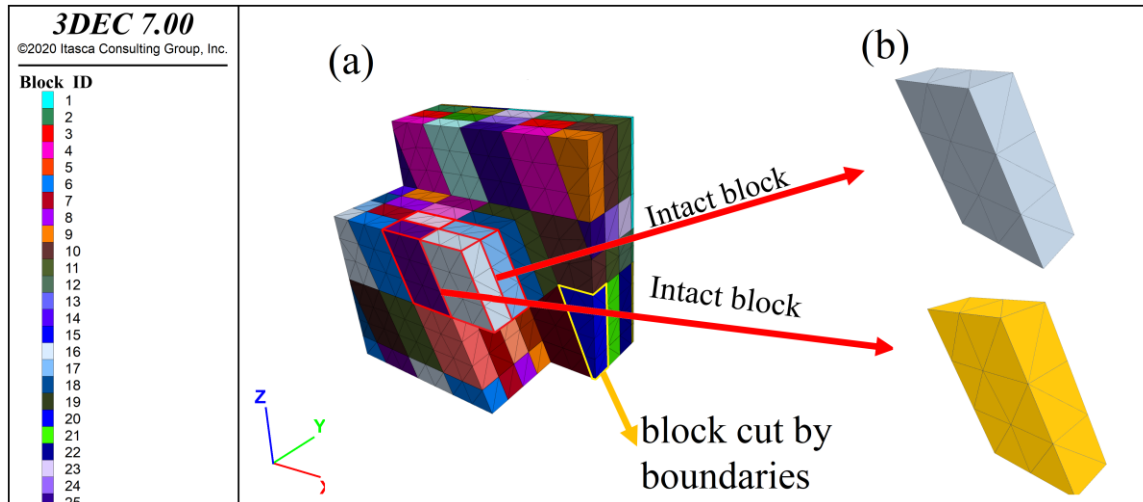
Fig 7-3. The basics for block volume and surface calculation. (a) the core view of the fractured rock mass for selection of the intact blocks. As the boundary blocks are cut by the model boundaries, they are not considered for the model development. (b) the intact blocks that were used for development of the analytical model as per [220, 240]

According to Fig 7-3, in order to numerically calculate the block volume and surface, it is important to consider the intact block; i.e., the block that is not cut by the boundaries of the numerical model. For this purpose, the size of the model should be increased until at least one intact block exists in the model. Actually, this block is the representative block that could be formed by cross of three persistent joint sets without being affected by the boundaries of the model and is demonstrated by Fig 7-3b. The results of analytical and numerical calculations of volume and surface of the intact blocks for the cases of Table 7-2, are listed in Table 7-3.

Table 7-3. Comparison of the analytical and numerical calculation of the volume and surface of the blocks for the cases of Table 7-2. N/A means that the parameter is unmeasurable by analytical model and depends to the size of the model in numerical models.

Case	Block surface (m^2)		Block volume (m^3)	
	Analytical (Eq.7-10)	Numerical (3DEC)	Analytical (Eq.7-9)	Numerical (3DEC)
1	11.74	11.76	1.16	1.17
2	274.91	272.93	40.49	40.49
3	40.05	40.02	11.67	11.64
4	783.83	783.83	257.31	257.29
5	91.36	91.36	13.05	13.07
6	70.9	70.88	8.9	8.9
7	7.4	7.4	0.35	0.35
8	6.65	6.64	0.54	0.54
9	2.68	2.68	0.20	0.21
10	145.92	145.92	30.1	30.1
11	45.56	45.54	6.85	6.84
12	17.15	17.14	1.00	1.01
13	2.11	2.11	0.09	0.09
14	40.07	40.08	1.62	1.62
15	1.79	1.79	0.08	0.08
16	47.66	47.65	5.39	5.38
17	29.38	29.38	5.32	5.34
18	2.11	2.12	0.09	0.09
19	N/A	N/A	N/A	N/A
20	213.4	213.3	31.43	31.44

According to Table 7-3, the analytical method for calculation of block volume and surface is in a good agreement with the results of the numerical models. In addition, the analytical and numerical models couldn't specify a value for the block volume and block surface for the case number 19 since the constructed blocks are columnar and stretched in *z* direction (all dips are 90° with various dip directions). Therefore, by extending the numerical model, the block volume and surface increase, and as a result, the numerical calculations are fully depending on the size of the numerical model for this case.

7.5 DISCUSSION

7.5.1 Stereographic illustration of the angles

As it is demonstrated in section 7.4.2, Eq.7-9 and Eq.7-10 could be used for calculation of the volume and surface of the block, respectively. However, determination of some parameters in these equations

might be obscured. In this section, the method for specifying these parameters is shown by using the stereographic projection. For this purpose, the volume and surface of the blocks for a few examples of rock mass are calculated in order to better clarifying the issue.

In Eq.7-9 and Eq.7-10, the true spacings of the joint sets are assumed to be known. However, the angles θ_1, θ_2 and θ_3 and γ_{AB}, γ_{AC} and γ_{BC} should be specified. For this purpose, Fig 7-4 shows the stereographic projection of the poles and planes of three joint sets as 1, 2 and 3. According to Fig 7-2, the edge vectors A, B and C are the lines of intersection between joint sets 2&3, 1&3 and 1&2, respectively. Therefore, the crossline of the planes of each pair of joint sets are the points that show the edge vectors. Accordingly, γ_{AB}, γ_{AC} and γ_{BC} are the angles between each pairs of edge vector and could simply measure by the defining the angle between each pair of points A, B and C in Fig 7-4. In addition, θ_1, θ_2 and θ_3 are the angles between normal to joint set and its relevant edge vector, as it is illustrated in Fig 7-2. For example, θ_1 is the angle between edge vector A and normal to joint set 1 (N_{J1}) as it is illustrated by the angle between P1 and A in Fig 7-2. θ_2 and θ_3 could be measured by the same method. Therefore, all the required angles in Eq.7-9 and Eq.7-10 could be measured by the stereographic projection of joint sets.
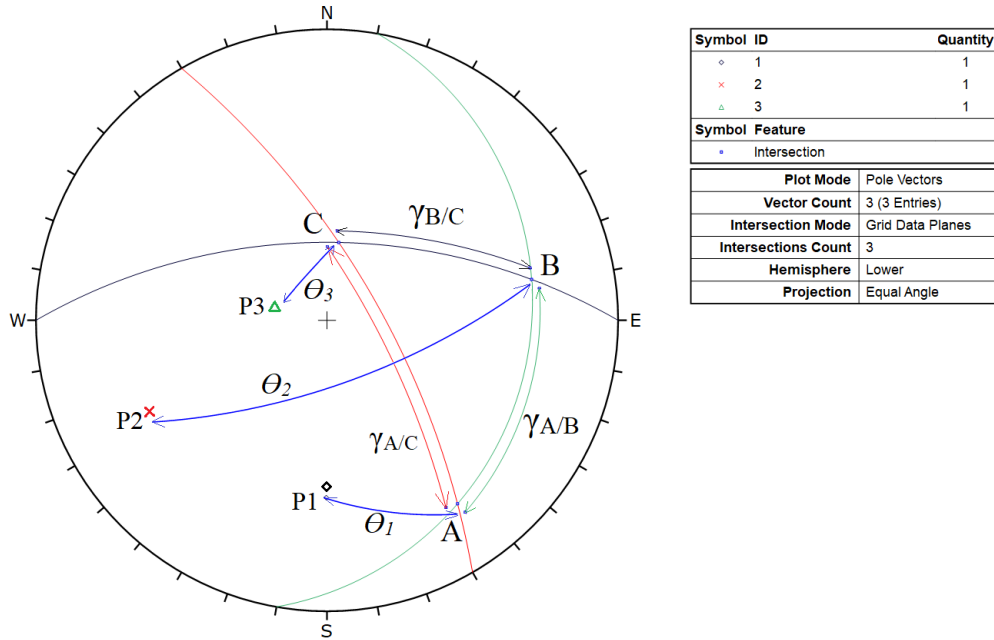
Fig 7-4. Stereographic projection of three joint sets and the method for measuring angles θ₁, θ₂ and θ₃ and γ_A/B, γ_A/C and γ_B/C. P₁, P₂ and P₃ are the poles of joint sets 1, 2 and 3, respectively.

In order to more clarifying the measurement method using Fig 7-4, four cases of rock mass that each of which include three joint sets are considered in Table 7-4 and the volume and surface of the produced block as well as all required angles for calculations are specified.

Table 7-4. Example cases of the fractured rock mass with various arrangements of join sets and the relevant block surface area and volume. N/A means that it is not possible to assign a value for that characteristics.

Case	(Dip/DD)	Spacing (m)	θ_1	θ_2	θ_3	γ_{AB}	γ_{AC}	γ_{BC}	Volume (m³)	Surface (m²)
									Block characteristics	
1	(60/0), (70/60), (20/100)	1, 2, 3	36	43	35	63	98	64	9	33
2	(20/30), (45/120), (90/330)	2, 1, 4	99	83	99	9	168	170	65	228
3	(90/0), (90/90), (0/0)	4, 1, 3	0	0	0	90	90	90	12	38
4	(90/0), (90/60), (90/120)	5, 7, 2	90	90	90	0	0	0	N/A	N/A

According to Table 7-4, the block that is formed in case number 1 and 2 is a parallelepiped. However, in case 3, the formed block is a rectangular cuboid and in case 4, it is a columnar block that vertically

stretched. That's why the Eq.7-9 and Eq.7-10 couldn't assign a value to the volume and surface of the block for case 4, as the size of this block is directly relevant to the extent of the model and changes by its variation.

7.5.2 Effect of parameters on block volume and surface

Following the discussion that is provided on section 7.4.1 for selection of the parameters that have effect on block volume and surface area, apart from the persistence that is not considered in this study, the spacing and orientation of the joint sets are defined to be the effective parameters that have impact on block characteristics. In this section and by using the response surface methodology (RSM), the effect of joint spacing (S_i) and the angle between them (γ_i) on the volume and surface area of the block that are calculated by Eq.7-9 and Eq.7-10, are evaluated. For this purpose, it is assumed that the S_i and γ_i for three joint sets are identical and by changing the values of the parameters, the variation of block volume and surface is evaluated. In this regard, the central composite design (CCD) has been applied for identifying the required experiments by using the Design-Expert® software. In addition, for the range of variation of parameters, it is assumed that S_i varies between 0.4 and 4 meters and γ_i changes between 10 to 90 degree. The number and type of calculations that is required for this purpose are listed in Table 7-5.

Table 7-5. The number and types of experiments that are required for evaluation of the effect of spacing and angle between joint sets on the block volume and surface, using central composite design by Design-Expert software- the volume and surface area of the blocks (Responses) are calculated using Eq.7-9 and Eq.7-10

Run	Space Type	Factors		Responses	
		Angle between sets (γ-deg)	Spacing (S-m)	Block volume (m^3)	Block surface (m^2)
1	Axial	50	0.4	0.11848	1.7772
2	Axial	90	2.2	10.648	29.04
3	Center	50	2.2	19.7122	53.7604
4	Axial	50	4	118.48	177.72
5	Factorial	78.2843	0.927208	0.843524	5.45848
6	Center	50	2.2	19.7122	53.7604
7	Factorial	78.2843	3.47279	44.3203	76.5729
8	Factorial	21.7157	3.47279	349.118	603.177
9	Center	50	2.2	19.7122	53.7604
10	Center	50	2.2	19.7122	53.7604
11	Factorial	21.7157	0.927208	6.64458	42.9973
12	Center	50	2.2	19.7122	53.7604
13	Axial	10	2.2	406.529	1108.72

Fig 7-5 illustrates the variation of the block volume and surface area with spacing and angle between joint sets that obtained by the analysis that performed by using the Design-Expert software on the data of

Table 7-5. It should be mentioned that the volume and surface area are calculated using Eq.7-9 and Eq.7-10.
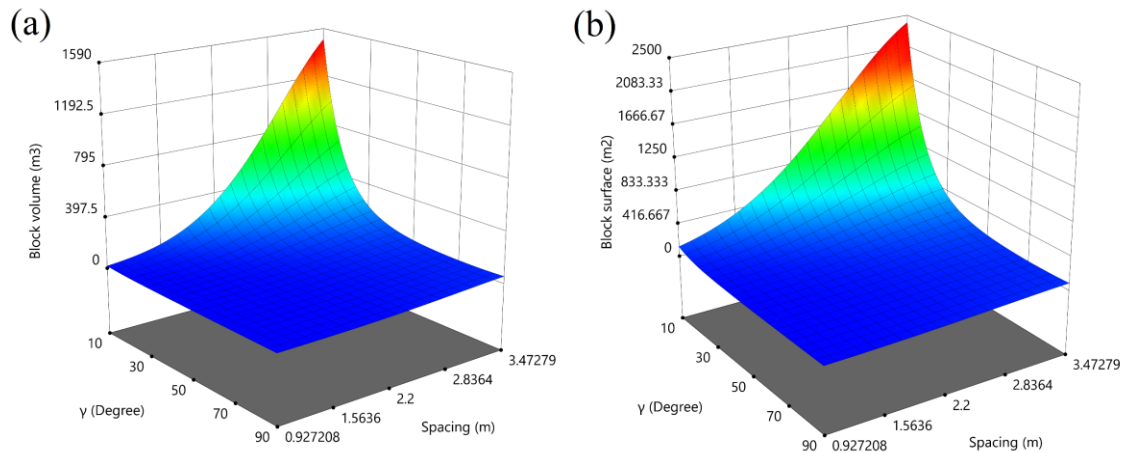
Fig 7-5. The effect of interaction between spacing (S) and the angle between joint sets (γ) on the volume and surface area of the block, by using the response surface methodology

Based on Fig 7-5, it could be deduced that:

- For a constant value of the spacing, the minimum and maximum values of block volume/surface are obtained in the perpendicular and inclined cross of joint sets, respectively.
- The impact of the spacing on block volume/surface increases by deviation from perpendicular cross of joint sets.
- The angle between joint sets has more impacts on the block volume/surface at grater values of spacings.

7.5.3 Error of previous methods for block volume calculation

As it was listed in Table 7-1, a number of equations have been developed for calculation of the volume of the block that is formed by cross of three joint sets. However, the accuracy of previous models is frequently questioned by the researchers [229, 240, 241]. In this section, the error of the previous models for calculation of the block volume is evaluated by central composite design type (CCD) of response surface methodology (RSM) by using the Design-Expert software. As the range of variation of input parameters are

same as what was considered in section 7.5.2, the considered factors are identical to Table 7-5; however, the responses are assumed to be the error of the methods that are listed in Table 7-1, by assuming that the joint sets are fully persistent. As a result, the error of the method that were listed in Table 7-1 for calculation of the block volume for the cases of Table 7-5, are listed in Table 7-6.

Table 7-6. Error values that are produced by methods of Table 7-1 for calculation of the block volume comparing with Eq.7-9.

Run	Error %		
	Palmstrom 1996	Palmstrom 1982	Latham 2006
1	0.661531	0.661531	325.2521
2	20.16337	20.16337	143.0785
3	136.8385	136.8385	-46.0146
4	20.16337	20.16337	143.0785
5	0.661531	0.661531	325.2521
6	3.34E-14	3.34E-14	350
7	20.16337	20.16337	143.0785
8	400.225	400.225	-88.2134
9	20.16337	20.16337	143.0785
10	20.16337	20.16337	143.0785
11	20.16337	20.16337	143.0785
12	20.16337	20.16337	143.0785
13	136.8385	136.8385	-46.0146

According to Table 7-6, only four methods are selected among the equations that are listed in Table 7-1 for calculation of the block volume. The reason is the compatibility of calculation methods with Eq.7-9, as the methods of Table 7-6 are selected in a way that the considered parameters for calculation of the block volume are the same as what was considered in Eq.7-9. In this regard, Fig 7-6 and Fig 7-7 show the variation of the error of Palmström equation [228] and [227] with spacing and γ.
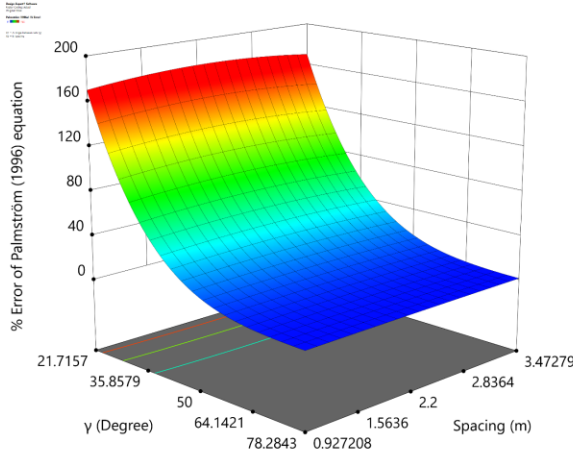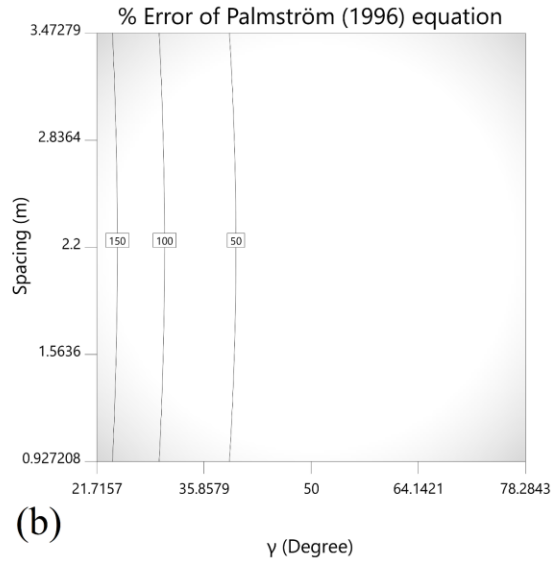
Fig 7-6. (a) 3D surface plot and (b) contour plot of the error of Palmström method [228] for calculation of the block volume
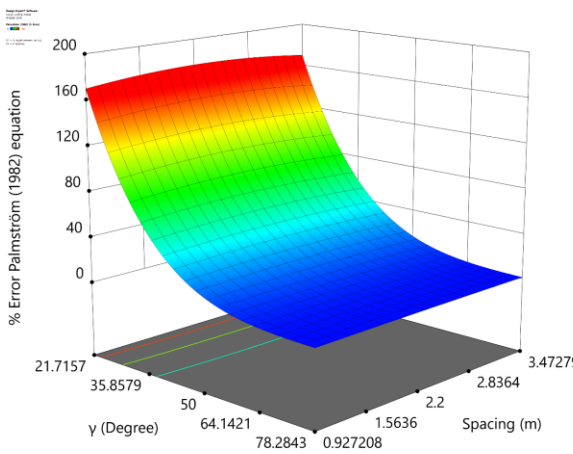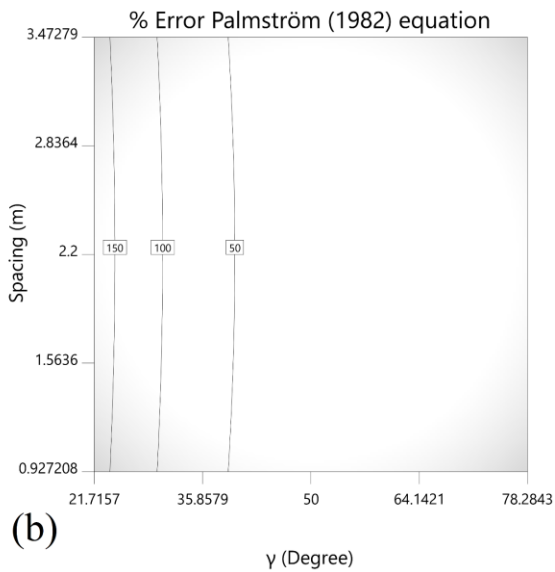
Fig 7-7. (a) 3D surface plot and (b) contour plot of the error of Palmström method [227] for calculation of the block volume

Generally, based on Fig 7-6 and Fig 7-7, the error of these methods is always greater than zero and it means that these methods are always overestimate the volume of the block. In addition, it is clear that the variation of joint spacing has no impact on the error of these method by itself and the angle between joint sets is the cause of error. In other words, the angle between joint sets was not considered properly by Palmström in development of the models for block volume calculation. The error of Latham equation in block volume calculation is illustrated by Fig 7-8.
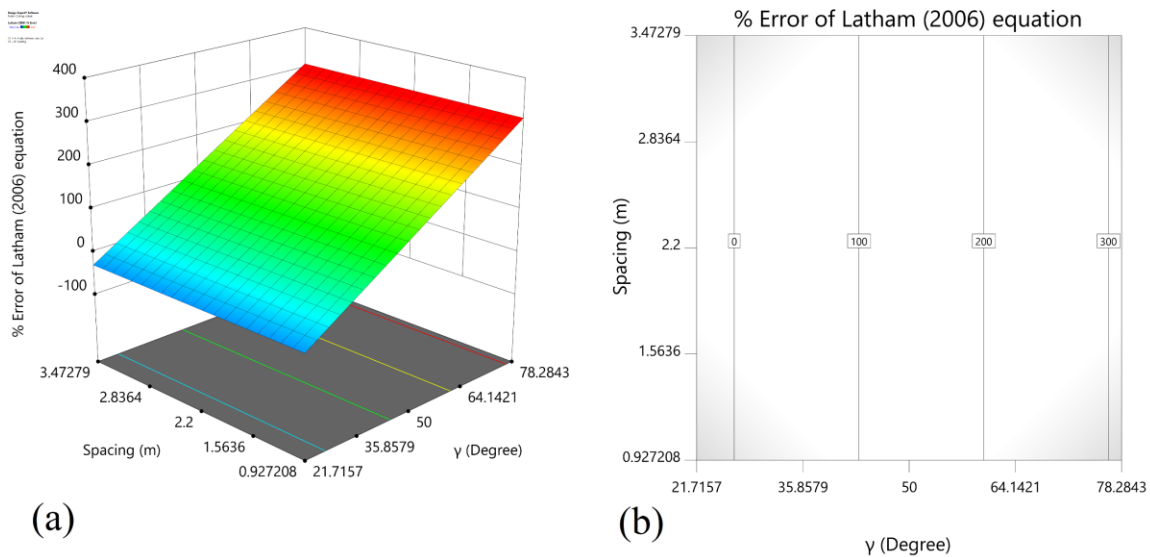
Fig 7-8. (a) 3D surface plot and (b) contour plot of the error of Latham method [232] for calculation of the block volume

The equation of Latham is mostly overestimating the volume of the block. However, in γ lower than around 25°, this method underestimates the block volume. In addition, the error of this method is very sensitive to γ, as this parameter is not included in development of this model and hence, in a constant value of spacing, a large value of error produces by variation of γ.

As a conclusion to section 7.5.3, application of the previous methods for block volume calculation is associated with error. Since the role of angles between joint sets is not properly considered in the equations, this parameter is responsible for most of the errors associated with calculation of the block volume, while the spacing (or multiplication of spacings), is the common parameter in most of the equations and in this regard, it has no contribution in the amount of produced error. Regarding the accuracy of the models, Palmström equations give more reliable results by getting close to the orthogonal joint sets and by deviation from perpendicularity, its accuracy reduces.

7.6 CONCLUSION

In this article, analytical methods are developed for calculation of the volume and surface area of the rock blocks that are created by cross of three persistent joint sets, as well as the volumetric fracture intensity (P_{32}). In order to prepare a reliable model, either in this study or for its next modification, i.e., presence of

non-persistence joint sets, it is assumed that the rock mas includes three persistent joint sets and hence, the effective parameters were selected to be the true spacings and the orientation of joint sets. It is obvious that the next modification of Eq.7-9 and Eq.7-10 will include the effect of other parameters on block volume and surface, e.g., joint persistence and joint set number.

The block volume and surface area could be stereographically calculated using Eq.7-9 and Eq.7-10. The equation for calculation of the surface area of the block (Eq.7-10) is developed for the first time through this article. In addition, by development of the block volume model, it was identified that the angles that were considered by previous studies for calculation of the block volume, e.g., angle between joint sets, were selected improperly and instead, the correct angles are shown in the current study. However, the impact of true spacing on block volume was almost correctly considered by the former models.

The block volume and surface area calculation by Eq.7-9 and Eq.7-10 represents the most reliable results among all previously developed models. This claim is validated by using the numerical simulation with 3DEC software, since the results of Eq.7-9 and Eq.7-10 are fully compatible with numerical results. An important issue that was rarely noticed in numerical calculation of block volume, is the representativeness of the numerical model, as the average block volume that is calculated by the small models is not expected to be the representative of the block volume of the rock mass. In order to avoid this problem, the dimension of the numerical model should be large enough to include a high portion of the intact blocks, as it is illustrated in Fig 7-3.

Regarding the impact of spacing and orientation of the joint sets on block volume and surface, it is identified that they have both individual and interactional effects on block characteristics. However, the impact of spacing will be more sensible in small values of angle between joint sets, and vice versa for the impact of γ. Furthermore, it is illustrated that the source of error of previous models for block volume calculation is the improperly consideration of the angle between joint sets (γ) instead of angle between edge vector and normal to joint set (θ). As a result, the error of previous models mostly increases by deviation from perpendicular cross of joint sets.

The volumetric fracture intensity (P_{32}) is another useful parameter that is widely used in geomechanical and hydrogeological investigations of the rock mass. In this article, an equation is developed for this purpose by Eq.7-11 and using the stereonet. As Eq.7-9 and Eq.7-10 were already validated by numerical simulation, this parameter is automatically validated.

7.7 DECLARATION OF COMPETING INTEREST

The authors declare that there is no conflict of interest associated with this publication.

7.8 ACKNOWLEDGEMENTS

CHAPTER 8

CONCLUSION

In addition to the conclusions listed in separate sections in the text of each article, the conclusions for each chapter are summarized in this section. The last section of this chapter presents suggestions for future research.

This thesis developed practical methods for predicting the amount of inflow rate to a tunnel excavated in fractured rock mass. Given that field data on the values of inflow rate to such tunnel are unavailable, the experimental method was not considered; this research adopted only analytical and numerical methods. However, similar to other analytical and numerical models, the methods developed in this study contain a set of simplifying assumptions. Consequently, their applications have limitations. In the development of all the models, including those for the inflow rate to the tunnel and calculation of block geometry, the following assumptions were adopted: the rock mass included three persistent joint sets, the permeability of the intact rock was negligible, and fluid flowed only through the fractures via the laminar flow mode. In addition, the level of the water table was fixed in the models, and the tunnel had a circular cross section. Furthermore, the effect of overburden load (stress) on the inflow rate was neglected in this research. As a result, all of the above-mentioned simplification assumptions limit the application of the models. For example, the analytical model for the calculation of block geometry is applicable only to a rock mass that includes three persistent joint sets.

In the analytical method for the calculation of the inflow rate to the tunnel, rock mass is regarded as a fractured network, and its hydraulic conductivity matrix is formed on this basis. In this study, Darcy's law and cubic law were applied as the basic equations for developing this model. For this purpose, the hydraulic gradient on the wall of the tunnel must be defined. Therefore, by using numerical simulation via Rocscience RS2 software, an empirical–numerical equation was introduced for the determination of the vertical hydraulic gradient on the tunnel wall in accordance with the geometrical characteristics of the discontinuities. Parallel to the analytical model, by using 3DEC software version 7, empirical–numerical equations were developed for the calculation of the inflow rate to the tunnel. For this purpose, the same

parameters that were adopted in the development of the analytical model were used. The required number of numerical simulations was performed using RSM and Design-Expert software. Then, the equation of the inflow rate to the tunnel and the individual and interaction effects of the parameters on the inflow rate to the tunnel were investigated using RSM.

In addition to the geometrical characteristics of the joint sets, the relationship between inflow rate to the tunnel and block geometries were studied in this work. For this purpose, new analytical models for the calculation of block volume, block surface area, and volumetric fracture intensity (P_{32}) were developed. After obtaining the numerically calculated inflow rate and analytically determined block geometries for each case, the relationship between the inflow rate to the tunnel and block geometries was specified.

The practical importance of this thesis is related to scientific and practical aspects. The practical applications of the thesis results may be of interest to specialists, mining engineers, and geologists. The flow rate into a tunnel is an important parameter that must be predicted before excavating underground structures. Eq. (3-13) can be used to help prevent rockfall and achieve tunnel stability. In addition, the numerically determined equation for calculating the inflow rate (Eq. (5-2)) can be used for this purpose if the rock mass consists of three joint sets. In addition, this thesis contributes an important innovation to 3D numerical simulation of tunnel inflow rate by introducing the concept of STL (CHAPTER 4). In all 3D numerical simulations of the tunnel inflow rate, tunnel length is more important than the volume of the numerical model (REV). Another important achievement of this work that can be considered by rock mechanics engineers is the analytical model for calculating block volume (Eq. (7-9)). This model can be widely used in field work where knowing the volume of blocks in a fractured rock mass is required. Another application parameter that is considered by rock mechanics and geologists is the volumetric fracture intensity (P_{32}), which can be determined analytically by Eq.7-11.

The conclusions from each article are summarized below.

8.1 ARTICLE 1

□ The hydraulic conductivity of the rock mass and the inflow rate to the tunnel were investigated in literature by using empirical, analytical, numerical, or a combination of these methods.

□ Experimental methods for determining rock mass permeability in formations other than the experimental data to which they belong cannot be used.

□ The analytical models for the calculation of the hydraulic conductivity or inflow rate to the tunnel are always accompanied by a series of simplifying assumptions. In the case of the inflow rate, the basic assumption is to regard the fractured rock mass (heterogeneous and anisotropic media) as a homogeneous (and isotropic) formation.

□ The numerical simulation methods for the evaluation of the hydraulic conductivity of rock mass, inflow rate to the tunnel, and sensitivity analysis of the effective parameters were mainly developed via 2D modeling. The effect of the interaction between parameters on the inflow rate/hydraulic conductivity and sensitivity analysis using 3D numerical models were not studied properly.

8.2 ARTICLE 2

□ A semi-analytical model was developed for the prediction of the inflow rate to a tunnel excavated in a fractured rock mass by knowing the aperture, spacing, and orientation of the joint sets; the direction and radius of the tunnel; and the water head above the tunnel.

□ Unlike in previously developed analytical models for the calculation of the inflow rate to the tunnel, predefining the equivalent hydraulic conductivity of the rock mass is not required when using the developed model.

□ The existing hydraulic gradient on the wall of the tunnel is an important parameter that affects the amount of inflow to the tunnel. A semi-empirical equation was developed in this study for defining the vertical hydraulic gradient on the wall of the tunnel. The results proved that horizontal hydraulic gradients have no major impact on the overall hydraulic gradient on the

tunnel wall. The vertical hydraulic gradient depends on the depth of the tunnel below the water table, the ratio of the principal hydraulic conductivities, and the angle between them.

8.3 ARTICLE 3

☐ A new concept regarding the REV of the numerical models for the case wherein a tunnel is excavated in a fractured rock mass was introduced in this study and called STL (specific tunnel length). STL is the length of the tunnel in 3D numerical simulations that has to be considered to avoid the impact of boundary effects on the value of the inflow rate to the tunnel. STL is equal to the least common multiple (LCM) of the apparent spacings of the joint sets on the wall of the tunnel and is the representative length of the tunnel for hydrogeologic purposes.

☐ STL is independent of the hydraulic aperture of the joint sets.

☐ An analytical model based on vectoral multiplication was developed for the calculation of the surface of the block formed by the intersection of three persistent joint sets. The accuracy of the model was validated by 3DEC version 7 software.

☐ The block volume calculated using existing analytical models is different from the actual block volume; therefore, these models must be modified to improve their accuracy.

☐ When the block volume and block surface decrease and the volumetric fracture intensity (P_{32}) increases, the inflow rate to the tunnel increases.

☐ The developed method for the calculation of block geometries considers the blocks created by the intersection of three joint sets (not the blocks that are placed at the boundaries of the model).

8.4 ARTICLE 4

☐ Empirical–numerical equations were developed for the calculation of the average inflow rate to the tunnel by determining the geometrical characteristics of the joint sets (hydraulic aperture, spacing, and orientation), tunnel radius, and water head above the tunnel.

- The average inflow rate to the tunnel (inflow rate from unit surface area of the tunnel wall) is independent of the tunnel radius.

- The lowest unit inflow rate to the tunnel is at the perpendicular intersection of the joint sets and the tunnel. By deviating from the perpendicularity, the inflow rate increases accordingly.

- The orientation of the joint sets is mostly demonstrated by dip and dip direction. However, for the case where the inflow rate to the tunnel is of interest, these two parameters and the direction of the tunnel can be substituted by the angle between joint sets and the direction of the tunnel.

- Among all the parameters that affect the inflow rate to the tunnel, hydraulic aperture is the most important.

8.5 ARTICLE 5

- An analytical model based on vectoral multiplication was developed for the calculation of the volume of the block formed by the intersection of three persistent joint sets by determining their dip, dip direction, and spacing.

- The developed analytical equation for calculating block volume was validated with the numerical simulation method by using 3DEC software.

- A set of field data on block volume was used to compare the result of the developed model with those of existing models. The findings revealed that many differences exist between the results of the models and the actual values of block volume.

8.6 ARTICLE 6

- A practical model based on stereographic projection was developed for the calculation of the block volume, block surface, and volumetric fracture intensity (P_{32}) of a rock mass that includes three persistent joint sets by determining their dip, dip direction, and spacing.

- Previously developed analytical models for calculating block volume and the current model consider the blocks that are not cut by the boundary of the numerical model (intact blocks).

- In the case where block geometry is of interest, the ratio of the boundary blocks to all blocks of the model is an index for assessing the representativeness of the model. In this regard, the numerical model must be large enough to include a large portion of intact blocks relative to all model blocks.

- The accuracy of previous models for block volume calculation decreases by deviating from the perpendicularity of the joint sets in a rock mass.

8.7 PERSPECTIVES FOR FUTURE RESEARCHES

This thesis studied the fluid flow through a fractured rock mass, with focus on the inflow rate to the tunnel. The research team also dealt with issues that have not been well discussed before but appear to be interesting and widely used in the study of the hydrogeological behavior of rock mass. The items that are relevant to the main or sub-objectives of the thesis are listed in this section as recommendations for future research.

- The inflow rate to the tunnel was formulated in this research by considering the effective parameters, such as hydraulic aperture, spacing, and orientation of the joint sets. These parameters are not fully independent, and each of them depends on secondary parameters. For example, hydraulic aperture is highly affected by the joint roughness coefficient (JRC); hence, the impact of this parameter could be included in the equations of the inflow rate to the tunnel.

- To simplify the problem, the ideal conditions of the parameters were considered in the development of the equations. Future research could consider reducing these simplifying assumptions to increase the applicability and accuracy of the analytical and numerical models. For example, joint persistence could be incorporated into the proposed equations for the calculation of the inflow rate to the tunnel or block geometry.

- Modification of existing methods or development of a new method for the determination of joint persistence could be undertaken to meet the requirements of the proposed models for the calculation of block geometry and inflow rate to the tunnel.

An analytical index could be developed for the qualitative evaluation of the inflow rate to a tunnel excavated in a fractured rock mass (inflow index) by determining the geometrical characteristics of the discontinuities, tunnel radius, and groundwater level. The input rate can be classified based on its value, and each class can be assigned to a specific range of the input index.

CHAPTER 9

Appendix A: Supplementary data of article 4

Alireza Shahbazi, Ali Saeidi[*], Romain Chesnaux, Alain Rouleau

Université du Québec à Chicoutimi, 555 boulevard de l'Université, Chicoutimi, Québec G7H 2B1, Canada

*Email: ali_saeidi@uqac.ca

9.1 The interaction between parameters

In this section, the diagrams that show the interactions between parameters are listed. The discussion on these diagrams are provided in sections 5.5.3 and 5.6 of the articles.
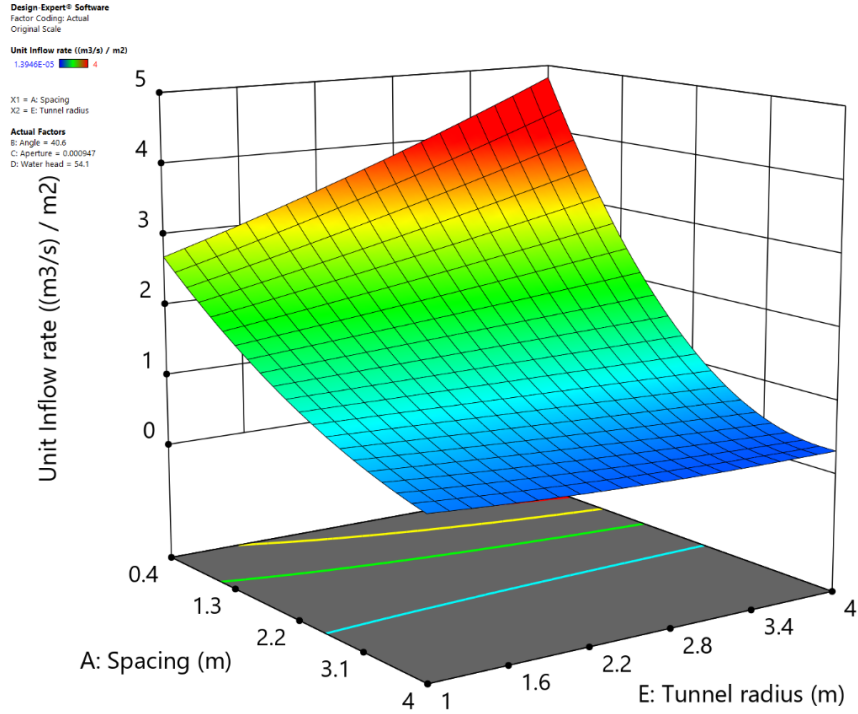
Fig A 9-1. The effect of interaction between mean spacing and tunnel radius on unit inflow rate
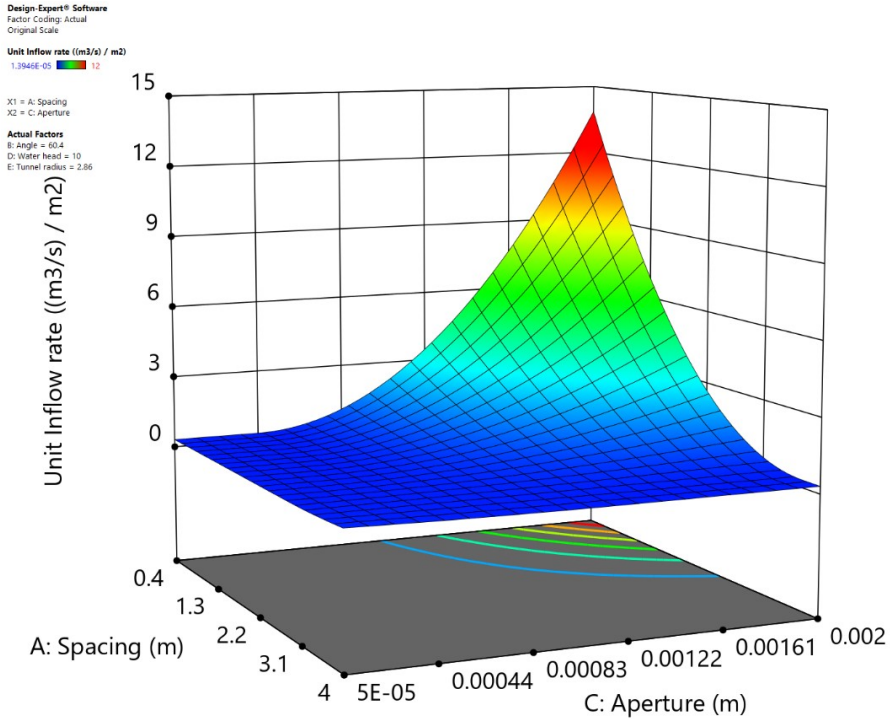
Fig A 9-2. The effect of interaction between mean spacing and average hydraulic aperture on unit inflow
rate
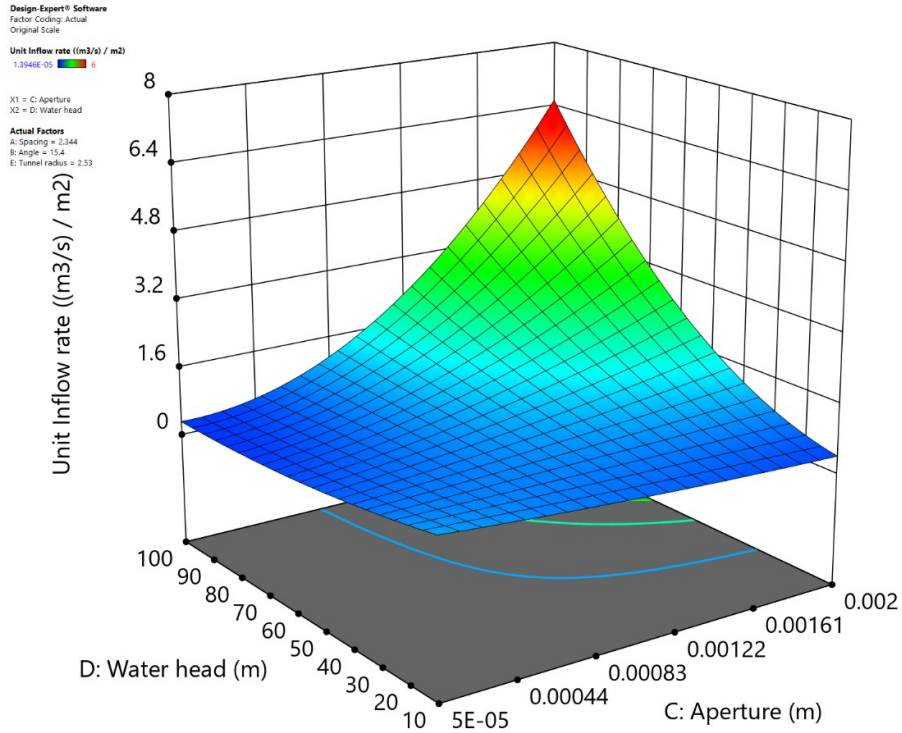
Fig A 9-3. The effect of interaction between average hydraulic aperture and water head above tunnel on unit inflow rate
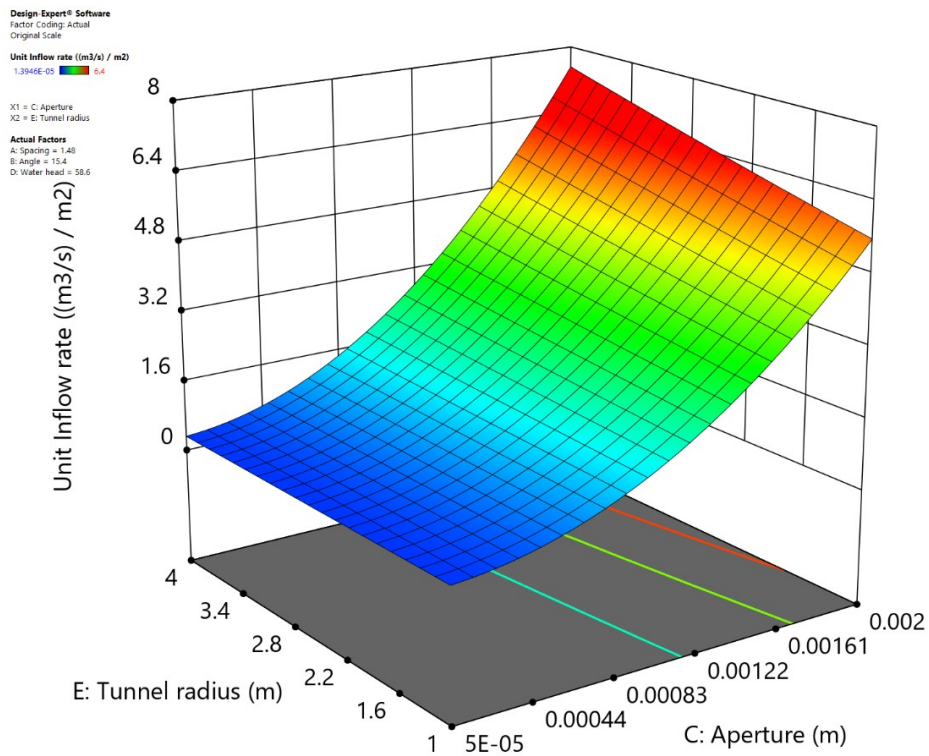
Fig A 9-4. The effect of interaction between average hydraulic aperture and tunnel radius on unit inflow rate
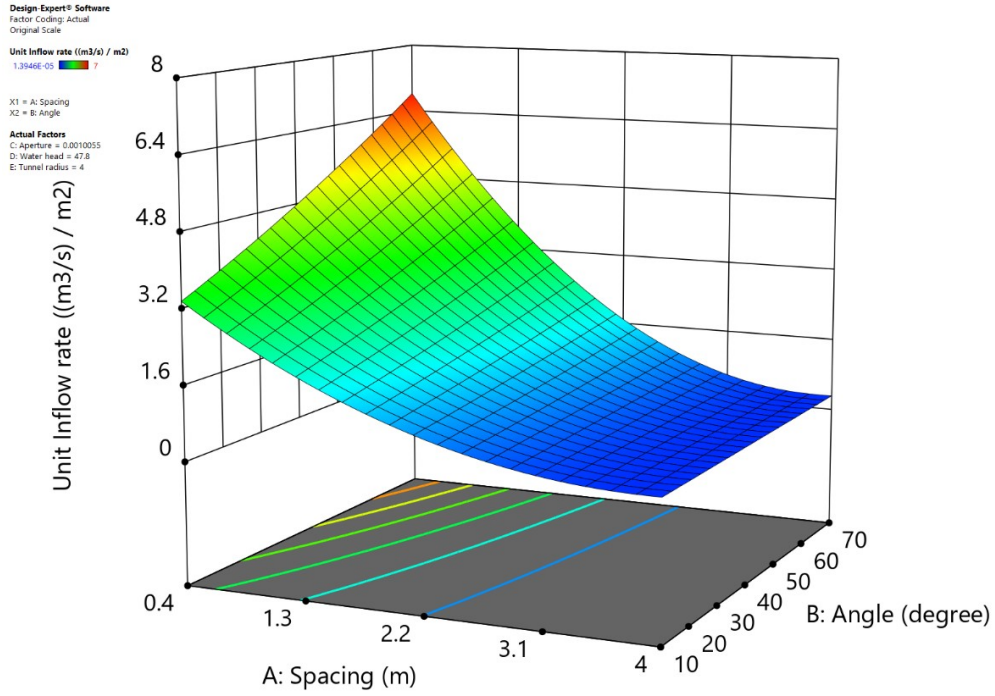
Fig A 9-5. The effect of interaction between mean spacing and average angle between tunnel and normal to joint sets on unit inflow rate
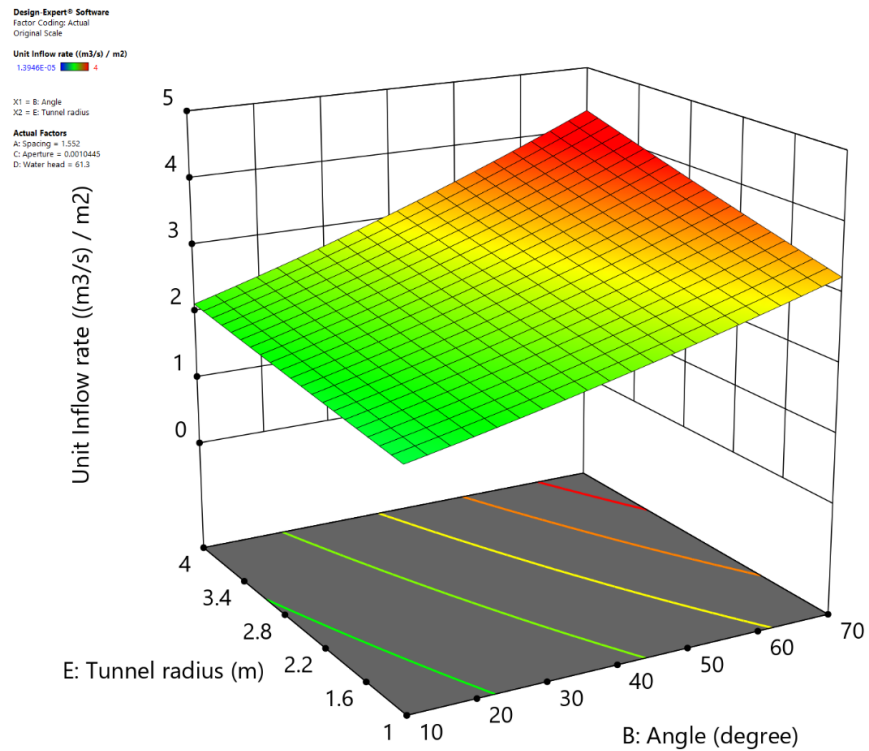
Fig A 9-6. The effect of interaction between average angle between tunnel and normal to joint sets, and tunnel radius on unit inflow rate
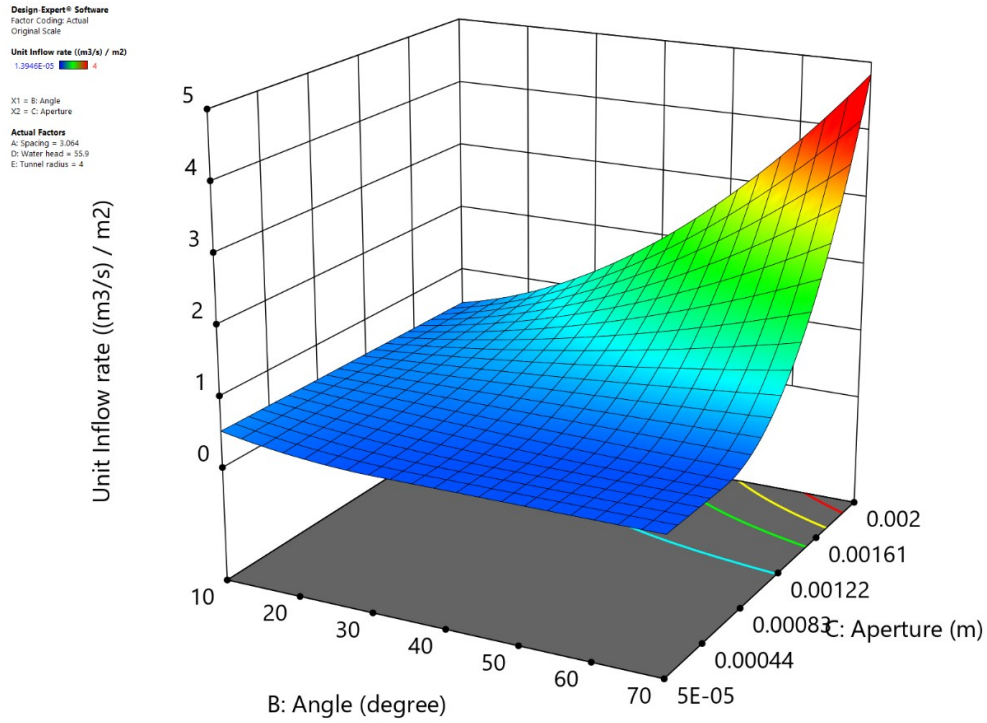
Fig A 9-7. The effect of interaction between average angle between tunnel and normal to joint sets, and average hydraulic aperture on unit inflow rate
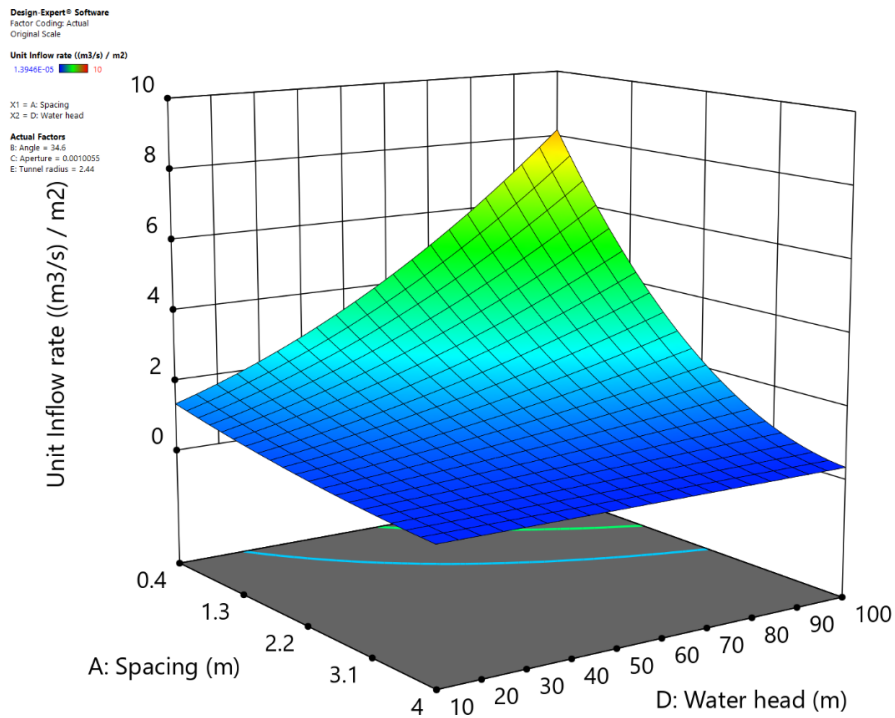
Fig A 9-8. The effect of interaction between mean spacing and water head above the tunnel on unit inflow rate

9.2 Statistical analysis

The complete list of numerical experiments that is designed by the Design-Expert ® software as well as design characteristics for exact and mean values of the parameters are provided in section 9.2.1 and 9.2.2, respectively.

9.2.1 Numerical experiments design for the exact values of the parameters

Table A 1 lists the details of 88 numerical experiments as well as the response (unit inflow rate) of the model. Each row refers to one run that consists of the arrangement of values of input parameters.

Table A 1. Design of experiments and the responses (unit inflow rate) for the exact values of the parameters

Run	Space Type	A: Spacing 1 (m)	B: Spacing 2 (m)	C: Spacing 3 (m)	D: Angle 1 (degree)	E: Angle 2 (degree)	F: Angle 3 (degree)	G: App 1 (m)	H: App 2 (m)	J: App 3 (m)	K: hw (m)	L: Tr (m)	Unit Inflow rate ((m³/s) / m²)
1	Plane	1	1	0.4	10	30	30	0.002	5E-05	0.002	40	4	2.24585
2	Plane	4	0.4	4	10	30	10	0.002	0.002	0.0005	10	1	0.518672
3	Plane	4	4	4	10	70	70	0.0005	0.002	0.0005	10	4	0.0995077
4	Edge	1	4	4	10	10	10	5E-05	0.002	0.002	10	4	0.155529
5	Plane	1	4	4	70	30	30	0.0005	5E-05	0.002	40	2	0.188979
6	Plane	0.4	1	4	10	30	30	5E-05	0.0005	0.0005	100	4	0.0299533
7	Plane	1	4	0.4	70	30	70	0.002	0.002	0.0005	10	1	0.533161
8	Plane	1	1	4	70	70	30	0.002	0.0005	0.0005	40	2	2.34748
9	Plane	1	1	1	70	10	70	0.0005	5E-05	0.0005	40	4	0.072122
10	Plane	1	1	4	30	10	10	0.002	0.0005	0.0005	40	1	0.383153
11	Plane	1	1	1	10	30	30	0.0005	0.0005	5E-05	40	1	0.0174497
12	Plane	1	4	0.4	10	30	70	0.002	5E-05	5E-05	100	4	0.569439
13	Vertex	0.4	0.4	0.4	10	10	70	5E-05	5E-05	0.002	10	1	0.918928
14	Plane	0.4	0.4	0.4	10	70	10	0.002	0.002	0.0005	100	2	31.6968
15	Plane	1	0.4	1	30	70	70	5E-05	0.002	0.0005	10	2	1.11374
16	Plane	1	4	0.4	30	70	10	5E-05	5E-05	5E-05	10	1	1.3946E-05
17	Plane	1	1	4	10	10	70	5E-05	0.0005	0.0005	10	2	0.00568132
18	Plane	0.4	0.4	0.4	70	10	10	5E-05	5E-05	5E-05	40	2	0.00139819
19	Plane	0.4	4	1	30	10	10	0.0005	0.002	0.0005	100	2	0.577101
20	Edge	4	4	0.4	10	10	30	0.002	0.002	5E-05	100	1	0.97228
21	Plane	4	0.4	0.4	70	70	30	0.0005	0.002	0.002	10	4	3.44806
22	Plane	1	1	1	10	30	30	0.0005	0.0005	5E-05	40	1	0.00539314
23	Vertex	4	4	4	70	10	10	0.002	0.002	0.002	100	1	2.17628
24	Plane	1	1	1	70	30	30	0.0005	0.0005	5E-05	10	1	0.0107798
25	Plane	1	1	4	70	70	10	5E-05	0.002	0.002	100	4	6.6014
26	Edge	4	0.4	0.4	30	70	10	0.002	5E-05	0.002	10	1	0.862385
27	Plane	0.4	0.4	4	70	10	10	0.0005	5E-05	5E-05	100	2	0.136178
28	Plane	1	0.4	4	10	10	30	5E-05	0.002	0.002	100	1	7.40678
29	Vertex	4	0.4	0.4	10	10	70	5E-05	5E-05	5E-05	100	4	0.000411224
30	Plane	1	1	1	70	10	70	0.0005	5E-05	0.0005	40	4	0.0986451
31	Plane	4	4	1	30	30	30	0.002	0.002	0.002	100	4	2.10609
32	Vertex	0.4	0.4	4	10	10	10	0.002	5E-05	5E-05	10	4	0.597561
33	Plane	0.4	1	4	10	30	10	0.002	0.002	0.002	100	4	4.29322
34	Vertex	4	0.4	4	70	10	70	0.002	5E-05	5E-05	10	1	0.0517309

35	Plane	4	4	1	70	10	10	0.0005	5E-05	0.0005	40	1	0.0155915
36	Plane	4	1	0.4	30	10	30	0.0005	0.002	5E-05	10	4	0.252559
37	Plane	4	0.4	4	30	30	10	0.0005	0.0005	0.002	40	4	0.189298
38	Vertex	0.4	0.4	0.4	70	70	70	0.002	5E-05	5E-05	100	1	5.02228
39	Edge	0.4	0.4	0.4	10	70	70	0.002	0.0005	5E-05	10	4	1.65003
40	Plane	1	4	1	10	10	70	5E-05	0.0005	5E-05	10	4	0.00117876
41	Plane	4	1	1	30	30	30	5E-05	0.002	0.0005	100	1	0.692792
42	Plane	4	4	1	30	70	30	0.002	0.0005	5E-05	40	1	0.130439
43	Plane	1	0.4	1	30	70	10	0.002	5E-05	5E-05	100	4	0.400226
44	Plane	1	1	1	10	70	10	0.002	0.002	0.0005	10	4	1.38471
45	Plane	1	1	4	30	70	70	0.0005	0.002	0.002	10	1	0.57682
46	Plane	4	1	4	70	10	70	0.0005	0.002	0.002	100	2	3.31048
47	Edge	4	4	1	70	10	70	5E-05	0.002	0.002	10	4	0.515587
48	Plane	1	0.4	1	30	10	30	0.002	0.002	0.002	10	1	0.927799
49	Plane	0.4	1	1	30	70	30	0.0005	5E-05	0.002	100	2	2.17384
50	Plane	4	1	1	70	70	70	0.002	0.002	5E-05	40	4	2.55828
51	Plane	1	4	0.4	30	10	30	0.0005	0.0005	0.002	100	1	3.61091
52	Plane	0.4	4	1	10	10	30	0.002	0.0005	0.0005	10	2	0.489615
53	Plane	1	1	1	10	30	10	0.0005	0.0005	0.002	10	2	0.115066
54	Plane	0.4	0.4	0.4	70	10	30	0.002	0.002	0.0005	100	4	40.9046
55	Edge	0.4	4	1	70	10	10	0.002	5E-05	5E-05	100	1	1.48171
56	Plane	4	4	0.4	70	10	30	5E-05	0.0005	5E-05	100	4	0.00167632
57	Plane	1	4	1	70	70	70	0.0005	5E-05	0.002	10	4	0.369845
58	Plane	1	1	4	70	70	30	0.002	0.0005	0.0005	40	2	1.96111
59	Edge	0.4	0.4	4	70	30	70	5E-05	0.002	0.002	10	4	1.70941
60	Plane	4	1	1	70	30	10	5E-05	5E-05	0.0005	10	4	0.00472948
61	Plane	4	1	0.4	30	30	70	5E-05	0.0005	0.002	40	2	1.06505
62	Plane	4	1	1	10	10	70	0.002	0.0005	0.0005	100	2	0.615032
63	Plane	0.4	4	4	70	70	70	5E-05	0.0005	5E-05	40	1	0.00614171
64	Plane	1	0.4	1	70	70	10	0.0005	0.0005	0.0005	100	1	0.411994
65	Plane	0.4	4	1	70	70	30	5E-05	0.002	0.002	40	1	1.73334
66	Plane	4	1	4	10	10	30	0.002	5E-05	0.002	10	2	0.0665308
67	Plane	1	4	4	30	70	30	0.002	0.002	0.0005	100	2	2.04328
68	Plane	4	1	0.4	70	30	10	0.002	5E-05	5E-05	100	2	1.03052
69	Plane	1	1	4	30	10	10	0.002	0.0005	0.0005	40	1	0.443286
70	Edge	4	4	4	70	70	10	5E-05	0.002	0.002	10	2	0.166215
71	Plane	4	4	4	30	30	10	0.002	0.0005	5E-05	10	4	0.0555941
72	Plane	1	0.4	4	10	70	70	5E-05	5E-05	0.002	100	2	0.18559
73	Plane	1	0.4	1	70	30	70	0.002	0.0005	0.002	40	2	4.36442
74	Plane	0.4	1	0.4	70	10	10	0.002	0.0005	0.002	10	4	14.1809
75	Edge	4	4	1	10	10	10	5E-05	5E-05	0.002	100	4	1.34399
76	Plane	1	1	4	70	10	10	0.0005	0.002	5E-05	40	4	0.765068
77	Plane	1	1	1	10	30	10	0.0005	0.0005	0.002	10	2	0.206164
78	Plane	0.4	4	4	30	10	70	0.002	0.0005	0.002	100	4	4.67945
79	Edge	4	1	4	70	70	70	0.002	5E-05	0.002	100	4	2.58731
80	Vertex	0.4	4	4	10	70	10	0.002	5E-05	0.002	100	1	4.03693
81	Plane	4	4	0.4	10	70	30	0.0005	0.0005	0.0005	40	4	0.0416265
82	Plane	4	1	4	10	70	10	5E-05	5E-05	5E-05	100	2	6.56544E-05
83	Edge	0.4	4	4	70	10	70	0.002	0.002	5E-05	40	4	1.79953
84	Edge	1	4	0.4	10	70	70	5E-05	0.002	0.002	100	4	10.1847
85	Edge	0.4	4	0.4	70	70	10	0.0005	0.002	5E-05	10	4	0.29491
86	Plane	0.4	1	4	10	30	70	0.002	0.002	5E-05	100	2	7.68358
87	Plane	4	4	4	30	30	70	0.0005	0.0005	0.0005	100	2	0.0086078
88	Edge	0.4	0.4	4	30	70	10	5E-05	0.002	5E-05	10	1	0.405854

Table A 2 lists the design characteristics that considered by Design-Expert ® software. In this regard, I-optimal method of response surface methodology has been used for the exact values of the parameters.

Table A 2. Design characteristics applied for the type and number of required numerical experiments for exact values of the parameters

File Version	11.0.3.0			
Study Type	Response Surface		**Subtype**	Randomized
Design Type	I-optimal	Coordinate Exchange	**Runs**	88
Design Model	Quadratic		**Blocks**	No Blocks
Build Time (ms)	7468.00			

Fig A 9-9 illustrates the predicted values of the unit inflow rate by Eq.(5-1) versus the actual values that were calculated by the 3DEC software. As the trendline is almost *x=y* line, the predicted and actual values are almost equal and hence, the values of the R^2 (adjusted and predicted) will be near to unity.
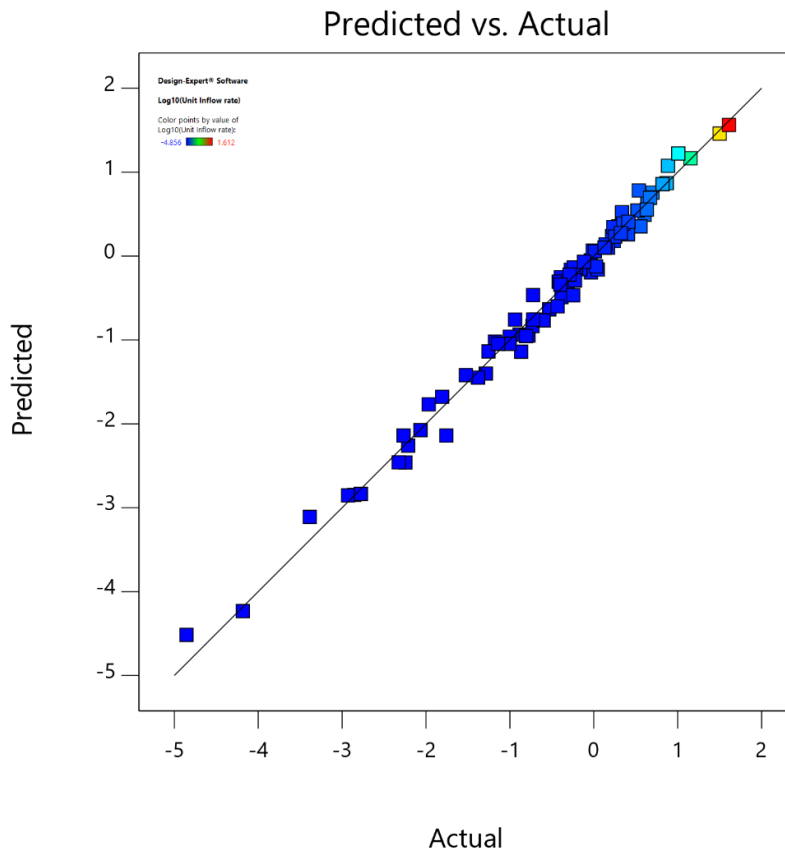
Fig A 9-9. predicted unit inflow rate by Eq.(5-1) versus the actual values. As much as the actual and predicted values be equal, the accuracy of the model and the higher values of the R^2 obtained.

9.2.2 Numerical experiments design for the mean values of the parameters

Table A 3 lists the details of 88 numerical experiments as well as the response (unit inflow rate) of the model. Each row refers to one run that consists of the arrangement of values of input parameters.

Table A 3. Design of experiments and the responses (unit inflow rate) for the mean values of the parameters

Run	Build Type	Space Type	A: Spacing (m)	B: Angle (degree)	C: Aperture (m)	D: Water head (m)	E: Tunnel radius (m)	Unit Inflow rate ((m³/s) / m²)
1	NA	Unknown	0.8	23.3333	0.00135	40	4	2.24585
2	NA	Unknown	2.8	16.6667	0.0015	10	1	0.518672
3	NA	Unknown	4	50	0.001	10	4	0.0995077
4	NA	Unknown	3	10	0.00135	10	4	0.155529
5	NA	Unknown	3	43.3333	0.00085	40	2	0.188979
6	NA	Unknown	1.8	23.3333	0.00035	100	4	0.0299533
7	NA	Unknown	1.8	56.6667	0.0015	10	1	0.533161
8	NA	Unknown	2	56.6667	0.001	40	2	2.34748
9	NA	Unknown	1	50	0.00035	40	4	0.072122
10	NA	Unknown	2	16.6667	0.001	40	1	0.383153
11	NA	Unknown	1	23.3333	0.00035	40	1	0.0174497
12	NA	Unknown	1.8	36.6667	0.0007	100	4	0.569439
13	NA	Unknown	0.4	30	0.0007	10	1	0.918928
14	NA	Unknown	0.4	30	0.0015	100	2	31.6968
15	NA	Unknown	0.8	56.6667	0.00085	10	2	1.11374
16	NA	Unknown	1.8	36.6667	5E-05	10	1	0.000346
17	NA	Unknown	2	30	0.00035	10	2	0.00568132
18	NA	Unknown	0.4	30	5E-05	40	2	0.00139819
19	NA	Unknown	1.8	16.6667	0.001	100	2	0.577101
20	NA	Unknown	2.8	16.6667	0.00135	100	1	0.97228
21	NA	Unknown	1.6	56.6667	0.0015	10	4	3.44806
22	NA	Unknown	1	23.3333	0.00035	40	1	0.00539314
23	NA	Unknown	4	30	0.002	100	1	2.17628
24	NA	Unknown	1	43.3333	0.00035	10	1	0.0107798
25	NA	Unknown	2	50	0.00135	100	4	6.6014
26	NA	Unknown	1.6	36.6667	0.00135	10	1	0.862385
27	NA	Unknown	1.6	30	0.0002	100	2	0.136178
28	NA	Unknown	1.8	16.6667	0.00135	100	1	7.40678
29	NA	Unknown	1.6	30	5E-05	100	4	0.000411224
30	NA	Unknown	1	50	0.00035	40	4	0.0986451
31	NA	Unknown	3	30	0.002	100	4	2.10609
32	NA	Unknown	1.6	10	0.0007	10	4	0.597561
33	NA	Unknown	1.8	16.6667	0.002	100	4	4.29322
34	NA	Unknown	2.8	50	0.0007	10	1	0.0517309
35	NA	Unknown	3	30	0.00035	40	1	0.0155915
36	NA	Unknown	1.8	23.3333	0.00085	10	4	0.252559
37	NA	Unknown	2.8	23.3333	0.001	40	4	0.189298
38	NA	Unknown	0.4	70	0.0007	100	1	5.02228
39	NA	Unknown	0.4	50	0.00085	10	4	1.65003
40	NA	Unknown	2	30	0.0002	10	4	0.00117876
41	NA	Unknown	2	30	0.00085	100	1	0.692792
42	NA	Unknown	3	43.3333	0.00085	40	1	0.130439
43	NA	Unknown	0.8	36.6667	0.0007	100	4	0.400226
44	NA	Unknown	1	30	0.0015	10	4	1.38471
45	NA	Unknown	2	56.6667	0.0015	10	1	0.57682
46	NA	Unknown	3	50	0.0015	100	2	3.31048
47	NA	Unknown	3	50	0.00135	10	4	0.515587
48	NA	Unknown	0.8	23.3333	0.002	10	1	0.927799
49	NA	Unknown	0.8	43.3333	0.00085	100	2	2.17384
50	NA	Unknown	2	70	0.00135	40	4	2.55828
51	NA	Unknown	1.8	23.3333	0.001	100	1	3.61091
52	NA	Unknown	1.8	16.6667	0.001	10	2	0.489615

53	NA	Unknown	1	16.6667	0.001	10	2	0.115066
54	NA	Unknown	0.4	36.6667	0.0015	100	4	39.811
55	NA	Unknown	1.8	30	0.0007	100	1	1.48171
56	NA	Unknown	2.8	36.6667	0.0002	100	4	0.00167632
57	NA	Unknown	2	70	0.00085	10	4	0.369845
58	NA	Unknown	2	56.6667	0.001	40	2	1.96111
59	NA	Unknown	1.6	56.6667	0.00135	10	4	1.70941
60	NA	Unknown	2	36.6667	0.0002	10	4	0.00472948
61	NA	Unknown	1.8	43.3333	0.00085	40	2	1.06505
62	NA	Unknown	2	30	0.001	100	2	0.615032
63	NA	Unknown	2.8	70	0.0002	40	1	0.00614171
64	NA	Unknown	0.8	50	0.0005	100	1	0.411994
65	NA	Unknown	1.8	56.6667	0.00135	40	1	1.73334
66	NA	Unknown	3	16.6667	0.00135	10	2	0.0665308
67	NA	Unknown	3	43.3333	0.0015	100	2	2.04328
68	NA	Unknown	1.8	36.6667	0.0007	100	2	1.03052
69	NA	Unknown	2	16.6667	0.001	40	1	0.443286
70	NA	Unknown	4	50	0.00135	10	2	0.166215
71	NA	Unknown	4	23.3333	0.00085	10	4	0.0555941
72	NA	Unknown	1.8	50	0.0007	100	2	0.18559
73	NA	Unknown	0.8	56.6667	0.0015	40	2	4.36442
74	NA	Unknown	0.6	30	0.0015	10	4	14.1809
75	NA	Unknown	3	10	0.0007	100	4	1.34399
76	NA	Unknown	2	30	0.00085	40	4	0.765068
77	NA	Unknown	1	16.6667	0.001	10	2	0.206164
78	NA	Unknown	2.8	36.6667	0.0015	100	4	4.67945
79	NA	Unknown	3	70	0.00135	100	4	2.58731
80	NA	Unknown	2.8	30	0.00135	100	1	4.03693
81	NA	Unknown	2.8	36.6667	0.0005	40	4	0.0416265
82	NA	Unknown	3	30	5E-05	100	2	6.56544E-05
83	NA	Unknown	2.8	50	0.00135	40	4	1.79953
84	NA	Unknown	1.8	50	0.00135	100	4	10.1847
85	NA	Unknown	1.6	50	0.00085	10	4	0.29491
86	NA	Unknown	1.8	36.6667	0.00135	100	2	7.68358
87	NA	Unknown	4	43.3333	0.0005	100	2	0.0086078
88	NA	Unknown	1.6	36.6667	0.0007	10	1	0.405854

Table A 4 lists the design characteristics that considered by Design-Expert ® software. In this regard, I-optimal method of response surface methodology has been used for the exact values of the parameters.

Table A 4. Design characteristics applied for the type and number of required numerical experiments for mean values of the parameters

File Version	11.0.3.0		
Study Type	Response Surface	Subtype	Randomized
Design Type	Historical Data	Runs	88
Design Model	Quadratic	Blocks	No Blocks
Build Time (ms)	11.00		

Fig A 9-10 illustrates the predicted values of the unit inflow rate by Eq.(5-2) versus the actual values that were calculated by the 3DEC software. As the trendline is almost *x=y* line, the predicted and actual values are almost equal and hence, the values of the R^2 (adjusted and predicted) will be near to unity.
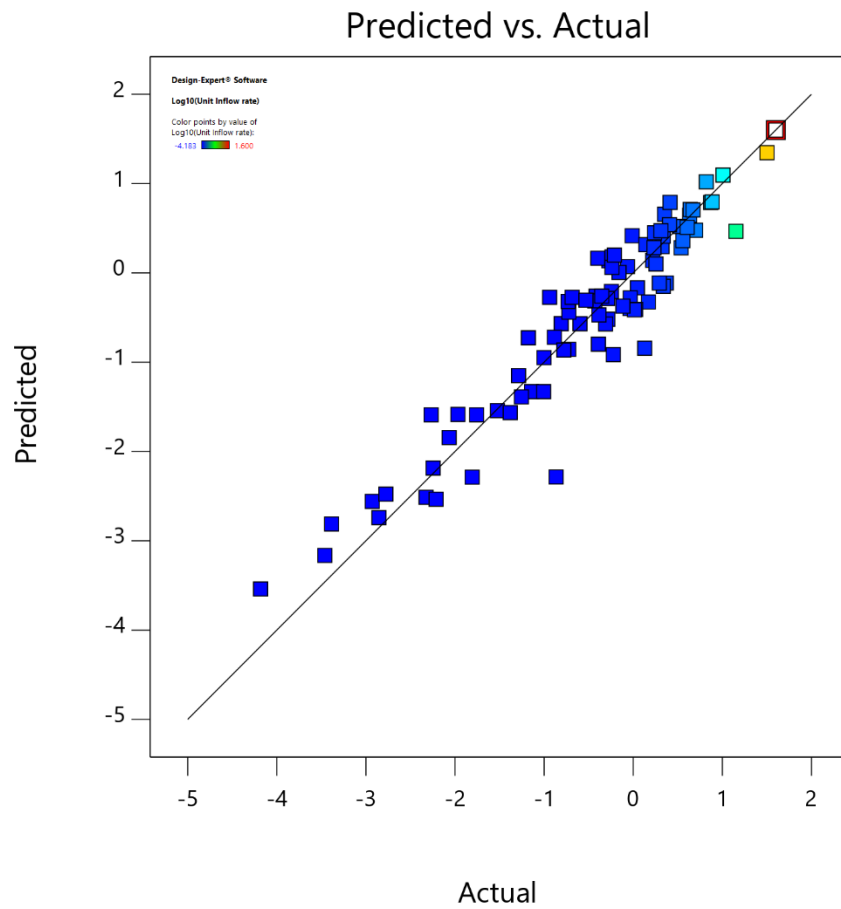
Fig A 9-10. Predicted unit inflow rate by Eq.(5-2) versus the actual values. As much as the actual and predicted values be equal, the accuracy of the model and the higher values of the R^2 obtained.

REFERENCES

1. Bieniawski, Z.T., *Determining rock mass deformability: experience from case histories.* International Journal of Rock Mechanics and Mining Sciences & Geomechanics Abstracts, 1978. 15: p. 237-247

2. Chen, Y.-F., et al., *Statistical distribution of hydraulic conductivity of rocks in deep-incised valleys, Southwest China.* Journal of Hydrology, 2018. 566: p. 216-226.http://dx.doi.org/10.1016/j.jhydrol.2018.09.016

3. Ajalloeian, R. and A.F. Dardashti, *Evaluation of fluid flow from a dam foundation using numerical modeling technique by UDEC software.* Electronic Journal of Geotechnical Engineering, 2013. 18: p. 1787-1800

4. Borbély, D., *Tunnel-excavation-induced permeability change of rock mass around a radioactive waste repository tunnel.* Central European Geology, 2018. 61: p. 73–84.https://doi.org/10.1556/24.61.2018.05

5. El Tani, M., *Water inflow into tunnels*, in *Proceedings of the World Tunnel Congress ITA-AITES*. 1999, International Tunneling and Underground Space Association: Switzerland. p. 61–70.

6. Fernandez, G. and J. Moon, *Excavation-induced hydraulic conductivity reduction around a tunnel – Part 1: Guideline for estimate of ground water inflow rate.* Tunnelling and Underground Space Technology, 2010. 25(5): p. 560-566.https://doi.org/10.1016/j.tust.2010.03.006

7. Lei, Q., et al. *Influence of stress on the permeability of a three-dimensional fractured sedimentary layer*. in *50th US Rock Mechanics/Geomechanics Symposium*. 2016. American Rock Mechanics Association.

8. Jing, L., et al., *Understanding coupled stress, flow and transport processes in fractured rocks.* Geosystem Engineering, 2013. 16(1): p. 2-25.http://dx.doi.org/10.1080/12269328.2013.780709

9. Snow, D.T., *The frequency and apertures of fractures in rock.* International Journal of Rock Mechanics and Mining Sciences & Geomechanics Abstracts, 1970. 7(1): p. 23-40

10. Carlsson, A. and T. Olsson, *Hydraulic properties of Swedish crystalline rocks*, in *Bulletin of the Geological Institution of the University of Uppsala*, U.o. Uppsala, Editor. 1977, Swedish State Power Board Civil Engineering Development: Uppsala, Sweden. p. 71-84.

11. Öge, İ.F., *Assessing rock mass permeability using discontinuity properties.* Procedia Engineering, 2017. 191: p. 638-645.http://dx.doi.org/10.1016/j.proeng.2017.05.373

12. Qureshi, M.U., et al., *An empirical relationship between in-situ permeability and RQD of discontinuous sedimentary rocks.* Electronic Journal of Geotechnical Engineering, 2014. 19 (R): p. 4781-4790

13. El-Naqa, A., *The hydraulic conductivity of the fractures intersecting Cambrian sandstone rock masses, central Jordan.* Environmental Geology, 2001. 40(8): p. 973-982.https://doi.org/10.1007/s002540100266

14. Cha, S.-S., et al., *Engineering characterization of hydraulic properties in a pilot rock cavern for underground LNG storage.* Engineering geology, 2006. 84(3-4): p. 229-243.https://doi.org/10.1016/j.enggeo.2006.02.001

15. Jiang, X.W., et al., *Estimation of rock mass deformation modulus using variations in transmissivity and RQD with depth.* International Journal of Rock Mechanics and Mining Sciences, 2009. 46(8): p. 1370-1377.https://doi.org/10.1016/j.ijrmms.2009.05.004

16. Muskat, M. and M.W. Meres, *The flow of homogeneous fluids through porous media.* Soil Science, 1938. 46(2): p. 524-530

17. Goodman, R.E., et al., *Groundwater inflow during tunnel driving*. 1965, University of California, .

18. Park, K.-H., A. Owatsiriwong, and J.-G. Lee, *Analytical solution for steady-state groundwater inflow into a drained circular tunnel in a semi-infinite aquifer: A revisit.* Tunnelling and Underground Space Technology, 2008. 23(2): p. 206-209.https://doi.org/10.1016/j.tust.2007.02.004

19. Snow, D.T., *Anisotropic permeability of fractured media.* Water Resources Research, 1969. 5(6): p. 1273-1289.https://doi.org/10.1029/WR005i006p01273

20.   Oda, M., *Permeability tensor for discontinuous rock masses.* Geotechnique, 1985. 35(4): p. 483-495.https://doi.org/10.1680/geot.1985.35.4.483

21.   Zhou, C.B., et al., *Flow–stress coupled permeability tensor for fractured rock masses.* International Journal for Numerical Analytical Methods in Geomechanics, 2008. 32(11): p. 1289-1309.https://doi.org/10.1002/nag.668

22.   Gattinoni, P. and L. Scesi, *An empirical equation for tunnel inflow assessment: application to sedimentary rock masses.* Hydrogeology Journal, 2010. 18(8): p. 1797-1810.https://doi.org/10.1007/s10040-010-0674-1

23.   Saeidi, O., H. Stille, and S.R. Torabi, *Numerical and analytical analyses of the effects of different joint and grout properties on the rock mass groutability.* Tunnelling and Underground Space Technology, 2013. 38: p. 11-25.http://dx.doi.org/10.1016/j.tust.2013.05.005

24.   Fernandez, G. and J. Moon, *Excavation-induced hydraulic conductivity reduction around a tunnel-Part 2: Verification of proposed method using numerical modeling.* Tunnelling and Underground Space Technology, 2010. 25: p. 567–574.https://doi.org/10.1016/j.tust.2010.04.001

25.   Min, K.-B., et al., *Stress-dependent permeability of fractured rock masses: a numerical study.* International Journal of Rock Mechanics and Mining Sciences, 2004. 41(7): p. 1191-1210.https://doi.org/10.1016/j.ijrmms.2004.05.005

26.   Lei, Q., et al., *Polyaxial stress-induced variable aperture model for persistent 3D fracture networks.* Geomechanics for Energy and the Environment 2015. 1: p. 34–47.https://doi.org/10.1016/j.gete.2015.03.003

27.   Zhang, X., et al., *Evaluation of the 2-D permeability tensor for fractured rock masses.* International Journal of Rock Mechanics and Mining Sciences & Geomechanics Abstracts, 1996. 33 p. 17-37.https://doi.org/10.1016/0148-9062(95)00042-9

28.   Baghbanan, A. and L. Jing, *Hydraulic properties of fractured rock masses with correlated fracture length and aperture.* International Journal of Rock Mechanics and Mining Sciences, 2007. 44(5): p. 704-719.https://doi.org/10.1016/j.ijrmms.2006.11.001

29.   Min, K.-B., L. Jing, and O. Stephansson, *Determining the equivalent permeability tensor for fractured rock masses using a stochastic REV approach: Method and application to the field data from Sellafield, UK.* Hydrogeology Journal, 2004. 12(5): p. 497-510.https://doi.org/10.1007/s10040-004-0331-7

30.   Lin, H.-I. and C.-H. Lee, *An approach to assessing the hydraulic conductivity disturbance in fractured rocks around the Syueshan tunnel, Taiwan.* Tunnelling and Underground Space Technology, 2009. 24(2): p. 222-230.http://dx.doi.org/10.1016/j.tust.2008.06.003

31.   Mortimer, L., et al., *Is in situ stress important to groundwater flow in shallow fractured rock aquifers?* Journal of Hydrology, 2011. 399: p. 185–200.http://dx.doi.org/10.1016/j.jhydrol.2010.12.034

32.   Chen, D., Z. Pan, and Z. Ye, *Dependence of gas shale fracture permeability on effective stress and reservoir pressure: Model match and insights.* Fuel, 2015. 139: p. 383–392.https://doi.org/10.1016/j.fuel.2014.09.018

33.   Baghbanan, A. and L. Jing, *Stress effects on permeability in a fractured rock mass with correlated fracture length and aperture.* International Journal of Rock Mechanics and Mining Sciences, 2008. 45(8): p. 1320-1334.https://doi.org/10.1016/j.ijrmms.2008.01.015

34.   Latham, J.P., et al., *Modelling stress-dependent permeability in fractured rock including effects of propagating and bending fractures.* International Journal of Rock Mechanics and Mining Sciences, 2013. 57: p. 100-112.http://dx.doi.org/10.1016/j.ijrmms.2012.08.002

35.   Jacquemyn, C., et al., *Multi-scale three-dimensional distribution of fracture-and igneous intrusion-controlled hydrothermal dolomite from digital outcrop model, Latemar platform, Dolomites, northern ItalyThree-dimensional Dolomite Distribution.* AAPG Bulletin, 2015. 99(5): p. 957-984.https://doi.org/10.1306/10231414089

36.   Lei, Q., J.-P. Latham, and C.-F. Tsang, *The use of discrete fracture networks for modelling coupled geomechanical and hydrological behaviour of fractured rocks.* Computers and Geotechnics, 2017. 85: p. 151-176.https://doi.org/10.1016/j.compgeo.2016.12.024

37.   Louis, C., *Rock Hydraulics*, in *Rock Mechanics*, L. Müller, Editor. 1972, Springer Vienna: Vienna. p. 299-387.

38. Burgess, A., *Groundwater movements around a repository*. 1977, Kaernbraenslesaekerhet: Sweden. p. 116.

39. Black, J.H., *Flow and flow mechanisms in crystalline rock.* Geological Society, London, Special Publications, 1987. 34(1): p. 185-200.https://doi.org/10.1144/GSL.SP.1987.034.01.13

40. Wei, Z.Q., P. Egger, and F. Descoeudres, *Permeability predictions for jointed rockmasses.* International Journal of Rock Mechanics and Mining Sciences & Geomechanics Abstracts, 1995. 32: p. 251–261.https://doi.org/10.1016/0148-9062(94)00034-Z

41. Zhao, J., *Rock mass hydraulic conductivity of the Bukit Timah granite, Singapore.* Engineering Geology, 1998. 50: p. 211–216.https://doi.org/10.1016/S0013-7952(98)00021-0

42. Hamm, S.-Y., et al., *Relationship between hydraulic conductivity and fracture properties estimated from packer tests and borehole data in a fractured granite.* Engineering Geology, 2007. 92(1-2): p. 73-87.https://doi.org/10.1016/j.enggeo.2007.03.010

43. Huang, Z., et al., *Influence of structure and water pressure on the hydraulic conductivity of the rock mass around underground excavations.* Engineering Geology, 2016. 202: p. 74-84.https://doi.org/10.1016/j.enggeo.2016.01.003

44. Coli, N., et al., *Evaluation of rock-mass permeability tensor and prediction of tunnel inflows by means of geostructural surveys and finite element seepage analysis.* Engineering Geology, 2008. 101(3-4): p. 174-184.http://dx.doi.org/10.1016/j.enggeo.2008.05.002

45. Piscopo, V., et al., *Estimation of rock mass permeability using variation in hydraulic conductivity with depth: experiences in hard rocks of western Turkey.* Bulletin of Engineering Geology and the Environment, 2018. 77(4): p. 1663–1671.https://doi.org/10.1007/s10064-017-1058-8

46. Talbot, C.J. and M. Sirat, *Stress control of hydraulic conductivity in fracture-saturated Swedish bedrock.* Engineering geology, 2001. 61(2-3): p. 145-153.https://doi.org/10.1016/S0013-7952(01)00047-3

47. Lee, C.H., B.W. Deng, and J.L. Chang, *A continuum approach for estimating permeability in naturally fractured rocks* Engineering Geology, 1995. 39(1-2): p. 71-85.https://doi.org/10.1016/0013-7952(94)00064-9

48. Jiang, X.W., et al., *Estimation of fracture normal stiffness using a transmissivity-depth correlation.* International Journal of Rock Mechanics and Mining Sciences, 2009. 46(1): p. 51-58.https://doi.org/10.1016/j.ijrmms.2008.03.007

49. Snow, D.T., *Closure on rock fracture spacings, openings and porosities.* Journal of the Soil Mechanics and Foundations Division, 1969. Vol 95: p. 880-883.https://doi.org/10.1061/JSFEAQ.0001290

50. Louis, C., *Introduction a l'hydraulique des roches*. BULL BRGM. Vol. III. 1974, Orleans: Bureau Recherches Geologique Miniers. 114.

51. Priest, S.D. and J.A. Hudson, *Discontinuity spacings in rock.* International Journal of Rock Mechanics and Mining Sciences & Geomechanics Abstracts, 1976. 13: p. 135-148.https://doi.org/10.1016/0148-9062(76)90818-4

52. Swan, G., *Determination of stiffness and other joint properties from roughness measurements.* Rock Mechanics and Rock Engineering 1983. 16: p. 19-38.https://doi.org/10.1007/BF01030216

53. Ku, C.-Y., et al., *An empirical model for estimating hydraulic conductivity of highly disturbed clastic sedimentary rocks in Taiwan.* Engineering Geology, 2009. 109(3-4): p. 213-223.https://doi.org/10.1016/j.enggeo.2009.08.008

54. Singhal, B.B.S. and R.P. Gupta, *Applied hydrogeology of fractured rocks*. 2010: Springer Science & Business Media.

55. Spitz, K. and J. Moreno, *A practical guide to groundwater and solute transport modeling*. 1996: John Wiley and sons.

56. Bear, J., *Dynamics of fluids in porous media*. 1972: Courier Corporation.

57. Lei, S., *An Analytical Solution for Steady Flow into a Thnnel.* Ground Water, 1999. 37: p. 23-26.https://doi.org/10.1111/j.1745-6584.1999.tb00953.x

58. Király, L., *Anisotropie et hétérogénéité de la perméabilité dans les calcaires fissurés.* Eclogae Geologicae Helvetiae, 1969. 62(2): p. 613-619

59. Liu, J., D. Elsworth, and B.H. Brady, *Linking stress-dependent effective porosity and hydraulic conductivity Fields to RMR.* International Journal of Rock Mechanics and Mining Sciences, 1999. 36(5): p. 16.https://doi.org/10.1016/S0148-9062(99)00029-7

60. Chen, Y.F., C.B. Zhou, and Y.Q. Sheng, *Formulation of strain-dependent hydraulic conductivity for a fractured rock mass.* International Journal of Rock Mechanics and Mining Sciences, 2007. 44(7): p. 981-996.https://doi.org/10.1016/j.ijrmms.2006.12.004

61. Darcy, H., *Les fontaines publiques de la ville de Dijon: exposition et application*. 1856: Victor Dalmont.

62. Zhao, Z., et al., *Numerical modeling of stress effects on solute transport in fractured rocks.* Computers and Geotechnics 2011. 38: p. 113–126.https://doi.org/10.1016/j.compgeo.2010.10.001

63. Lee, C.-H. and I.W. Farmer, *Fluid Flow in Discontinuous Rocks*. 1993, London: Chapman & Hall.

64. Witherspoon, P.A., et al., *Validity of cubic law for fluid flow in a deformable rock fracture.* Water Resources Research, 1979. 16(6): p. 1016-1024.https://doi.org/10.1029/WR016i006p01016

65. Zimmerman, R.W. and G.S. Bodvarsson, *Hydraulic conductivity of rock fractures.* Transport in Porous Media, 1996. 23: p. 1-30.https://doi.org/10.1007/BF00145263

66. Todd, D.K., *Groundwater hydrology*. Second ed. 1980: John Wiley.

67. Barton, N., S. Bandis, and K. Bakhtar, *Strength, deformation and conductivity coupling of rock joints.* International Journal of Rock Mechanics and Mining Sciences & Geomechanics Abstracts, 1985. 22: p. 121-140.https://doi.org/10.1016/0148-9062(85)93227-9

68. Zoorabadi, M., B. Indraratna, and J. Nemcik, *A new equation for the equivalent hydraulic conductivity of rock mass around a tunnel.* International Journal of Rock Mechanics and Mining Sciences, 2012. 54: p. 125-128.http://dx.doi.org/10.1016/j.ijrmms.2012.05.017

69. Rouleau, A. and J.E. Gale, *Statistical characterization of the fracture system in the Stripa granite, Sweden.* International Journal of Rock Mechanics and Mining Sciences & Geomechanics Abstracts, 1985. 22(6): p. 353-367.https://doi.org/10.1016/0148-9062(85)90001-4

70. Xu, C., et al., *A connectivity index for discrete fracture networks.* Mathematical geology, 2006. 38(5): p. 611-634.https://doi.org/10.1007/s11004-006-9029-9

71. Reynolds, O., *Experiments showing dilatancy, a property of granular material, possibly connected with gravitation*. 1886, Royal Institution Great Britain: Great Britain. p. 217-227.

72. Brown, S.R. and R.L. Bruhn, *Fluid permeability of deformable fracture networks.* Journal of Geophysical Research: Solid Earth, 1998. 103(B2): p. 2489-2500.https://doi.org/10.1029/97JB03113

73. Ivars, D.M., et al., *The synthetic rock mass approach for jointed rock mas modelling.* International Journal of Rock Mechanics and Mining Sciences, 2011. 48: p. 219–244.https://doi.org/10.1016/j.ijrmms.2010.11.014

74. Farahmand, K., et al. *Effect of fracture dilation angle on stress-dependent permeability tensor of fractured rock*. in *49th US Rock Mechanics/Geomechanics Symposium*. 2015. American Rock Mechanics Association.

75. Yeo, I.W., M.H.D. Freitas, and R.W. Zimmerman, *Effect of shear displacement on the aperture and permeability of a rock fracture.* International Journal of Rock Mechanics and Mining Sciences, 1998. 35: p. 1051-1070.https://doi.org/10.1016/S0148-9062(98)00165-X

76. Huang, T.H., C.S. Chang, and C.Y. Chao, *Experimental and mathematical modeling for fracture of rock joint with regular asperities.* Engineering Fracture Mechanics 2002. 69 p. 1977–1996.https://doi.org/10.1016/S0013-7944(02)00072-3

77. Zhao, Z., L. Jing, and I. Neretnieks, *Evaluation of hydrodynamic dispersion parameters in fractured rocks.* Journal of Rock Mechanics and Geotechnical Engineering, 2010. 2(3): p. 243-254.https://doi.org/10.3724/sp.J.1235.2010.00243

78. Hossain, M., M. Rahman, and S. Rahman, *A shear dilation stimulation model for production enhancement from naturally fractured reservoirs.* SPE Journal, 2002. 7(02): p. 183-195.https://doi.org/10.2118/78355-PA

79. Brady, B.H.G. and E.T. Brown, *Rock mechanics For underground mining*, ed. 3. 2013: Springer science & business media.

80. Karlsrud, K., *Control of water leakage when tunneling under urban areas in the Oslo region.* NFF Publication, 2001. 4(12): p. 27-33

81. Farhadian, H. and H. Katibeh, *New empirical model to evaluate groundwater flow into circular tunnel using multiple regression analysis.* International Journal of Mining Science and Technology, 2017. 27(3): p. 415-421.http://dx.doi.org/10.1016/j.ijmst.2017.03.005

82. Polubarinova, P.Y. and N. Kochina, *Theory of ground water movement*. 1962: Princeton University Press.

83. Heuer, R.E., *Estimating rock tunnel water inflow*, in *Rapid Excavation and Tunneling Conference*. 1995, Society for mining, metallurgy and exploration, INC: San Francisco, California. p. 41-60.

84. El Tani, M., *Circular tunnel in a semi-infinite aquifer.* Tunnelling and Underground Space Technology, 2003. 18(1): p. 49-55.http://dx.doi.org/10.1016/s0886-7798(02)00102-5

85. Kolymbas, D. and P. Wagner, *Groundwater ingress to tunnels – The exact analytical solution.* Tunnelling and Underground Space Technology, 2007. 22(1): p. 23-27.https://doi.org/10.1016/j.tust.2006.02.001

86. Ickblom, G.B. and C.D. Martin, *Recent experiments in hard rocks to study the excavation response: implications for the performance of a nuclear waste geological repository.* Tunnelling and Underground Spae.e Technology, 1999. 14(3): p. 377-394.https://doi.org/10.1016/S0886-7798(99)00053-X

87. Kelsall, P.C., J.B. Case, and C.R. Chabannes, *Evaluation of excavation-induced changes in rock permeability.* International Journal of Rock Mechanics and Mining Sciences & Geomechanics Abstracts, 1984. 21(3): p. 123-135.https://doi.org/10.1016/0148-9062(84)91530-4

88. Pusch, R., *Alteration of the hydraulic conductivity of rock by tunnel excavation.* International Journal of Rock Mechanics and Mining Sciences & Geomechanics Abstracts, 1989. 26(I): p. 79-83.https://doi.org/10.1016/0148-9062(89)90528-7

89. Hoteit, H. and A. Firoozabadi, *Compositional modeling by the combined discontinuous Galerkin and mixed methods.* SPE Journal, 2006. 11(01): p. 19-34.https://doi.org/10.2118/90276-PA

90. Karimi-Fard, M., L.J. Durlofsky, and K. Aziz. *An efficient discrete fracture model applicable for general purpose reservoir simulators*. in *SPE Reservoir Simulation Symposium*. 2003. Society of Petroleum Engineers.

91. Dreuzy, J.R., Y. Méheust, and G. Pichot, *Influence of fracture scale heterogeneity on the flow properties of three‐dimensional discrete fracture networks (DFN).* Journal of Geophysical Research: Solid Earth, 2012. 117(B11): p. 1-21.https://doi.org/10.1029/2012JB009461

92. Chesnaux, R., D. Allen, and S. Jenni, *Regional fracture network permeability using outcrop scale measurements.* Engineering Geology, 2009. 108(3-4): p. 259-271.https://doi.org/10.1016/j.enggeo.2009.06.024

93. Belayneh, M. and J.W. Cosgrove, *Fracture-pattern variations around a major fold and their implications regarding fracture prediction using limited data: an example from the Bristol Channel Basin.* Geological Society, London, Special Publications, 2004. 231(1): p. 89-102.https://doi.org/10.1144/GSL.SP.2004.231.01.06

94. Long, J.C.S., et al., *Porous media equivalents for networks of discontinuous fractures.* Water Resources Research, 1982. 18(3): p. 645-658.http://dx.doi.org/10.1029/wr018i003p00645

95. Priest, S.D. and J.A. Hudson, *Estimation of discontinuity spacing and trace length using scanline surveys.* International Journal of Rock Mechanics and Mining Sciences & Geomechanics Abstracts, 1981. 18: p. 183-197.https://doi.org/10.1016/0148-9062(81)90973-6

96. Kulatilake, P.H.S.W. and T.H. Wu, *Estimation of mean trace length of discontinuities.* Rock Mechanics and Rock Engineering 1984. 17: p. 215-232

97. Zhang, L. and H. Einstein, *Estimating the intensity of rock discontinuities.* International Journal of Rock Mechanics and Mining Sciences, 2000. 37(5): p. 819-837.https://doi.org/10.1016/S1365-1609(00)00022-8

98. Bonnet, E., et al., *Scaling of fracture systems in geological media.* Reviews of geophysics, 2001. 39(3): p. 347-383.https://doi.org/10.1029/1999RG000074

99. Davy, P., *On the frequency‐length distribution of the San Andreas fault system.* Journal of Geophysical Research: Solid Earth, 1993. 98(B7): p. 12141-12151.https://doi.org/10.1029/93JB00372

100. Liu, R., et al., *Review: Mathematical expressions for estimating equivalent permeability of rock fracture networks.* Hydrogeology Journal, 2016. 24(7): p. 1623-1649.https://doi.org/10.1007/s10040-016-1441-8

101. Rives, T., et al., *Joint spacing: analogue and numerical simulations.* Journal of Structural Geology, 1992. 14(8-9): p. 925-937.https://doi.org/10.1016/0191-8141(92)90024-Q

102.	Barton, C.A. and M.D. Zoback, *Self-similar distribution and properties of macroscopic fractures at depth in crystalline rock in the Cajon Pass Scientific Drill Hole.* Journal of Geophysical Research: Solid Earth, 1992. 97(B4): p. 5181-5200.https://doi.org/10.1029/91JB01674

103.	Hooker, J., et al., *Aperture-size scaling variations in a low-strain opening-mode fracture set, Cozzette Sandstone, Colorado.* Journal of Structural Geology, 2009. 31(7): p. 707-718.https://doi.org/10.1016/j.jsg.2009.04.001

104.	Priest, S.D., *Discontinuity analysis for rock engineering.* 2012: Springer Science & Business Media.

105.	Ren, F., et al., *Equivalent discrete fracture networks for modelling fluid flow in highly fractured rock mass.* Engineering Geology, 2017. 229: p. 21-30.https://doi.org/10.1016/j.enggeo.2017.09.013

106.	Damjanac, B., C. Fairhurst, and T. Brandshaug. *Numerical simulation of the effects of heating on the permeability of a jointed rock mass.* in *9th ISRM Congress.* 1999. International Society for Rock Mechanics.

107.	Takatoshi, I., D. Swenson, and K. Hayashi, *Effect of thermal deformation on fracture permeability in stressed rock masses*, in *Elsevier Geo-Engineering Book Series.* 2004, Elsevier. p. 673-678.

108.	Figueiredo, B., et al., *A study of changes in deep fractured rock permeability due to coupled hydro-mechanical effects.* International Journal of Rock Mechanics and Mining Sciences, 2015. 79: p. 70-85.http://dx.doi.org/10.1016/j.ijrmms.2015.08.011

109.	Rutqvist, J., et al., *Linked multicontinuum and crack tensor approach for modeling of coupled geomechanics, fluid flow and transport in fractured rock.* Journal of Rock Mechanics and Geotechnical Engineering, 2013. 5(1): p. 18-31.http://dx.doi.org/10.1016/j.jrmge.2012.08.001

110.	Oda, M., et al., *Elastic stress and strain in jointed rock masses by means of crack tensor analysis.* Rock Mechanics and Rock Engineering, 1993. 26(2): p. 89-112.https://doi.org/10.1007/BF01023618

111.	Kobayashi, A., T. Fujita, and M. Chijimatsu, *Continuous approach for coupled mechanical and hydraulic behavior of a fractured rock mass during hypothetical shaft sinking at Sellafield, UK.* International Journal of Rock Mechanics and Mining Sciences, 2001. 38(1): p. 45-57.https://doi.org/10.1016/S1365-1609(00)00063-0

112.	Gan, Q. and D. Elsworth, *A continuum model for coupled stress and fluid flow in discrete fracture networks.* Geomechanics Geophysics for Geo-Energy Geo-Resources, 2016. 2(1): p. 43-61.https://doi.org/10.1007/s40948-015-0020-0

113.	COMSOL, *Multiphysics C user guide*, C, Editor. 2010, COMSOL Consulting Services: Stockholm, Sweden.

114.	Zhang, X. and D.J. Sanderson, *Effects of stress on the two-dimensional permeability tensor of natural fracture networks.* Geophysical Journal International, 1996. 125: p. 912-924.https://doi.org/10.1111/j.1365-246X.1996.tb06034.x

115.	Rouainia, M., et al., *Hydro-geomechanical modelling of seal behaviour in overpressured basins using discontinuous deformation analysis.* Engineering Geology, 2006. 82(4): p. 222-233.https://doi.org/10.1016/j.enggeo.2005.11.004

116.	Itasca Consulting Group, I., *Particle Flow Code (PFC).* 2000: Minneapolis, Minnesota, USA.

117.	Kozicki, J. and F.V. Donze, *A new open-source software developed for numerical simulations using discrete modeling methods.* Computer Methods in Applied Mechanics and Engineering, 2008. 197(49-50): p. 4429-4443.https://doi.org/10.1016/j.cma.2008.05.023

118.	Kozicki, J. and F.V. Donze, *Yade-open dem: an open-source software using a discrete element method to simulate granular material.* Engineering Computations, 2009. 26(7): p. 786-805.https://doi.org/10.1108/02644400910985170

119.	Rockfield Software, L., *ELFEN User's Manual.* 2011: Swansea (UK).

120.	Munjiza, A.A., *The combined finite-discrete element method.* 2004: John Wiley & Sons.

121.	Itasca Consulting Group, I., *Universal Distinct Element Code (UDEC).* 2000: Minneapolis, Minnesota, USA.

122.	Lang, P.S., A. Paluszny, and R.W. Zimmerman, *Permeability tensor of three-dimensional fractured porous rock and a comparison to trace map predictions.* Journal of Geophysical Research: Solid Earth, 2014. 119(8): p. 6288-6307.https://doi.org/10.1002/2014jb011027

123. Huang, N., et al., *Estimation of permeability of 3-D discrete fracture networks: An alternative possibility based on trace map analysis.* Engineering Geology, 2017. 226: p. 12-19.https://doi.org/10.1016/j.enggeo.2017.05.005

124. Liu, R., et al., *A numerical approach for assessing effects of shear on equivalent permeability and nonlinear flow characteristics of 2-D fracture networks.* Advances in Water Resources, 2018. 111: p. 289-300.https://doi.org/10.1016/j.advwatres.2017.11.022

125. Ren, F., et al., *Investigation of the permeability anisotropy of 2D fractured rock masses.* Engineering Geology, 2015. 196: p. 171–182.https://doi.org/10.1016/j.enggeo.2015.07.021

126. Mortimer, L., et al., *Determining the directional hydraulic conductivity of a rock mass*, in *Proceedings World Geothermal Congress.* 2010: Bali, Indonesia.

127. Xu, Z., et al., *Back-analysis approach for the determination of hydraulic conductivity in rock caverns.* Tunnelling and Underground Space Technology, 2015. 47: p. 233-238.http://dx.doi.org/10.1016/j.tust.2015.01.008

128. Dang, W., et al., *Effect of shear-induced aperture evolution on fluid flow in rock fractures.* Computers and Geotechnics, 2019. 114: p. 103152.https://doi.org/10.1016/j.compgeo.2019.103152

129. Liao, Q.H. and S.R. Hencher, *Numerical modelling of the hydro-mechanical behaviour of fractured rock masses.* International Journal of Rock Mechanics and Mining Sciences, 1997. 34(3-4): p. e1-e17.http://dx.doi.org/10.1016/s1365-1609(97)00052-x

130. Olssona, R. and N. Barton, *An improved model for hydromechanical coupling during shearing of rock joints.* International Journal of Rock Mechanics and Mining Sciences 2001. 38: p. 317–329.https://doi.org/10.1016/S1365-1609(00)00079-4

131. Xiong, X., et al., *Experimental and numerical study of the geometrical and hydraulic characteristics of a single rock fracture during shear.* International Journal of Rock Mechanics and Mining Sciences, 2011. 48(8): p. 1292-1302.http://dx.doi.org/10.1016/j.ijrmms.2011.09.009

132. Paluszny, A. and S.K. Matthäi, *Numerical modeling of discrete multi-crack growth applied to pattern formation in geological brittle media.* International Journal of Solids and Structures, 2009. 46(18-19): p. 3383-3397.http://dx.doi.org/10.1016/j.ijsolstr.2009.05.007

133. Lei, Q., et al., *Effects of geomechanical changes on the validity of a discrete fracture network representation of a realistic two-dimensional fractured rock.* International Journal of Rock Mechanics and Mining Sciences, 2014. 70: p. 507-523.http://dx.doi.org/10.1016/j.ijrmms.2014.06.001

134. Rutqvist, J. and O. Stephansson, *The role of hydromechanical coupling in fractured rock engineering.* Hydrogeology Journal, 2003. 11(1): p. 7-40.https://doi.org/10.1007/s10040-002-0241-5

135. Lomize, G., *Flow in fractured rocks.* Gosenergoizdat, Moscow, 1951. 127(197): p. 496

136. Louis, C., *A study of groundwater flow in jointed rock and its influence on the stability of rock masses, Imperial College.* Rock Mechanics Research Report, 1969. 10: p. 1-90

137. Patir, N. and H.S. Cheng, *An average flow model for determining effects of three-dimensional roughness on partial hydrodynamic lubrication.* Journal of Lubrication Technology, 1978. 100(1): p. 12-17.https://doi.org/10.1115/1.3453103

138. Walsh, J.B., *Effect of pore pressure and confining pressure on fracture permeability.* International Journal of Rock Mechanics and Mining Sciences & Geomechanics Abstracts, 1981. 18(5): p. 429-435.https://doi.org/10.1016/0148-9062(81)90006-1

139. Hakami, E., *Water flow in single rock joints.* 1989, Swedish Nuclear Fuel and Waste Management Co.

140. Renshaw, C.E., *On the relationship between mechanical and hydraulic apertures in rough‑walled fractures.* Journal of Geophysical Research: Solid Earth, 1995. 100(B12): p. 24629-24636.https://doi.org/10.1029/95JB02159

141. Rasouli, V. and A. Hosseinian, *Correlations developed for estimation of hydraulic parameters of rough fractures through the simulation of JRC flow channels.* Rock Mechanics and Rock Engineering, 2011. 44(4): p. 447-461.https://doi.org/10.1007/s00603-011-0148-3

142. Xie, L.Z., et al., *Numerical investigation of geometrical and hydraulic properties in a single rock fracture during shear displacement with the Navier–Stokes equations.* Environmental Earth Sciences, 2015. 73(11): p. 7061-7074.https://doi.org/10.1007/s12665-015-4256-3

143.   Zimmerman, R.W., et al., *Non-linear regimes of fluid flow in rock fractures.* International Journal of Rock Mechanics and Mining Sciences, 2004. 41: p. 163-169.https://doi.org/10.1016/j.ijrmms.2004.03.036

144.   Olson, J.E., *Sublinear scaling of fracture aperture versus length: An exception or the rule?* Journal of Geophysical Research: Solid Earth, 2003. 108(B9): p. 1-11.https://doi.org/10.1029/2001jb000419

145.   Renshaw, C.E. and J.C. Park, *Effect of mechanical interactions on the scaling of fracture length and aperture.* Nature, 1997. 386(6624): p. 482-484.http://dx.doi.org/10.1038/386482a0

146.   Rossen, W., Y. Gu, and L. Lake. *Connectivity and permeability in fracture networks obeying power-law statistics.* in *SPE Permian Basin Oil and Gas Recovery Conference.* 2000. Society of Petroleum Engineers.

147.   Barton, C.A., M.D. Zoback, and D. Moos, *Fluid flow along potentially active faults in crystalline rock.* Geology 1995. 23: p. 683–686.https://doi.org/10.1130/0091-7613(1995)023<0683:FFAPAF>2.3.CO;2

148.   Raven, K.G. and J.E. Gale, *Water flow in a natural rock fracture as a function of stress and sample size.* International Journal of Rock Mechanics and Mining Sciences & Geomechanics Abstracts, 1985. 22: p. 251-261.https://doi.org/10.1016/0148-9062(85)92952-3

149.   Cheng, Y., *Inherent and stress-dependent anisotropy of permeability for jointed rock masses.* 2006, National Central University: Taiwan, 2006.

150.   Xu, Z., et al., *Determination of hydraulic conductivity of fractured rock masses: A case study for a rock cavern project in Singapore.* Journal of Rock Mechanics and Geotechnical Engineering, 2015. 7(2): p. 178-184.http://dx.doi.org/10.1016/j.jrmge.2014.10.006

151.   Neuman, S.P., *Trends, prospects and challenges in quantifying flow and transport through fractured rocks.* Hydrogeology Journal, 2005. 13(1): p. 124-147.https://doi.org/10.1007/s10040-004-0397-2

152.   Snow, D.T., *A parallel plate model of fractured permeable media.* 1965, Univ. of California: California.

153.   Min, K.-B., *Determination of equivalent hydraulic and mechanical properties of fractured rock masses using the distinct element method*, in *Department of Land and Water Resources Engineering.* 2002, Mark och vatten: Stockholm.

154.   Liu, E.R., *Effects of fracture aperture and roughness on hydraulic and mechanical properties of rocks: implication of seismic characterization of fractured reservoirs.* Journal of Geophysics and Engineering, 2005. 2(1): p. 38-47.http://dx.doi.org/10.1088/1742-2132/2/1/006

155.   Xing Zhang and D.J. Sanderson, *Anisotropic features of geometry and permeability in fractured rock masses.* Engineering Geology, 1995. 40: p. 65-75.https://doi.org/10.1016/0013-7952(95)00040-2

156.   Rasouli, M., *Engineering geological studies of the diversion tunnel, focusing on stabilization analysis and support design, Iran.* Engineering Geology, 2009. 108(3-4): p. 208-224.https://doi.org/10.1016/j.enggeo.2009.07.007

157.   Font-Capó, J., et al., *Groundwater inflow prediction in urban tunneling with a tunnel boring machine (TBM).* Engineering Geology, 2011. 121(1): p. 46-54.https://doi.org/10.1016/j.enggeo.2011.04.012

158.   Moon, J. and G. Fernandez, *Effect of excavation-induced groundwater level drawdown on tunnel inflow in a jointed rock mass.* Engineering Geology, 2010. 110(3-4): p. 33-42.https://doi.org/10.1016/j.enggeo.2009.09.002

159.   Kavvadas, M.J., *Monitoring ground deformation in tunnelling: current practice in transportation tunnels.* Engineering Geology, 2005. 79(1-2): p. 93-113.https://doi.org/10.1016/j.enggeo.2004.10.011

160.   Pujades, E., et al., *Deep enclosures versus pumping to reduce settlements during shaft excavations.* Engineering Geology, 2014. 169: p. 100-111.https://doi.org/10.1016/j.enggeo.2013.11.017

161.   Molinero, J., J. Samper, and R. Juanes, *Numerical modeling of the transient hydrogeological response produced by tunnel construction in fractured bedrocks.* Engineering Geology, 2002. 64(4): p. 369-386.https://doi.org/10.1016/S0013-7952(01)00099-0

162.   Moon, J. and S. Jeong, *Effect of highly pervious geological features on ground-water flow into a tunnel.* Engineering Geology, 2011. 117(3): p. 207-216.https://doi.org/10.1016/j.enggeo.2010.10.019

163.   Hubbert, M.K., *The theory of ground-water motion.* The Journal of Geology, 1940. 48(8, Part 1): p. 785-944.https://doi.org/10.1086/624930

164.   Hassani, A.N., H. Katibeh, and H. Farhadian, *Numerical analysis of steady-state groundwater inflow into Tabriz line 2 metro tunnel, northwestern Iran, with special consideration of model dimensions.* Bulletin of Engineering Geology and the Environment, 2016. 75(4): p. 1617-1627.http://dx.doi.org/10.1007/s10064-015-0802-1

165.   Shahbazi, A., A. Saeidi, and R. Chesnaux, *A review of existing methods used to evaluate the hydraulic conductivity of a fractured rock mass.* Engineering Geology, 2020. 265: p. 105438.https://doi.org/10.1016/j.enggeo.2019.105438

166.   Zhang, D., et al., *Ground and tunnel responses induced by partial leakage in saturated clay with anisotropic permeability.* Engineering Geology, 2015. 189: p. 104-115.https://doi.org/10.1016/j.enggeo.2015.02.005

167.   Sun, Z., et al., *A new method for determining the hydraulic aperture of rough rock fractures using the support vector regression.* Engineering Geology, 2020. 271: p. 105618.https://doi.org/10.1016/j.enggeo.2020.105618

168.   Schleiss, A., *Design of concrete linings of pressure tunnels and shafts for external water pressure*, in *Proceedings Tunelling Asia'97*. 1997. p. 291-300.

169.   Pudasaini, S.P., *A novel description of fluid flow in porous and debris materials.* Engineering Geology, 2016. 202: p. 62-73.https://doi.org/10.1016/j.enggeo.2015.12.023

170.   Pan, J.-B., et al., *Application of fracture network model with crack permeability tensor on flow and transport in fractured rock.* Engineering Geology, 2010. 116(1-2): p. 166-177.https://doi.org/10.1016/j.enggeo.2010.08.007

171.   Wu, C., et al., *3D characterization of microbially induced carbonate precipitation in rock fracture and the resulted permeability reduction.* Engineering Geology, 2019. 249: p. 23-30.https://doi.org/10.1016/j.enggeo.2018.12.017

172.   Bandis, S.C., A.C. Lumsden, and N.R. Barton, *Fundamentals of Rock Joint Deformation.* International Journal of Rock Mechanics and Mining Sciences & Geomechanics Abstracts, 1983. 20: p. 249-268.https://doi.org/10.1016/0148-9062(83)90595-8

173.   Chen, S.G. and J. Zhao, *A study of UDEC modelling for blast wave propagation in jointed rock masses.* International Journal of Rock Mechanics and Mining Sciences, 1998. 35(1): p. 93-99.http://dx.doi.org/10.1016/s0148-9062(97)00322-7

174.   Lee, I.-M., S.-W. Nam, and J.-H. Ahn, *Effect of seepage forces on tunnel face stability.* Canadian Geotechnical Journal, 2003. 40(2): p. 342-350.https://doi.org/10.1139/T02-120

175.   Shin, Y., J. Shin, and I.M. Lee. *Ground reaction due to tunnelling below groundwater table*. in *6th International Symposium on Geotechnical Aspects of Underground Construction in Soft Ground, IS-Shanghai*. 2009.

176.   Rocscience, *RS2, 2D Geotechnical finite element analysis*. 2019, Rocscience Inc.: Toronto, Canada.

177.   Zhang, L. and J. Franklin, *Prediction of water flow into rock tunnels: an analytical solution assuming an hydraulic conductivity gradient.* International journal of rock mechanics and mining sciences & geomechanics abstracts, 1993. 30(1): p. 37-46.https://doi.org/10.1016/0148-9062(93)90174-C

178.   Liu, Q., et al., *An Analytical Investigation on the Estimation of Water Inflow into a Circular Tunnel Based On-site Data.* Rock Mechanics and Rock Engineering, 2020. 53(8): p. 3835-3844.https://doi.org/10.1007/s00603-020-02114-2

179.   Nilsen, B. and A. Palmström, *Stability and water leakage of hard rock subsea tunnels*, in *Modern Tunnelling Science and Technology*. 2001, Proceedings of International Symposium IS-Kyoto: Kyoto, Japan. p. 497-502.

180.   Tan, Y., et al., *Predicting external water pressure and cracking of a tunnel lining by measuring water inflow rate.* Tunnelling and Underground Space Technology, 2018. 71: p. 115-125.https://doi.org/10.1016/j.tust.2017.08.015

181.   Butscher, C., *Steady-state groundwater inflow into a circular tunnel.* Tunnelling and Underground Space Technology, 2012. 32: p. 158-167.https://doi.org/10.1016/j.tust.2012.06.007

182.   Zhang, P., et al., *Ground settlement induced by tunneling crossing interface of water-bearing mixed ground: A lesson from Changsha, China.* Tunnelling and Underground Space Technology, 2020. 96: p. 103224.https://doi.org/10.1016/j.tust.2019.103224

183.   Saeidi, A., et al., *Development of a damage simulator for the probabilistic assessment of building vulnerability in subsidence areas.* International Journal of Rock Mechanics and Mining Sciences, 2015. 73: p. 42-53.https://doi.org/10.1016/j.ijrmms.2014.10.007

184.   Vanarelli, M.J., *A Geostatistical Solution to Estimating Groundwater Inflows in Deep Rock Tunnels with Validation Through Case Studies.* Mining, Metallurgy & Exploration, 2020.https://doi.org/10.1007/s42461-020-00321-7

185.   Lin, F., et al., *Effectiveness analysis of water-sealing for underground LPG storage.* Tunnelling and Underground Space Technology, 2016. 51: p. 270-290.https://dx.doi.org/10.1016/j.tust.2015.10.039

186.   Kayabasi, A., N. Yesiloglu-Gultekin, and C. Gokceoglu, *Use of non-linear prediction tools to assess rock mass permeability using various discontinuity parameters.* Engineering Geology, 2015. 185: p. 1-9.https://doi.org/10.1016/j.enggeo.2014.12.007

187.   Hsu, S.-M., et al., *Rock mass permeability classification schemes to facilitate groundwater availability assessment in mountainous areas: a case study in Jhuoshuei river basin of Taiwan.* Geosciences Journal, 2020. 24(2): p. 209-224.https://doi.org/10.1007/s12303-019-0017-8

188.   Zhang, Y., et al., *Analytical solutions of non-Darcy seepage of grouted subsea tunnels.* Tunnelling and Underground Space Technology, 2020. 96: p. 103182.https://doi.org/10.1016/j.tust.2019.103182

189.   Shahbazi, A., R. Chesnaux, and A. Saeidi, *A new combined analytical-numerical method for evaluating the inflow rate into a tunnel excavated in a fractured rock mass.* Engineering Geology, 2021. 283: p. 106003.https://doi.org/10.1016/j.enggeo.2021.106003

190.   Farhadian, H., et al., *Optimum model extent for numerical simulation of tunnel inflow in fractured rock.* Tunnelling and Underground Space Technology, 2016. 60: p. 21-29.https://dx.doi.org/10.1016/j.tust.2016.07.014

191.   Wang, Z., et al., *The effects of hydro-mechanical coupling in fractured rock mass on groundwater inflow into underground openings.* Tunnelling and Underground Space Technology, 2020. 103: p. 103489.https://doi.org/10.1016/j.tust.2020.103489

192.   Nikvar Hassani, A., H. Farhadian, and H. Katibeh, *A comparative study on evaluation of steady-state groundwater inflow into a circular shallow tunnel.* Tunnelling and Underground Space Technology, 2018. 73: p. 15-25.https://doi.org/10.1016/j.tust.2017.11.019

193.   Yu, C., et al., *The anisotropic seepage analysis of water-sealed underground oil storage caverns.* Tunnelling and Underground Space Technology, 2013. 38: p. 26-37.https://doi.org/10.1016/j.tust.2013.05.003

194.   Ivars, D.M., *Water inflow into excavations in fractured rock—a three-dimensional hydro-mechanical numerical study.* International Journal of Rock Mechanics and Mining Sciences, 2006. 43(5): p. 705-725.https://doi.org/10.1016/j.ijrmms.2005.11.009

195.   Palmström, A., *RMi-a rock mass characterization system for rock engineering purposes*, in *Department of Geology*. 1995, University of Oslo.

196.   Esmaieli, K., J. Hadjigeorgiou, and M. Grenon, *Estimating geometrical and mechanical REV based on synthetic rock mass models at Brunswick Mine.* International Journal of Rock Mechanics and Mining Sciences, 2010. 47(6): p. 915-926.https://doi.org/10.1016/j.ijrmms.2010.05.010

197.   Wang, M., et al., *Estimation of REV size and three-dimensional hydraulic conductivity tensor for a fractured rock mass through a single well packer test and discrete fracture fluid flow modeling.* International Journal of Rock Mechanics and Mining Sciences, 2002. 39(7): p. 887-904.https://doi.org/10.1016/S1365-1609(02)00067-9

198.   Palmström, A., *Measurements of and correlations between block size and rock quality designation (RQD).* Tunnelling and Underground Space Technology, 2005. 20(4): p. 362-377.https://doi.org/10.1016/j.tust.2005.01.005

199.   Barton, N., *Scale effects or sampling bias?* Publikasjon-Norges Geotekniske Institutt, 1990. 182: p. 31-55

200. Cai, M., et al., *Estimation of rock mass deformation modulus and strength of jointed hard rock masses using the GSI system.* International Journal of Rock Mechanics and Mining Sciences, 2004. 41(1): p. 3-19.https://doi.org/10.1016/S1365-1609(03)00025-X

201. Li, P., et al., *Investigation of steady water inflow into a subsea grouted tunnel.* Tunnelling and Underground Space Technology, 2018. 80: p. 92-102.https://doi.org/10.1016/j.tust.2018.06.003

202. Lv, Y., et al., *A review of the effects of tunnel excavation on the hydrology, ecology, and environment in karst areas: Current status, challenges, and perspectives.* Journal of Hydrology, 2020. 586: p. 124891.https://doi.org/10.1016/j.jhydrol.2020.124891

203. Chen, Y., C. Zhou, and H. Zheng, *A numerical solution to seepage problems with complex drainage systems.* Computers and Geotechnics, 2008. 35(3): p. 383-393.https://doi.org/10.1016/j.compgeo.2007.08.005

204. Wang, X., et al., *An interval risk assessment method and management of water inflow and inrush in course of karst tunnel excavation.* Tunnelling and Underground Space Technology, 2019. 92: p. 103033.https://doi.org/10.1016/j.tust.2019.103033

205. Jin, X.G., H.W. Liu, and S.X. Zhou, *Research of Water Inflow Impact on Ecological Environment for Cimushan Tunnel.* Advanced Materials Research, 2012. 594-597: p. 1263-1268.https://doi.org/10.4028/www.scientific.net/AMR.594-597.1263

206. Zhang, L., et al., *Prediction of water inflow in Tsingtao subsea tunnel based on the superposition principle.* Tunnelling and Underground Space Technology, 2020. 97: p. 103243.https://doi.org/10.1016/j.tust.2019.103243

207. Zhou, J.-Q., et al., *A semi-empirical model for water inflow into a tunnel in fractured-rock aquifers considering non-Darcian flow.* Journal of Hydrology, 2021. 597: p. 126149.https://doi.org/10.1016/j.jhydrol.2021.126149

208. Katibeh, H. and A. Aalianvari, *Development of a new method for tunnel site rating from groundwater hazard point of view.* Journal of Applied Sciences, 2009. 9(8): p. 1496-1502.https://doi.org/10.3923/jas.2009.1496.1502

209. Zarei, H.R., A. Uromeihy, and M. Sharifzadeh, *A new tunnel inflow classification (TIC) system through sedimentary rock masses.* Tunnelling and Underground Space Technology, 2013. 34: p. 1-12.https://doi.org/10.1016/j.tust.2012.09.005

210. Su, K., et al., *An Analytical Method for Groundwater Inflow into a Drained Circular Tunnel.* Groundwater, 2017. 55(5): p. 712-721.https://doi.org/10.1111/gwat.12513

211. Chen, Y.-F., et al., *Non-Darcian flow effect on discharge into a tunnel in karst aquifers.* International Journal of Rock Mechanics and Mining Sciences, 2020. 130: p. 104319.https://doi.org/10.1016/j.ijrmms.2020.104319

212. Quinn, P.M., J.A. Cherry, and B.L. Parker, *Relationship between the critical Reynolds number and aperture for flow through single fractures: Evidence from published laboratory studies.* Journal of Hydrology, 2020. 581: p. 124384.https://doi.org/10.1016/j.jhydrol.2019.124384

213. Sharifzadeh, M., S. Karegar, and M. Ghorbani, *Influence of rock mass properties on tunnel inflow using hydromechanical numerical study.* Arabian Journal of Geosciences, 2013. 6(1): p. 169-175.https://doi.org/10.1007/s12517-011-0320-9

214. Yang, Z.-M., et al., *Time and technique of rehabilitation for large deformation of tunnels in jointed rock masses based on FDM and DEM numerical modeling.* Tunnelling and Underground Space Technology, 2018. 81: p. 669-681.https://doi.org/10.1016/j.tust.2018.08.036

215. Clauser, C., *Permeability of crystalline rocks.* Eos, Transactions American Geophysical Union, 1992. 73(21): p. 233-238.https://doi.org/10.1029/91EO00190

216. Brown, E.T., *ISRM Suggested Method: Rock Characterization, Testing and Monitoring.* 1981, London: Pergamon press.

217. Farhadian, H., H. Katibeh, and P. Huggenberger, *Empirical model for estimating groundwater flow into tunnel in discontinuous rock masses.* Environmental Earth Sciences, 2016. 75(6): p. 471.https://doi.org/10.1007/s12665-016-5332-z

218. Masset, O. and S. Loew, *Hydraulic conductivity distribution in crystalline rocks, derived from inflows to tunnels and galleries in the Central Alps, Switzerland.* Hydrogeology Journal, 2010. 18(4): p. 863-891.https://doi.org/10.1007/s10040-009-0569-1

219. Barton, N. and E.F. de Quadros, *Joint aperture and roughness in the prediction of flow and groutability of rock masses.* International Journal of Rock Mechanics and Mining Sciences, 1997. 34(3): p. 252.e1-252.e14.https://doi.org/10.1016/S1365-1609(97)00081-6

220. Shahbazi, A., et al., *The Specific Length of an Underground Tunnel and the Effects of Rock Block Characteristics on the Inflow Rate.* Geosciences, 2021. 11(12).https://doi.org/10.3390/geosciences11120517

221. ISRM, *Suggested methods for the quantitative description of discontinuities in rock mass.* International journal of rock mechanics and mining sciences & geomechanics abstracts, 1978. 15: p. 319-368

222. Bieniawski, Z.T., *Rock mechanics design in mining and tunneling*. 1984, Rotterdam: A.A. Balkema.

223. Bieniawski, Z.T., *The Rock Mass Rating (RMR) System (Geomechanics Classification) in Engineering Practice*, L. Kirkaldie, Editor. 1988, ASTM International: West Conshohocken, PA. p. 17-34.

224. Palmström, A., *Measurement and characterization of rock mass jointing*, in *In-situ characterization of rocks*, V.M. Sharma and K.R. Saxena, Editors. 2001, A.A. BalkemaA Publishers: India. p. 1-40.

225. Itasca Consulting Group, I., *3DEC — Three-Dimensional Distinct Element Code*. 2021, Itasca: Minneapolis.

226. Boumaiza, L., A. Saeidi, and M. Quirion, *A method to determine relevant geomechanical parameters for evaluating the hydraulic erodibility of rock.* Journal of Rock Mechanics and Geotechnical Engineering, 2019. 11(5): p. 1004-1018.https://doi.org/10.1016/j.jrmge.2019.04.002

227. Palmström, A. *The volumetric joint count—a useful and simple measure of the degree of rock mass jointing*. in *International Association of Engineering Geology. International congress*. 1982. India / Netherlands: A.A. Balkema.

228. Palmström, A., *The Rock Mass Index (RMi) applied in rock mechanics and rock engineering.* Joumal of Rock Mechanics and Tunnelling Technology, 1996. 2: p. 40

229. Elci, H. and N. Turk, *Block Volume Estimation from the Discontinuity Spacing Measurements of Mesozoic Limestone Quarries, Karaburun Peninsula, Turkey.* The Scientific World Journal, 2014. 2014: p. 363572.https://doi.org/10.1155/2014/363572

230. Barton, N., R. Lien, and J. Lunde, *Engineering classification of rock masses for the design of tunnel support.* Rock mechanics, 1974. 6(4): p. 189-236.https://doi.org/10.1007/BF01239496

231. Cai, M., et al., *Estimation of rock mass deformation modulus and strength of jointed hard rock masses using the GSI system.* International Journal of Rock Mechanics and Mining Sciences, 2004. 41(1): p. 3-19

232. Latham, J.-P., J. Van Meulen, and S. Dupray, *Prediction of in-situ block size distributions with reference to armourstone for breakwaters.* Engineering Geology, 2006. 86(1): p. 18-36.https://doi.org/10.1016/j.enggeo.2006.04.001

233. Kirsten, H.A.D., *A classification system for excavating in natural materials.* Civil Engineering = Siviele Ingenieurswese, 1982. 24(7): p. 293-308

234. Bieniawski, Z.T., *Engineering classification of jointed rock masses.* Civil Engineer in South Africa, 1973. 15(12): p. 11.https://doi.org/10.1016/0148-9062(74)92075-0

235. Edelbro, C., *Rock mass strength : a review*, in *Teknisk rapport / Luleå tekniska universitet*. 2003, Luleå tekniska universitet: Luleå. p. 92.

236. Grenon, M. and J. Hadjigeorgiou, *Open stope stability using 3D joint networks.* Rock Mechanics and Rock Engineering, 2003. 36(3): p. 26.https://doi.org/10.1007/s00603-002-0042-0

237. Pells, P.J., et al., *Rock quality designation (RQD): time to rest in peace.* Canadian Geotechnical Journal, 2017. 54(6): p. 10.https://doi.org/10.1139/cgj-2016-0012

238. Bergh-Christensen, J., *On the blastability of rocks*, in *Geological Institute*. 1968, Technical University of Norway: Trondheim, Norway. p. 320.

239. Pells, S., *Erosion of rock in spillways*, in *School of Civil and Environmental Engineering, Faculty of Engineering*. 2016, University of New South Wales: Australia. p. 1982.

240. Sidiki Koulibaly, A., et al., *Rock block volume calculation by analytical method for geological engineering applications.* Submitted to Engineering Geology Journal, 2021

241. Shahbazi, A., A. Saeidi, and R. Chesnaux, *Numerical investigation of the relationship between the inflow rate to the tunnel, block volume and block surface area*, in *The Evolution of Geotech-25 Years of Innovation*, R.E. Hammah, et al., Editors. 2022, CRC Press, Taylor & Francis: Netherlands.